GROUP 4 METALLOCENES AS CATALYSTS FOR DEHYDROCOUPLING OF ORGANOSILANES

by

Ying Mu

A thesis submitted to the
Faculty of Graduate Studies and Research
in partial fulfilment of the requirements for
the degree of Doctor of Philosophy

Department of Chemistry
McGill University
Montreal, Quebec, Canada

June 1991

National Library of Canada
Bibliothèque nationale du Canada

Canadian Theses Service
Service des thèses canadiennes

Ottawa, Canada
K1A 0N4

ISBN 0-315-72017-4

GROUP 4 METALLOCENES AS CATALYSTS FOR DEHYDROCOUPLING OF ORGANOSILANES

PH.D. Ying Mu Chemistry

ABSTRACT

The dehydrocoupling of phenylsilane in the presence of dimethyltitanocene (DMT) or dimethylzirconocene (DMZ) was proved to be a stepwise reaction. The reaction profiles for phenylsilane, 1,2-diphenyldisilane and 1,2,3-triphenyltrisilane were studied in detail by following the reactions by ^1H NMR, GC and GPC. Dimer was produced as the only product in the dehydrocoupling of diphenylsilane, while dimer and trimer were obtained from the phenylmethylsilane system. Butylmethylsilane showed no reactivity toward the dehydrocoupling reaction. A kinetic study indicated that the dehydrocoupling of diphenylsilane is a second order reaction with respect to the silane. The dehydrocoupling of methylsilane under pressures around 10 atmospheres, catalyzed by either DMT or DMZ produced high molecular weight polymethylsilane quantitatively. Pyrolysis of polymethylsilane gave high yields (75-80%) of near stoichiometric SiC. The amorphous SiC was converted to β-SiC at temperatures about 1000°C. Stoichiometric reactions of DMZ with a number of organosilanes gave a variety of dimeric silylzirconocene complexes, $Cp_2ZrR^1(\mu\text{-}H)_2R^2ZrCp_2$ (where R^1 is a silyl group, R^2 can be H, Me, or a silyl group) and $[Cp_2ZrSiRR'H]_2$ (where R = Ph, R′ = Ph, Me, H; R = Me, R′ = Bu, Me, H). Reactions of DMT with organosilanes in the presence of trimethylphosphine or pyridine usually gave silyl titanocene(III) complexes of the type $Cp_2Ti(R)L$, where R is a silyl group, L = PMe_3 or Py. However, a pyridyl-bridged complex $Cp_2Ti(\mu\text{-}H)(\mu\text{-}N,C\text{-}Py)TiCp_2$ was isolated from reactions of DMT with phenylmethylsilane and butylmethylsilane.

DÉSHYDROCOUPLAGE DES ORGANOSILANES CATALYSÉ PAR DES MÉTALLOCÈNES DU GROUPE 4

Ph.D. Ying Mu Chimie

RÉSUMÉ

Il fut démontré que le couplage déshydrogénatif du phénylsilane en présence du diméthyltitanocène (DMT) ou du diméthylzirconocène (DMZ), est effectué par étapes successives. Les réactions de couplage du phénylsilane, du diphényl-1,2 disilane et du triphényl-1,2,3 trisilane furent étudiées en détail en suivant leurs progressions par résonance magnétique nucléaire (RMN) de ^{1}H, par chromatographie en phase gazeuse (CG) et par chromatographie de perméation de gel (CPG). Le couplage du diphénylsilane n'a permis d'obtenir que son dimère alors que pour le méthylphénylsilane, le dimère et le trimère furent obtenus. Aucune réactivité reliée au couplage déshydrogénatif du butylméthylsilane ne fut observée. Une étude cinétique du couplage du diphénylsilane a démontré que cette réaction est du deuxième ordre par rapport au silane. Le couplage du méthylsilane avec le DMT ou le DMZ, sous une pression d'environ 10 atmosphères, a permis de produire quantitativement du polyméthylsilane à haut poids moléculaire. Le pyrolyse de ce polymère a donné de bon rendements (75-80%) de carbure de silicium (SiC) possédant une proportion stoichiométrique voisine du SiC idéal. Ce carbure de silicium amorphe fut converti en β-SiC par une autre pyrolyse à environ 1000°C. Les réactions stoichiométriques du DMZ avec certains organosilanes ont permis d'obtenir une variété de nouveaux complexes dimériques tels que: $Cp_2ZrR^1(\mu\text{-}H)_2R^2ZrCp_2$ (où R^1 est un groupement silyle et R^2 peut être H, Me ou un groupement silyle) et $[Cp_2ZrSiR^1R^2H]_2$ (où R^1 = Ph, R^2 = Ph, Me, H; R^1 = Me, R^2 = Bu, Me, H). Les réactions du DMT avec des organosilanes en présence de

triméthylphosphine ou de pyridine ont permis de former les complexes silyltitanocène(III) du type suivant: $Cp_2Ti(R)L$, où R est un groupement silyle et L = PMe_3 ou Py. Néanmoins, de nouveaux complexes pontés par un ligand pyridyle, $Cp_2Ti(\mu\text{-}H)(\mu\text{-}N,C\text{-}Py)TiCp_2$, furent isolés à partir des réactions du DMT avec le méthylphénylsilane et le butylméthylsilane.

To my parents

and my wife, shufen

ACKNOWLEDGMENTS

I would like to express my sincere appreciation and gratitude to my supervisor, Dr. John F. Harrod, for his consistent enthusiasm and patience in guiding me throughout the course of this work. His constant encouragement and extensive knowledge of chemistry are particularly appreciated.

I am grateful to all my colleagues in Room 435 (i.e., Abdul Malek, Bernadette Soo Lum, Bruno Côte, Clair Aitken, Darlene Trojansek, François Gauvin, Helene Boily, Huaqin Liu, Jacques Demers, Lei Wang, Pierre-Yves Plouffe, Ricardo Turin, Shixuan Xin and Steven Morris) for their friendship and help; in particular, Clare Aitken for showing me how to conduct the air-sensitive silane dehydrocoupling reaction, François Gauvin for helpful discussions and for translating the abstract, Pierre-Yves Plouffe for showing me how to get the crystal structures on an IBM personal computer and put them into my thesis.

I wish to thank Dr. E. Samuel at the Ecole Nationale Superieure de Chimie de Paris for measuring the EPR spectra, Dr. R. Laine at the University of Washington for providing the IR spectra in Fig. III-13, Dr. F. Babonneau at Université de Pierre et Marie Curie (Paris VI) for providing the solid state ^{29}Si NMR spectra in Fig. III-12, Dr. J. Britten for solving one of the crystal structures, Dr. F. Morin for measuring a number of solid state NMR spectra.

I would also like to acknowledge all members of the support staff in the Department of Chemistry, in particular Ms. Renée Charron for helping in dealing with the bureaucratic red tape during the past five years.

Finally, I wish to express my gratitude to my parents for their support and encouragement over many years of study, and to my wife Shufen for her constant support.

TABLE OF CONTENTS

CHAPTER I - GENERAL INTRODUCTION

PAGE

CHAPTER II - DEHYDROCOUPLING OF PHENYLSILANE, DIPHENYLDISILANE AND TRIPHENYLTRISILANE CATALYZED BY DIMETHYLTITANOCENE AND DIMETHYLZIRCONOCENE

CHAPTER III - SYNTHESIS, CHARACTERIZATION AND PYROLYSIS OF POLYMETHYLSILANE

PAGE

PAGE

CHAPTER VI - REACTIONS OF SOME SILANES WITH DIMETHYLTITANOCENE IN THE PRESENCE OF TRIMETHYLPHOSPHINE AND PYRIDINE

---- SYNTHESIS AND STRUCTURE OF SOME NOVEL SILYL BIS(CYCLOPENTADIENYL)TITANIUM(III) COMPLEXES

PAGE

LIST OF TABLES

LIST OF FIGURES

FIGURE PAGE

LIST OF COMPOUNDS

COMPOUND	SUBSTITUENT		LABEL
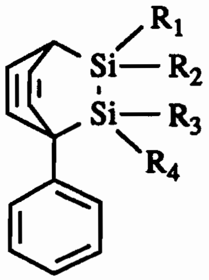			I
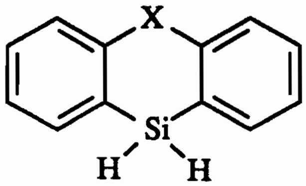	X = CH_2		II
	X = CH_2CH_2		III
	X = a bond		IV
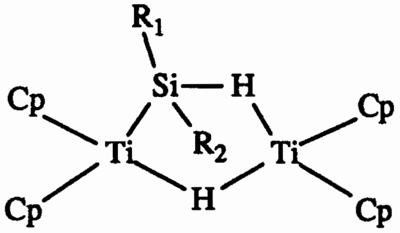	R_1 = Ph,	R_2 = H	Va
	R_1 = Hx,	R_2 = H	Vb
	R_1 = Bz,	R_2 = H	Vc
	R_1 = Ph,	R_2 = Ph	Vd
	R_1 = Me,	R_2 = H	Ve
	R_1 = Bu,	R_2 = Me	Vf
	R_1 = Ph,	R_2 = Me	Vg
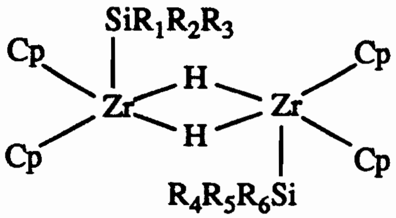	$SiR_1R_2R_3$	$SiR_4R_5R_6$	
	SiH_2Ph	SiHMePh	VIa
	SiH_2Ph	SiH_2Ph	VIb
	SiH_2Ph	$SiHPhSiH_2Ph$	VIc
	SiH_2Me	$SiHMe_2$	VId
	SiH_2Me	SiH_2Me	VIe
	SiHMePh	$SiMe_2Ph$	VIf
	SiHMePh	SiHMePh	VIg
	$SiMe_2Ph$	$SiMe_2Ph$	VIh
	$SiHPh_2$	$SiMePh_2$	VIi
	$SiHPh_2$	$SiHPh_2$	VIj
	$SiPh_2SiHPh_2$	$SiPh_2SiHPh_2$	VIk
	SiHBuMe	SiHBuMe	VIl

COMPOUND	SUBSTITUENT	LABEL
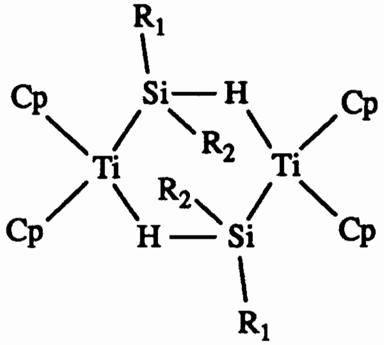	R_1 = Ph, R_2 = H	**VIIa**
	R_1 = Hx, R_2 = H	**VIIb**
	R_1 = Bz, R_2 = H	**VIIc**
	R_1 = Ph, R_2 = Ph	**VIId**
	R_1 = Me, R_2 = H	**VIIe**
	R_1 = Bu, R_2 = Me	**VIIf**
	R_1 = Ph, R_2 = Me	**VIIg**
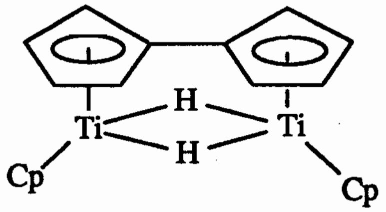		**VIII**
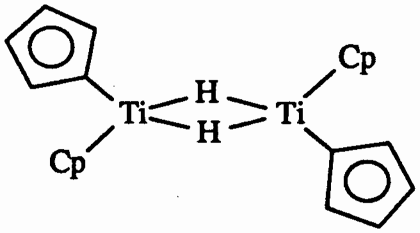		**IX**
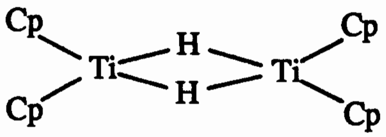		**X**
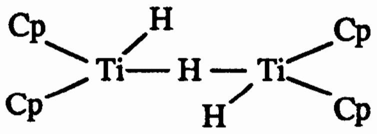		**XI**
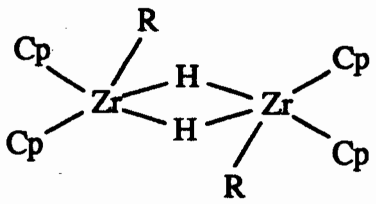	R = H or an alkyl group	**XII**
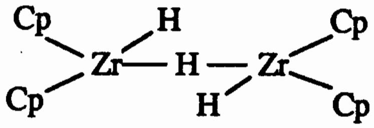		**XIII**

COMPOUND	SUBSTITUENT		LABEL
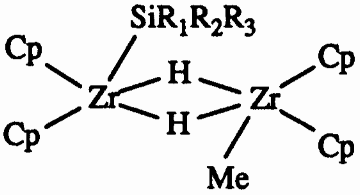	$SiR_1R_2R_3$		
	SiH_2Ph		**XIVa**
	$SiHPhSiH_2Ph$		**XIVb**
	SiHMePh		**XIVc**
	$SiHPh_2$		**XIVd**
	$SiPh_2SiHPh_2$		**XIVe**
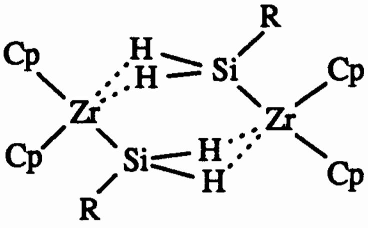	R = Ph		**XVa**
	R = Me		**XVb**
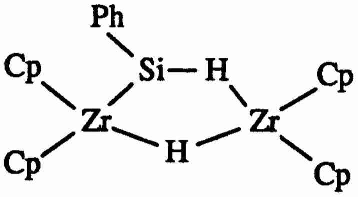			**XVIa**
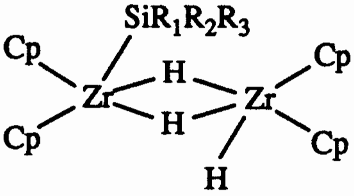	$SiR_1R_2R_3$		
	SiHMePh		**XVIIa**
	$SiHPh_2$		**XVIIb**
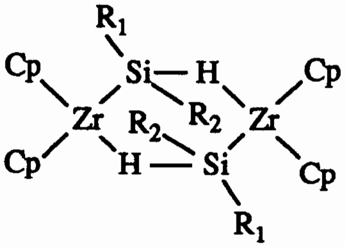	R_1 = Ph,	R_2 = Me	**XVIIIa**
	R_1 = Ph,	R_2 = Ph	**XVIIIb**
	R_1 = Bu,	R_2 = Me	**XVIIIc**
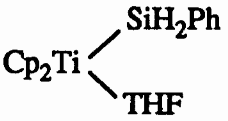			**XIX**
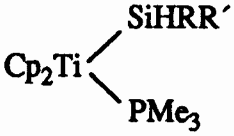	R = Ph,	R′ = Ph	**XXa**
	R = Ph,	R′ = Me	**XXb**
	R = Ph,	R′ = H	**XXc**
	R = Ph,	R′ = SiH_2Ph	**XXd**
	R = Me,	R′ = H	**XXe**

COMPOUND	SUBSTITUENT		LABEL
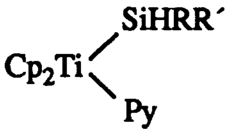	R = Ph,	R′ = H	**XXIa**
	R = Ph,	R′ = Ph	**XXIb**
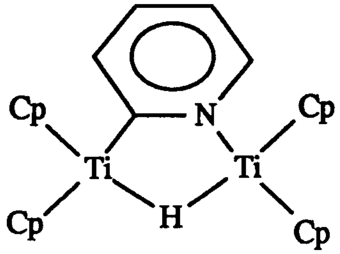			**XXII**

LIST OF ABBREVIATIONS

Å	angstrom (1 = 10^{-10} m)
BM	Bohr magneton
n-Bu	*normal*-butyl
i-Bu	*iso*-butyl
Bz	benzyl
COD	cycloocta-1,5-diene
Cp	η^5-cyclopentadienyl (η^5-C_5H_5)
Cp*	η^5-pentamethylcyclopentadienyl (η^5-$C_5(CH_3)_5$)
D	Dalton (1 D = 1 atomic mass unit)
DEPT	distortionless enhancement by polarization transfer
DMT	dimethyltitanocene
DMZ	dimethylzirconocene
$\overline{DP}_n$	number average degree of polymerization
DRIFT	diffuse reflectance infrared Fourier transform
DTA	differential thermal analysis
EPR	electron paramagnetic resonance
Et	ethyl
GPC	gel permeation chromatography
Hx	normal-hexyl
Ind	indenyl
IR	infra-red
Me	methyl
Mes	mesityl

$\bar{M}_n$	number average molecular weight
$\bar{M}_w$	weight average molecular weight
NMR	nuclear magnetic resonance
ORTEP	Oak Ridge Thermal Elipsoid Plot
Ph	phenyl
ppm	parts per million
i-Pr	*iso*-propyl
n-Pr	*normal*-propyl
Py	pyridine
RCp	η^5-alkylcyclopentadienyl
THF	tetrahydrofuran
TMS	tetramethylsilane
TGA	thermogravimetric analysis
$\nu_{1/2}$	line width at half-height

Abbreviations used to describe NMR peaks

ABq	AB quartet
br	broad band
d	doublet
dd	doublet of doublets
ddd	doublet of doublets of doublets
q	quartet
qd	quartet of doublets
t	triplet

Chapter I

General introduction

I.1 INTRODUCTION TO POLYORGANOSILANES

To date, Most industrial polymers are carbon-based, with main chains consisting entirely of carbon atoms or mainly of carbon atoms. There are, however, a number of important synthetic polymers based on inorganic main chains. Some examples of these include polymeric sulphur, poly(sulphur nitride), polyphosphazanes, polysilazanes, polysiloxanes and polyorganosilanes (1). Two of them now are commercially important: the polysiloxanes, with polymer chains made up of alternating silicon and oxygen atoms, and the polyphosphazanes, with alternating phosphorus and nitrogen atoms in the backbone. The polyorganosilanes represent a new class of polymers, which may now be approaching commercialization. Polyorganosilanes are those organosilane polymers in which the polymer chain or ring is made up entirely of silicon atoms with at least one Si-C bond. The unique feature of the polyorganosilane structure is their uninterrupted chain of silicon atoms, which allows significant delocalization of electrons along the polymer chain. This gives these polymers highly unusual properties, and some potential applications based on these properties have arisen. These remarkable properties and potential applications are currently stimulating intense interest in the synthesis, properties and applications of polyorganosilanes.

I.1.1 Historical

The first compound containing a Si-Si bond, hexaethyldisilane, was prepared by Friedel and Ladenburg in 1869 (2), only six years after the first organosilicon compound, tetraethylsilane, was obtained (3). It was however nearly a century before detailed investigations were undertaken into the properties and chemistry of oligo- and polysilanes(4).

The first organosilane polymers were made by F.S. Kipping and his coworkers in the early 1920's (5,6), from the condensation of diphenyldichlorosilane with sodium, but these highly insoluble and intractable materials were not well characterized and evoked little scientific interest. This reaction was restudied by Gilman and Schwebke in the 1960's. Their results show that Kipping had in fact obtained a number of perphenylcyclosilanes, $(Ph_2Si)_n$, where n = 4, 5 and 6 (7,8). More detailed studies on this reaction have shown that the relative amounts of each ring formed may be controlled by varying the reaction conditions (4). The first clear description of a polysilane was made by Burkhard in 1949 (9). In this paper, the synthesis of both permethylsilane linear polymer $(Me_2Si)_n$ and six-membered ring oligomer $(Me_2Si)_6$ were reported. It was reported that $(Me_2Si)_n$ was a white powder, extremely insoluble in organic solvents, which decomposed without melting when heated above 250°C. Such a completely intractable solid was discouraging. As a result, the chemistry of polysilanes was neglected for many years. However, in 1975 Yajima and Hayashi discovered that polydimethylsilane can be converted in a two-step process to silicon carbide by heating to high temperatures (10,11). This important discovery revived interest in the chemistry of organosilane polymers.

The condensation of dimethyldichlorosilane with alkali metal has been widely studied by West *et al.* (12,13,14) and Nagai *et al.* (15) in the later 1970's and early 1980's. The permethylcyclosilanes are usually obtained from the condensation of Me_2SiCl_2 with Na/K alloy in refluxing THF. The main product is $(Me_2Si)_6$ (85-90%) under standard reaction conditions. Medium and large rings can be obtained by slow addition of the dimethyldichlorosilane to Na/K alloy in refluxing THF. The largest ring isolated so far is $(Me_2Si)_{24}$, but much larger rings, up to $(Me_2Si)_{35}$, have been found in the high-pressure liquid chromatogram of the reaction mixture (16,17). During this period, a number of cyclic polysilanes containing other groups such as Et, *n*-Pr, *n*-Bu, *i*-Pr and *i*-Bu (18-20) have been obtained. In addition, a series of polyspirocyclopolysilanes $((CH_2)_4Si)_n$ where n = 5-12, and $((CH_2)_5Si)_n$ where n = 4-6 have also been prepared (21,22).

Another important advance in polysilane chemistry, made in late 1970's, was the discovery of soluble, high molecular weight polyorganosilanes. In 1980 Wesson and Williams (23) reported the synthesis of soluble random copolymers from the condensation of dimethyldichlorosilane with either ethylmethyldichlorosilane or methyl-*n*-propyldichlorosilane. These copolymers are soluble in common organic solvents, but they were found to have poor film-forming properties and were not extensively studied. Several months later, a number of soluble block copolymers with acceptable film-forming properties were reported by the same authors (24). These block copolymers with number-average molecular weights ranging 5,000 to 10,000 were prepared by the coupling of various α,ω-dichlorosilane oligomers with 1,5-dilithiodecaphenylpentasilane in yield of 30-35%. In 1981 West and coworkers (25-27) reported the preparation of a soluble copolymer from methylphenyldichlorosilane and dimethyldichlosilane. It was found that the introduction of phenyl groups along the chain has a dramatic effect on the nature of the polymer. Crystallinity drops and solubility increases sharply with increasing numbers of phenyl groups. At Me_2Si/PhMeSi ratios near 1:1 the polymer is amorphous, with a softening temperature near 220 °C, and highly soluble in organic solvents at room temperature. The polymer can be cast into transparent films, and melt- or solution-spun into fibers. Samples with number-average molecular weight of 300,000 have been obtained at Me_2Si/PhMeSi ratios near 2:1. At about the same time, Trujillo (28) reported the preparation of a soluble homopolymer from the condensation of methylphenyldichlorosilane with sodium in refluxing dodecane. This material had a broad bimodal molecular weight distribution, and considerable quantities of insoluble material were generated. These pioneering studies suggested that high molecular weight organosilane polymers were not necessarily insoluble, intractable materials, and they stimulated intense interest in the synthesis, characterization and application of polysilane materials.

Since the first reports of soluble organopolysilanes, the synthesis and characterization of a large number of soluble homo- and copolymers have been reported, and properties and applications of these polymers have also been intensely studied (29,30). However, almost all of the polysilanes studied so far are disubstituted organosilane polymers, including homo- and copolymers, prepared by Wurtz-Fittig coupling of suitable diorganodichlorosilanes with molten sodium in hydrocarbon solvents. In the middle of 1980's, Harrod and coworkers (31-34) discovered that monosubstituted organosilane polymers can been obtained from the dehydrocoupling of primary organosilanes catalyzed by dimethyltitanocene and dimethylzirconocene. This discovery opened a new field in the polysilane chemistry. The polymers prepared from primary silanes by this route, containing between 10 and 20 silicon atoms, are soluble in common organic solvents. These polymers have an unusual structure as follows:

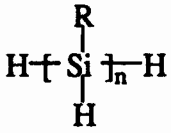

$$H\!-\!\!\left[\begin{array}{c}R\\ |\\ Si\\ |\\ H\end{array}\right]_n\!\!-\!H$$

This kind of polysilane can not be prepared by classical Wurtz-Fittig coupling reactions. In addition to general properties possessed by organosilane polymers, the presence of Si-H along the backbone and at the chain ends offers the opportunity for a wide variety of functionalizations including hydrosilations with olefins and alkynes and reactions with a wide variety of transition metal complexes with formation of metal-Si bonds. These kinds of reactions allow the preparation of a large new range of polymeric materials. Such materials would be expected to exhibit their own interesting physical and chemical properties.

I.1.2 Synthesis

Polysilanes are usually synthesized by Wurtz-Fittig coupling reactions of suitable diorganodichlorosilanes with sodium metal in an inert hydrocarbon solvent at above 100 °C (35-41). Homopolymers can be made from a single dichlorosilane (eq. I-1), while copolymers can be synthesized from mixtures of two or more dichlorosilanes (eq. I-2):

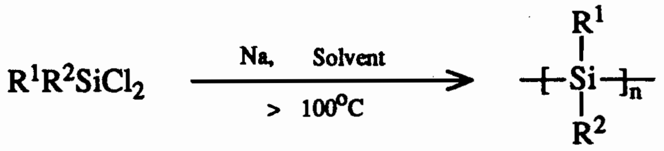

$$R^1R^2SiCl_2 \xrightarrow[>\ 100^{o}C]{Na,\quad Solvent} -\!\left[\overset{\displaystyle R^1}{\underset{\displaystyle R^2}{Si}}\right]_n\!- \qquad (\text{I-1})$$

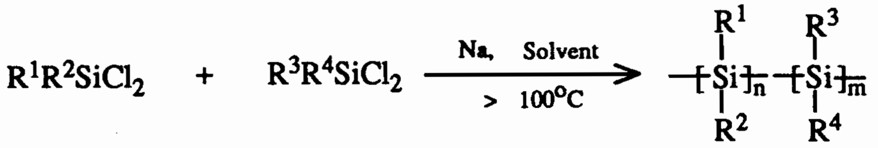

$$R^1R^2SiCl_2 \quad + \quad R^3R^4SiCl_2 \xrightarrow[>\ 100^{o}C]{Na,\quad Solvent} -\!\left[\overset{\displaystyle R^1}{\underset{\displaystyle R^2}{Si}}\right]_n\!-\!\left[\overset{\displaystyle R^3}{\underset{\displaystyle R^4}{Si}}\right]_m \qquad (\text{I-2})$$

Because the groups R^1- R^4 can include a wide variety of aryl and alkyl groups, the number of possible kinds of polysilane polymers is very large. The sodium is normally employed as a dispersion in an inert solvent such as toluene, xylene or a high-boiling alkane. The preformed sodium dispersion can be added to the dichlorosilane dissolved in the reaction solvent at elevated temperature or vice versa. The latter procedure constitutes the normal addition mode , while the former procedure is termed inverse addition. The inverse addition mode generally results in lower yields of higher molecular weight polymer.

Polymers made by Wurtz-Fittig coupling reactions usually have bimodal molecular weight distributions, a low molecular weight polymer ($\overline{M}_n = 10^3$) and a high molecular weight polymer ($\overline{M}_n > 10^5$). Considerable amounts of cyclic and other oligomers are always obtained along with high polymer, so that the yield of high molecular weight polymers is often less than 50%. In general, the polymer yields are strongly affected by the reaction conditions, the solvent and the steric bulk of the substituents (30). For *n*-alkyl substituents, the substituent bulk is approximately cylindrically symmetric and steric interactions can not be alleviated by rotation around the carbon-silicon bond. However, simple aryl substituents are sterically unsymmetrical and the aryl substituents in perarylpolysilane derivatives can minimize substituent interactions by rotation around the carbon-silicon bond.

Recently, a number of low molecular weight ($\overline{M}_w$ = 1,000-1,500) homo- and copolymers containing -SiRH- linkages in the backbone have also been prepared by condensation of phenyldichlorosilane (29,42). The molecular weight of the homopolymer end-capped with diphenylmethylsilyl group is very low ($\overline{M}_w$ = 1,000). These Si-H containing polysilanes are relatively sensitive to air, and also extremely reactive with water and methanol used in the workup. As a result, all of the polymers reported in references 29 and 42 contain considerable Si-O-Si and Si-OH in the polymer chain. So much, in some cases that the products are better described as polysiloxanes.

Although Wurtz-Fittig coupling is highly versatile and can give linear polymers with molecular weights up to ca. 10^6, as mentioned above, it has several difficulties. Among the most serious difficulties are the poor control of structure, molecular weight and polydispersity, the production of low molecular weight cyclics, the low yield of high polymers, the hazards associated with handling hot, molten alkali metals, the limited tolerance of functional groups on the silicon to the reaction conditions, and relatively high cost. Recently, several alternative procedures have been developed.

One of these procedures is ultrasonic activation polymerization (43-46). Matyjaszewski and co-workers (43,44) have shown that the polymerization of methylphenyldichlorosilane yields monomodal high molecular weight polymers ($\overline{M}_w \approx 10^5$) in toluene at ambient temperature with ultrasound. The polydispersity of these polymers can be below $\overline{M}_w/\overline{M}_n < 1.3$. The ultrasonic activation homopolymerization of dichlorosilanes is successful at ambient temperatures in toluene or xylenes only for monomers with aryl substituents. Dialkyldichlorosilanes do not react with sodium dispersion under these conditions, but they can be copolymerized with methylphenyldichlorosilane. It has also been reported that the homopolymerization of dialkyldichlorosilanes can be initiated by adding 25-30% by volume of diglyme into the system (47). The use of the ultrasonic activation technique for the polymerization of alkyltrichlorosilanes with sodium has also been reported recently (45,46). Without ultrasound, the coupling reaction is incomplete and residual silicon-halogen bonds remain. The ultrasound activation technique also suffers from low yields of high polymers and it has been found that high molecular weight polysilanes are rapidly degraded in the presence of ultrasound.

More recently, Sakurai and co-workers (48) reported an entirely novel method of preparing polysilanes based on anionic polymerization of masked disilenes. In this method, a series of 1-phenyl-7,8-disilabicyclo[2.2.2]octa-2,5-dienes (I) were used for anionic polymerization. In principle, the substituents R_1- R_4 can include a wide variety of alkyl or

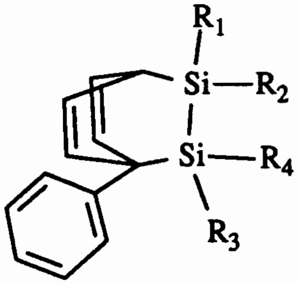

I

aryl groups. However, the number of available monomers is very limited due to the difficulties in preparation. The anionic polymerization was carried out using a break-seal method under high vacuum conditions ($<10^{-5}$mmHg) at or below room temperature. Alkyllithiums such as *n*- and *i*-butyllithium and phenyllithium were used as initiators, ethanol as terminator and THF as solvent (eq. I-3):

$$\mathrm{I} \xrightarrow{\mathrm{RLi,\ THF}} \mathrm{R[SiR_1R_2SiR_3R_4]_nLi} \xrightarrow{\mathrm{EtOH}} \mathrm{R[SiR_1R_2SiR_3R_4]_nH} \qquad (\mathrm{I\text{-}3})$$

The molecular weight distribution of the polymers synthesized by this method ($\overline{M}_n = 10^4$- 10^5, $\overline{M}_w/\overline{M}_n \approx 1.5$) is much narrower than that prepared by the conventional Wurtz-Fittig coupling reaction.

Very recently, Matyjaszewski *et al.* (49) reported a new reaction to prepare high molecular weight polysilanes, the anionic ring-opening polymerization of strained cyclopolysilanes. By this method they have successfully prepared polyphenylmethylsilane ($\overline{M}_n = 30{,}000$, $\overline{M}_w/\overline{M}_n \approx 2$) from 1,2,3,4-tetraphenyl-1,2,3,4-tetramethylcyclotetrasilane with butyllithium or 1,4-dipotassiooctaphenyltetrasilane as initiator. The ring-opening polymerization is an important reaction because cyclopolysilanes are always formed in the Wurtz-Fittig coupling reaction and the catalytic dehydrocoupling reaction. However, the application of the ring-opening polymerization seems to be very limited. So far, only tetraphenyltetramethylcyclotetrasilane has been polymerized to a high molecular weight product by this method.

The catalytic dehydrocoupling of primary organosilanes in the presence of alkyl or hydride derivative of titanocene or zirconocene discovered by Harrod and co-workers (31-34) provides an important synthetic route for linear and cyclic monosubstituent polysilane oligomers. A variety of substituents, including phenyl, tolyl, benzyl, *n*-hexyl, cyclohexyl, *n*-butyl, etc., have been successfully utilized. The oligomers prepared by this route contain 10 - 20 silicon atoms, and are terminated by $SiRH_2$ groups. The dehydrocoupling reaction is highly selective and the steric constraints are significant. Only primary silanes can produce oligomers. Secondary silanes can only produce dimers and trimers. The dehydrocoupling reaction of primary silanes is very easy to control, and the only by-product is hydrogen.

I.1.3 Properties and applications

Polysilane polymers possess some rather remarkable properties. Although they formally resemble polyalkanes, they exhibit physical properties similar to polyenes. All of the polysilanes absorb strongly in the near ultraviolet region, with absorption bands from 300-400 nm, and exhibit a strong delocalization of electrons in the main chain. In addition to special spectroscopic properties they also have excellent photoconductivity and very interesting nonlinear optical properties. These remarkable properties have stimulated intense interest in the polysilane polymers as (i) photoconductors (50,51), (ii) a new class of sensitive radical photoinitiators for olefin polymerizations (52), (iii) radiation sensitive materials for microlithographic applications (53-56) and (iv) nonlinear optical materials (57,58). Another application of polysilanes is as thermal precursors to silicon carbide ceramics (59,60).

Physical properties of the polysilanes depend greatly upon the nature of the organic groups bound to silicon. They can be crystalline or glassy solids, or elastomers depending on the nature of organic side-chain groups. The glass transition temperatures range from -75°C to over +120°C (61). Polysilanes with symmetrical alkyl substituents smaller than propyl are not soluble, probably due to high crystallinity and strong interactions in the solid state. Polymers with longer alkyl substituents are soluble in common organic solvents, but still preserve short distance order above a transition which was first ascribed to true melting (46). Polymers with two different substituents at each silicon atom are atactic and can not form large microcrystalline regions (62). These polymers dissolve easily in some common organic solvents. Lengthening an alkyl chain changes the properties rapidly. $(Me(n\text{-}Pr)Si)_n$ is a soluble glass, and $(Me(n\text{-}Hex)Si)_n$ is an elastomeric material. Aryl groups raise the softening point of the polymer, $(PhMeSi)_n$ is a glassy solid which flows only at temperatures > 200°C. The glass transition temperatures vary correspondingly from > -50°C for elastomeric polysilanes to > 120°C for the aryl compounds.

Light-scattering studies on some high molecular weight polydiorganosilanes indicate that polysilanes form random coils in solution, but they show greater persistence lengths, and hence reduced flexibility, compared to polyolefins. The polysilanes may be "semiflexible" polymers, with properties intermediate between those of rigid rods and highly flexible coils (63).

The spectroscopic properties of soluble, high molecular weight substituted silane polymers are unusual and interesting (64-66). All of these materials absorb strongly in the UV suggesting extensive sigma bond delocalization in the backbone. The position of the absorption maximum and the absorptivity at the absorption maximum are quite dependent upon the polymer chain length and the nature of the organic substituent groups, and also upon solvent and temperature. Increasing chain length results in a marked red-shift of the absorption maximum, finally reaching a constant value in high molecular weight polymers at 300-327 nm for polyorganosilanes containing alkyl substituents and 335-360 nm for polyorganosilanes containing aryl substituents. Aryl substituents directly attached to the backbone result in red-shifts of 20-30 nm. The absorption properties also depend strongly on the conformation (47,67-71) of the polysilane backbone. It has been suggested that the trans coplanar arrangement absorbs at longer wavelengths than any nonplanar conformations. The thermochromism of polysilanes, due to temperature dependent conformational changes along the backbone, has been observed both in solution and solid films. The position of the absorption maximum shifts gradually and reversibly to longer wavelength as the temperature is lowered due to the increase in the proportion of the trans conformations.

The unusual absorption spectra of the polysilanes suggest potentially interesting electroconducting and photoconducting characteristics. The preparation of some electrically conductive polysilanes by doping has been reported (72). Conducting films have recently been prepared from a variety of polysilanes by heating to high temperatures in sulfuric acid

(73). The photoconducting (51,74) and charge-transporting (50,75) characteristics of a variety of polysilane derivatives has also been studied, and these polysilane derivatives were found to be excellent photoconductors.

Polysilane derivatives are sensitive to light and various types of radiation. Irradiation either in solution, or in the solid state, results in strong spectral bleaching at the original absorption maximum. This phenomenon is associated with photodegradation of the polysilane (29,64,76). Chain scission is usually the main photochemical processes for alkylpolysilanes, but photocrosslinking becomes more competive for arylpolysilanes. It was found that the major products in the photolysis of alkylpolysilanes are silylenes and silyl radicals. This finding suggests that there are at least two primary steps, simple scission to silyl radicals (eq. I-4) and elimination of silylenes, R_2Si (eq. I-5):

$$-SiR^1R^2\text{-}SiR^1R^2- \xrightarrow{h\nu} 2\ -R^1R^2Si\cdot \qquad (\text{I-4})$$

$$-SiR^1R^2\text{-}SiR^1R^2\text{-}SiR^1R^2- \xrightarrow{h\nu} R^1R^2Si: \ + \ 2\ -R^1R^2Si\cdot \qquad (\text{I-5})$$

Photochemical crosslinking of any polysilane can be carried out if the polymer is mixed with a multiply-unsaturated compound such as phenyl trivinylsilane, via radical addition to the carbon-carbon double bonds of the additive (77).

The photochemical reactions of polysilanes suggested the possible utility of polysilane polymers as photoinitiators for vinyl-type polymerization. West and co-workers (52,78,79) have demonstrated that a variety of vinyl monomers can be polymerized when certain polysilanes are incorporated as photoinitiators.

Polysilane derivatives have a number of unique characteristics that make them suitable for many potential lithographic applications (80). In this regard, the polysilanes are (i) thermally and oxidatively stable yet photochemically labile; (ii) strongly absorbing over a broad spectral range yet photobleachable, allowing uniform irradiation throughout the entire sample; (iii) good film formers which are compatible with most common polymers; (iv) high in silicon content and therefore resistant to oxygen etching in plasma environments. Recently, a large number of studies on the use of polysilanes in bi- or multilayer lithographic processes have been reported (30). Polysilane derivatives have been successfully utilized as (i) soluble O_2-etch barrier alternatives in trilayer lithographic processes, (ii) combination imaging and oxygen-etch-resistant barrier layers in bilayer lithographic processes, (iii) short-wavelength contrast-enhancing layers, and (iv) new resist materials for ionizing radiation.

The use of polysilanes for the generation of β-silicon carbide fibers was first described by Yajima *et al.* (10,11) in a two-step thermal conversion process starting with polydimethylsilane. Heating the polymer converted it to a polycarbosilane, a polymer with alternating Si and C atoms in the backbone. The polycarbosilane was fractionated and spun into fibers, which were oxidized on the surface to make them rigid, and then pyrolyzed above 800°C to amorphous silicon carbide. As the temperature was raised to 1300°C, crystals of β-silicon carbide formed in the fibers (eq. I-6):

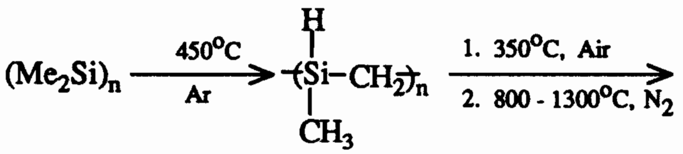

$$(Me_2Si)_n \xrightarrow[Ar]{450^oC} \left(\overset{\overset{H}{|}}{\underset{\underset{CH_3}{|}}{Si}}-CH_2\right)_n \xrightarrow[2.\ 800-1300^oC,\ N_2]{1.\ 350^oC,\ Air} \beta\text{-}SiC + CH_4 + H_2 \qquad (\text{I-6})$$

More recently developed formable polysilanes can also be transformed into silicon carbide, and it is not necessary to preform the polycarbosilane. The polysilane itself can be drawn into fibers, crosslinked and then fired directly to form silicon carbide (36).

I.2 CATALYTIC DEHYDROCOUPLING OF HYDROSILANES

Catalytic dehydrocoupling reactions of hydrosilanes could provide important routes to produce Si-Si bonded species which could be small molecules, oligomers, or polymers depending on the nature of the starting material and the employed approach (eq. I-7).

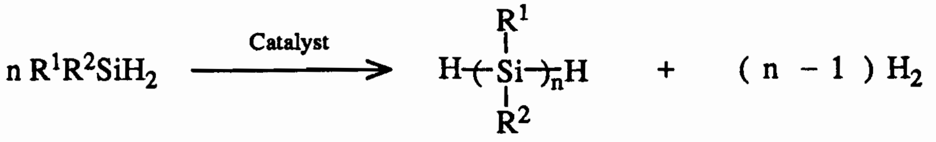

$$n\,R^1R^2SiH_2 \xrightarrow{\text{Catalyst}} H\!\left(\overset{R^1}{\underset{R^2}{Si}}\right)_{n}\!H \quad + \quad (n-1)\,H_2 \qquad (\text{I-7})$$

Where R^1 could be alkyl or aryl and R^2 could be alkyl, aryl, or H. This type of reaction could have a number of advantages such as providing a clean route to polysilanes with hydrogen gas as the only side-product, allowing control of chain length, molecular weight distribution, tacticity and yield etc. To date, a number of transition-metal complexes have been reported to catalyze the dehydrocoupling reaction of the hydrosilanes. These include some late transition-metal complexes such as rhodium, palladium, and platinum complexes, and some early transition-metal complexes such as titanium, zirconium, hafnium, vanadium complexes etc.

The catalytic dehydrocoupling of hydrosilanes in the presence of transition metal catalyst was first reported by Ojima and coworkers (81) in 1973. They obtained 14% of 1,2-dimethyl-1,2-diphenyldisilane, 30% of 1,2,3-trimethyl-1,2,3-triphenyltrisilane, 30% of diphenylmethylsilane and trace of triphenylmethylsilane by heating phenylmethylsilane in the presence of 0.1 mole% of Wilkinson's catalyst, $(Ph_3P)_3RhCl$, at 70^0C for one hour. Similar treatment of diphenylsilane at 80^0C gave 45% of the unchanged starting material, 38% of 1,1,2,2-tetraphenyldisilane, 8% of triphenylsilane and trace of phenylsilane and tetraphenylsilane. Similarly, phenylsilane and diethylsilane gave dimer, trimer, disproportionation products and some higher polymers. Similar results have also been obtained (82) by using a carbenerhodium(I) complex, cis-$[RhCl(COD)L^{Me}]$ (COD = cycloocta-1,5-diene, L^{Me}= :$\overline{CN(Me)(CH_2)_2N}Me$) or trans-$[RhCl(PPh_3)_2L^{Me}]$ as catalyst. In addition to disproportionation, oxidation of silicon-silicon bonds to siloxanes in the presence of these rhodium catalysts was found to be a problem. Recently, a number of other late transition metal complexes have also been examined as dehydrocoupling catalysts (83), including $(Ph_3P)_2Pt(C_2H_4)$, H_2PtCl_6, $(Ph_3P)_2PtCl_2$, $Pt(COD)Cl_2$, $[Rh(CO)_2Cl]_2$, $CpRh(C_2H_4)_2$, $RhCl_3$, $[Rh(COD)Cl]_2$, $[Ir(COD)Cl]_2$, and $[Pd(allyl)Cl]_2$. Some of these compounds did catalyze the dehydrocoupling reaction, but they show much lower catalytic activity than Wilkinson's catalyst, and disproportionation was the predominant reaction in some cases. For example, 27% of 1,2-dimethyl-1,2-diphenyldisilane and 52% of diphenylmethylsilane were obtained from the reaction of phenylmethylsilane in the presence of catalytic amounts of $(Ph_3P)_2Pt(C_2H_4)$ at room temperature for 75 hours.

Very recently, Corey and coworkers (84,85) reported reactions of secondary silanes, of the type shown below, in the presence of Wilkinson's catalyst. Reaction of II in toluene with Wilkinson's catalyst in the absence of air gave disilane and trisilane in varying ratios depending on a number of factors which include concentration, catalyst/silane ratio, temperature and reaction time. Higher temperature (85°C) and longer reaction time (96 h) favored the formation of trisilane. Disiloxane and trisiloxane were also produced in some cases. The trimer can be formed from II due to smaller steric bulk of this compound than that of Ph_2SiH_2. The major product from the reaction of the silepin III is disilane even at the higher temperature that favored trisilane formation from II. The reaction of III requires higher Rh/silane ratios and higher concentrations of silane. Good results (>50% dimer) were obtained by running reactions with neat silane under vacuum at higher temperatures (85°C). Dihydrosilafluorene IV reacted rapidly with Wilkinson's catalyst accompanied by evolution of hydrogen and gave an insoluble precipitate within 30min. The insoluble precipitate

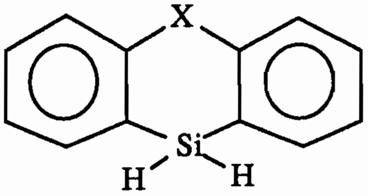

II X = CH_2
III X = CH_2CH_2
IV X = a bond

which was not well characterized perhaps is a cross-linked polymer produced by both the dehydrocoupling of the Si-H bond and the disproportionation of the Si-C bond, although the authors did not mention this possibility.

Although there is little substantive detail concerning reaction mechanism and conditions for dehydrogenative coupling of hydrosilanes in the presence of these late transition metal compounds, some generalizations can still be drawn from these reports: Dimers and trimers can be formed from primary silanes and a number of secondary silanes, but disproportionation reactions compete with the dehydrogenative coupling reaction. The dehydrocoupling reaction is sensitive to the size of substituents on the silicon since trisilane can be formed as one of the products from $PhMeSiH_2$ or **II** but disilane is the only coupling product from Ph_2SiH_2 or **III**. In the presence of air and water some catalysts promote the conversion of silicon-silicon bonds to siloxanes. Generally, tertiary silanes do not form silicon-silicon bonded products but a recent report described the dehydrocoupling of $PhMe_2SiH$ to dimer with platinum catalysts (86).

Recently, Harrod and coworkers (31-34,87-90) have discovered a class of more promising catalysts --titanocene and zirconocene derivatives Cp_2MR_2 (M = Ti or Zr; R = methyl or H), which catalyze the dehydrocoupling of primary silanes to polysilanes. Polymerization reactions of a number of primary silanes, $RSiH_3$, (R = phenyl, benzyl, *n*-hexyl, and *p*-tolyl) in the presence of these catalysts have been studied and it was found that these reactions produce mixtures of linear and cyclic oligomers. With titanocene-based catalysts the average degree of polymerization is about 10 and does not vary very much with the R group on silicon or experimental conditions. Zirconocene-based catalysts are more active, and can give higher molecular weight polysilanes with an average degree of polymerization of ca. 20.

A number of metallocene derivatives of early transition metals and actinides have been studied for catalytic activity for the polymerization of primary silanes. The results of these studies indicated that both steric effects and electronic effects of ligands and central metal on the catalytic activity are very important. Diphenyltitanocene is too stable and shows no catalytic activity at ambient temperature (31), but it can catalyze the polymerization of phenylsilane at elevated temperature (110°C) (91). Dimethylbis-(methylcyclopentadienyl)- titanium and -zirconium both have similar catalytic activities to the cyclopentadienyl analogues and give polysilanes with the same degree of polymerization. The mixed cyclopentadienyl-pentamethylcyclopentadienyl (CpCp*) complexes are also active, although the reactions are much slower, but the bis Cp* complexes are not (90). However, $Cp^*_2HfH_2$ catalyzes a slow stepwise oligomerization of phenylsilane (92) although Cp_2HfMe_2 shows no catalytic activity, probably due to the failure of the starting complex to be transformed into an active species. $Cp^*_2ThMe_2$ and $Cp^*_2UMe_2$ are also catalytically active, the former for the dimerization of primary silanes and the latter for their oligomerization (34). Bis(indenyl)dimethyltitanium catalyzes the slow oligomerization of phenylsilane to dimer and trimer at room temperature while the bis(indenyl)zirconium analogue is active as a polymerization catalyst, giving essentially the same product as the bis(cyclopentadienyl) complex (34).

Trialkyl(cyclopentadienyl)titanium and zirconium complexes show no evident catalytic activity for the polymerization of phenylsilane at ambient temperature (90). It is thus clear that the catalytic activity is strongly dependent on electronic factors. None of the metallocenes, metallocene alkyls, metallocene hydrides of groups 5 and 6 have shown any measurable activity for polymerization under ambient conditions, although vanadocene catalyzes the slow stepwise oligomerization of phenylsilane in refluxing toluene. The nonreactivity of groups 5 and 6 metallocene derivatives points to a unique electronic feature of the group 4 compounds and extremely severe constraint on the catalytic activity of compounds for the dehydrocoupling reaction.

These dehydrocoupling reactions catalyzed by early transition metal complexes are more selective than those based on late transition metal catalysts, since no side products from redistribution are formed. These catalytic reactions are quite sensitive to the steric bulk of silanes, so that primary silanes and secondary silanes react but tertiary silanes do not. Primary silanes can react to give polysilanes, but secondary silanes usually give only dimer and trimer as products (31,32,34,85,89,91). Although Corey *et al.* have recently reported that the special type secondary silane IV (dihydrosilafluorene) can be oligomerized by titanocene catalyst, the product obtained from their reaction is insoluble in all solvents and can not be well characterized (85). The tertiary hydrogens of the polysilane backbone show no detectable further reactivity under polymerization conditions, since no branched or cross-linked polysilanes have been obtained so far from the dehydrocoupling reaction.

The dehydrocoupling reactions of germanes are very different from those of silanes probably due to the slightly larger atomic radius of germanium and the weaker Ge-H bond. Phenylgermane is rapidly polymerized to a three dimensional gel and diphenylgermane undergoes a rapid stepwise oligomerization to give dimer, trimer, and higher oligomers in the presence of catalytic amounts of dimethyltitanocene (89).

In many cases, it was found that the dehydrocoupling reaction takes place in a stepwise fashion. For example, when a more steric bulky complex such as Ind_2TiMe_2 or $Cp^*_2HfH_2$ was used as catalyst, or a less reactive silane such as $BuSiH_3$ (93) was used as substrate, a slow stepwise oligomerization was observed. However, for the polymerization reactions of phenylsilane and a number of other primary silanes in the presence of titanocene and zirconocene derivatives, no dimer, trimer etc. low molecular weight oligomers have been observed upon following the reactions by NMR. It was believed that these observed differences in reaction behavior probably represent two mechanistically distinct processes, and a mechanism for the polymerization reaction of primary silanes (34,89) involving a rapid repetitive addition of monosilane to a silylenetitanium intermediate, produced by α-hydride elimination from hydridosilyltitanium(IV) species, has

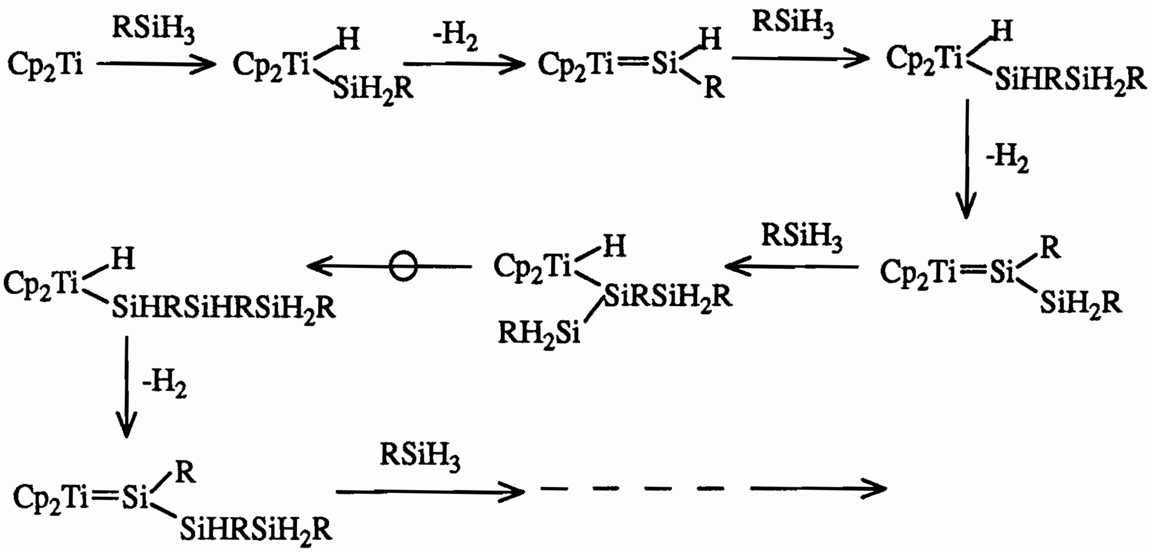

Scheme I-1. Mechanism for $RSiH_3$ polymerization proposed by Harrod et al. (34,89).

been suggested (Scheme I-1). Although this mechanism was proposed based on the titanocene catalyzed silane dehydrocoupling reaction, it was believed that the zirconocene catalyzed silane dehydrocoupling reaction might occur by the same route as shown in Scheme 1, since most of the observed behaviors for both catalytic systems are similar to each other. According to such a mechanism, most of the observed features of the dehydrocoupling reaction of primary silanes can be explained on the condition of supposing that intermediate products can not be liberated. On considering that intermediate products might be liberated from the metal center in some cases, such a silylene-based mechanism can also be used to explain the stepwise silane dehydrocoupling reaction (93). However, this type of mechanism is difficult to test in the absence of any evidence for the existence of early transition metal silylene complexes in these systems.

Very recently, Tilley and Woo (92) proposed a σ-bond metathesis mechanism for the silane dehydrogenative coupling reaction by zirconocene and hafnocene catalysts (Scheme I-2), which involves some σ-bond metathesis processes of M-H and M-Si bonds with Si-H,

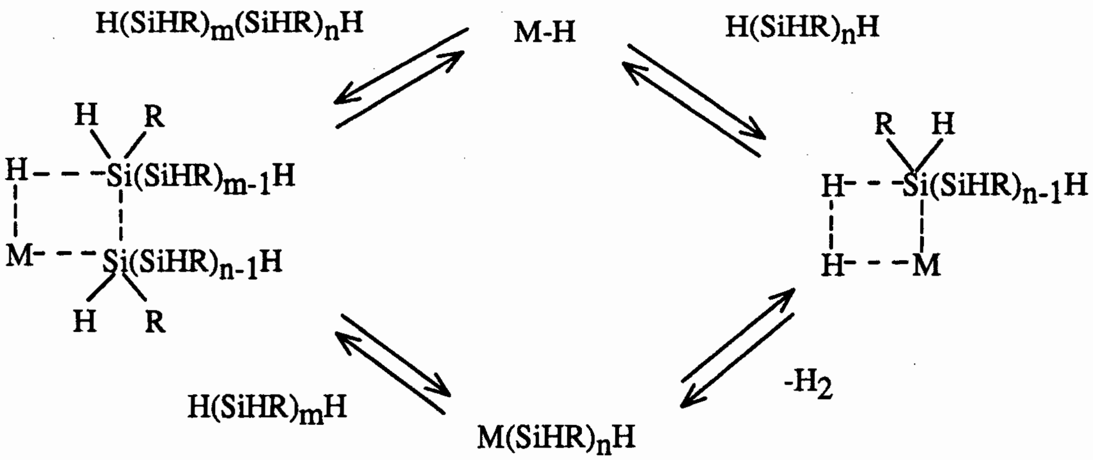

Scheme I-2. Tilley's mechanism for dehydrogenative silane polymerization by zirconocene and hafnocene catalysts (92).

Si-Si and H-H bonds, observed in the course of their studies of silyl derivatives of zirconocene and hafnocene chloride $CpCp^*M(SiR_3)Cl$ (M = Zr, Hf; R = Me, Ph, $SiMe_3$) as catalysts (94). Tilley's mechanism is appealingly simple and can explain most of their experimental observations. However, it seems that further evidence is necessary to confirm such a mechanism. The dehydrocoupling reaction of $PhSiH_3$ in the presence of the chloride derivatives of zirconocene and hafnocene is so slow that they did not obtain enough oligosilanes from this kind of reaction to carry out molecular weight measurements (94). For instance, the catalytic dehydrocoupling reaction of $PhSiH_3$ to disilane and trisilane in the presence of $CpCp^*Hf(SiH_2Ph)Cl$ (50 mol%) only gave a conversion of 33% after 24 hours (92). Such a conversion can be achieved within a few minutes with 1 mol% dimethyl-titanocene or -zirconocene as catalyst. Tilley *et al.* have also found that the dehydrocoupling of phenylsilane is violent at room temperature with $CpCp^*Zr[Si(SiMe_3)_3]Me$ as catalyst (95). It is difficult to ascertain, because of their slowness, that the dehydrocoupling reactions of phenylsilane in the presence of the chloride derivatives of zirconocene and hafnocene are really due to the chloride derivatives themselves, while the direct involvment of these chloride derivatives in the catalytic cycle is the basis of the σ-bond metathesis mechanism. It is also possible that these slow dehydrocoupling reactions are catalyzed by a small amount of chlorine-free metallocenes, produced from the redistribution of chloride derivatives, given the very high concentration of chloride derivatives is employed in the reactions. The production of Cp_2ZrCl_2 and chlorine-free zirconocene derivatives by the redistribution reaction in alkyl and hydridozirconocene chloride systems has been reported (96-98).

In summary, although some σ-bond metathesis reactions have been observed, the most important evidence to support the σ-bond metathesis mechanism seems to be still in question. It is thus obvious that still further experimental observations are necessary to understand the polymerization mechanism.

I.3 INTRODUCTION TO SOME ASPECTS OF THE CHEMISTRY OF BIS(CYCLOPENTADIENYL)TITANIUM/ZIRCONIUM AND THEIR DERIVATIVES

Organometallic compounds of the group 4 metals could not be isolated until good inert atmosphere techniques were developed in the early 1950's, due to their high sensitivity to air, moisture and other hydroxylic species. The first organotitanium compound, $TiPh(O\text{-}i\text{-}Pr)_3$, was isolated in 1952 (99). Since that time, the organometallic chemistry of the group 4 metals has been developed rapidly due in large part to the discovery of the catalytic role played by titanium halides with aluminium alkyls in the polymerization of ethene (100), together with the discovery of ferrocene (101,102). The discovery of ferrocene and its sandwich structure (103,104) stimulated research interest in this kind of sandwich transition metal compounds. As a result many bis(cyclopentadienyl) complexes of the first row transition metals have been prepared. The first bis(cyclopentadienyl) compounds of titanium and zirconium, Cp_2TiBr_2 and Cp_2ZrBr_2, were reported in 1953 by Wilkinson *et al.*

(105). By far the majority of the organometallic compounds of titanium and zirconium contain the cyclopentadienyl anion ligand bonded in the pentahapto fashion (η^5-C_5H_5). The unique stabilizing influence of this ligand allows the isolation of many organometallic compounds.

The most common oxidation state for group 4 metallocene derivatives is +4. This is the maximum that can be observed for the group, giving a d^0 configuration. A major difference between the first member Ti and subsequent members Zr and Hf of the group is the relative accessibility of lower oxidation states (106). Thus Ti(IV) reduces much more easily than Zr(IV) and Hf(IV). In addition, Zr(III) complexes tend to be more kinetically labile than their Ti(III) analogues. As a result, Zr(III) metallocene derivatives are not common, and Hf(III) compounds even less so. In a recent report, it has been shown that the elusiveness of Cp_2ZrX (X = Cl, I) species is due to the ease of their disproportionation to Cp_2ZrX_2 and "Cp_2Zr" (107).

I.3.1 Structure and bonding of bis(cyclopentadienyl)transition metal complexes

Normal bis(cyclopentadienyl) transition metal complexes such as ferrocene are highly symmetric molecules with two parallel cyclopentadienyl rings. Their symmetry is D_{5h} if the two rings are eclipsed, or D_{5d} if the rings are staggered. In bent bis(cyclopentadienyl) transition metal complexes the rings are not parallel, that is the angle (θ) between the normals from the metal to the planes of the cyclopentadienyl ligands is less than 180°, and there are from one to three additional ligands bound to the metal. A bent Cp_2M fragment has C_{2v} symmetry, and only C_s symmetry if the rings are staggered.

The electronic structure of the bis(cyclopentadienyl)transition metal complexes has been studied in detail by Hoffmann *et al.* (108) and Ballhausen *et al.* (109). The bonding in a normal metallocene Cp_2M in D_{5d} symmetry can be described as follows: the π orbitals of two parallel $C_5H_5^-$ ligands yield three sets of approximately degenerate orbitals: a low-lying

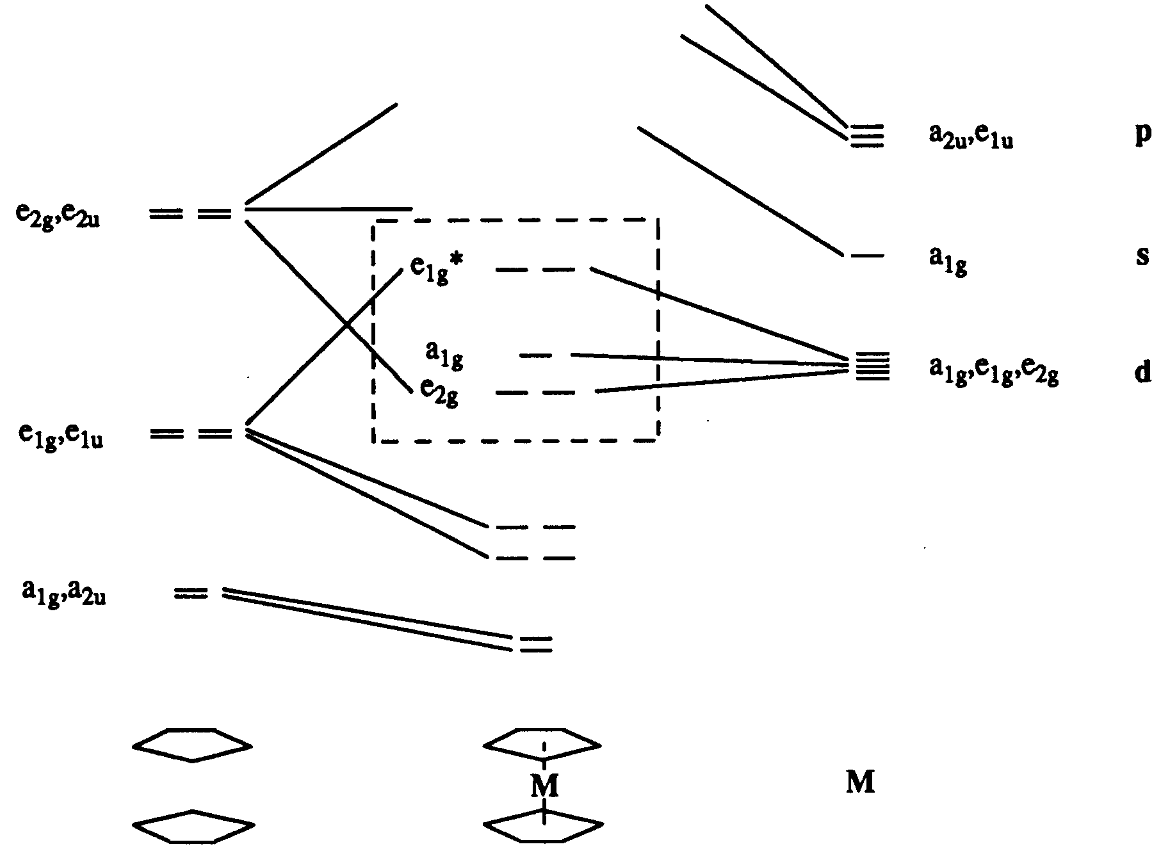

Fig. I-1. Interaction diagram for a D_{5d} metallocene. The frontier orbitals are in the box (as shown in reference 108).

filled pair of a_{1g} and a_{2u} symmetry, a set of filled orbitals, e_{1g} and e_{1u}, and a high-lying empty set of antibonding orbitals of symmetry e_{2g} and e_{2u}. These orbitals interact with the orbitals of the metal as shown in Figure I-1. There is a strong interaction with the metal s and p orbitals and also a strong bonding interaction with the e_{1g} (d_{xz}, d_{yz}) set. The remaining three d orbitals of the metal, the a_{1g} (d_{z^2}) and the e_{2g} ($d_{x^2-y^2}$, d_{xy}) set, remain essentially nonbonding. Thus the d-level splitting is $e_{2g} \leq a_{1g} < e_{1g}^*$. The three nonbonding frontier orbitals play a prime role in bonding further ligands.

Ferrocene has the ideal number of electrons for Cp_2M complexes. Considering each

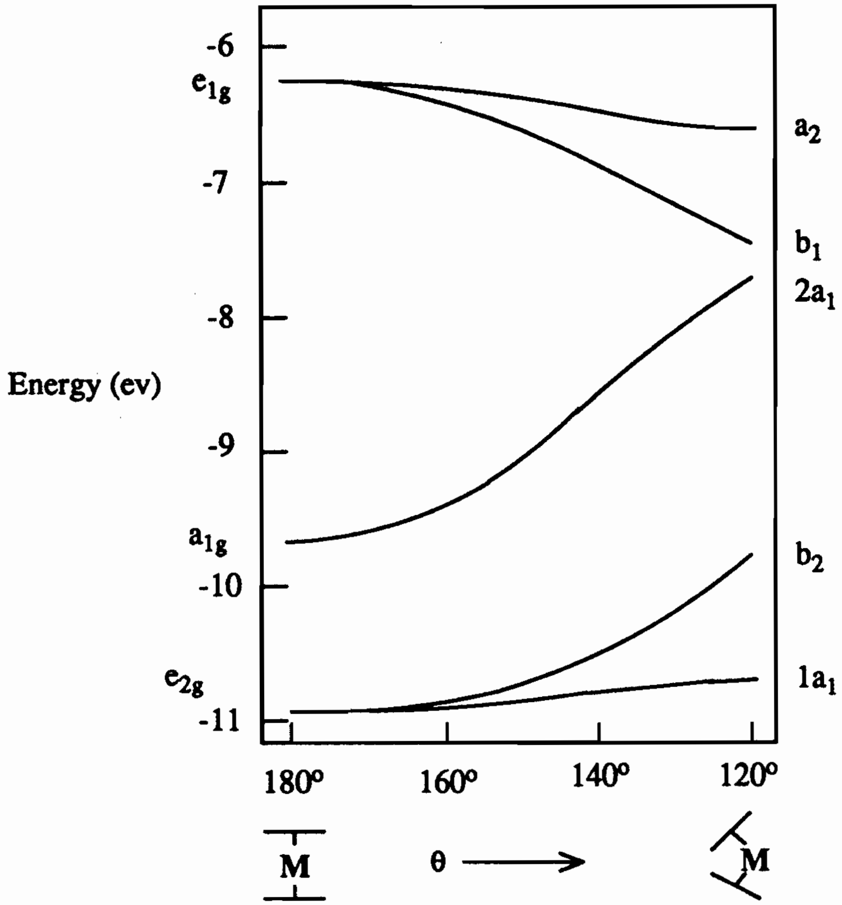

Fig. I-2. Cp_2M orbitals as a function of the bending angle θ in D_{5d} geometry (as shown in reference 108).

$C_5H_5^-$ ligand as a six-electron donor, together with the six d electrons of Fe(II), one achieves an 18-electron configuration by filling precisely the nonbonding e_{2g} and a_{1g} levels. It is therefore the most stable of the metallocenes. Cobaltocene (d^7- 19 electrons) and nickelocene (d^8- 20 electrons) which have an excess number of electrons in the high-lying e_{1g}* orbitals are less stable and are easily oxidized. On the other hand, titanocene and zirconocene (d^2- 14 electrons) are highly electron deficient, having fewer than 6 d electrons. These two compounds are paramagnetic if they exist as monomeric Cp_2M with two unpaired electrons in e_{2g} orbitals. In fact, $[C_5(CH_3)_5]_2Ti(II)$ has an effective magnetic moment of 2.60 BM at 298°K (110), which is in reasonable agreement with a spin-only magnetic moment of 2.84 BM expected for a monomeric Ti(II) species with two unpaired electrons. To achieve the desired 18-electron configuration, the electron-deficient complexes acquire additional ligands which can contribute electrons. This addition of the additional ligands leads to bending back of the two $C_5H_5^-$ ligands, and thus results in the change of symmetry from D_{5h} or D_{5d} to C_{2v} or C_s. This is accompanied by a transformation of the nonbonding orbitals from e_{2g} and a_{1g} to $1a_1$, b_2 and $2a_1$ as shown in Figure I-2. The interaction of the three low-lying frontier orbitals of the bent Cp_2M fragment with two σ-donor ligand orbitals in complexes of the type Cp_2MX_2 (where the X can be a variety of ligands), together with the shapes of these frontier orbitals and the associated coordinate system are shown in Figure I-3. With the new ordering of these orbitals, the d^2 complexes of this type are predicted to have their $1a_1$ filled hence they are expected to be diamagnetic.

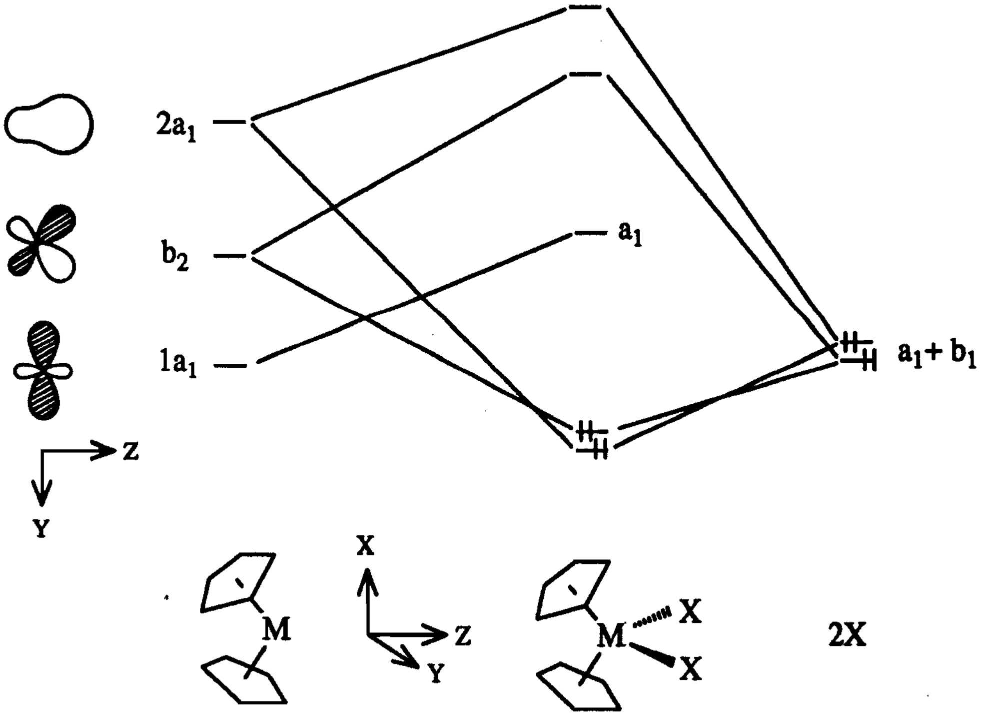

Fig. I-3. Interaction diagram for Cp_2MX_2 (as shown in reference 108).

The d^1 complexes will have one unpaired electron in the $1a_1$ orbital and hence be paramagnetic, while the d^0 complexes will be diamagnetic.

I.3.2 Bis(cyclopentadienyl)titanium and zirconium alkyl complexes

Bis(cyclopentadienyl)titanium and -zirconium alkyl complexes usually possess general formula Cp_2MR_2 where M = Ti, Zr and R = alkyl, with the metal being in the +4 oxidation state. The first complex of this type, Cp_2TiMe_2, was prepared in 1956 (111). Initially it was obtained in low yield from the reaction of MeMgI with Cp_2TiCl_2 in THF. Subsequent workers obtained higher yields using MeLi as a alkylating agent and this method is now preferred (112). It was however 15 years or so before the analogous complex Cp_2ZrMe_2 was first isolated, from the reaction of MeLi with Cp_2ZrCl_2 (113,114). This is likely due to the extreme sensitivity of dimethylzirconocene toward moisture and other hydroxylic compounds. A number of other complexes of this type have also been isolated for both titanium and zirconium (115-123). The general preparative routes are as outlined above for the dimethyl complexes.

A number of lower oxidation state Cp_2TiR derivatives with large sterically hindered alkyl groups have also been prepared (124-126). Examples of complexes of this type isolated include Cp_2TiBz, and $Cp_2TiCH_2C(CH_3)_3$. The large size of the alkyl groups was found to preclude dimerization. To date, it seems that no neutral complex of the type Cp_2ZrR has been reported. The only alkyl zirconocene(III) compounds to have been isolated in the solid state are some dinitrogen complexes, *e.g.*, $(C_5H_4R)_2Zr(\eta^2\text{-}N_2)CH(SiMe_3)_2$ (127). Several phosphine complexes, *e.g.*, $Cp_2ZrBu(PPh_2Me)$ (128) and $Cp_2Zr(CH(SiMe_3)C_6H_4Me\text{-}o)(PMe_3)$ (129) have also been reported, but none of these compounds has been isolated and the only evidence for their existence was the observation of EPR signals during reaction. Another interesting compound reported recently is a diamagnetic methylzirconocene complex which was characterized as the dimer $[Cp_2ZrMe]_2$ with a Zr-Zr bond (130). This complex was not isolated as a solid, but only obtained as a red oil.

The most widely studied compounds to date remain dimethyltitanocene and -zirconocene. A number of thermolysis and photolysis studies have been undertaken, primarily to determine the decomposition pathways of these two complexes. In particular, Cp_2TiMe_2 is very heat and light sensitive, decomposing in a spectacular autocatalytic manner, unless stored at low temperature and in the dark. The thermal decomposition of Cp_2TiMe_2 has been studied in the solid state and in a number of solvents (131,132). In all cases methane was the predominant product, together with trace amounts of ethane. Deuterium labelling studies showed that the methane resulted from hydrogen abstraction from either the cyclopentadienyl rings or from the methyl groups themselves, and from the solvent in the case of diethyl ether. At temperatures greater than 100°C solid state decomposition was found to give rise to ethene, cyclopentadiene and methylcyclopentadiene, in addition to methane and ethane (131). Labelling studies showed that the ethene arose exclusively from decomposition of the cyclopentadienyl ligands and that the methylcyclopentadiene was produced by a simple combination of methyl and cyclopentadienyl groups.

Cp_2ZrMe_2 is much more thermally stable than Cp_2TiMe_2 and does not decompose in an autocatalytic manner. In the solid state, thermal decomposition of dimethylzirconocene at 230°C has been shown to produce methane and cyclopentadiene together with very small amounts of methylcyclopentadiene (131).

Bamford *et al.* studied the photolysis of Cp_2TiMe_2 and reported that Cp_2TiMe_2-d_6 in toluene-d_8 gave only CD_3H with no CD_4 (133). This suggests that hydrogen abstraction occurs exclusively from the cyclopentadienyl rings and precludes involvement by both the solvent and the other methyl group. Free methyl radicals were not thought to exist.

Photolysis studies on Cp_2ZrMe_2 have shown the products to be methane and "zirconocene", the former being produced from hydrogen abstraction from the cyclopentadienyl rings (134). An EPR study detected the presence of an unidentified zirconium(III) hydride during the photolysis of Cp_2ZrMe_2 in toluene solution (135).

The chemical reactivity of dimethyltitanocene and -zirconocene toward H_2, silanes, or donor ligands has also been widely studied. Under certain circumstances, they could readily lose their methyl ligands to become an *in situ* source of the corresponding metallocenes. these *in situ* metallocenes are very reactive intermediates for some reactions (136,137), and very effective catalysts for the hydrogenation of olefins (138,139), the polymerization of organosilanes (34,89), and the polymerization of acetylene (140,141).

The reaction between solid crystalline dimethyltitanocene and hydrogen gas was reported to yield a violet titanocene hydride compound $[Cp_2TiH]_2$ (eq I-8) (142), while the same reaction, between dimethyltitanocene and hydrogen gas, led to the dark green compound $[CpTiH]_2[C_{10}H_8]$, if carried out in hydrocarbon solvents (eq. I-9) (112).

$$2\,Cp_2Ti(CH_3)_2 \quad + \quad 3\,H_2 \longrightarrow [Cp_2TiH]_2 \quad + \quad 4\,CH_4 \qquad (\text{I-8})$$

$$2\,Cp_2Ti(CH_3)_2 \quad + \quad 2\,H_2 \xrightarrow[\text{as solvent}]{C_6H_{14}} [CpTiH]_2[C_{10}H_8] \quad + \quad 4\,CH_4 \qquad (\text{I-9})$$

In both cases, an incubation period from several to tens of minutes was observed. The reaction began at a point and spread rapidly throughout the system after the incubation.

It seemed reasonable to expect the analogous reaction, between $[C_5(CH_3)_5]_2Ti(CH_3)_2$ and H_2, to lead to $Cp^*_2Ti(II)$, with the evolution of 2 mol of methane. However, $[C_5(CH_3)_5]_2Ti(CH_3)_2$ was found to show little or no reactivity toward hydrogen gas even when exposed to 100 atm of H_2 (143). A reaction, however, did take place with evolution of the stoichiometric 2 mol of CH_4 in the presence of small amounts of $[C_5(CH_3)_5][C_5(CH_3)_4CH_2]TiCH_3$, which readily reacts with H_2 to yield $[C_5(CH_3)_5]_2Ti(II)$, via a hydride complex (eq. I-10).

$$[C_5(CH_3)_5][C_5(CH_3)_4CH_2]TiCH_3 \quad + \quad H_2 \longrightarrow [C_5(CH_3)_5]_2Ti \quad + \quad CH_4 \qquad (I\text{-}10)$$

It seems clear that $Cp^*{}_2Ti(II)$ is an important initiator and intermediate in the reaction of $Cp^*{}_2TiMe_2$ with H_2. The low reactivity of $Cp^*{}_2TiMe_2$ toward hydrogen is presumably due to its greater thermal stability compared to that of the unsubstituted Cp_2TiMe_2. Cp_2TiMe_2 decomposes at room temperature in the course of several minutes, whereas $Cp^*{}_2TiMe_2$ can be stored at room temperature for days without decomposition and is stable in solution to 90°C. This leads to the difficulty of the production of the initial $Cp^*{}_2Ti(II)$ and thus to the low reactivity.

The reaction of Cp_2ZrMe_2 with H_2 was reported to yield a white insoluble (polymeric or dimeric) dihydride compound at elevated H_2 pressure (60 atm) and temperature (80°C) (144,145). Under 1 atm of H_2 pressure and at room temperature, however, the reaction proceeded slowly to yield white, insoluble $[Cp_2Zr(CH_3)(\mu\text{-}H)]_2$ (38%, 5 days) and CH_4 (146). Unreacted Cp_2ZrMe_2 was found to be the only other Zr compound in the solution at the end of the reaction. The lower reactivity of Cp_2ZrMe_2 toward hydrogen is probably related to the insolubility of the reaction products. As discussed above for the titanium case, the formation of $Cp_2Zr(II)$ in the reaction solution might also be important to promote the hydrogenolysis of Cp_2ZrMe_2. In fact, $Cp^*{}_2ZrMe_2$ can react with H_2 (50-100 atm) at room temperature to give a quantitative yield of pure soluble $Cp^*{}_2ZrH_2$(147).

The reaction of Cp_2TiMe_2 with a primary silane (such as phenylsilane, benzylsilane, hexylsilane etc.) is very similar to that with H_2. After an induction period, generally lasting from a few seconds to a few minutes, the reaction occurred suddenly and proceeded rapidly to give methane, methylated silane $MeRSiH_2$, and a dimeric titanocene silyl complex

$(Cp_2Ti)_2(\mu\text{-}H)(\mu\text{-}HSiRH)$ (<u>V</u>) as products (148). Although the detailed mechanism is not clear at present, the reaction can be expressed as follows:

$$Cp_2TiMe_2 + RSiH_3 \longrightarrow CH_4 + MeRSiH_2 + Cp_2Ti \qquad (I\text{-}11)$$

$$2\,Cp_2Ti + RSiH_3 \rightleftharpoons \underset{\underline{\mathbf{V}}}{Cp_2Ti(\mu\text{-}H)(\mu\text{-}HSiRH)TiCp_2} \qquad (I\text{-}12)$$

The reactivity of Cp_2ZrMe_2 toward primary silanes is lower than that of Cp_2TiMe_2. The spectacular sudden colour change observed in the titanium reactions did not occur in the analogous zirconium reactions, rather a slow change from colourless to orange occurred together with slow evolution of methane gas (148). Deuterium labelling studies have shown that the silane is the source of hydrogen for methane formation in both cases. Based on these observations, several possible mechanisms for the initial reaction between silane and Cp_2TiMe_2 or Cp_2ZrMe_2 have been suggested (148).

I.3.3 Bis(cyclopentadienyl)titanium and zirconium silyl complexes

The first zirconocene silyl derivative $Cp_2ZrCl(SiPh_3)$ was prepared in 1967 by the reaction of Ph_3SiLi with Cp_2ZrCl_2 at -50°C in THF (149). This was in fact the first group 4 silyl complex to be obtained. It is interesting to note that only the monosilyl complex was obtained. Attempts to obtain the bis(silyl) complex were not successful. About a year later, the first titanocene silyl complex $Cp_2Ti(SiPh_3)_2$ was reported (150). However, this compound was prepared by the reaction of Cp_2TiCl_2 with Ph_3SiK in air, and it was later suggested that instead of $Cp_2Ti(SiPh_3)_2$, $CP_2Ti(OSiPh_3)_2$ had been obtained (151). Since that time, a number of silyl and mixed alkyl silyl derivatives of bis(cyclopentadienyl)titanium(IV) and -zirconium(IV) have been prepared and characterized. These include $Cp_2TiCl(SiMe_3)$ (152), $Cp_2\overline{Ti(SiPh_2)_3Si}Ph_2$ (153), $Cp_2ZrCl(SiMe_3)$ (154,155), $Cp_2Zr[Si(SiMe_3)_3]Cl$, $Cp_2Zr[Si(SiMe_3)_3]Me$, $Cp_2Zr[Si(SiMe_3)_3]BH_4$, $Cp_2Zr[Si(SiMe_3)_3]SiMe_3$ (156), $Cp_2Zr(SiMe_3)Me$ (157) and $Cp_2Zr(SiHMes_2)Me$ (158) and so on. It is interesting to note that each of these complexes possesses at least one large sterically hindered silyl group, which is obviously very important to stabilize the complex. It was reported that $Cp_2Zr(SiHMes_2)Me$ decomposes at ambient temperature in the solid and has to be stored below 0°C, while $Cp_2Zr[Si(SiMe_3)_3]Me$ and $Cp_2Zr(SiMe_3)Me$, both of which possess a more bulky silyl group, are very stable even at the melting point. To date, no mixed alkyl silyl titanocene derivative has been reported. This is an indication that this type of complex is probably very unstable.

In addition to the complexes mentioned above, a particularly interesting binuclear titanium silyl compound, $Cp_2Ti(\mu\text{-}SiH_2)_2TiCp_2$, was reported in 1973 by Hencken and Weiss (159) from the reaction of $KSiH_3$ with Cp_2TiCl_2. A crystal structure revealed the presence of a dimer with a planar Si_2Ti_2 ring. Unfortunately, the structure was only refined to an R value of 9%. In view of the structure of $[Cp_2Ti(\mu\text{-}HSiPhH)]_2$ obtained by Aitken *et al.*(32), the structure $[Cp_2Ti(\mu\text{-}HSiH_2)]_2$ would probably fit the data at least as well.

Recently, an unusual silylzirconocene hydride complex, $Cp_2Zr(SiMePhH)(\mu\text{-}H)_2(PhH_2Si)ZrCp_2$ (VIa), was isolated from the catalytic dehydrocoupling reaction of phenylsilane by Clare Aitken in this laboratory (33). This compound was characterized mainly by ^1H-NMR and ^{29}Si-NMR. A crystallographic study was carried out, but the crystal structure was not refined to a satisfactory level due to severe disorder problems. The proposed structure for VI is shown in next page.

It is rather surprising that only a few lower valent titanium silyl complexes have been reported, although lower valent titanium such as Ti(III) might well provide increased stability to a Ti-Si bond by $d\pi$-$p\pi$ backbonding. It is very likely that this is a result of a lack

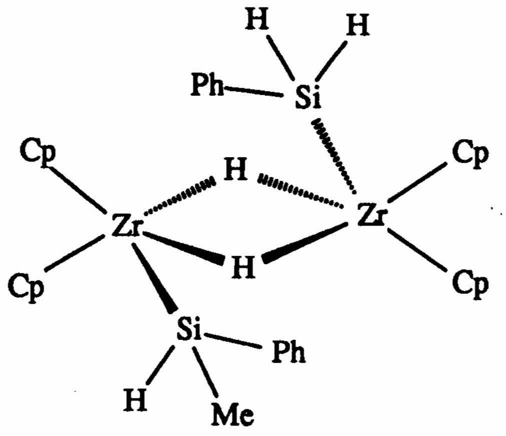

VIa

of preparative methods together with difficult isolation and purification procedures. In addition, the oxygen sensitivity of titanium and zirconium organometallic compounds has already been shown to be a problem. To our knowledge, only two Ti(III) silyl complexes, $[Cp_2Ti(\mu\text{-}H)(\mu\text{-}HSiHPh)TiCp_2]$ (**Va**) and $[Cp_2Ti(\mu\text{-}HSiHPh)]_2$ (**VIIa**), have been reported (32). They were obtained from the reaction of Cp_2TiMe_2 and $PhSiH_3$, and structurally characterized by X-ray crystallography. Several analogous complexes **Vb**, **Vc**, **VIIb**, and **VIIc** have also been obtained with the same method. The structures for these complexes are as follows:

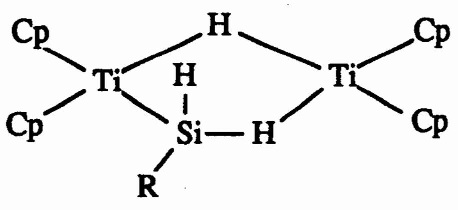

Va R = Ph

Vb R = Hx

Vc R = Bz

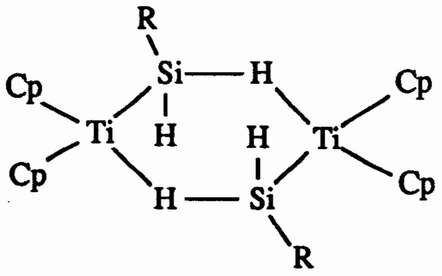

VIIa R = Ph

VIIb R = Hx

VIIc R = Bz

On the other hand, it appears that to date no Zr(III) or Zr(II) silyl complexes have been reported, although Zr has been reported to form Zr(III) alkyl complexes (129). As discussed previously, oxidation states of less than +4 are not readily accessible for Zr complexes, and so it is not surprising that no Zr(III) or Zr(II) silyl complexes have been obtained.

I.3.4 Bis(cyclopentadienyl)titanium/zirconium and their hydride derivatives

Bis(cyclopentadienyl)titanium and -zirconium, *i.e.*, titanocene and zirconocene, although frequently referred to in the literature, have never actually been isolated as discrete chemical compounds. However, these molecules have been implicated as highly reactive intermediates in a wide variety of chemical reactions involving hydrogen, dinitrogen and some unsaturated molecules such as olefins, alkynes and carbon monooxide. Since the early 1960s, some discrete, well-characterized bis(cyclopentadienyl) and bis(pentamethylcyclopentadienyl) complexes of low-valent titanium and zirconium, and their hydride derivatives have been isolated and studied. However, many such species are poorly characterized and remain elusive. Even now very few definitive X-ray structural studies are available because of the difficulty in obtaining suitable crystals of the air-sensitive materials.

As early as 1956, an air-sensitive, dark-green, diamagnetic crystalline solid from the reaction of titanium dichloride with cyclopentadienyl sodium was reported to be titanocene $(C_5H_5)_2Ti$ (160). Watt and Baye (161) later tried to repeat this synthesis, but were unable to obtain any product of composition $(C_5H_5)_2Ti$, and they therefore expressed considerable doubt about the existence of titanocene. Clauss and Bestian (112) reported that a similar green solid was obtained from the reaction of Cp_2TiMe_2 with hydrogen in hexane at 20°C, but they formulated this solid as a dimeric species $[(C_5H_5)_2Ti]_2$. Subsequent workers tried to prepare titanocene by de-halogenation of Cp_2TiCl_2 with sodium amalgam (162), or with sodium naphthalene (163). These reactions were reported to yield green, air-sensitive products, formulated as $[(C_5H_5)_2Ti]_2$ and $(C_5H_5)_2Ti$, respectively. A related "titanocene" material, obtained by reduction of Cp_2TiCl_2 with sodium sand, was considered on the basis of its infrared spectrum not to be a simple π-sandwich complex, but a more complicated dimer containing both π- and σ-bonded cyclopentadienyl groups (164).

The precise nature of "titanocene" therefore remained uncertain up to the late 1960s. A series of reports appeared to be consistent with the presence of the $(C_5H_5)_2Ti$ unit in some form in the various reaction mixtures. The green solution, for example, obtained as in reference (163), absorbed CO and N_2 slowly to give $Cp_2Ti(CO)_2$ (165) and $[(C_5H_5)_2Ti]_2N_2$ (166), respectively. Meanwhile, some other reports indicated the presence of titanium hydride species in many reduced Ti(IV) solutions. The problem regarding the precise nature of the green "titanocene" $[C_{10}H_{10}Ti]_2$ was resolved by Brintzinger and Bercaw in the early 1970s (167). While several reports had indicated that treatment of the green "titanocene" with hydrogen chloride gas did not afford Cp_2TiCl or Cp_2TiCl_2, they established that the product of this reaction was in fact $[C_{10}H_9TiCl]_2$ (167), and suggested that a $Ti(\mu\text{-}H)_2Ti$ group must be present in the structure of the green 'titanocene" according to the IR spectrum which contains a strong metal-hydride streching band at 1230 cm^{-1}. Two possible structures, $(CpTiH)_2(C_{10}H_8)$ (<u>VIII</u>) and $[Cp(C_5H_4)TiH]_2$ (<u>IX</u>), were then postulated depending on the mode of bonding of the C_5H_4 units.

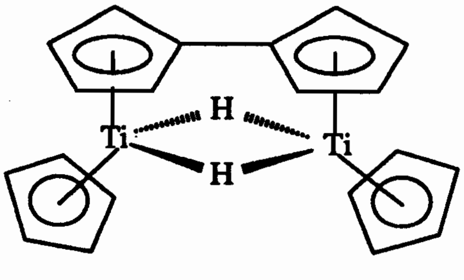

<u>VIII</u>

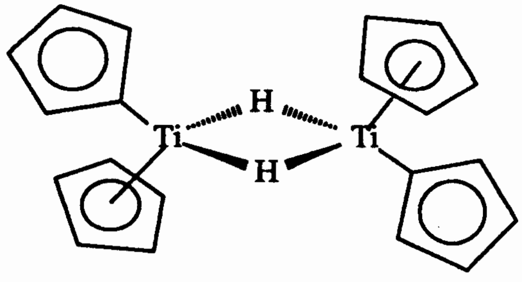

<u>IX</u>

The structure of VIII was later proved by ^{13}C NMR studies (168). Although crystals suitable for x-ray diffraction have never been obtained, the structure of VIII was indirectly confirmed by X-ray structural determination of the bis-hydroxyl derivative $(CpTiOH)_2(C_{10}H_8)$ (169).

A series of investigations by Brintzinger and Bercaw in the early 1970s largely clarified the relationship between these titanocene and hydride derivatives. They obtained the first isolated hydride $[Cp_2TiH]_2$ (X), a violet diamagnetic bridging dihydride dimer, by treating solid Cp_2TiMe_2 with hydrogen at 0°C in the absence of solvent (142). Upon heating to 150°C *in vacuo*, X was found to convert to VIII via the loss of hydrogen. It was also found that X slowly converted to a polymeric form, a grey-green complex formulated as $[Cp_2TiH]_n$ at room temperature (143). The grey-green hydride complex could also be prepared directly from the reaction of Cp_2TiMe_2 with H_2 in solution at 0°C instead of 20°C. The polymeric hydride has been found to be a good source of a reactive form of titanocene. On stirring in toluene at 20°C, it evolved 0.5 mol of H_2 per mol of Ti, giving rise to a dark species with the composition $[Cp_2Ti]_n$. A simple metallocene type of IR spectrum was obtained, showed no evidence of σ-bonded cyclopentadienyl groups. Molecular weight studies showed $[Cp_2Ti]_n$ to be dimeric in solution. The presence of normal η^5-C_5H_5 rings in $[Cp_2Ti]_2$ is also supported by its chemical behavior. When exposed to HCl gas at -80°C, solutions of $[Cp_2Ti]_2$ rapidly reacted to form Cp_2TiCl_2. The dark titanocene $[Cp_2Ti]_2$, initially called "metastable" titanocene, is different from , but isomeric with, the green

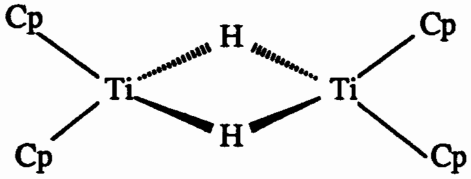

X

titanocene VIII. It is a much more reactive compound than the latter, and it is transformed into the green form by heating in toluene at 100°C. It is noteworthy that magnetic susceptibility determinations on solutions of $[Cp_2Ti]_2$ in toluene indicated a noticeable paramagnetism, which has been explained by the presence of a small fraction of the complex as monomeric Cp_2Ti with two unpaired electrons (143).

Attempts to isolate the monomeric Cp_2Ti have never been successful. However, its analogue, decamethyltitanocene Cp^*_2Ti, has been obtained as a monomer (143). $[Cp_2Ti]_2$ and Cp^*_2Ti resemble each other in many of their reaction patterns, so the latter provided an opportunity to investigate the reactivity associated with such a bis(cyclopentadienyl) -titanium(II) intermediate in detail (170). It was found that Cp^*_2Ti, just as $[Cp_2Ti]_2$, reversibly interacts with gaseous hydrogen. When solutions of decamethyltitanocene in toluene or pentane were exposed to an atmosphere of H_2, hydrogen was absorbed concurrent with the formation of a bright orange hydride $Cp^*_2TiH_2$. If Cp^*_2Ti was desired, the solutions of $Cp^*_2TiH_2$ were stirred at room temperature *in vacuo*, and the coordinated hydrogen was slowly released over a period of several hours.

Another particularly interesting titanocene hydride complex is a paramagnetic, mixed oxidation state Ti(III)/Ti(IV) dimer $(Cp_2TiH)_2H$ (XI), which was obtained by Samuel and Harrod from the reaction of certain organosilanes with Cp_2TiMe_2 (171). The structure suggested based on IR and EPR spectroscopic evidence is as follows:

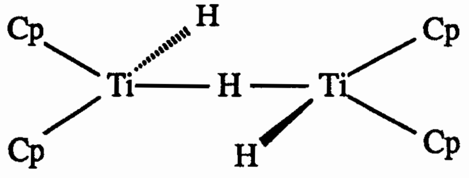

XI

It is very interesting to note that the hydride <u>XI</u> can been obtained only from the reactions of a number of organosilanes with some reactive titanocene derivatives. This indicates that <u>XI</u> is formed by a special mechanism which is closely related to the polymerization of organosilanes. Thus the isolation and characterization of <u>XI</u>, together with <u>V</u> and <u>VII</u>, might provide some insights into the mechanism of organosilane polymerization.

Zirconium is analogous to titanium in that no stable monomer Cp_2Zr has ever been isolated. Many attempts to obtain zirconocene by various methods, usually involving a reduction of Cp_2ZrCl_2, have resulted in failure (172-176). Watt and Drummond were the first to report a synthesis and characterization of a species they called zirconocene (172). Although the correct stoichiometry was obtained and IR spectroscopy showed that there was no apparent evidence of Zr-H bonds, subsequently other workers prepared the same material and showed that hydrides were in fact present (177). Schwartz *et al.* (178) have suggested that "zirconocenes", prepared by reduction of Cp_2ZrCl_2 with sodium amalgam, or by decomposition of hydridoalkylzirconocenes, are polymeric Zr(IV) compounds containing hydride and $\eta^1:\eta^5$-C_5H_4 bridges. It was believed that "zirconocene" is not isostructural with the green, stable form of "titanocene", nor does it remain in solution as a metastable species, as does the titanocene.

The first hydride derivatives of zirconocene, $Cp_2ZrH(BH_4)$ and $[Cp_2ZrH_2]_n$, were obtained by James *et al.* from the reaction of $Cp_2Zr(BH_4)_2$ with trialkylamines in 1967 (179). Later, Wailes and Weigold obtained several hydrides, including Cp_2ZrHCl, $Cp_2ZrH(AlH_4)$, $Cp_2ZrH(CH_3)$, by the reaction of $LiAlH_4$ with the corresponding chloride derivative (180). A number of hydrides of the formula Cp_2ZrHR, where R = ethyl, cyclohexyl, (cyclohexyl)methyl, neopentyl, *n*-octyl (181), or $CH(SiMe_3)_2$ (182), were subsequently prepared by this method. Although $Cp_2ZrH(CH_3)$ and $[Cp_2ZrH_2]_n$ were presumed to be polymeric based on their characteristic insolubility, other hydrides all appear to exist in dimeric form in solution. The structure of these dimeric hydrides is as follows:

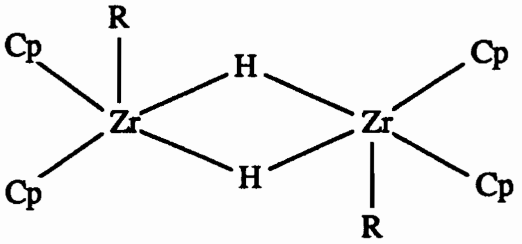

XII

Recently, $[Cp_2ZrH_2]_n$ (183) and $Cp_2ZrH(CH_3)$ (146) have also been reported to be dimeric. Attempts to solubilize the dihydride complex by using substituted cyclopentadienyl ligands have been partially successful, and a number of $[(RCp)_2ZrH_2]_2$ compounds (R = Me, *i*-Pr, *t*-Bu) have been prepared by hydrogenolysis of the corresponding $(RCp)_2ZrMe_2$ compounds (97). These hydrides were characterized as dimers by mass spectrometry and ^1H NMR spectroscopy. The dimeric structure has also been confirmed with the crystal structure of the $[(C_5H_4Me)_2ZrH(\mu\text{-}H)]_2$ derivative (184).

Preparation of the decamethylzirconocene, Cp^*_2Zr, has been achieved by reduction of $Cp^*_2ZrCl_2$ with excess Na amalgam in toluene under N_2 (185). Initially the dinitrogen complex, $[Cp^*_2ZrN_2]_2N_2$ was obtained, which was found to slowly release its coordinated nitrogen *in vacuo*. The decamethylzirconocene dihydride, $Cp^*_2ZrH_2$, has also been prepared by the reaction of $[Cp^*_2ZrN_2]_2N_2$ with H_2 (186). Treatment of $Cp^*_2ZrH_2$ with isobutylene was found to yield $Cp^*_2Zr(H)(CH_2CHMe_2)$, which decomposes slowly to evolve isobutane. Dimerization or polymerization does not happen to these decamethylzirconocene derivatives due to steric crowding.

To date, no zirconocene(III) hydride has been isolated. However, several reports have indicated that the paramagnetic Zr hydrides can be detected by EPR during the photolysis of Cp_2ZrMe_2 (187), Cp_2ZrPh_2 (188) and $[(C_5H_4Me)_2ZrH(\mu\text{-}H)]_2$ (189). A weak EPR signal, assigned to a mixed-valence zirconocene hydride similar to **XI**, has also been observed during the reaction of Cp_2ZrMe_2 with phenylsilane (33). The existence of the mixed-valence zirconocene hydride in this system implies that the mechanism of the organosilane polymerization in the presence of Cp_2ZrMe_2 is probably the same as, or similar to, that in the presence of Cp_2TiMe_2.

I.4 SCOPE OF THE THESIS

In the first part of this thesis, the dehydrocoupling of a number of organosilanes, including $PhSiH_3$, $MeSiH_3$, Ph_2SiH_2, $PhMeSiH_2$ and n-$BuMeSiH_2$, and the kinetics of the dimerization of Ph_2SiH_2 in the presence of Cp_2TiMe_2 and Cp_2ZrMe_2 were investigated. The pyrolysis of polymethylsilane to SiC was also studied. In the second part of the thesis, the stoichiometric reactions of Cp_2TiMe_2 and Cp_2ZrMe_2 with the above listed organosilanes were studied, and a number of new silylzirconocene complexes of the type $Cp_2ZrR^1(\mu\text{-}H)_2R^2ZrCp_2$, where R^1 is a silyl group, and R^2 could be H, Me, or a silyl group, were isolated or observed in reaction solutions. In addition, the mechanism of the silane dehydrocoupling reaction is discussed. In the last part of the thesis, a series of novel silyltitanocene(III) complexes $Cp_2Ti(R)L$, where R is a silyl group, L = PMe_3 or Py, were prepared and the X-ray crystal structures of some of them were determined.

Chapter II

Dehydrocoupling of phenylsilane, diphenyldisilane and triphenyltrisilane catalyzed by dimethyltitanocene and dimethylzirconocene

II.1 INTRODUCTION

As mentioned in chapter I, polysilanes have unusual physical and chemical properties and a number of potential applications (29,30). However, a very limited number of synthetic routes to high molecular weight polysilanes so far have been developed (35,37,43,48). Of these, the most widely employed route has been the Wurtz-Fittig coupling reaction. This method however has several commercial drawbacks: (1) poor control over molecular weight and large polydispersity, (2) potential hazards associated with the use of molten metals, and (3) large amounts of salt waste generated. More versatile synthetic methods are thus expected to promote the development of the applications of polysilanes. The discovery of catalysts for the facile dehydrocoupling of primary organosilanes aroused hopes that such reactions might provide another, and perhaps superior, synthetic route to polysilanes.

Since titanocene and zirconocene alkyl derivatives were found by Harrod and co-workers (31-34) to catalyze the dehydrogenative polymerization of primary organosilanes, a number of groups (91-94) in the world have focused on the catalytic dehydrocoupling reaction of organosilanes and a variety of metallocene, metallocene alkyl (90), aryl (91), silyl, and hydride (92,94) complexes of group 4-6 metals as catalysts for the dehydrocoupling reaction of primary silanes, particularly phenylsilane, have been studied. It was found that the molecular weight of the polysilanes obtained from the dehydrocoupling reaction can vary as a function of reaction conditions and catalysts (90,92). To date, the best catalysts found for the dehydrocoupling of primary silanes to polysilanes are titanocene and zirconocene alkyl and hydride derivatives, which can give polysilanes with 10 - 20 Si atoms, well below the chain length required for a polymer with useful mechanical and electronic properties.

Improvement of this method relies heavily on the understanding of the polymerization procedure and mechanism. However, the mechanism is still very much in question (32,34,87-89). For the polymerization of phenylsilane, and a number of other primary silanes, in the presence of titanocene and zirconocene alkyl derivatives, it is even not very clear if the polymerization takes place in a stepwise fashion or a chain growth fashion, because no dimer, trimer and other low molecular weight oligomers were observed when the reactions were followed by NMR (31,32). However, when a more sterically encumbered complex such as Ind_2TiMe_2 (90) was used as catalyst, or a less reactive silane such as butylsilane (93) was used as substrate, a slow stepwise oligomerization was observed. Does the dehydrocoupling reaction go through different mechanisms when different catalysts or substrates are used, or do the experimental observations give wrong information? It is obvious that further experimental observations are necessary to understand the polymerization mechanism.

On the other hand, although the molecular weight and molecular weight distribution for the polysilanes made from these primary silanes have been studied, and it was found that these material have bimodal molecular weight distributions (88), the reason why they have bimodal molecular weight distributions is not very clear. So far, nobody has studied the changes in molecular weight and molecular weight distribution during the polymerization reaction, while such studies might provide very important information to understand the reaction procedure and mechanism.

The polymerization reaction profiles of phenylsilane, diphenyldisilane and triphenyltrisilane in the presence of dimethyl-titanocene and -zirconocene have been studied in detail by following the reactions by ^{1}H NMR, GC and GPC, and some important information about the progress of the reactions was obtained from these studies. The results will be discussed in this chapter. Phenylsilane, as well as its dimer and trimer, were chosen as substrates because phenylsilane is the most typical primary silane. It has higher reactivity than alkyl silanes and has a simple NMR spectrum.

II.2 RESULTS AND DISCUSSION

II.2.1 Dehydrocoupling reaction of phenylsilane catalyzed by dimethyltitanocene

The present detailed studies of the polymerization of phenylsilane indicate that the polymerization reaction goes through a step growth mechanism rather than a chain growth mechanism. The dimer and trimer produced from the polymerization reaction have been successfully detected by GC and ^{1}H NMR. A typical GC trace for the phenylsilane polymerization reaction mixture is shown in Fig. II-1. The Si-H NMR signals for dimer and trimer are greatly broadened in the presence of the active titanocene catalyst and the catalyst must either be destroyed by oxidation, or removed by passing the reaction mixture through a Florisil column in order to observe the dimer and trimer at room temperature. This is the reason why they were not observed by NMR before. Even in the presence of active catalyst, these species can be observed at lower temperature. The typical NMR spectra of the phenylsilane polymerization reaction mixture, before and after the catalyst was removed, at room temperature and -40°C, are shown in Fig. II-2. It was found that the Si-H NMR signal for monomer is broadened much less than those for dimer and trimer, and the resonances for phenyl protons are not affected. These facts indicate that the selective catalyst broadening effect on the Si-H NMR signals results from a dynamic process between silanes and catalyst rather than a paramagnetic material. The latter should broaden all resonances in the system. This has been proved by adding a paramagnetic material, $FeCl_3$, into the mixture of phenylsilane and diphenyldisilane in benzene-d_6, which broadened all the NMR signals in the same way. A likely candidate for the dynamic process is a rapid, reversible oxidative addition reaction between titanocene and silane (90), as shown in eq. II-1. Such a reaction is analogous to the previously observed, reversible oxidative addition of H_2 to permethyltitanocene (110). The fact that the Si-H signals of

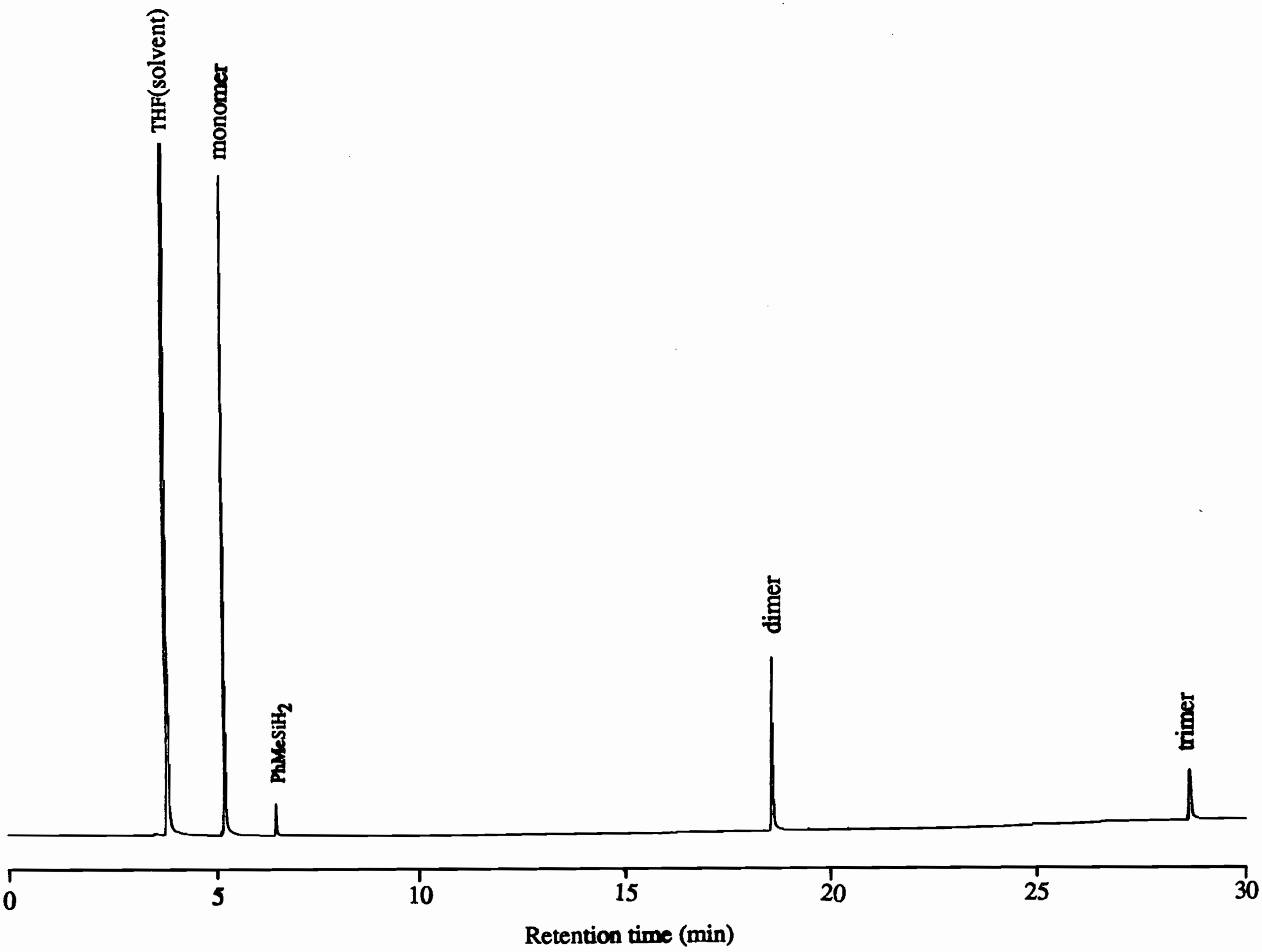

Figure II-1. A GC trace of the phenylsilane polymerization reaction mixture.

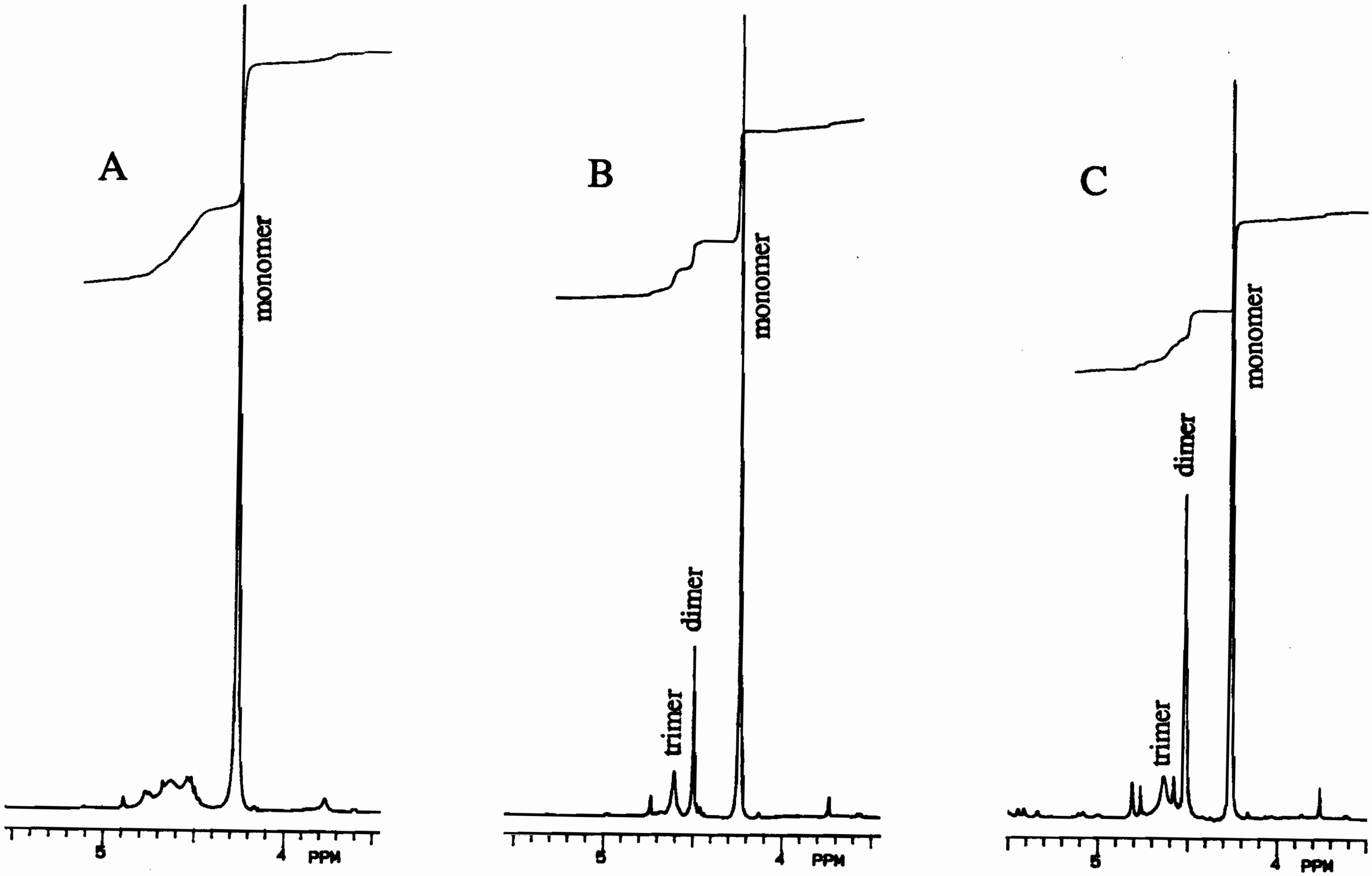

Figure II-2. NMR spectra of the $PhSiH_3$ polymerization reaction mixture after 30 minutes.
a) before and b) after the titanocene catalyst was removed, at room temperature;
c) with active catalyst, at -40°C.

$$Cp_2Ti \quad + \quad {\equiv}SiH \quad \rightleftarrows \quad Cp_2TiH(Si{\equiv}) \qquad (II-1)$$

dimer and trimer are broadened much more than that of the monomer can be attributed to the fact that the Si-H bonds in dimer and trimer are weaker(190,191) and more reactive than the ones in monomer, due at least in part to the σ-electron delocalization along the Si-Si bond, by which the Si-H bond is weakened to some extent (30). The higher reactivity of dimer has been proved by comparison of the dehydrocoupling reaction rate of the dimer with that of the monomer. After addition of 4 mg of Cp_2TiMe_2 (0.019 mmol) into a 1:1 (mole/mole) mixture of monomer and dimer (0.96 mmol) in benzene-d_6 (0.6 ml) for 40 minutes, it was found that 80% of the dimer had reacted into higher molecular weight oligomers, and only 10% of monomer was consumed. This result indicates that the reaction rate of the dimer is much faster than that of the monomer, and hence that the dimer is more reactive than the monomer.

The polymerization of phenylsilane has been followed by ^1H NMR, GC and GPC. The concentrations of the monomer, dimer and trimer with the passage of time can be estimated by GC or NMR integrations. The results from both methods are in good agreement. A reaction profile for the polymerization of phenylsilane is shown in Fig. II-3. This is a typical stepwise polymerization reaction, in which the dimer is formed first, followed by trimer and other higher molecular weight oligomers. A noticeable feature of this reaction is that the concentrations of both the dimer and the trimer are several times lower than that of the monomer throughout most of the reaction (the molar ratios of the monomer to dimer and trimer are 3 - 5). This indicates that both the dimer and trimer are more reactive than the monomer in this system. It is difficult to compare the reactivity between dimer and trimer based only on the reaction profile shown in Fig. II-3. However, we can get some information about the reactivity of the oligomers by following the reaction

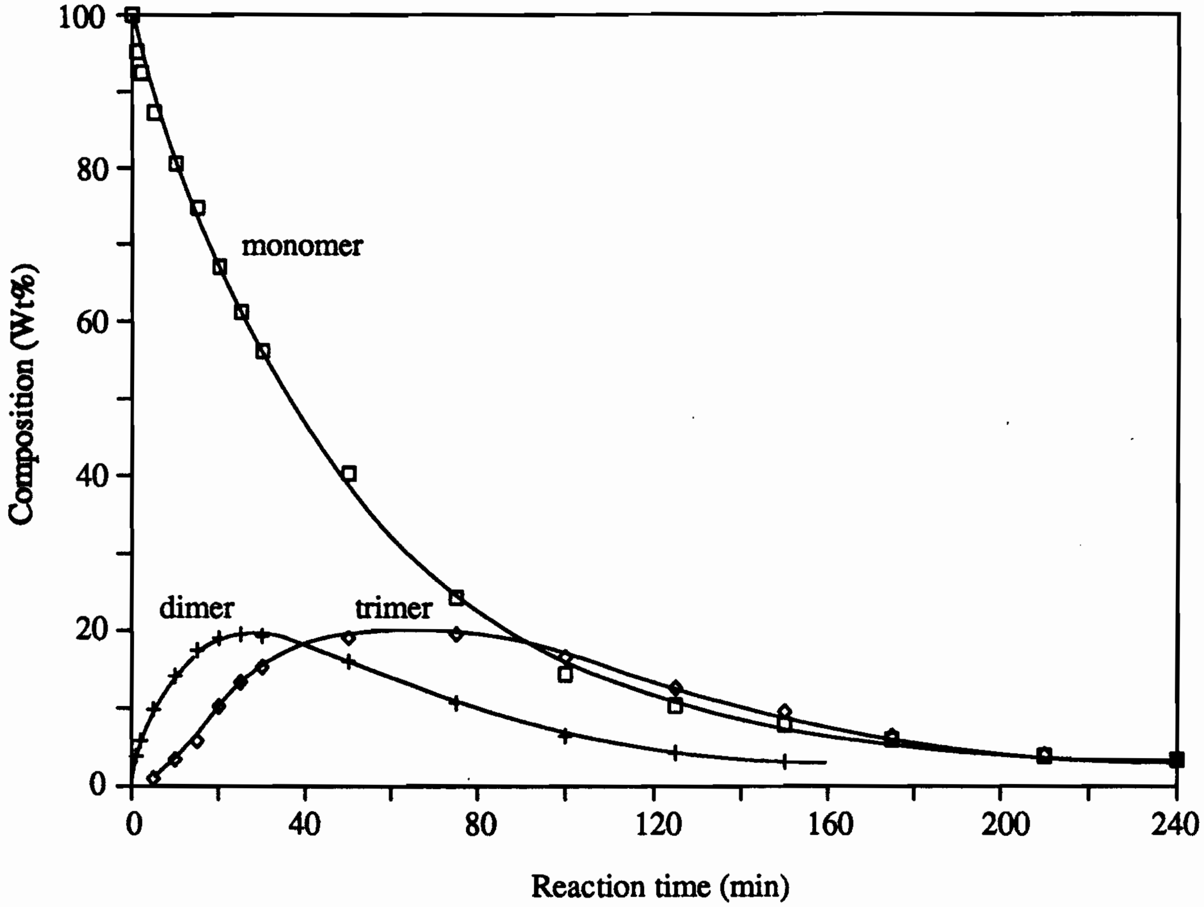

Figure II-3. Reaction profile for the titanocene catalyzed $PhSiH_3$ polymerization reaction. $[Cp_2TiMe_2] = 0.08$ M in neat $PhSiH_3$ at room temperature.

with GPC.

The GPC traces for the reaction mixture at different reaction times are shown in Figure II-4. Although the separation of the peaks for different species is not good enough to calculate the amount of each species, the GPC traces can still provide some important information about the reaction process. In the first place, all of the expected low molecular weight oligomers from dimer to pentamer have been clearly observed. The average molecular weight of the reaction products increases steadily with reaction time. These

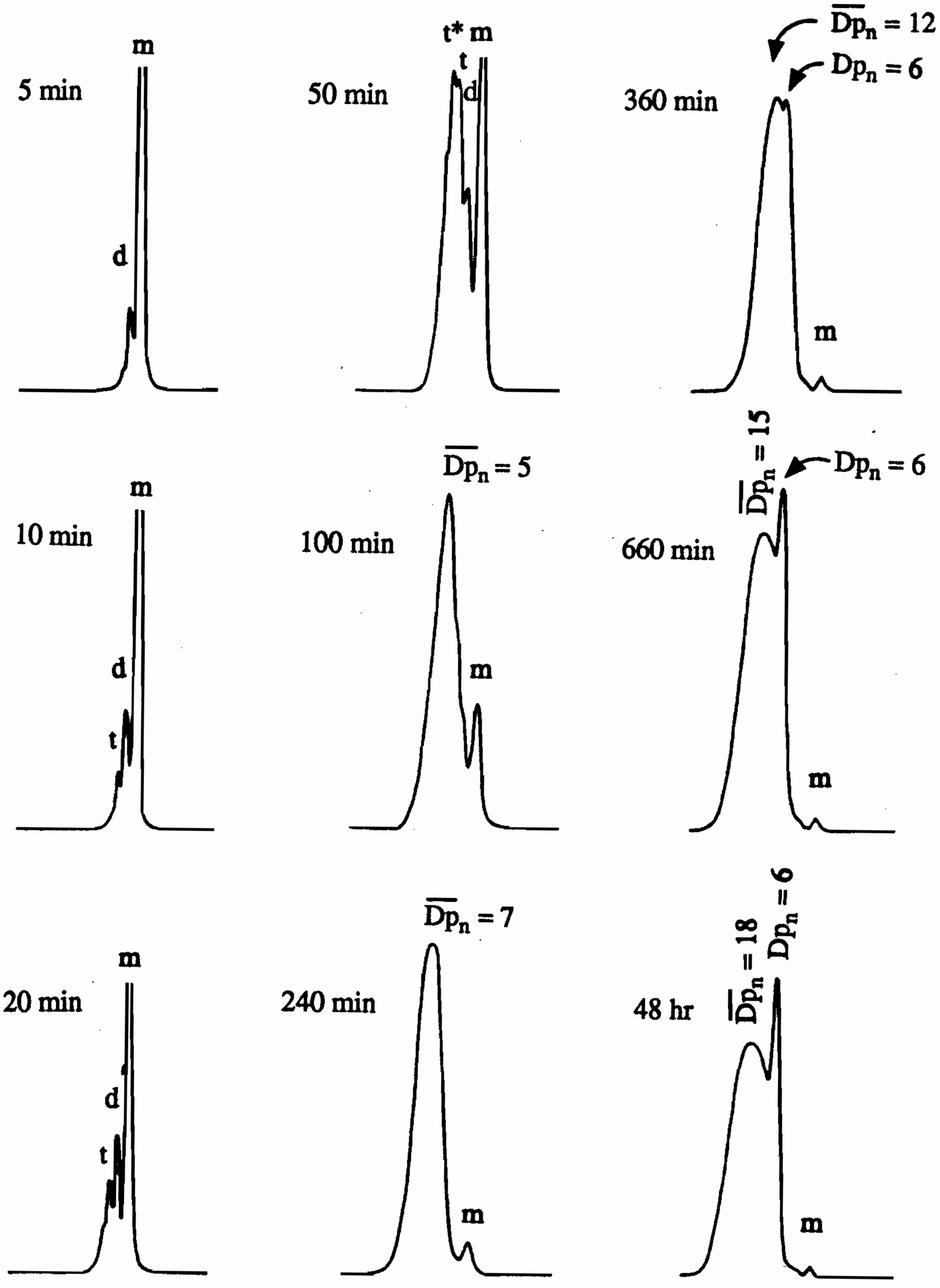

Figure II-4. GPC traces of the titanocene catalyzed $PhSiH_3$ polymerization reaction mixture at different reaction times. m - monomer; d - dimer; t - trimer; t*- tetramer.

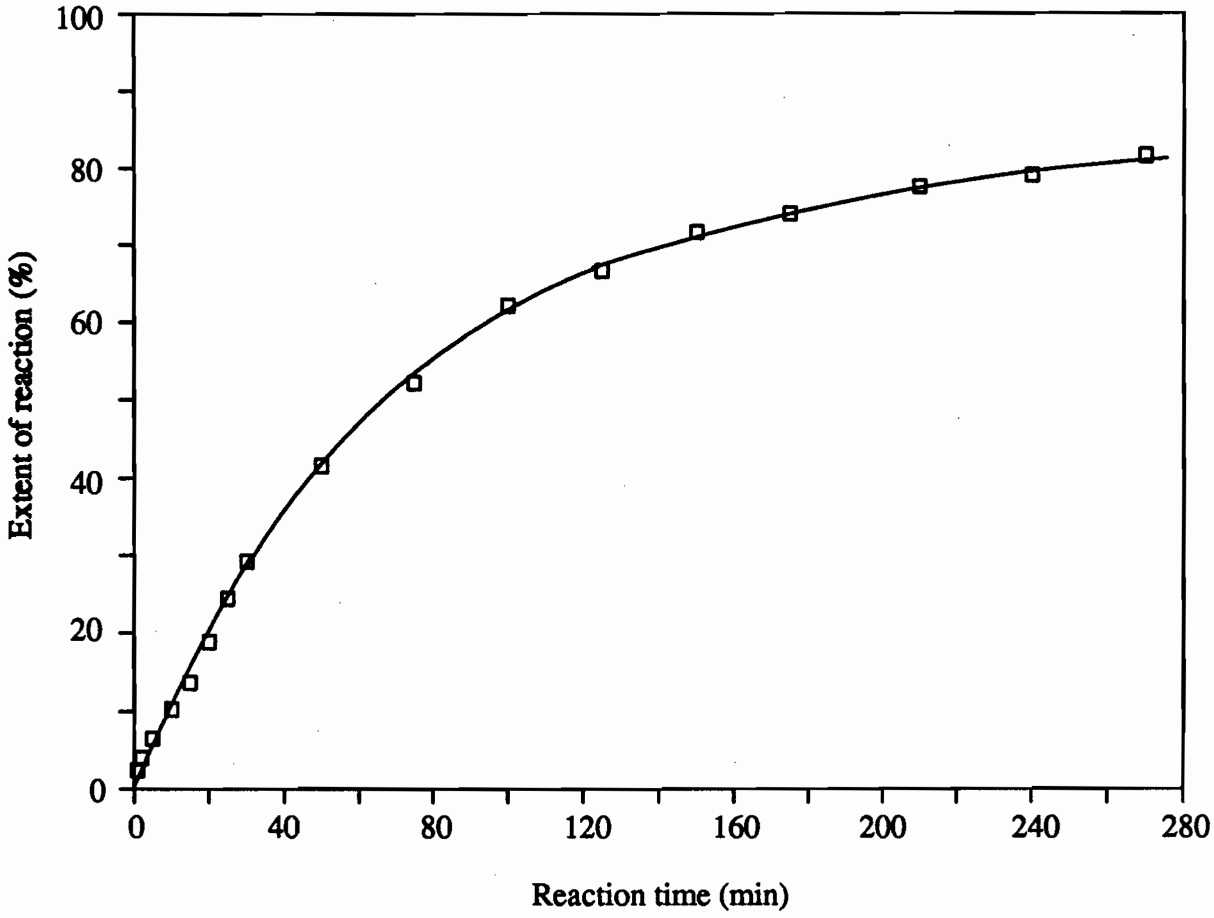

Figure II-5. Variation of the extent of reaction with time for the titanocene catalyzed $PhSiH_3$ polymerization reaction. $[Cp_2TiMe_2] = 0.08$ M in neat $PhSiH_3$ at room temperature.

further confirm the step growth nature of the polymerization reaction. Secondly, by following the reaction, we have also obtained some information about the extent and rate of the polymerization reaction at different times throughout the course of reaction. The extent of reaction, p, defined as the fraction of the reactive groups that have reacted at time t, has been estimated by GPC and the variation of p with reaction time is shown in Fig. II-5. One feature that should be noted from this figure is that the extent of reaction p increases rapidly in the early stages of the reaction and then changes slowly after about 2 hours, at which time the concentrations of monomer and dimer have become very low. This variation curve of *p* with time indicates that the polymerization reaction is faster when the concentrations of monomer and dimer in the reaction mixture are higher, and then becomes slower and slower with the increase in the degree of polymerization of the reaction mixture. The completion of the overall polymerization of phenylsilane requires about 2 days. The final extent of reaction is about 95%. Thirdly, when the monomer was almost totally consumed (about 5 hours), the degree of polymerization of the reaction products at the GPC peak position (Dp_n) was about 6 - 7 and the molecular weight distribution was monomodal (Fig. II-4). This probably indicates that the reactivity of those oligomers with 6 or more silicon atoms is lower than that of monomer. Generally speaking, the reactivity of polymers, particularly oligomers, decreases with increasing chain length because of both the dilution of functional groups and the increase in steric hindrance. In this regard, the order of reactivity of phenylsilane and its oligomers should be as follows:

$$PhSiH_3 << \text{dimer} > \text{trimer} > \text{tetramer} > \text{pentamer} > \text{hexamer} > \ldots$$

Finally, with the passage of time (about 6 hours), the GPC trace of the reaction mixture changed from monomodal to bimodal with a very narrow distribution low molecular weight fraction and a somewhat broader distribution higher molecular weight fraction. The low molecular weight fraction, which was accompanied by the appearance of a broad set of resonances in the region of 4.9 - 5.5 ppm in NMR spectra (Fig. II-6), has a constant Dp_n value of 6. The average degree of polymerization ($\overline{Dp_n}$) for the higher molecular weight fraction increased with time until the reaction mixture became hard solid (after about 48 hours), and then showed no notable further change. The final $\overline{Dp_n}$ for the higher molecular weight fraction is about 18. We attribute the higher molecular weight fraction to linear polymer and the lower molecular weight species to cyclosilane. It has been

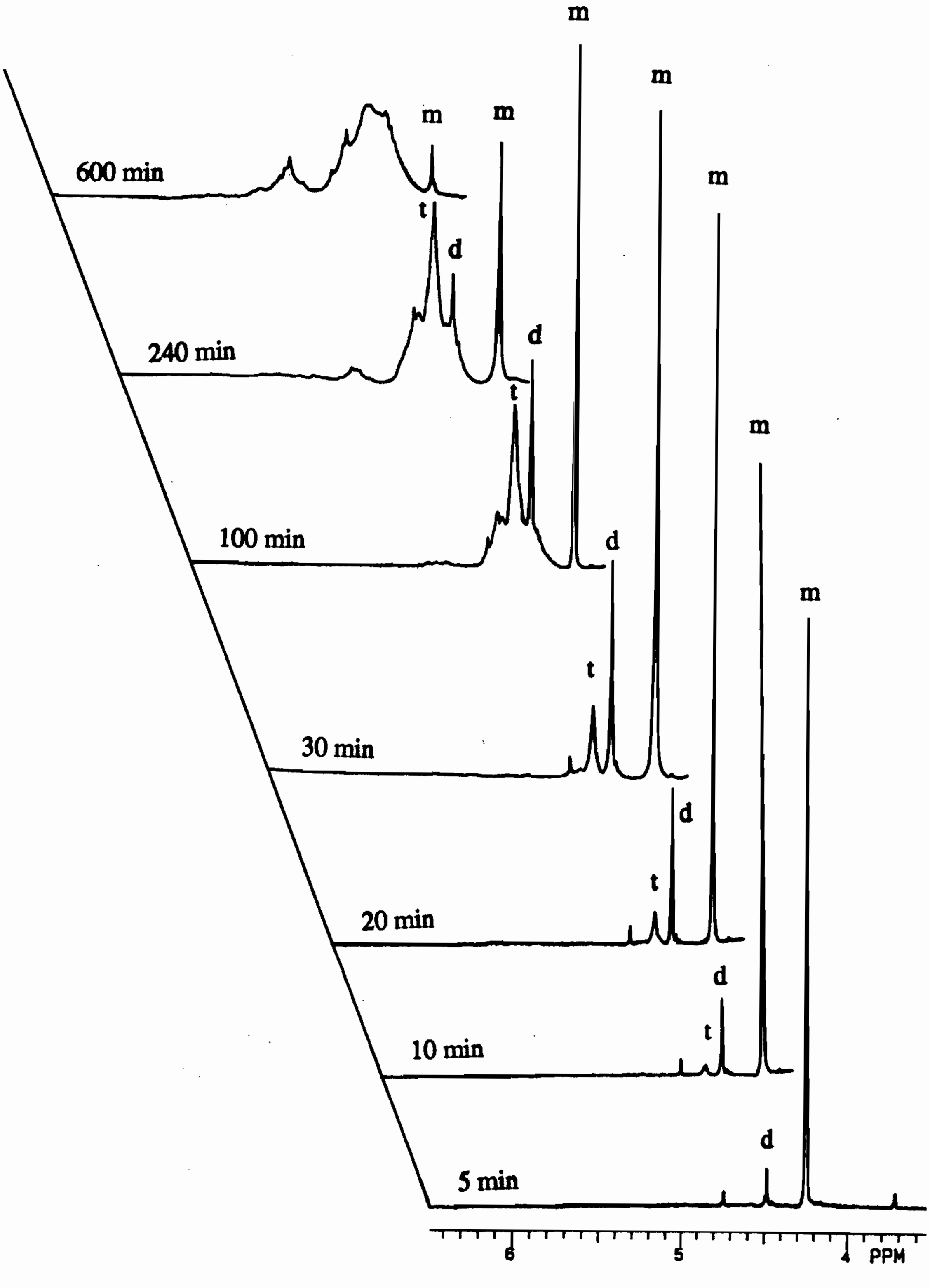

Figure II-6. ^{1}H NMR spectra of the titanocene catalyzed $PhSiH_3$ polymerization reaction mixture at different times. m - monomer; d - dimer; t - trimer.

previously observed that the formation of the lower molecular weight species is favored by low monomer concentration (88). A highly insoluble white material, all-trans isomer of hexaphenylcyclohexasilane, has also been obtained from the polymerization reaction of phenylsilane (90). When benzylsilane was used as substrate, the produced polymer, which was shown by ^{29}Si NMR (DEPT) spectra to be a mixture of cyclics with no linear species (34), gives a monomodal GPC trace. More recently, a X-ray crystal structure for the all-trans hexabenzylcyclohexasilane obtained from the polymerization of benzylsilane has been determined (192). Based on all these experimental results, it is almost beyond doubt that the lower molecular weight fraction consists of cyclics, which presumably result from an intramolecular ring closure, as opposed to a linear propagation via an intermolecular reaction.

Another important feature of the polymerization reaction is the cyclization of higher molecular weight linear polymer in solution with active catalyst. In an attempt to get still higher molecular weight polysilane by coupling the polymer obtained from the above reaction, the polymer was dissolved with active catalyst in toluene and left to react. However, instead of further chain growth, it was found that the higher molecular weight fraction was gradually converted to lower molecular weight cyclics. The NMR spectra and GPC traces of the reaction mixture before and after the cyclization reaction are shown in Fig. II-7 and Fig. II-8 respectively and the IR data is presented in Table II-1.

Table II-1. IR data for a polyphenylsilane sample before and after cyclization

note	ν_{Si-H}, cm^{-1}	δ_{SiH2}, cm^{-1}	I_δ / I_ν
before cyclization	2095	914	0.35
after cyclization	2100	914	0.16

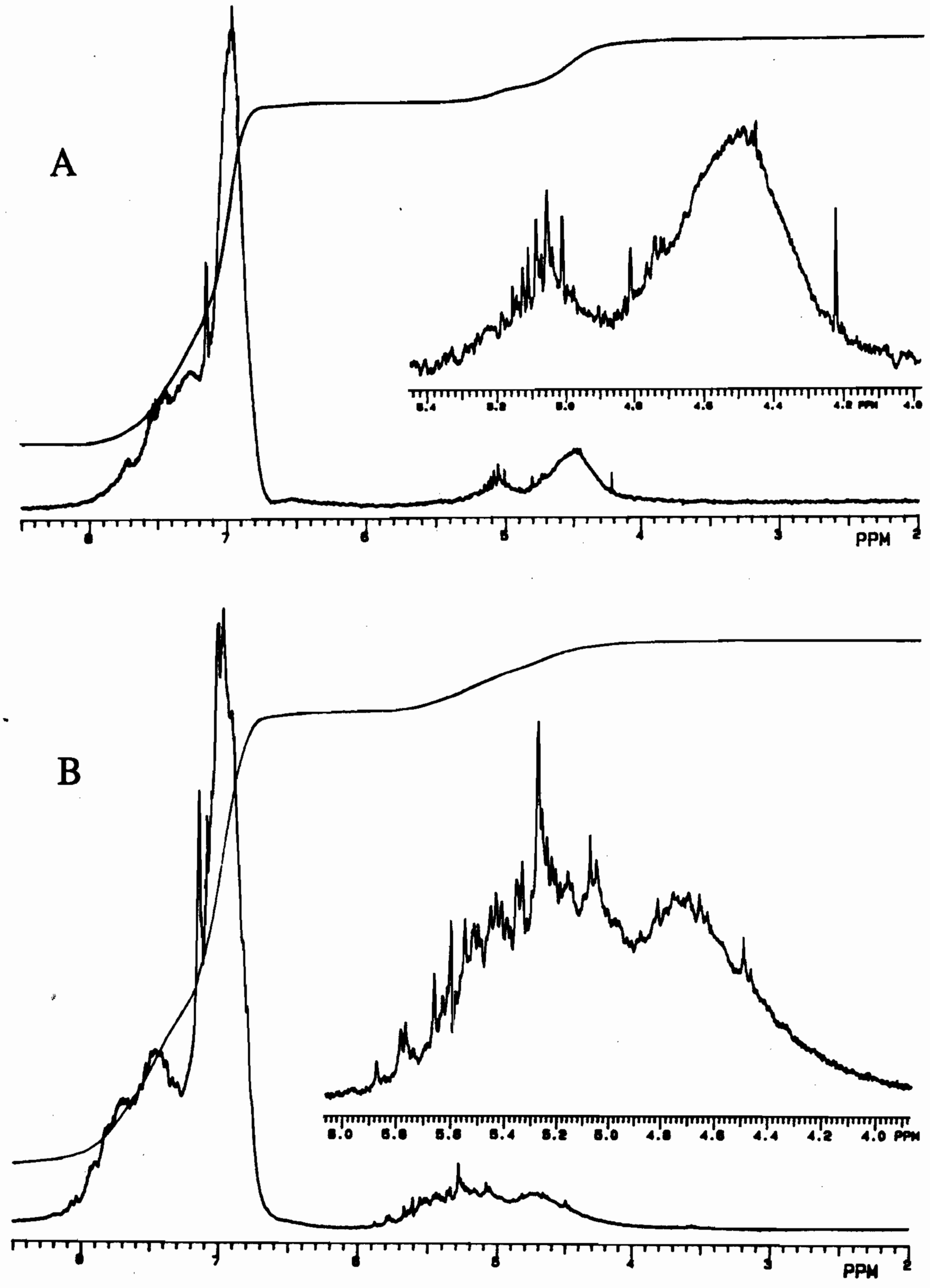

Figure II-7. ^{1}H NMR spectra of polyphenylsilane before and after cyclization catalyzed by titanocene. a) before cyclization; b) cyclization for 4 days.

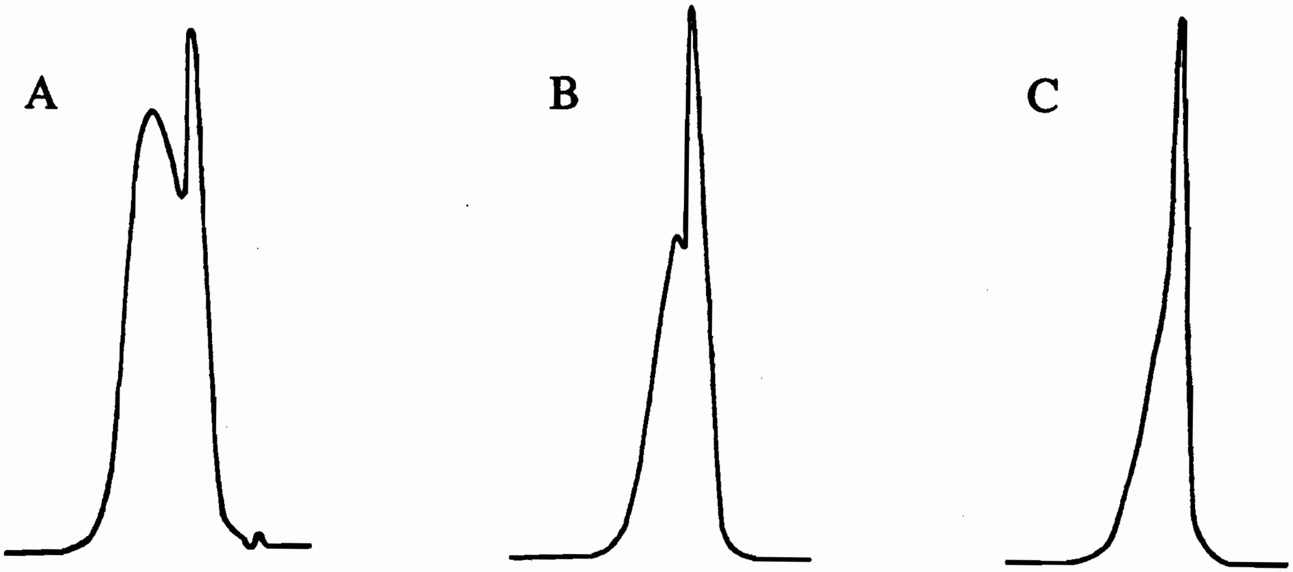

Figure II-8. GPC traces of polyphenylsilane before and after cyclization catalyzed by titanocene. a) before cyclization; b) cyclization for 4 days; and c) for 7 days.

The cyclization reaction in this case is quite slow, requiring 7 - 10 days to go to completion. A similar cyclization process has also been observed in the benzylsilane polymerization reaction (34). Although the detailed mechanism for the overall polymerization reaction is still obscure, it seems to be clear that the cyclosilanes are produced through two different routes. One is the intramolecular ring closure of the oligomers with suitable chain length mentioned above (eq. II-2), and the other is a back-biting depolymerization reaction of the polymers with longer chains (eq. II-3). Given

$$H_2PhSi(PhSiH)_{n-2}SiPhH_2 \longrightarrow (PhSiH)_n + H_2 \qquad \text{(II-2)}$$

$$H_2PhSi(PhSiH)_{m+n}SiPhH_2 \longrightarrow (PhSiH)_n + H_2PhSi(PhSiH)_mSiPhH_2 \qquad \text{(II-3)}$$

that the reactivity of oligomers for polymerization decreases gradually and the cyclization reaction becomes more and more dominant with the increase of their chain length, it is understandable that the average degree of polymerization of the polyphenylsilanes obtained so far by this method has been limited to 10 - 20.

II.2.2 Dehydrocoupling reaction of phenylsilane catalyzed by dimethylzirconocene

Dimethylzirconocene has been found to exhibit almost identical behavior to dimethyltitanocene in catalyzing the polymerization of primary organosilanes. The only evident differences between the two systems are the pronounced induction period observed for the titanium catalyzed reaction and the essentially complete reduction of the dimethyltitanocene to Ti(III) complexes at the onset of polymerization (32). The zirconocene catalyzed reaction exhibits an autoacceleration in the course of the reaction, but no obvious induction period. Stoichiometric reactions of the dimethylzirconocene with some primary and secondary silanes, followed by NMR, indicate that, unlike the case of dimethyltitanocene, the conversion of dimethylzirconocene into active catalyst is gradual. This might be the reason for the observed differences between the two catalytic systems.

The zirconocene catalyzed polymerization of phenylsilane was found to be much faster than the titanocene catalyzed reaction. When the polymerization reaction was carried out with neat phenylsilane as substrate, the reaction was violent and almost all of starting phenylsilane was consumed in several minutes, while the titanocene catalyzed polymerization under similar conditions required several hours to reach the same conversion. A reaction profile for the zirconocene catalyzed phenylsilane polymerization is shown in Fig. II-9 and the GPC traces for this reaction are shown in Fig. II-10. In order to illustrate the change of the reaction rate with time, a variation curve of the extent of reaction with time is also shown in Fig. II-9. Although dimer, trimer and other low molecular weight oligomers can be observed as products in the zirconocene catalyzed reaction, their concentrations are relatively lower than in the titanocene catalyzed reaction. By comparison of the reaction rate of the dimer with that of the monomer, it is revealed that the difference in reactivity between dimer and monomer in the zirconocene catalyzed reaction is larger than in titanocene system. In a typical reaction, after 4 mg of Cp_2ZrMe_2 (0.016 mmol) was added into a 1:1 (mole/mole) mixture of monomer and dimer (0.96 m mol) in benzene-d_6 (0.6 ml) for 5 minutes, 90% of the dimer has been converted to higher molecular weight oligomers, but only about 5% of monomer was consumed. In the zirconocene catalyzed polymerization, it was found that all the lower oligomers from dimer to hexamer, including cyclohexasilane, were produced almost at the same time as soon as the reaction began. When the monomer was almost totally consumed, the average degree of polymerization for the reaction mixture has reached about 10, and only traces of low oligomers smaller than hexamer were left in the reaction system at this point. The quick formation and consumption of these smaller oligomers suggest that all of them are probably more reactive than monomer in this system.

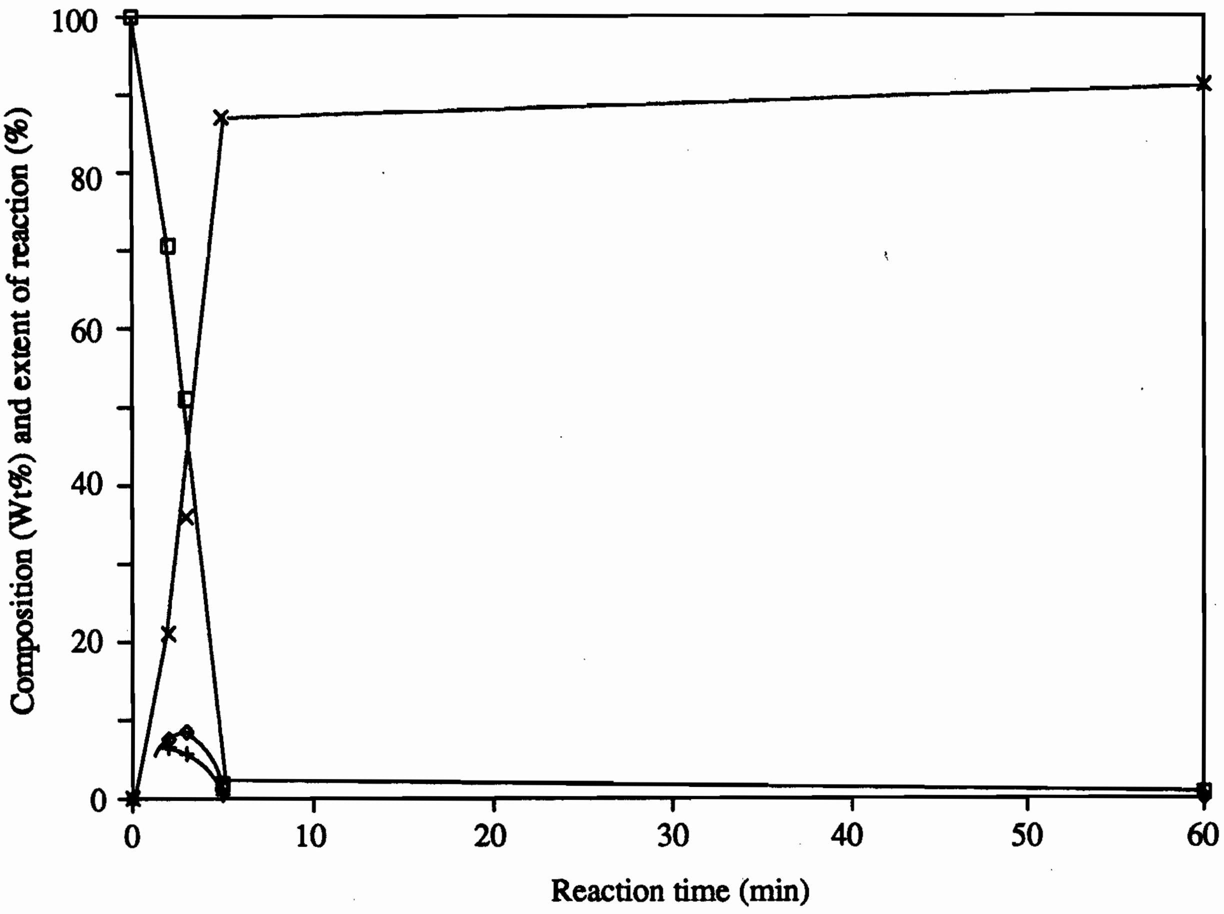

Fig. II-9. Reaction profile for the zirconocene catalyzed $PhSiH_3$ polymerization reaction. $[Cp_2ZrMe_2]$ = 0.08 M in neat $PhSiH_3$ at room temperature. □—monomer; + — dimer; ◇ — trimer; × — the extent of reaction.

As a result of the quick conversion of monomer and lower oligomers to higher oligomers mentioned above, the average molecular weight of the reaction mixture increases rapidly at the beginning of reaction, and then the reaction slows down dramatically after the monomer is consumed. As seen from Fig. II-9, more than 85% of the reactive Si-H groups have reacted within 5 minutes (see the extent of reaction curve). However, the total reaction took 1 - 2 days to go to completion. The extremely slow propagation in the later stages of the reaction indicates again the difficulty in coupling between higher oligomers due to

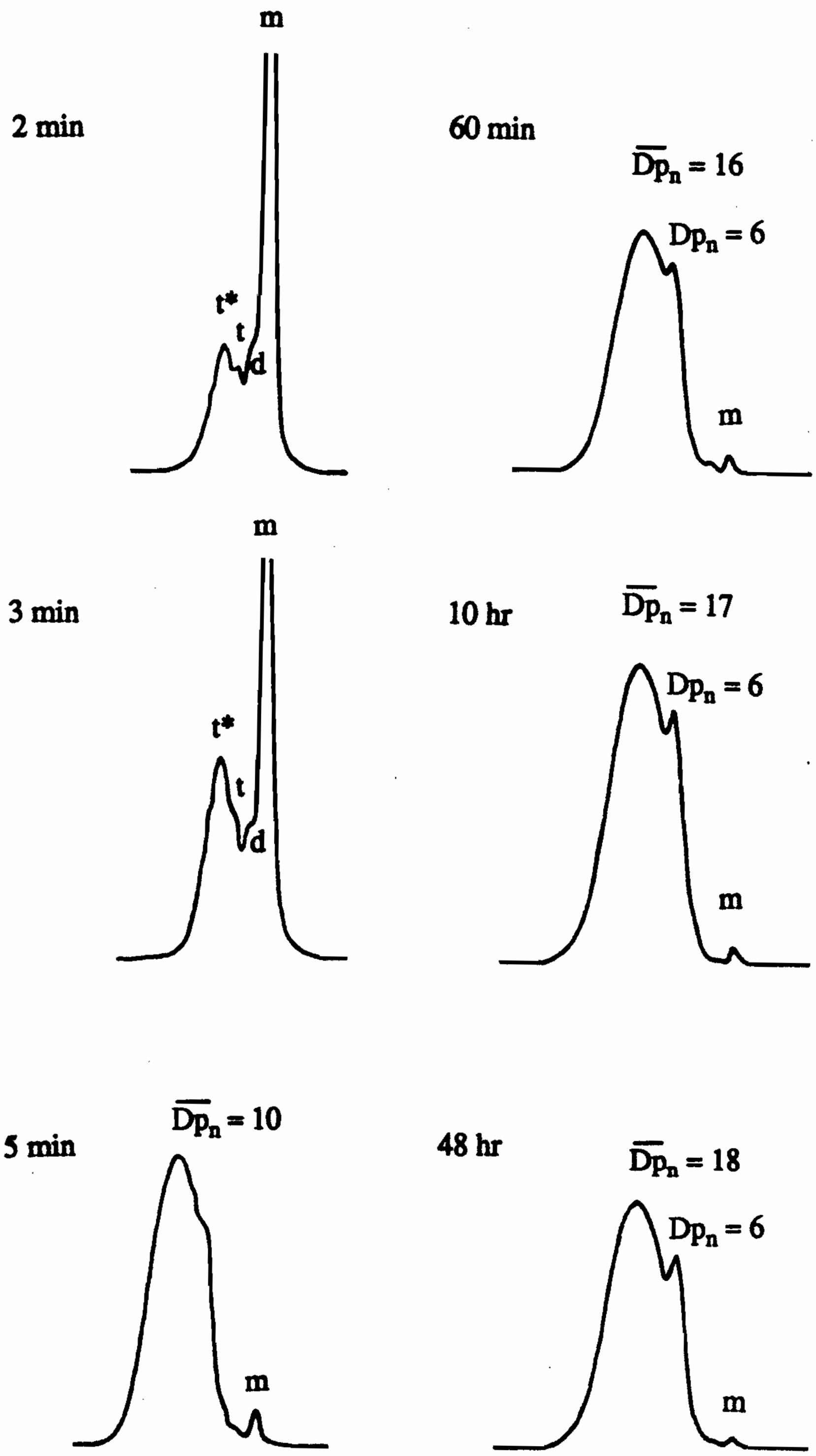

Figure II-10. GPC traces of the zirconocene catalyzed $PhSiH_3$ polymerization reaction mixture at different reaction times. m - monomer; d - dimer; t - trimer; t*- tetramer.

lower concentration of functional groups and higher steric hindrance, as well as lower diffusion rate.

The polyphenylsilane obtained from the zirconocene catalyzed polymerization reaction also gives a bimodal GPC trace similar to that from titanocene system. Although it was previously observed that the polyphenylsilane obtained from the zirconocene system has higher molecular weight than that obtained from titanocene system (34), the present molecular weight results, based on GPC measurements, indicate no evident difference in average molecular weight for the polymers obtained from the two systems.

The cyclization observed in titanocene catalyzed reactions does not seem to happen very much in the zirconocene system. When the polymer obtained from above reaction was dissolved in toluene with active catalyst in the same way as was done with the titanocene system, no evident change in molecular weight was observed after 3 days. However, it has been previously found that very long contact times (20 days) with zirconocene catalyst lead to a reversion of the higher molecular weight fraction to lower molecular weight species with a decrease in the $\overline{Dp_n}$ value of the higher molecular weight fraction (193).

The zirconocene catalyzed polymerization of neat phenylsilane is too fast to be followed very well. In order to have a better understanding of the zirconocene system, the polymerization of phenylsilane in hydrocarbon solvent (which is slower than the neat phenylsilane reaction and can be easily followed) was studied. The reaction profile and GPC traces for a typical polymerization reaction are shown in Fig. II-11 and Fig. II-12 respectively.

The polymerization reaction in solvent behaved in the same way as the neat phenylsilane polymerization at the beginning of reaction. All of the lower oligomers from dimer to hexamer, including cyclohexasilane, were produced at almost the same time, and the concentrations of the dimer and trimer were always several times lower than that of the monomer. With the passage of time, however, the polymerization in solvent showed a very

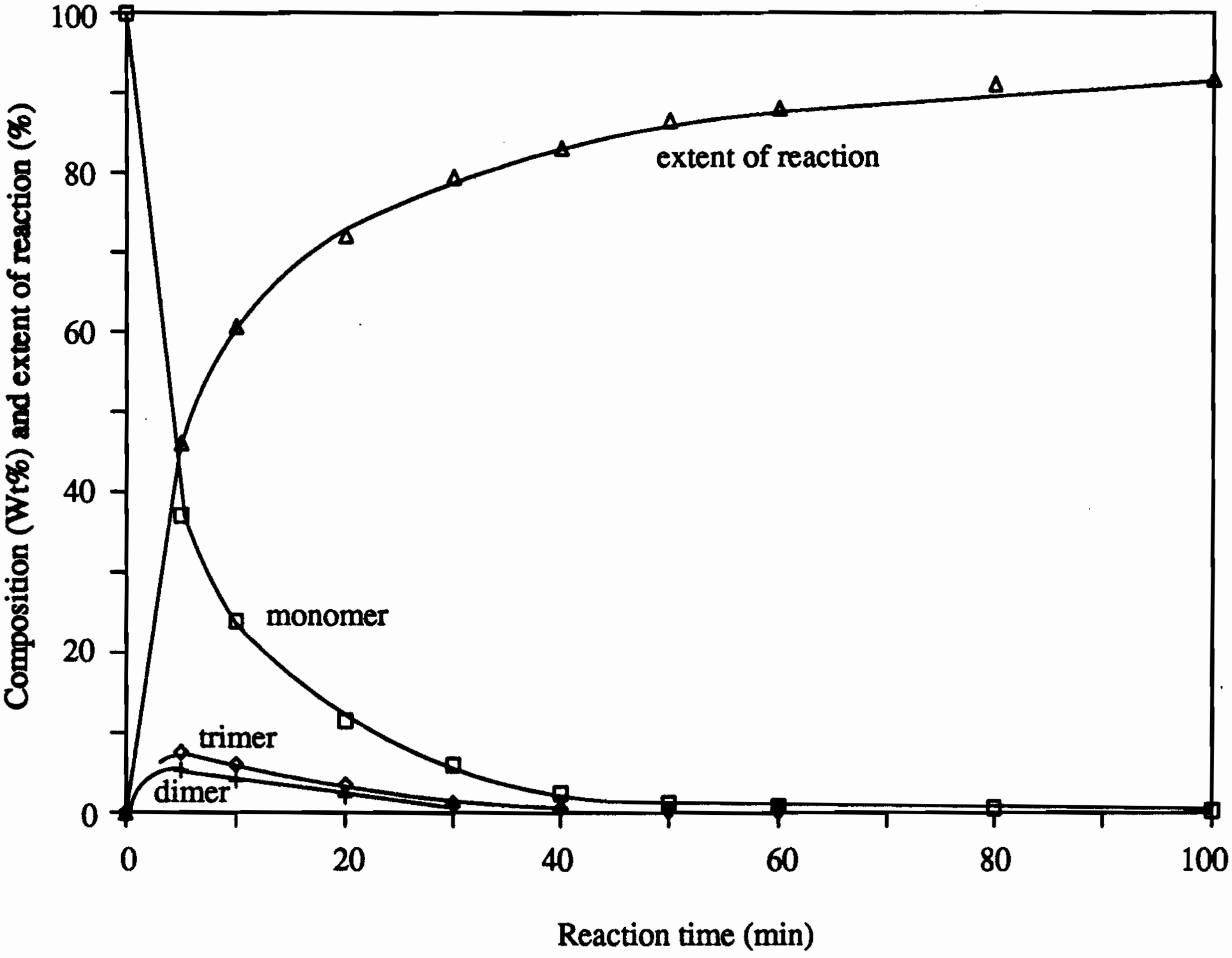

Figure II-11. Reaction profile for the zirconocene catalyzed $PhSiH_3$ polymerization reaction. $[Cp_2ZrMe_2] = 0.04$ M; $[PhSiH_3] = 3$ M in benzene-d_6 at room temperature.

different pattern of chain propagation from the neat phenylsilane polymerization. In the former case, the phenylsilane was first converted to lower oligomers with an average degree of polymerization about 6 and very narrow molecular weight distribution. The subsequent polymerization led to higher oligomers with discontinuous Dp_n values about 12, 18 and 24. This indicates that the higher oligomers were formed mainly from the coupling of hexamer with itself and higher oligomers. ^1H NMR studies indicated that about 30% of the reaction products were cyclosilanes when the average degree of polymerization was about 6. The

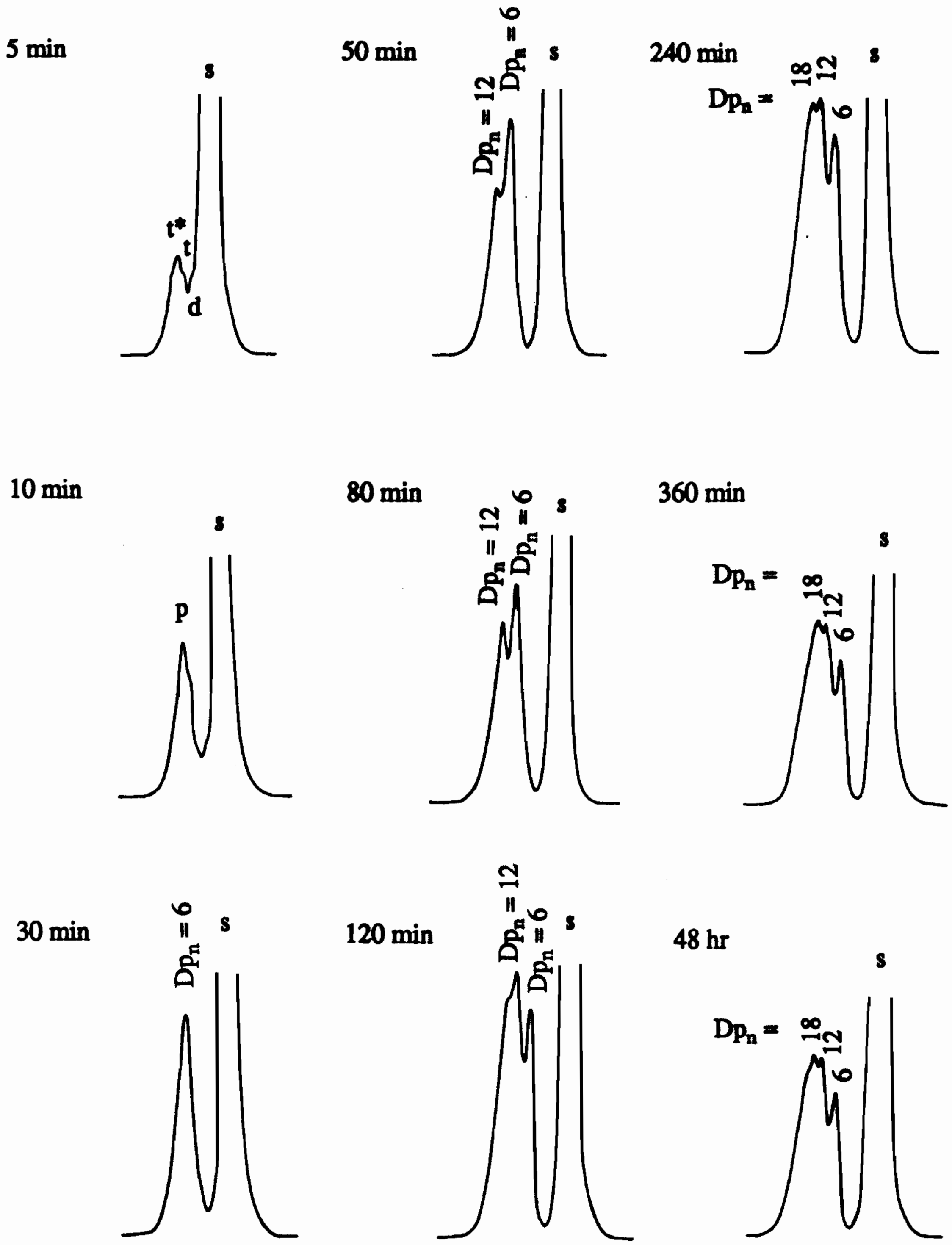

Figure II-12. GPC traces of the zirconocene catalyzed $PhSiH_3$ polymerization reaction mixture at different reaction times. $[Cp_2ZrMe_2] = 0.04$ M; $[PhSiH_3] = 3$ M in C_6D_6 at room temperature. s - solvent; d - dimer; t - trimer; t*- tetramer; p - pentamer.

amount of cyclosilanes increased with time. At the end of the reaction, the percentage of the cyclosilanes was about 45%. However, the GPC measurements showed that the percentage of hexamer in the final reaction mixture was only 20%. These results suggest the existence of cyclosilanes in the higher oligomers if the NMR assignment for cyclosilanes is correct. In the neat silane case, however, the phenylsilane was converted directly to higher oligomers with an average degree of polymerization about 10, and then the molecular weight of the reaction mixture increased gradually and continually. In this case, the percentage of cyclosilanes showed by ^{1}H NMR and GPC is in good agreement.

The reason for the difference in chain propagation process between the two reaction systems appears to be clear. When the polymerization is carried out in solvent, the propagation reaction is slower and the diffusion of the reactants is faster. Consequently, the selectivity of the dehydrocoupling reaction must be higher than that in the neat phenylsilane polymerization and thus the oligomerization of smaller molecules will be largely favored. In addition, the cyclization reaction should be more favored for the same reason. Based on these arguments, and considering the higher reactivity of the lower oligomers, it is not difficult to understand why the reaction mixture was composed mainly of linear and cyclic hexamers with a little other oligomers when the monomer was exhausted. The further coupling of these oligomers will naturally give rise to the observed discontinuous increase in polymer chain length. In the case of neat phenylsilane, the situation is reversed. The lower selectivity and higher reaction rate lead to more chances for the formation and reaction of higher oligomers, and thus lead to a broader molecular weight distribution and a continuous change in molecular weight during the reaction.

II.2.3 Dehydrocoupling reaction of 1,2-diphenyldisilane catalyzed by dimethyl-titanocene and -zirconocene

It has been mentioned in the previous paragraphs that 1,2-diphenyldisilane polymerizes more rapidly than its analogous monomer, phenylsilane, in the mixture of dimer and monomer or in the reaction mixture of phenylsilane polymerization. The polymerization of neat 1,2-diphenyldisilane is also much faster than that of phenylsilane under comparable conditions with titanocene or zirconocene as catalyst. As seen from a typical reaction profile (Fig. II-13) for the polymerization of 1,2-diphenyldisilane catalyzed by titanocene complex, the diphenyldisilane was consumed very quickly and only 1% of it was left after 95 minutes, while it requires 5 - 6 hours for the phenylsilane polymerization to reach the same extent with higher catalyst concentration under the condition of Fig. II-3. However, after the dimer was used up, the polymerization reaction slowed down rapidly and the overall reaction took 1 - 2 days, which is comparable to the phenylsilane polymerization reaction. In order to illustrate the change of the reaction rate with time, a variation curve of the extent of reaction with time is also shown in Fig. II-13 in the same way as above.

Although the dehydrocoupling reaction of diphenyldisilane is much faster than phenylsilane, a clear stepwise polymerization process passing from dimer to tetramer to hexamer etc. has been observed by following the reaction with NMR and GPC. The assignments for these compounds were made based mainly on their GPC retention time. The tetramer was also characterized by ^{1}H NMR (terminal Si-H: 4.56-4.66 ppm, m; internal Si-H: 4.66-4.72 ppm, m). The GPC traces of the titanocene catalyzed diphenyldisilane dehydrocoupling reaction mixture at different reaction times are shown in Fig. II-14. Two points should be stressed from these GPC traces. Firstly, unlike the situation in the phenylsilane polymerization where the concentrations of the dimer and trimer were always several times lower than that of the monomer, large amounts of tetramer formed from the

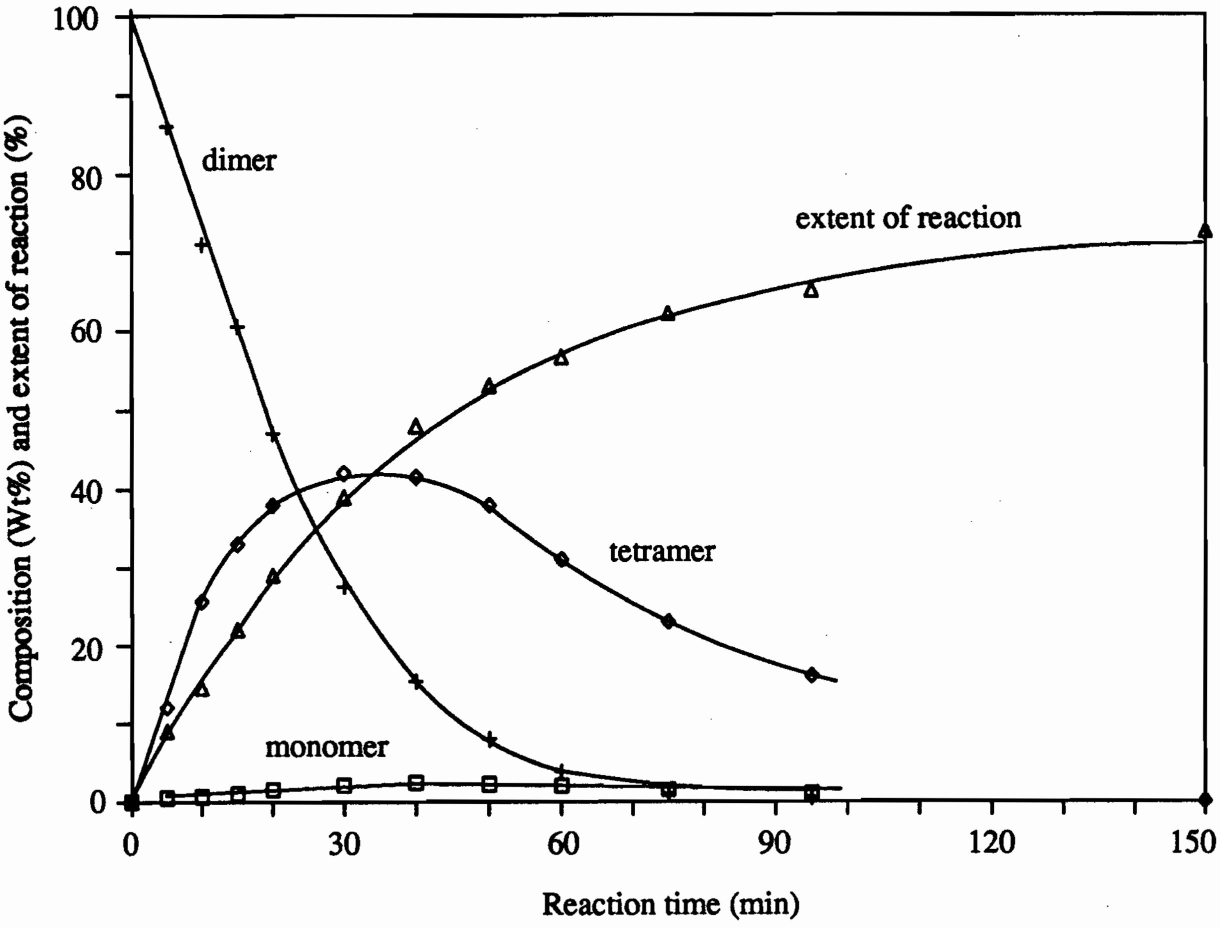

Figure II-13. Reaction profile for the titanocene catalyzed diphenyldisilane polymerization. $[Cp_2TiMe_2] = 0.02$ M in neat diphenyldisilane at room temperature.

dimerization of the starting material were accumulated with the consumption of dimer in this case. When the dimer was almost used up, the reaction mixture was reasonably simple and composed of mainly hexamer, followed by tetramer and octamer with small amounts of other oligomers. Based on these observations, it is evident that the reactivity of the oligomers for the dehydrocoupling reaction decreases rapidly with increasing chain length as a result of the dilution of the reactive end groups and the increase in steric hindrance. Secondly, the average degree of polymerization for the higher molecular weight fraction of

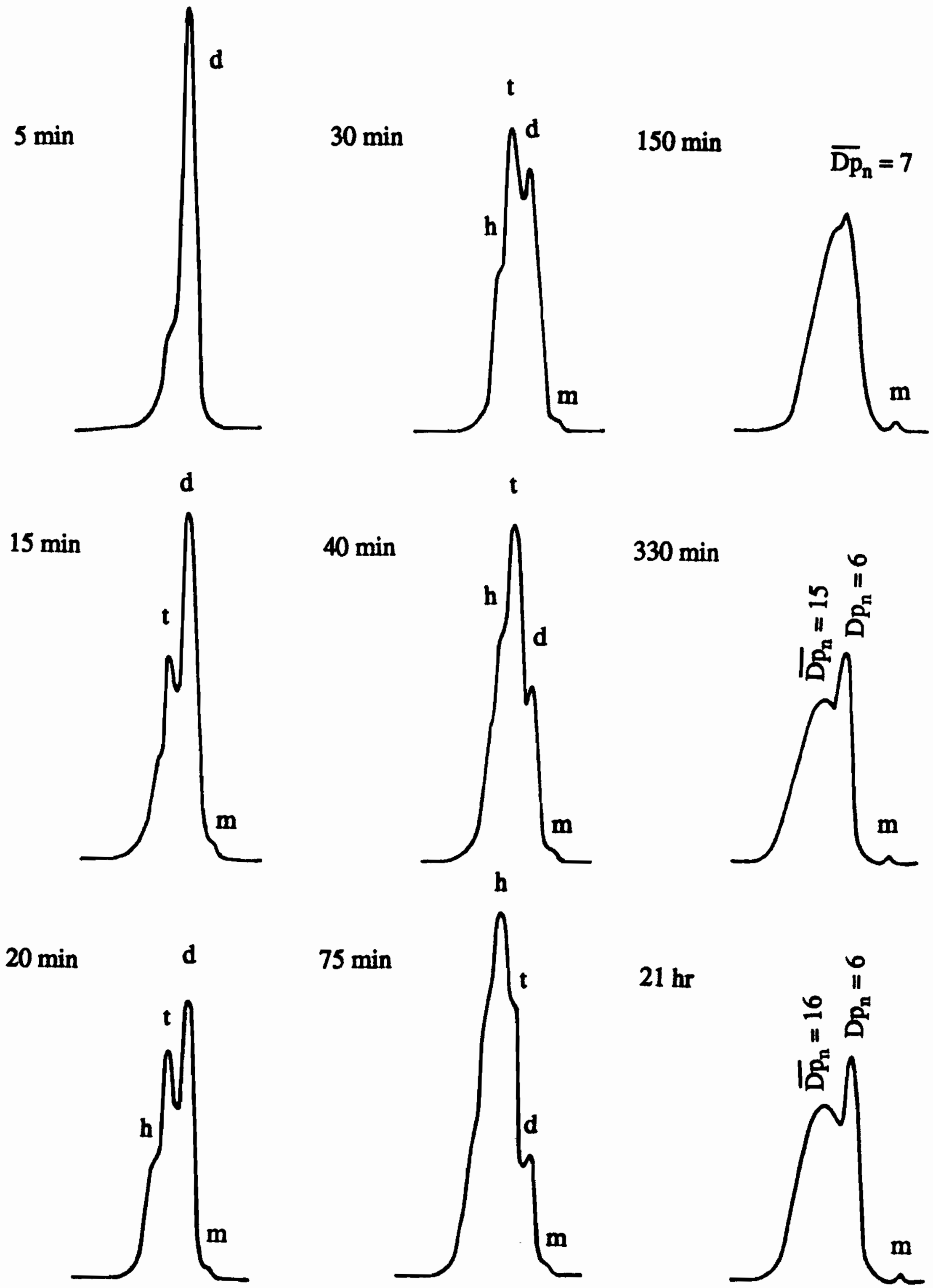

Figure II-14. GPC traces of the titanocene catalyzed diphenyldisilane polymerization reaction mixture at different reaction times. $[Cp_2TiMe_2] = 0.02$ M in neat silane at room temperature. m - monomer; d - dimer; t - tetramer; h - hexamer.

the final products is about 16, which is a little bit lower than that observed in the phenylsilane polymerization. The decrease in the average molecular weight of the linear polysilane is not unexpected. As mentioned above, the reactivity of the oligomers for the dehydrocoupling reaction decreases with the increase of their chain length, and thus the smaller oligomers take part in the reaction favorably. When the smallest oligomer in the reaction mixture reaches some chain length, for example, about 6 silicon atoms for the titanocene catalyzed reaction system, the linear propagation dramatically slows down if it does not stop. If this chain length is defined as the critical chain length for the dehydrocoupling reaction, it is possible that the chain length of one of the reacting silanes in a catalytic cycle might have to be shorter than this critical chain length in order to form an active intermediate (the detailed discussion on the reaction mechanism will be given in Chapter V). In the diphenyldisilane reaction system, as discussed above, dimer, tetramer etc. smaller oligomers are consumed preferentially. Therefore, the molecular weight distribution is narrower during and after the polymerization reaction. As a result, the average molecular weight of the final products is lower. In the phenylsilane reaction system, however, the situation is different from the disilane system. In this case, the reactivity of phenylsilane is lower than that of its lower oligomers, and thus phenylsilane itself is consumed slowly while its lower oligomers are converted to higher oligomers rapidly. As a result, there are more chances for higher oligomers to react with monomer and lower oligomers. Therefore, the molecular weight distribution is wider during the polymerization reaction and the average molecular weight of the final products is higher.

The zirconocene catalyzed polymerization of diphenyldisilane is similar to the titanocene catalyzed reaction, but is much faster. In a polymerization reaction of neat diphenyldisilane with 0.5 mol% of Cp_2ZrMe_2 (0.02 M) as catalyst, the reaction mixture was transformed into a viscous gum with a $\overline{Dp}_n$ value about 7 within 5 minutes. After that, the reaction became very slow and it took about 20 - 30 hours to go to completion. The $\overline{Dp}_n$

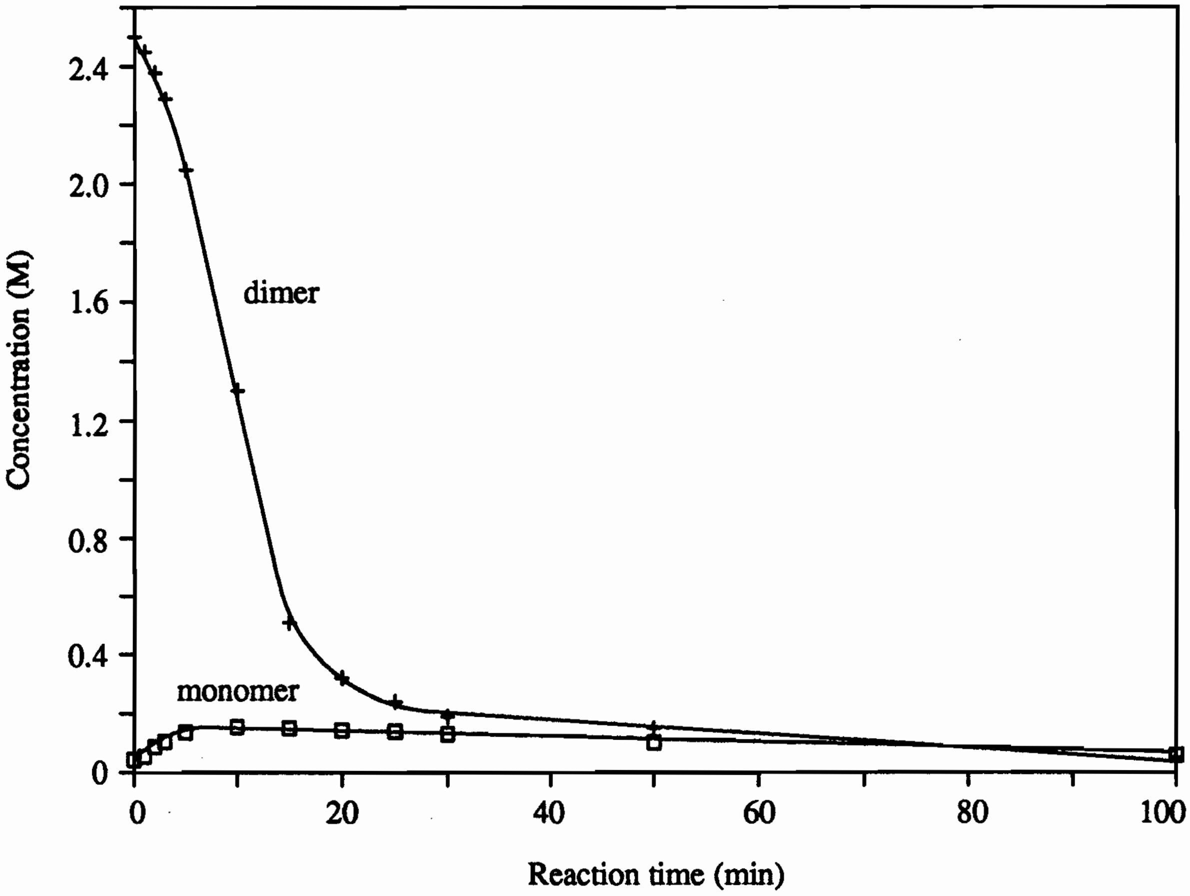

Fig. II-15 Reaction profile for the zirconocene catalyzed polymerization of diphenyldisilane. $[Cp_2ZrMe_2] = 0.025$ M; [silane] = 2.5 M; in benzene-d_6 at room temperature.

value for the higher molecular weight fraction of the final products is about 14-15, the same range as that from the titanocene catalyzed reaction.

Another interesting phenomenon is the formation of a small amount of phenylsilane from the polymerization reaction of diphenyldisilane in both cases of titanocene and zirconocene as seen from Fig. II-13 and Fig. II-15. We attribute this to a redistribution reaction and/or a depolymerization reaction of the diphenyldisilane as shown in eqs. II-4 and II-5. The triphenyltrisilane has also been detected by GC although its concentration in

$$2\ H_2PhSiSiPhH_2 \longrightarrow PhSiH_3 + H_2PhSiSiPhHSiPhH_2 + 3-4\ \text{Kcals} \qquad \text{(II-4)}$$

$$H_2PhSiSiPhH_2 + H_2 \longrightarrow 2\ PhSiH_3 - 2-4\ \text{Kcals} \qquad \text{(II-5)}$$

the reaction mixture is much lower than that of the monomer due to the fact that the trimer reacts more rapidly than monomer. More phenylsilane was produced when the reaction was carried out in a sealed NMR tube than in a open Schlenk tube. This indicates that the formation of phenylsilane is affected by the concentration of hydrogen in the reaction system. The slightly favorable energetics of redistribution reaction result from the trading of an Si-Si bond and a relatively weak Si-H bond of the disilane (190,191) for a new Si-Si bond of comparable strength and the somewhat stronger Si-H bond of the primary silane. The depolymerization reaction II-5 is endothermic by 2-4 Kcals (194), and thus is not expected to occur very much. The possible mechanism for these reactions will be discussed in Chapter V.

II.2.4 Dehydrocoupling reaction of 1,2,3-triphenyltrisilane catalyzed by dimethyl-titanocene and -zirconocene

Although the triphenyltrisilane was also found to polymerize more rapidly than phenylsilane in the reaction mixture of phenylsilane polymerization, the dehydrocoupling reaction of the neat triphenyltrisilane, unlike the case of diphenyldisilane, is considerably slower with both titanocene and zirconocene based catalysts. In a typical titanocene catalyzed reaction as shown in Fig. II-16, after 10 hours of reaction, there still was about 2% unreacted triphenyltrisilane in the reaction mixture, which is much slower than the dehydrocoupling of diphenyldisilane under comparable conditions. The zirconocene catalyzed reaction under the same conditions gave similar results. The slowness of the

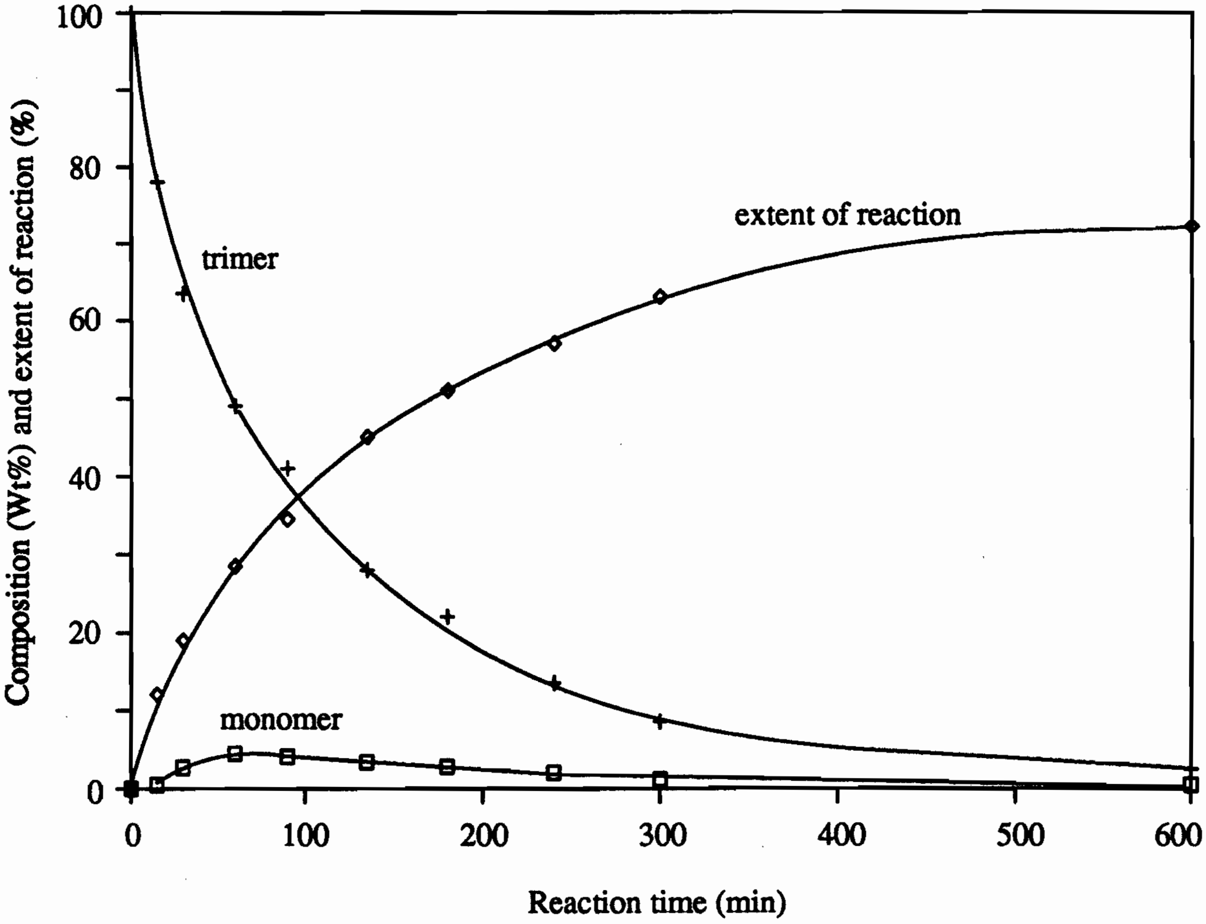

Fig. II-16. Reaction profile for the titanocene catalyzed polymerization of triphenyltrisilane. $[Cp_2TiMe_2]$ = 0.03 M in neat triphenyltrisilane at room temperature.

dehydrocoupling of triphenyltrisilane indicates again the effect of chain length on the reactivity of silanes toward dehydrocoupling. As discussed earlier, in addition to the concentration factor of the functional groups, the reactivity of silanes (toward the dehydrocoupling reaction) is also affected by the electronic and steric factors. When the steric hindrance is smaller, the reactivity is controlled dominantly by electronic effect. Therefore, the dimer, trimer etc. oligomers show higher reactivity than monomer because the Si-H bonds in these oligomers are weaker than the ones in monomer (190,191).

However, with the increase of the steric hindrance from both of the two reacting silanes in a catalytic cycle, the reactivity decreases rapidly. Given the fact that higher oligomers containing more than 10 silicon atoms can be formed rapidly in the zirconocene catalyzed phenylsilane polymerization, the slowness of triphenyltrisilane polymerization suggests that the existence of monomer and dimer in the reaction system is important to give a fast polymerization. In other words, the steric effect of the two reacting silanes in a catalytic cycle is different and one is more important than the other. That is, if one of the two reacting silanes is monomer or dimer, the reaction is faster even though the other is a larger oligomer such as decamer; but if both of the two reacting silanes are trimers or larger oligomers, the reaction is slower.

The dehydrocoupling reaction of triphenyltrisilane has also been found to be accompanied by a slow redistribution reaction and/or a depolymerization reaction as shown in eq. II-4 and II-5. The amount of the monomer produced in the trisilane polymerization is a little more than that produced in the diphenyldisilane reaction, but never rises to more than a few per cent of the initial amount of the trimer. A trace of dimer can also be observed by NMR during the trisilane polymerization.

In both catalytic systems, hexamer is formed first, followed by enneamer and small amounts of higher oligomers. The GPC traces for the titanocene catalyzed reaction mixture at different reaction times are shown in Fig. II-17. Because of the large difference in reactivity between trimer and hexamer, the hexamer is accumulated in large amounts with the consumption of the trimer. The conversion of the hexamer into higher oligomers is very slow. After the trimer is completely consumed, the GPC traces show little further change in the average molecular weight of the reaction mixture. The final average degree of polymerization for both catalytic systems is around 8-9 and the products consist mainly of hexamer and enneamer. ^1H NMR spectra indicate that about 30% - 35% of the final products are cyclosilane if the ^1H NMR assignment for the cyclosilane is correct. This

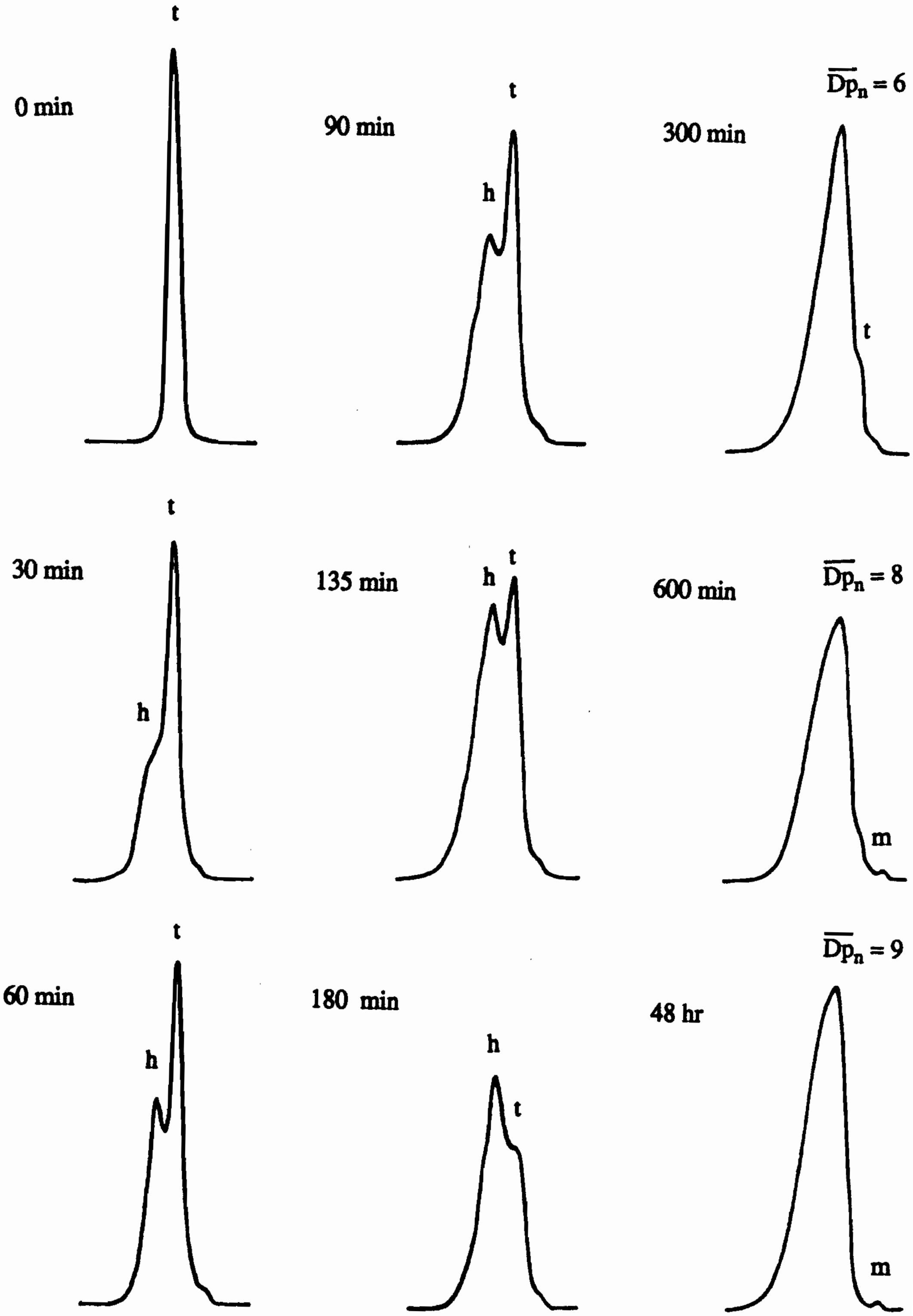

Figure II-17. GPC traces of the titanocene catalyzed triphenyltrisilane polymerization reaction mixture at different reaction times. $[Cp_2TiMe_2] = 0.03$ M in neat silane at room temperature. m - monomer; t - trimer; h - hexamer.

suggests that most or probably all of the hexamer in the final products are cyclosilane. The decrease in the average molecular weight of the polymerization products with the increase in the chain length of the starting material is what has been expected, and the reason for this has been discussed in last section.

II.3 EXPERIMENTAL

II.3.1 General procedures

All reactions were carried out in three-necked flasks or Schlenk tubes under argon (U.H.P., Linde) by using standard inert atmosphere techniques (195). Solvents were freshly distilled and degassed before use. Degassing was generally accomplished by the use of three freeze-pump-thaw cycles. All glassware was dried at 115°C and cooled under vacuum. Flasks or Schlenk tubes were evacuated and filled with argon tree times before or after reagents were put in, depending on the property of the reagents. Solvents and liquid reagents were transferred by syringe. All polymerizations catalyzed by titanocene and zirconocene complexes were carried out at room temperature in 20 mL Schlenk tubes. Typically, the tubes were charged with catalyst, degassed solvent, and the appropriate organosilane. The reaction mixture was periodically sampled and the course of the reaction was followed by ^{1}H NMR, GC and GPC. The catalyst was removed from the reaction mixture by passing it through a Florisil column. Florisil (100 - 200 mesh) was purchased from Aldrich.

^{1}H NMR spectra were recorded on a Varian XL-200 spectrometer and all chemical shifts are in δ ppm units. Shift values are accurate to ± 0.002 ppm. All NMR spectra were measured at ambient temperature (293 ± 2K) unless otherwise indicated. Variable temperature controllers calibrated with methanol and ethylene glycol gave temperatures that are considered accurate to ± 0.5K.

The GPC measurements were performed on a Varian 5000 liquid chromatograph interfaced to a Varian Vista 402 data station and equipped with a Waters Associates 10^3 Å Ultrastyragel column. All GPC measurements were carried out at 30.00 ± 0.05°C, using air-free chromatographic grade THF as solvent. Instead of polystyrene, the phenylsilane monomer, dimer, trimer, tetramer and hexamer were used as calibrants. Although the molecular weight range of these phenylsilane oligomers is not large enough to give very accurate results for higher molecular weight polymers, the molecular weight values calculated with these phenylsilane oligomer standards should be reasonably accurate because all the samples analyzed have quite low molecular weight ($Dp_n < 20$) and very narrow molecular weight distribution.

Gas chromatography (GC) analyses of the monomer, dimer and trimer from polymerization reactions were carried out on a Shimadzu GC-8A chromatograph equipped with a H_2 flame detector and a DB-5 30 m capillary column. Stationary phase: 95% dimethyl-, 5% diphenylpolysiloxane. Injection temperature 300°C. Column temperature 100-300°C, programmed at 8°C per min. Carrier gas flow rate 0.5 mL min^{-1}. Calibration was carried out with pure samples of these compounds.

Infrared spectra for polysilanes as films between KBr plates were recorded on an Analect AQS-20 fourier-transform infrared (FT-IR) spectrophotometer referenced using the red line (632.8 nm) of a He/Ne laser. A triglycine sulfate (TGS) detector was used with a standard resolution of 4 cm^{-1}.

II.3.2 Chemicals

Toluene, hexanes, cyclohexane and tetrahydrofuran (THF) were refluxed over sodium/benzophenone and collected by distillation under nitrogen. Subsequent freeze-thaw degassing was performed under argon. Anhydrous diethylether was obtained from Fisher Scientific Co., and used straight from the freshly opened can. Benzene-d_6 and toluene-d_8 were purchased from Merk, Sharp and Dohme, and were generally used as received after degassing and purging with argon. For polymerization reactions, deuterated solvents were trap-to-trap distilled from sodium/benzophenone before use. Methyllithium was purchased from Aldrich as a 1.4 M solution in diethylether and used as received. $LiAlH_4$ was obtained from Aldrich. $PhSiCl_3$ was purchased from Petrarch Chemical Co. and used as received to prepare $PhSiH_3$ by a literature method (196). Diphenyldisilane and triphenyltrisilane were synthesized using the vanadocene catalyzed oligomerization of phenylsilane, and purified by microdistillation under high vacuum (90). Cp_2TiCl_2 and Cp_2ZrCl_2 were purchased from Aldrich and used as received. Cp_2TiMe_2 was prepared according to a published procedure (112), and after recrystallization it was stored in the mother liquor at -20°C in the dark. Cp_2ZrMe_2 was prepared from Cp_2ZrCl_2 and MeLi in diethylether according to a literature procedure (113). Purification of the material was accomplished by sublimation under high vacuum (10^{-4} torr) at 90°C.

II.3.3 Polymerization reactions

1. Cp_2TiMe_2 catalyzed polymerization of $PhSiH_3$

A sample of dimethyltitanocene (67 mg, 0.321 mmol) was placed in a Schlenk tube, equipped with a rubber septum and a magnetic stirrer. After the Schlenk tube was purged with argon, $PhSiH_3$ (4.0 mL, 32.1 mmol) was added and the catalyst was rapidly dissolved. The reaction took place immediately with a color change from orange to blue/black, accompanied by rapid gas evolution. The reaction mixture was periodically sampled and analyzed by ^1H NMR, GC and GPC. The concentration was estimated by GC for monomer, dimer and trimer; and also by NMR for monomer and dimer. The results from the two methods are in good agreement. After about 5 hours, the reaction mixture became very viscous and could not be stirred, and after 48 hours, the reaction had essentially ceased.

2. Cp_2ZrMe_2 catalyzed polymerization of $PhSiH_3$

In a typical reaction, dimethylzirconocene (80 mg, 0.32 mmol) was put in an argon-filled Schlenk tube, equipped as above, and then $PhSiH_3$ (4.0 mL, 32.1 mmol) was injected into the Schlenk tube. The catalyst was rapidly dissolved and gas evolution occurred immediately, accompanied by a progressive color change to orange. The reaction was slower at the beginning and then became faster and faster. After 3 minutes, the reaction got violent and the reaction mixture became a viscous gel within several minutes. Then the reaction slowed down rapidly, but continued for about another 48 hours. The reaction was followed in the same way as above.

As an example of the polymerization carried out in a solvent, $PhSiH_3$ (1.5 mL, 12.0 mmol) was added to a solution of Cp_2ZrMe_2 (40 mg, 0.16 mmol) in benzene-d_6 (2.5 mL) in a Schlenk tube. After a few seconds, the reaction took place with gas evolution, accompanied by a slow color change from colorless to orange. The gas evolution got faster with the color change at the beginning and then slowed down after about half an hour. The reaction was followed for 48 hours in the same way as above.

3. Diphenyldisilane polymerization reactions

In the titanocene catalyzed reaction, a sample of diphenyldisilane (3.00 g, 14.0 mmol) was injected into a Schlenk tube which had previously been charged with Cp_2TiMe_2 (14.5 mg, 0.07 mmol). The reaction took place immediately, accompanied by a color change and rapid gas evolution like the case of phenylsilane. After about two hours, the reaction mixture became too viscous to be stirred. The reaction was followed by ^1H NMR and GPC for 40 hours. The concentration was estimated by NMR for dimer and by GPC for tetramer.

The zirconocene catalyzed polymerization reaction was carried out under conditions identical with those used for the titanocene catalyzed reaction, using 18 mg of Cp_2ZrMe_2

(0.07 mmol) instead of Cp_2TiMe_2. In this case, the reaction was violent at the beginning and the reaction mixture became highly viscous in 2 - 3 minutes. After that, the reaction continued very slowly. This reaction was followed in the same way as above.

The zirconocene catalyzed reaction was also carried out in benzene-d_6. In this case, the Schlenk tube was charged with 20 mg of Cp_2ZrMe_2 (0.08 mmol) and a solution of diphenyldisilane (1.0 mL, 4.0 mmol) in benzene-d_6 (2 mL). 0.1 mL of cyclohexane was added as an internal standard in order to calculate the amount of monomer more accurately. This reaction was followed by NMR.

4. Triphenyltrisilane polymerization reactions

In a typical titanocene catalyzed reaction, a sample of Cp_2TiMe_2 (19.5 mg, 0.094 mmol) was dissolved in triphenyltrisilane (3.00 g, 9.36 mmol) in a Schlenk tube. The reaction was carried out and followed in the same way as the diphenyldisilane reactions. In the zirconocene case, 23.5 mg of Cp_2ZrMe_2 (0.094 mmol) was used instead of Cp_2TiMe_2, and the reaction was performed under the same conditions as the titanocene case. In both cases, the gas evolution throughout the course of the polymerization was slow, and after the reaction had essentially stopped (48 hours), the reaction mixture was still a viscous gum, while the polyphenylsilanes obtained from the polymerization of monomer or dimer were brittle glasses.

5. Cyclization of polyphenylsilane

Polyphenylsilane (1 g), obtained from the titanocene catalyzed phenylsilane polymerization, was dissolved in 2 mL of previously degassed toluene without destroying the active catalyst and the mixture was kept to react continuously. The reaction was followed by ^1H NMR, IR and GPC.

Chapter III

Synthesis, characterization and pyrolysis of polymethylsilane

III.1 INTRODUCTION

Polyorganosilanes have attracted a lot of attention to their potential applications recently, in particular as precursors to SiC via pyrolytic decomposition (10,11,59,197-203). Silicon carbide is a useful ceramic material made commercially by the high-temperature solid-state reaction between silicon dioxide and graphite. Material prepared by this method is infusible, intractable, and not applicable for the preparation of fibers or films. The original process for thermal generation of SiC ceramic from polysilane precursors was reported by Yajima and Hayashi (10,11). The starting material they used is the insoluble polydimethylsilane. The Yajima process entails essentially a two-step thermal conversion as shown in eq. I-6. The low temperature pyrolysis converts the intractable polydimethylsilane into a soluble carbosilane which can be processed into films or fibers. These films or fibers are then surface oxidized at 350-400°C to provide dimensional stability for further processing and pyrolyzed to 1300°C in an inert atmosphere to produce β-SiC crystals.

More recently, West *et al.* indicated that formable polysilanes, such as poly(phenylmethylsilane) and poly(phenylmethylsilane-*co*-dimethylsilane), can be converted to silicon carbide directly, without the necessity for preformation of polycarbosilane. The polysilanes can be formed into fibers, crosslinked by irradiation with UV light, and then pyrolyzed directly to silicon carbide in vacuum (36,60).

The considerable research in the area of pyrolytic transformations of polysilane derivatives to silicon carbide has demonstrated that this method has unquestionable practical utility. Theoretically, the ideal precursor to SiC is polymethylsilane $[MeSiH]_n$

Table III-1. Theoretical maximum ceramic yields for some polyorganosilanes

Polymer	Maximum SiC yield (%)
$[Me\text{-}Si\text{-}H]_n$	91
$[Me\text{-}Si\text{-}Me]_n$	69
$[Ph\text{-}Si\text{-}Me]_n$	33
$[Hex\text{-}Si\text{-}Me]_n$	31

(PMS). The maximum theoretical SiC yields for some polyorganosilanes are listed in Table III-1. In principle, the condensation of CH_3SiHCl_2 with an alkali metal could give polymethylsilane. In practice, however, the SiH function is also reactive toward alkali metals under the conditions of the condensation (204-206). The catalyzed dehydrocoupling reaction of primary organosilanes provides a possible route to prepare polymethylsilane since this reaction works reasonably well for higher n-alkylsilanes. Our initial efforts, which were confined to working at atmospheric pressure by bubbling methylsilane gas into reaction solution, gave no convincing evidence for the formation of polymethylsilane, even after very long reaction times (ca. 1 week). However, working at methylsilane pressures around 10 atmospheres gave reasonable reaction rates and essentially quantitative conversion. The polymer produced under carefully controlled conditions is completely soluble in most organic solvents, and contains considerably more high molecular weight material than is characteristic of other polyorganosilanes produced by this type of dehydrocoupling reaction. The pyrolysis of polymethylsilane gave relatively pure β-SiC in high yield. The polymer first undergoes a major rearrangement from polysilane to polycarbosilane at 400°C, and the resulting polycarbosilane decomposes to SiC above 400°C. The transformation of the amorphous SiC to β-SiC occurs at temperatures about 1000°C. To our knowledge, this is one of the best precursors, if not the best one, to SiC found to date.

III.2 RESULTS AND DISCUSSION

III.2.1 The polymerization reaction

So far, only oligomers with 10 to 20 silicon atoms have been obtained from the dehydrocoupling of phenylsilane and cyclohexylsilane (33). The dehydrocoupling of butylsilane gives even smaller oligomers (93). However, catalytic dehydrocoupling , using either dimethyltitanocene or dimethylzirconocene as catalyst, is an efficient method for the synthesis of polymethylsilane. Using this methodology, completely hydrocarbon-soluble polymethylsilane can be prepared with >90% yield by carefully controlling the reaction conditions. Insoluble material is, however, obtained if the reaction is conducted for too long. The results of a number of polymerization reactions under different conditions are given in Table III-2 and Table III-3.

Table III-2. Summary of methylsilane polymerization reactions.

Run	Solvent	Catalyst	CH_3SiH_3 (psi × L)	Temp. (°C)	Time (day)	Amount of PMS (g)	Yield (%)
1	5mL cyclohexene + 2mL toluene	50mg DMT	120 × 0.12	20	6	1.52	90
2	"	"	130 × 0.12	20	9	1.82	~100
3	"	"	140 × 0.12	20	12	1.96	~100
4	"	"	120 × 0.12	45	4	1.68	~100
5	"	"	110 × 0.12	65	1	1.53	~100
6	4mL toluene	"	100 × 0.12	20	9	0.37	26
7	same as run 1	60mg DMZ	110 × 0.12	20	5	1.43	92
8	"	"	130 × 0.12	20	7	1.81	~100
9	"	"	125 × 0.12	20	9	1.75	~100
10	"	"	100 × 0.12	65	1	1.40	~100
11	4mL toluene	"	110 × 0.12	20	7	0.99	64
12	20mL cyclohexene + 5mL toluene	300mg DMZ	120 × 1	20	20	13.1	88
13	25mL cyclohexene	200mg DMZ	130 × 1	45	16	15.0	92
14	20mL cyclohexene	120mg DMZ	85 × 1	45	14	9.50	91

Table III-3. Molecular weight properties and IR data of a series of polymethylsilanes.

Sample[a]	Higher MW fraction			Cyclics		Insoluble material(%)	I_δ / I_v [c]
	$\bar{M}_w$	$\bar{M}_n$	$\bar{M}_w/\bar{M}_n$	M_w[b]	% of weight		
1	1590	790	2.01	160	0.5		0.43
2	6350	1200	5.30	160	1.6	3	0.37
3	10100	1250	8.10	160	4.1	11	0.31
4	7890	1240	6.36	160	0.5	13	0.33
5	12990	1260	10.3	160	0.5	31	0.29
6	830	560	1.48	160	2.5		0.54
7	1730	800	2.16				0.39
8	6010	1080	5.56	160	0.8		0.36
9	9990	1350	7.40	160	2.5	64	0.30
10			insoluble gel			100	0.18
11	1020	620	1.65	160	2.0		0.51

[a] The samples are from the corresponding reaction in Table III-2.

[b] Peak molecular weight. [c] Relative intensity of the δ_{SiH2} band and the ν_{SiH} band.

In order to increase reaction rate and to avoid the inconvenience of large hydrogen pressures at the end of the reaction, it is necessary to take advantage of the simultaneous co-hydrogenation of cyclohexene to remove the hydrogen (87). This procedure works with both dimethyltitanocene and dimethylzirconocene in the present system, even though with other silanes, working at ambient temperature and pressure, dimethylzirconocene does not catalyze hydrogenation fast enough to suppress hydrogen evolution. Although the scavenging of hydrogen seems not to be essential to the polymerization reaction, the rates of reaction and the composition of the polymer are sensitive to the presence or absence of cyclohexene. As seen from Table III-2, in the absence of cyclohexene, the polymerization reaction proceeds to a conversion of about 25% for the titanocene system after 9 days, and about 65% for the zirconocene system after 7 days. In both cases, the molecular weight of the obtained polymethylsilane is lower. In the presence of cyclohexene, the polymerization reactions are much faster in both catalyst systems than in the absence of cyclohexene.

The fact that the polymerization of methylsilane proceeds, even in the presence of hydrogen pressure, is the first experimental confirmation of the exothermicity of the organosilane dehydrocoupling reaction. Calculations based on available thermodynamic data (190,191,194) suggest that the silane dehydrocoupling reaction should be exothermic to the extent of ca. 2-4 kcals/mol, which is certainly not out of line with the present results.

The polymerization of the methylsilane monomer is very slow at room temperature. The reaction profiles for two typical polymerization reactions, catalyzed by titanocene and zirconocene respectively, are shown in Figure III-1. After the methylsilane monomer is consumed, however, the molecular weight of the polymer increases rapidly (compare No.1 with 2, 3, and 7 with 8, 9 in Table III-3). The slowness of the methylsilane polymerization is in part due to the low reactivity and in part due to the low solubility of the methylsilane monomer. In all of the previously reported studies of catalyzed dehydrocoupling of organosilanes, monomer concentrations of about 3 to 10 M have been used to achieve reasonable reaction rates under ambient conditions. With monomers whose boiling points are well above room temperature this presents no problem, but with a monomer, like methylsilane, which is a gas at room temperature and whose solubility in hydrocarbon solvents is about 0.1 M at one atmosphere pressure, it is necessary to work at higher pressure. Our experiments were carried out in what may be considered to be the low end of the useful pressure (rate) scale and more useful rates would require pressures of an order of magnitude greater. The lower reactivity of alkylsilanes than arylsilanes has been reported previously (34). The reactivity of n-hexylsilane toward dehydrocoupling reaction is about 10 times lower than that of phenylsilane.

For both catalyst systems, during the course of polymerization of methylsilane, no detectable amounts of dimer, trimer etc. oligomers in either gas phase or solution has been

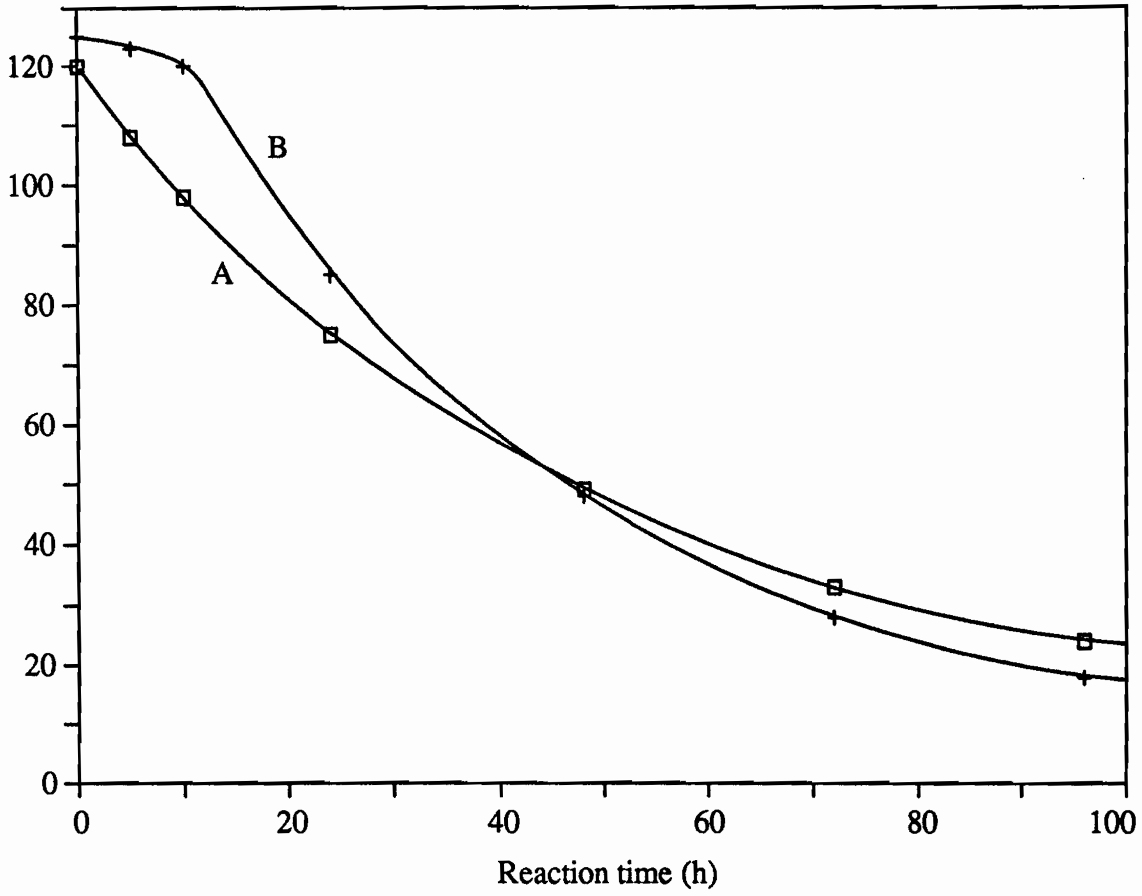

Figure III-1. Reaction profiles for methylsilane polymerizations catalyzed by (A) DMT and (B) DMZ, respectively. [catalyst] = 0.034 M in a mixture of 5 mL of cyclohexene and 2 mL of toluene. Volume of the reactor = 120 mL. Room temperature.

observed by GC analysis. GPC measurements indicate that the number average molecular weight of polymethylsilane is around 600 D (styrene equivalents) and does not change very much with time in the earlier stages of polymerization when there is a large amount of methylsilane in the reaction system. We attribute the lack of small oligomers in the reaction system to the fact that these small oligomers are more reactive than monomer and polymerize to larger oligomers rapidly. The higher reactivity of small oligomers than monomer has been observed in phenylsilane polymerization. Although small oligomers can be observed during the polymerization of phenylsilane and butylsilane (93), it has been found that the concentrations of dimer, trimer etc. oligomers are always several times lower than that of monomer in the phenylsilane system.

Although the rates of reaction under the conditions used in the present investigation are less than desirable for a practical application, it is clear that rates can easily be increased by working at higher pressure. We have not pursued this option since it requires, for reasons of safety, a major increase in the sophistication and cost of equipment. Rates of reaction can also be increased by raising the temperature. At first sight it appears that increasing temperature will diminish the selectivity for linear polymerization and it is difficult to avoid the production of insoluble polymer at higher temperature. However, after having carefully investigated the results in Table III-2 and III-3, we find that cross linking to form insoluble gel can occur only after the methylsilane monomer has been totally consumed. If there is an excess of methylsilane in the reaction system after cyclohexene has been consumed, the cross linking does not occur even at higher temperature. Otherwise, even at room temperature, if the reaction is continued for too long, gelation occurs to give a puffy, elastic gel. Also, storage of the soluble polymer in the solid state without first removing the catalyst eventually results in an almost completely insoluble material.

Both dimethyltitanocene and dimethylzirconocene catalyze the cross-linking reaction. However, dimethylzirconocene is a much more powerful catalyst. Some experimental observations on the cross-linking behaviour are presented in Table III-4. The higher molecular weight and the cross-linking are unexpected since higher alkylsilanes were earlier found to be less reactive than the arylsilanes (34). This cross-linking behaviour may facilitate the transformation of the polymer into SiC fibres since dense cross-linking is a prerequisite to high ceramic yields via the pyrolysis of polyorganosilanes.

Since the experimental evidence clearly indicates that cross-linking is taking place in these reactions, it is reasonable to conclude that the backbone SiH functions are reacting,

Table III-4. Observations on the cross-linking behaviour of polymethylsilane

Sample[a]	Catalyst	Observed Phenomena[b]			
		1 day	3 days	5 days	10 days
2	DMT			60% insoluble	100% insoluble
8	DMZ	100% insoluble	brittle glass		

[a] Samples are from the corresponding reaction in Table III-2. [b] The cross-linking behaviour was observed under argon after the solvent was removed.

although at a much lower rate than SiH_3 and SiH_2 functions. The initial hierarchy of reactions that can probably occur is :

$$SiH_3/SiH_3 > SiH_3/SiH_2 > SiH_2/SiH_2 > SiH_2/SiH > SiH/SiH$$

As the reaction proceeds, concentration effects lead to a diminishing importance of the reactions to the left of this series, and an increasing importance of the reactions to the right. The production of insoluble gel, due to reaction of the SiH functions along the polymer backbone, is a feature unique to polymethylsilane among the polyorganosilanes so far investigated. The phenomenon has, however, been previously encountered in the polymerization of phenylgermane (207). Since methylsilane does not polymerize at a significantly greater rate than other organosilanes, the origin of the cross-linking reaction is probably an increase in the relative rate of reaction of the tertiary SiH functions. This in turn is probably due to the smaller steric effect of the CH_3 group, relative to other organic substituents. It is already well established that the reactions of silanes with group 4 metallocene derivatives are quite sensitive to steric effects (89).

III.2.2 IR spectra of polymethylsilane.

The IR spectrum of polymethylsilane is shown in Figure III-2 and listed in Table III-5. Assignments are made by comparing the spectrum with those for polyphenylsilane (88,89) and permethylcyclosilanes (17), which have been previously investigated. This spectrum shows the expected features of the $\nu_{C\text{-}H}$, $\nu_{Si\text{-}H}$, $\nu_{Si\text{-}C}$, $\nu_{Si\text{-}Si}$ and $\delta_{H\text{-}Si\text{-}H}$. The absorptions below 550 cm^{-1} are assigned to Si-Si stretching modes which are known to lie in this frequency range. The bands between 600-750 cm^{-1} are assigned as Si-C stretching modes by analogy with previous work for dimethylsilane. The band at 930 cm^{-1} can be assigned to the bending mode of a SiH_2 group. The presence of this band indicates that the polymer chains are terminated at least in part by $MeSiH_2$ groups. The relative intensities of the $\nu_{Si\text{-}H}$ band at 2075 cm^{-1} and the $\delta_{H\text{-}Si\text{-}H}$ band at 930 cm^{-1} change with molecular weight

Table III-5. Infrared absorptions of polymethylsilane.

Absorption, cm^{-1}	Assignment
2956(m)	antisym C-H stretch
2894(m)	sym C-H stretch
2075(s, br)	Si-H stretch
1406(m)	CH_3 deformation
1247(m)	Si-CH_3 deformation
930(m)	SiH_2 deformation
865(vs)	CH_3 rocking
764(s, br)	antisym Si-C stretch
685(s) 650(s)	sym Si-C stretch
510(w) 483(w)	Si-Si stretch

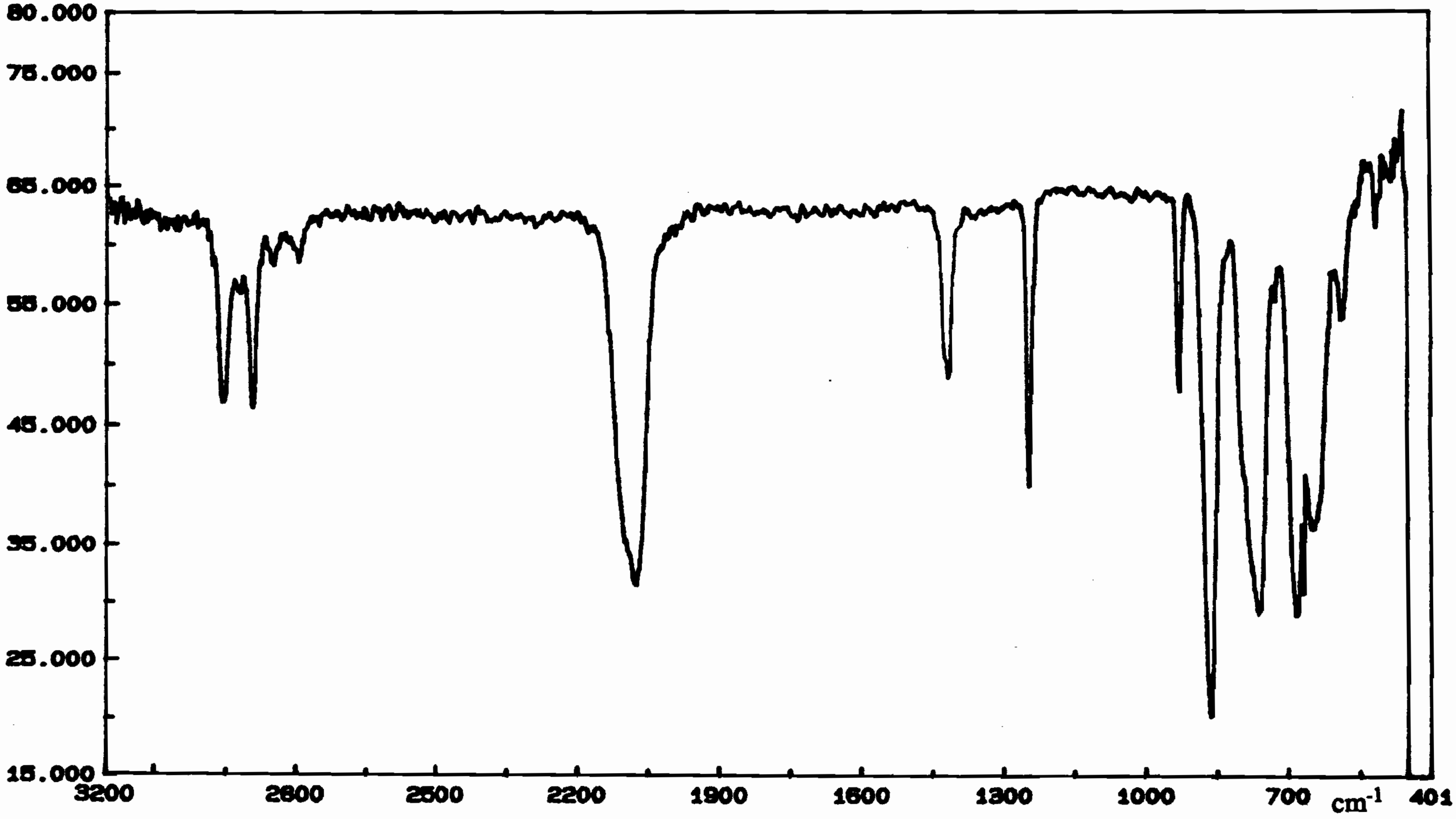

Figure III-2. IR spectrum of polymethylsilane. Thin film of pure material supported on KBr plate.

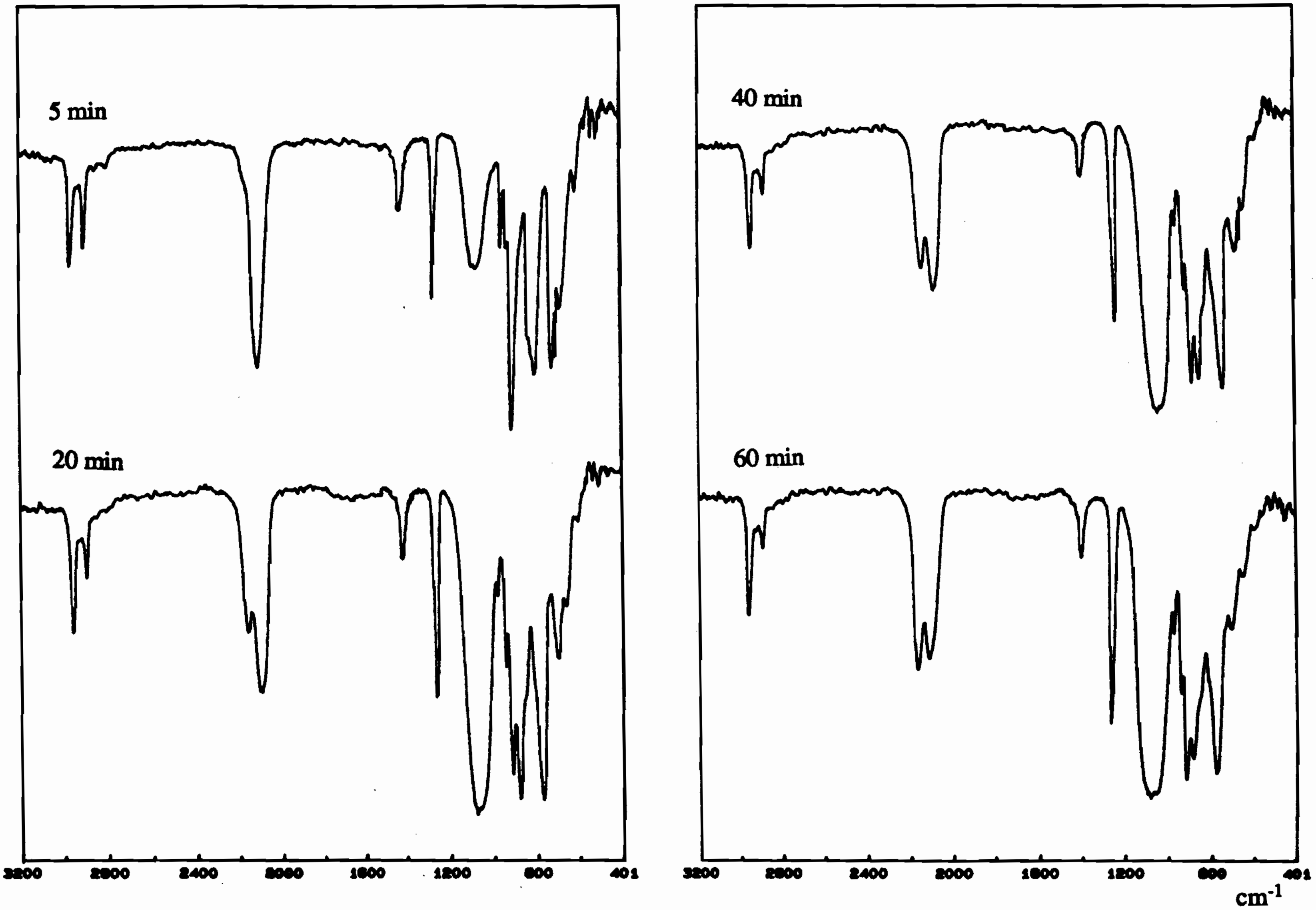

Figure III-3. The effect of oxidation on the IR spectrum of polymethylsilane. Thin film of pure material on KBr plate.

of the polymer (see Table III-3). The relative intensities of the ν_{C-H} band and the ν_{Si-H} band are also sensitive to molecular size. Polymethylsilane which has been extensively crosslinked by prolonged contact with the catalyst has a considerably higher intensity ratio of ν_{C-H}/ν_{Si-H} than the uncrosslinked polymer.

IR spectroscopy is useful in determining the degree of oxidation of polysilanes. In addition to the presence of a very strong band in the 1100 cm^{-1} region, changes to the ν_{Si-H} band are also apparent upon oxidation of the polymethylsilane. The effect of exposing polymethylsilane to air is shown in Figure III-3. In comparison with polyphenylsilane (148), polymethylsilane is much more sensitive to air. It needs about 1 month for polyphenylsilane to be oxidized to the same degree as polymethylsilane is oxidized within an hour. The extreme air-sensitivity of polymethylsilane requires that all manipulations must be carefully carried out under inert atmosphere. However, it should be emphasized that, although polymethysilane is quite air-sensitive, oxidation-free sample can be easily prepared and handled by using standard inert atmosphere techniques. The complete absence of the ν_{Si-O} band in the 1100 cm^{-1} region in Figure III-2 indicates that the sample is completely free of oxidation.

III.2.3 NMR spectra of polymethylsilane.

The ^1H NMR spectrum of polymethylsilane in benzene-d_6 solution is shown in Figure III-4. Only two bands are observed, corresponding to the Si-H (4.08 ppm) and C-H (0.45 ppm) protons. these bands are broad and featureless, as is typical of atactic polyorganosilanes. Unlike the case of polyphenylsilane, where two set of Si-H resonances, due to linear and cyclic species respectively, are observed, the polymethylsilane gives only one set of Si-H signals. This makes it impossible to estimate the amount of cyclic species by ^1H NMR.

The ^{13}C (-8.0 ppm) and ^{29}Si (-63 ppm) NMR spectra both exhibit single broad

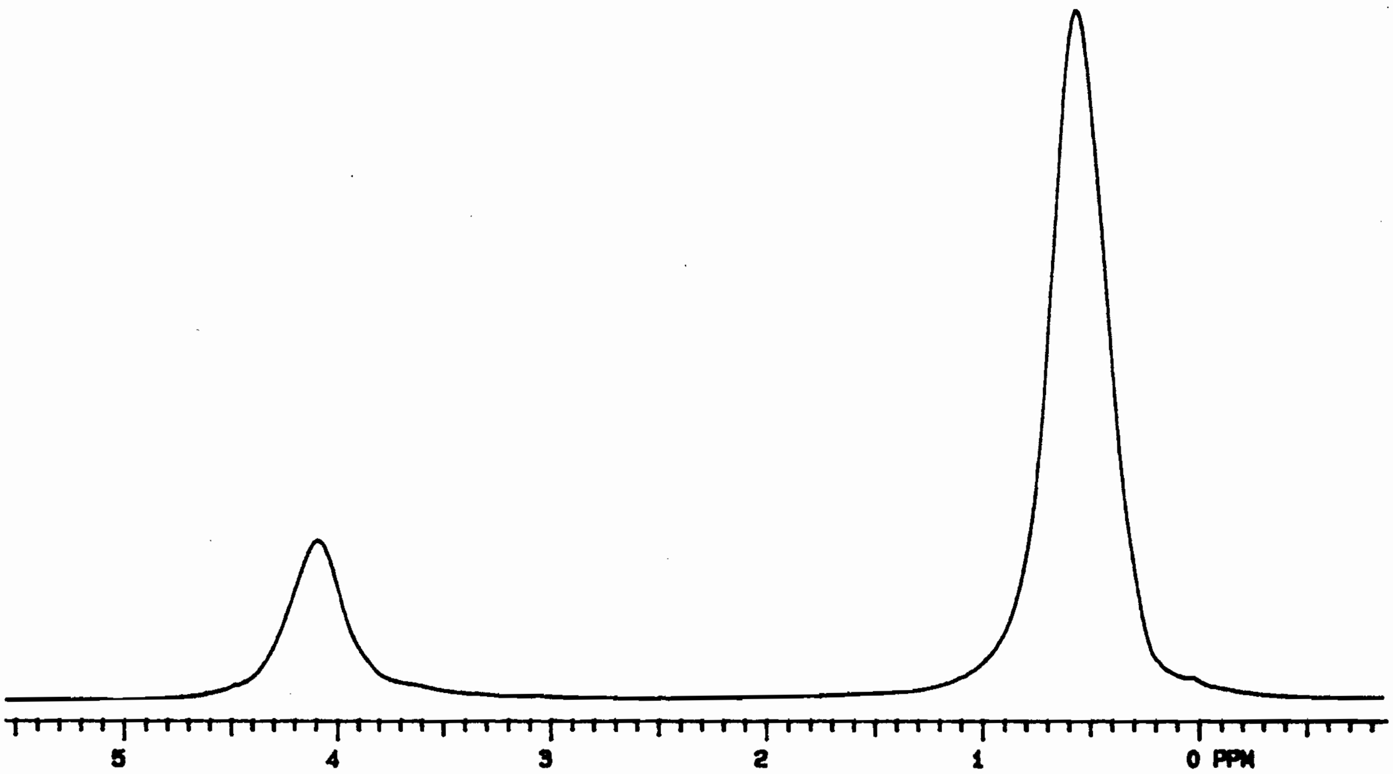

Figure III-4. ^{1}H-NMR spectrum of polymethylsilane in C_6D_6.

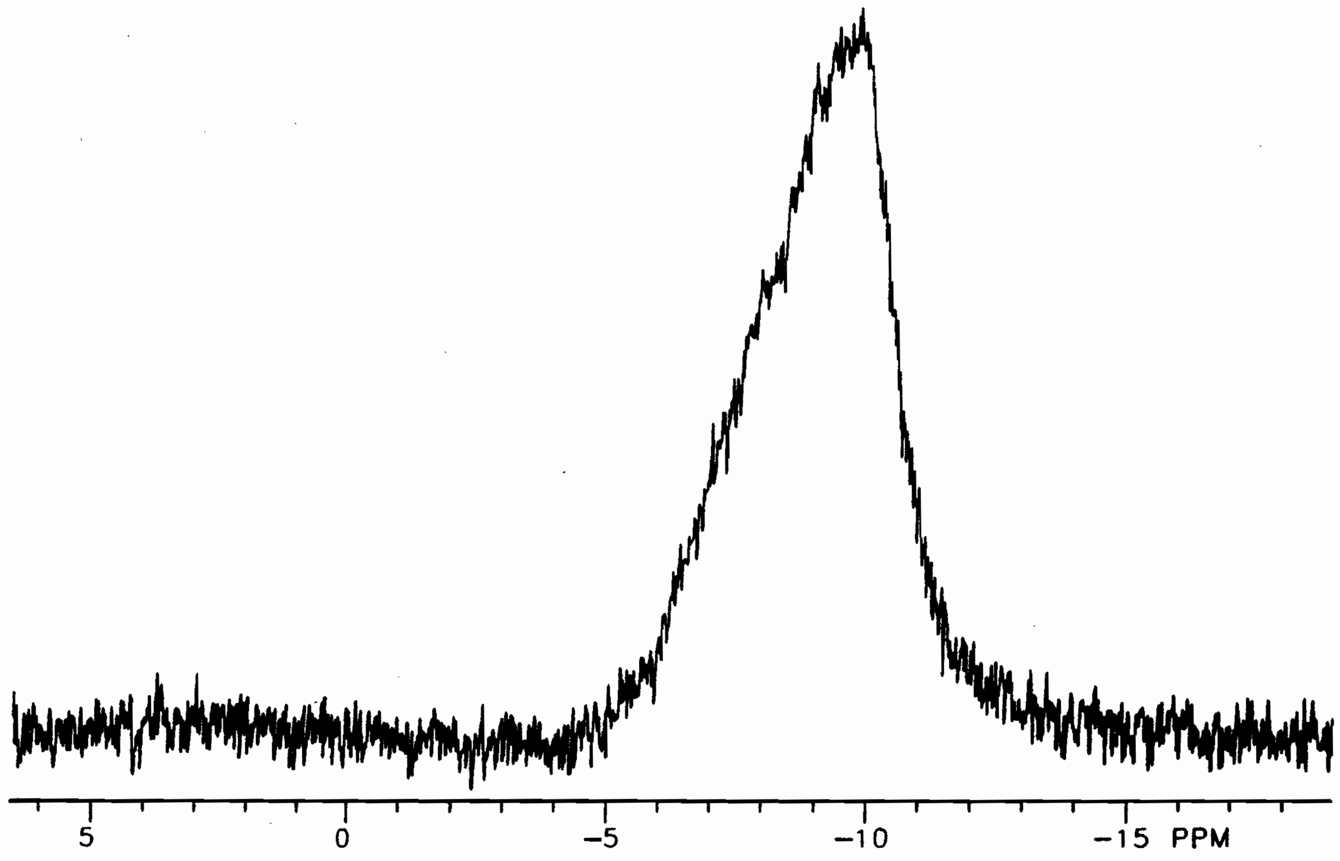

Figure III-5. ^{13}C-NMR spectrum of polymethylsilane in C_6D_6.

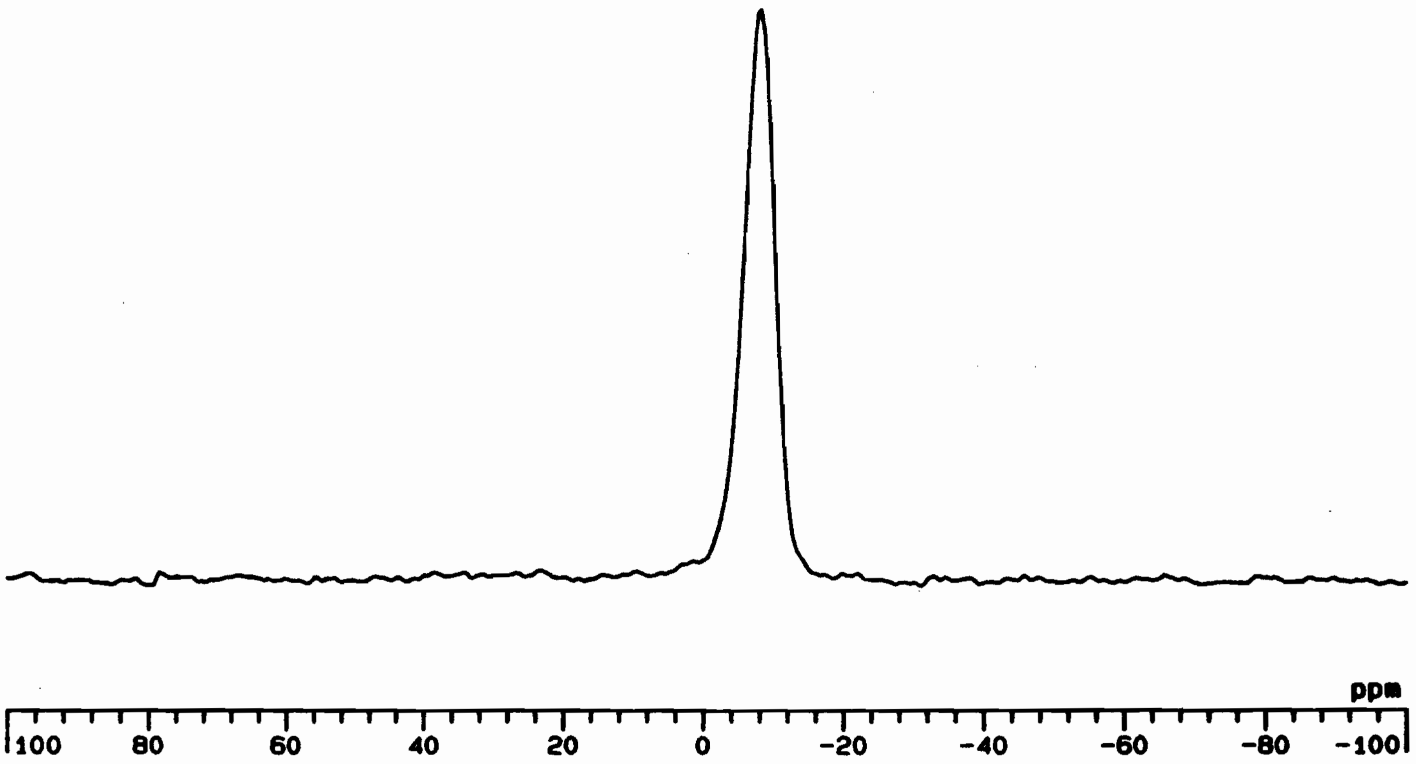

Figure III-6. Solid state ^{13}C-NMR spectrum of cross-linked polymethylsilane.

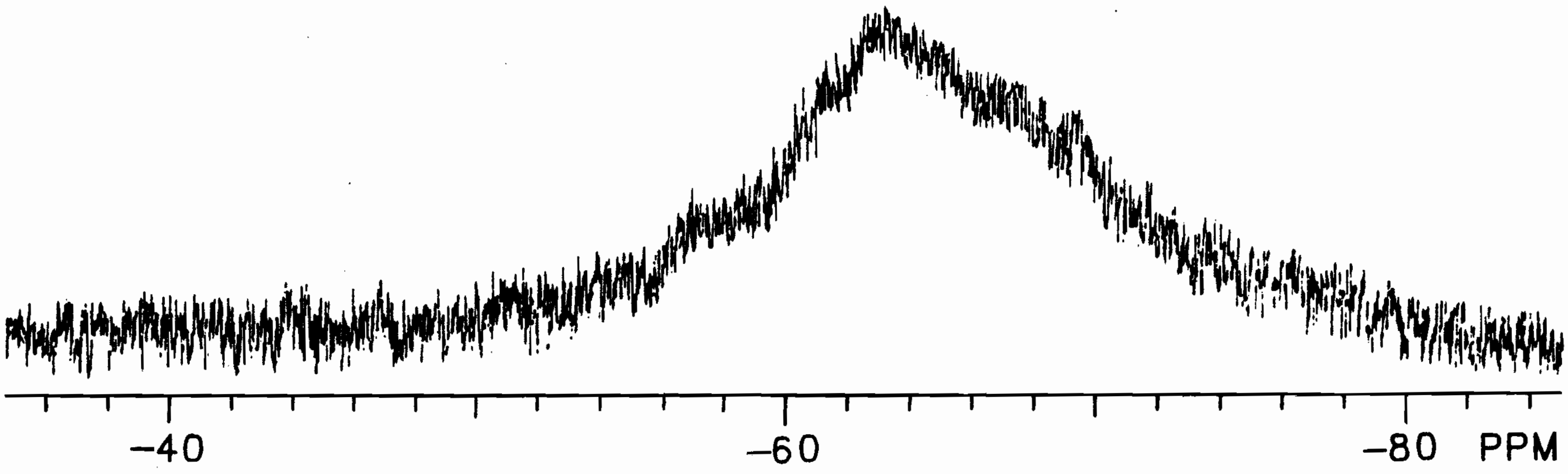

Figure III-7. Natural abundance ^{29}Si-NMR spectrum of polymethylsilane in C_6D_6.

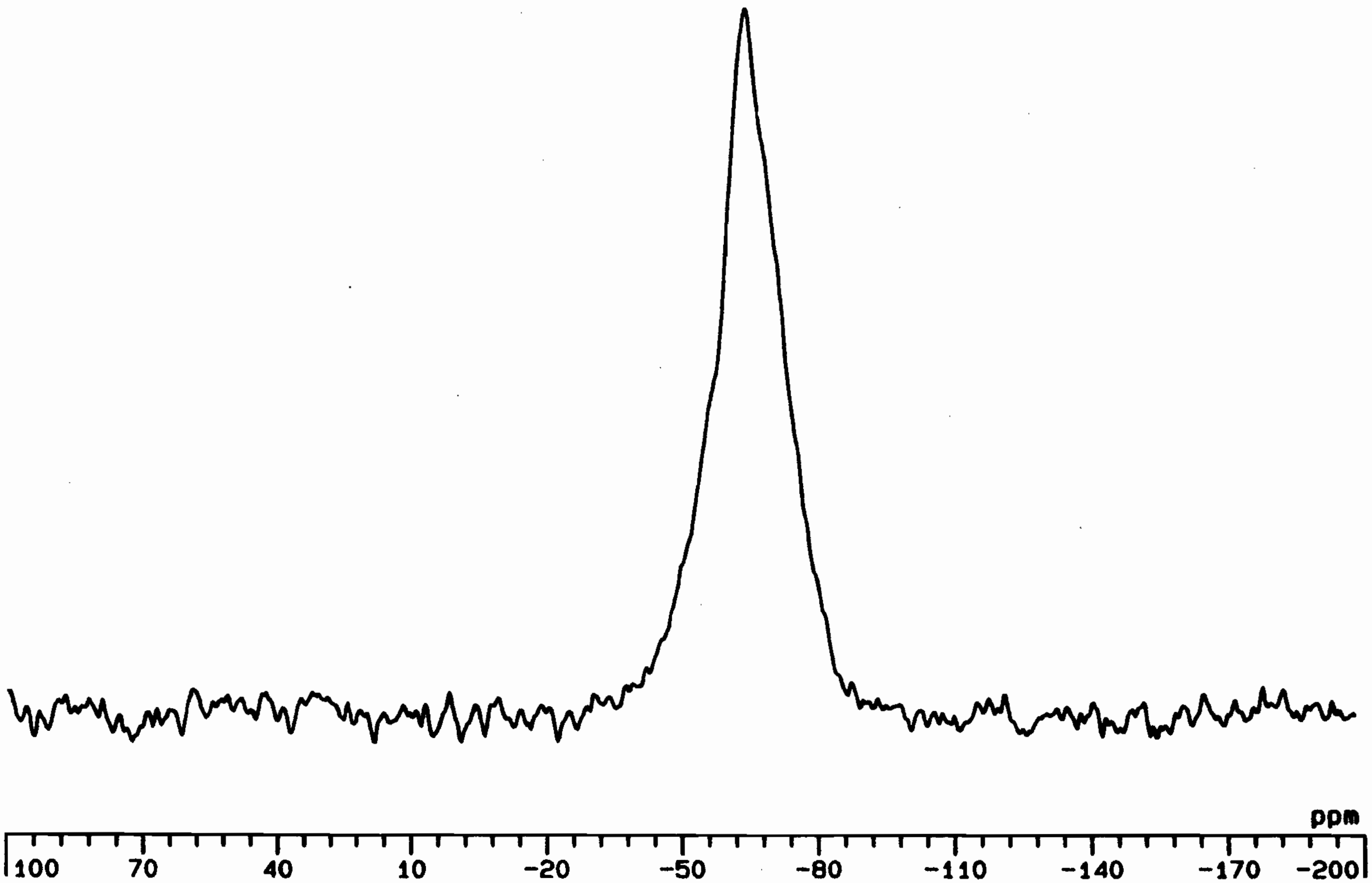

Figure III-8. Solid state ^{29}Si-NMR spectrum of cross-linked polymethylsilane.

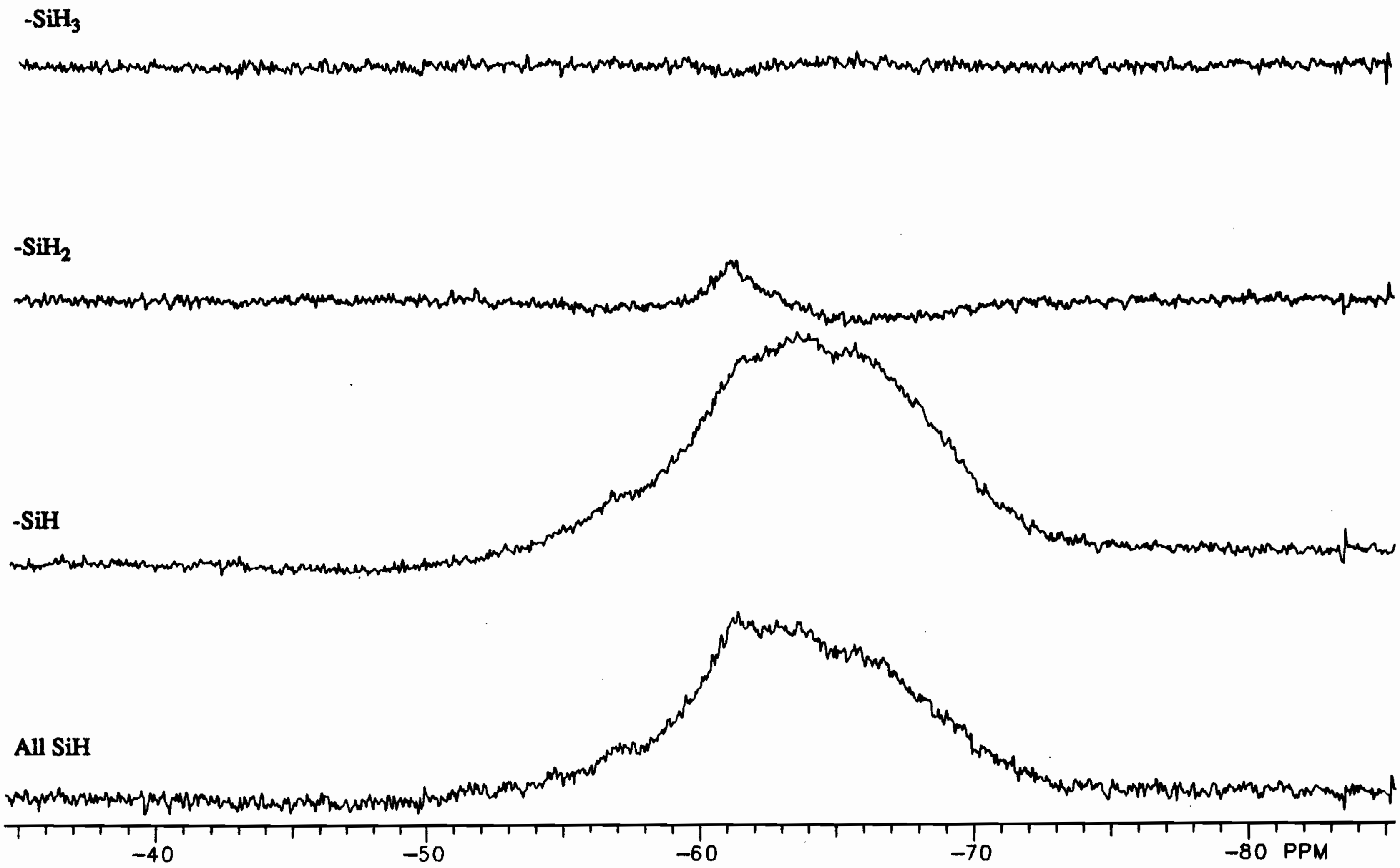

Figure III-9. ^{29}Si-NMR spectrum of polymethylsilane in C_6D_6, using a DEPT pulse sequence to detect silicons carrying different number of protons.

bands, giving little more information on the structure of polymethylsilane. These spectra for soluble and insoluble polymers are shown in Figure III-5, III-6, III-7 and III-8. The ^{29}Si DEPT spectra shown in Figure III-9 confirm that the soluble polymer contains mainly SiH units, together with a small amount of SiH_2 units. By comparison of the DEPT spectra with the natural abundance ^{29}Si spectrum of the same sample (Figure III-7), it can be found that the natural abundance ^{29}Si spectrum is slightly different in shape from the one for all SiH in DEPT spectra. This can probably be attributed to the presence of some quaternary silicons in the polymer.

III.2.4 Molecular weight properties.

The gel permeation chromatograms for a number of polymethylsilanes are shown in Figure III-10. From these chromatograms, the following points should be noted:

(1) Both the molecular weight and the polydispersity are lower and increase very slowly in the presence of large amounts of methylsilane monomer. After most of methylsilane has been consumed, the increase in molecular weight becomes fast. This indicates that the methylsilane polymerizes first to oligomers whose reactivity is lower than methylsilane itself. These oligomers polymerize further to larger polymers after the methylsilane has been exhausted.

(2) The polymethylsilane gives a bimodal GPC trace. The bimodal form of the distribution is typical of other polysilanes produced by catalytic dehydrocoupling. From studies on other systems we have concluded that the lower molecular weight peak is probably due to cyclic oligomers.

(3) A fairly dramatic difference between the higher molecular weight peak of polymethylsilane and those of other polysilanes is the extreme width of the former, particularly as a result of the presence of much higher molecular weight material than is usually observed. The polydispersity indices of other polysilanes of this type never exceed 2

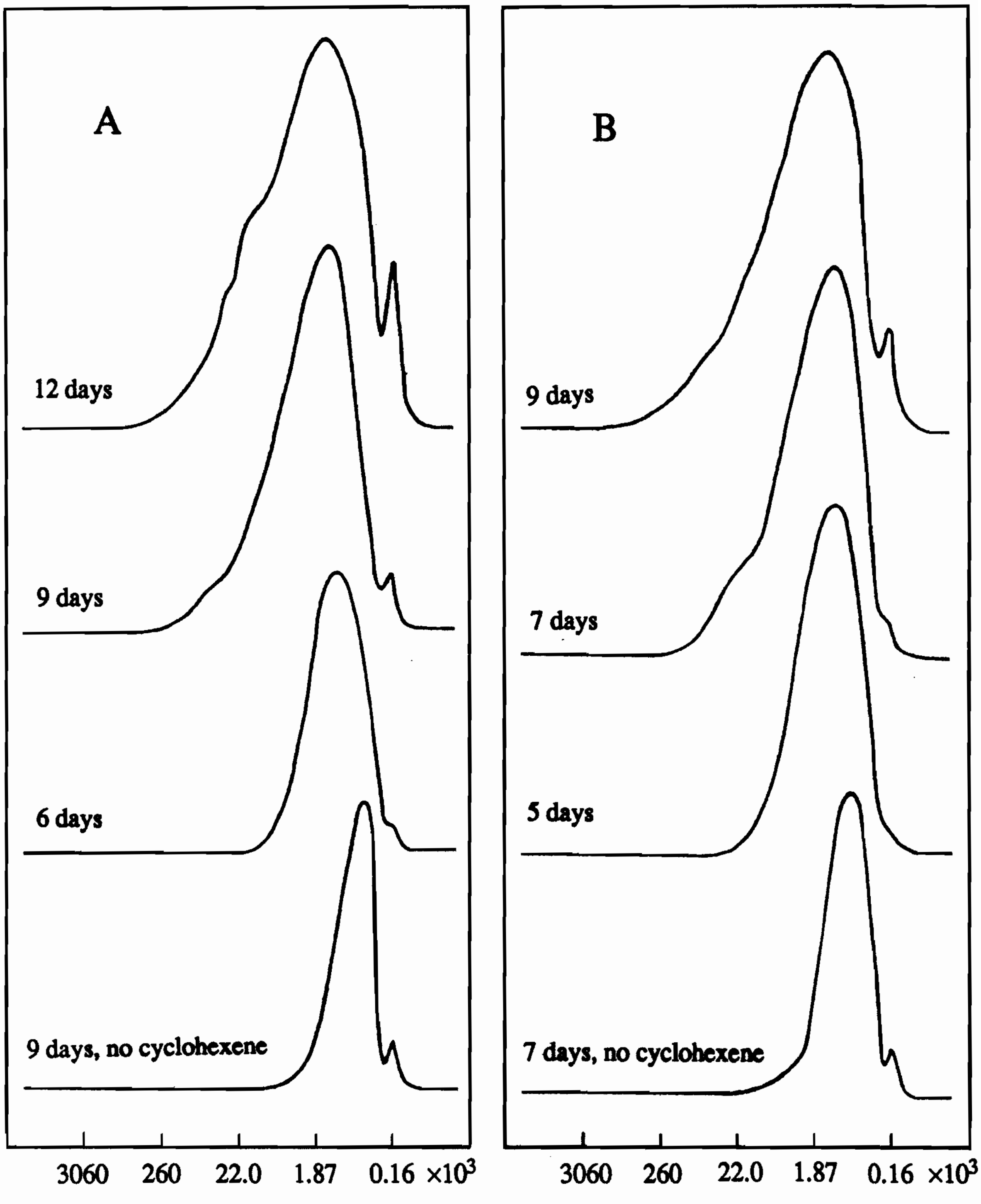

Figure III-10. Gel permeation chromatograms of a number of samples of polymethylsilane. (A) from titanocene and (B) from zirconocene catalyzed polymerization reactions. Reaction conditions are listed in Table III-2.

and are more often very close to 1, while polymethylsilane can have a polydispersity index as large as 10. The very high polydispersity of polymethylsilane can be attributed to the branching/crosslinking reactions. An important feature of the branching/crosslinking reactions is the low number-average molecular weight and high weight-average molecular weight (208).

(4) The molecular weight cut-off limit for polyphenylsilane is always in the range of 15,000 to 20,000 daltons (polystyrene equivalents) and less for other polysilanes. For a typical polymethylsilane sample, However, the cut-off is about 250,000 and ca. 50 per cent of the polymer has a MW in excess of 4000 (25 per cent in excess of 10,000). The increased molecular weight is obviously due to the unique steric properties of the methyl group, which lead to longer polymer chains and probably cross-linking via reaction of the tertiary SiH functions.

(5) For a typical polymethylsilane sample, an $\overline{M}_n$ of 1250 D, or a $\overline{DP}_n$ of ca. 12 (styrene equivalents), is calculated for the higher molecular weight fraction. The low molecular weight peak, due to small cyclic oligomers, gives a DP_n of 1.5, while the real DP_n should be about 6 based on the studies on other silanes. If we make a crude assumption that the real $\overline{DP}_n$ of polymethylsilane is about 4 times larger than that calculated from GPC, it can be expected that the $\overline{DP}_n$ of the higher molecular weight fraction is about 40~50. Such a figure is easily reconcilable with the ^{29}Si-NMR data. The ^{29}Si DEPT spectra indicate a ratio of SiH_2 to SiH functions of ca. 1:20 and if all of the molecules were linear and SiH_2 terminated, this would require a $\overline{DP}_n$ of ca. 42. Even if the cyclic and branching/crosslinking products were taken into account, it can be concluded that the GPC results are not out of line with those of ^{29}Si NMR. The lack of precision in this analysis is a consequence of the lack of good GPC calibrants for the polysilanes and the fact that the polymers are substantially non-linear. These factors result in a large margin of uncertainty in the estimates of molecular size by GPC. In addition, the peak areas in the DEPT spectra

are not proportional to the number of silicons for different types of H substitution, therefore there is a large margin of uncertainty in the estimate of $\overline{DP}_n$ using this data. Despite these uncertainties, the general conclusion is reasonably founded.

(6) Campbell and Hilty studied the polymerization of *n*-butylsilane with dimethylzirconocene catalyst and concluded that the product oligosilanes were mainly low molecular weight cyclics (Si_6 and Si_7) (93). Our analyses of the products of phenylsilane, *n*-hexylsilane and benzylsilane polymerizations with both dimethyltitanocene and dimethylzirconocene catalysts led us to conclude that they were mainly linear, mainly cyclic and entirely cyclic respectively (209). It was also concluded that the ratio of cyclic to linear products increases with increasing the dilution of the starting silane. From these results it might be anticipated that the products of the methylsilane polymerization would be mainly low molecular weight cyclics. However, the evidence of the gel permeation chromatograms shown in Figure III-10 does not support such an expectation. These chromatograms indicate that the low molecular weight cyclics in these samples never exceed a few per cent.

The fact that the methylsilane polymerization did not give very much cyclic oligomers can probably be attributed to the fact that the methylsilane oligomers with suitable chain-length for cyclization are more reactive than methylsilane itself and can polymerize to larger oligomers rapidly. The higher reactivity of these oligomers has been proved by their absence in reaction mixtures, even in the presence of a large amount of methylsilane.

III.2.5 Pyrolysis of polymethylsilane.

Thermogravimetric analysis (TGA), differential thermal analysis (DTA) and bulk sample pyrolysis of polymethylsilane have been performed. The thermogravimetric analysis indicates that polymethylsilane lost only 22% of its weight and gave a 78% ceramic yield upon heating to 1200°C under nitrogen at a rate of 8°C/min (Fig. III-11a). The pyrolysis of a bulk polymethylsilane sample in N_2 at 1°C/min to 1000°C left a ceramic residue in 77% yield (Fig. III-11b). To our knowledge, this is the highest ceramic residue yield obtained so far from polysilane precursors. In contrast, more than 70% of polyphenylmethylsilane and almost 99% of polydimethylsilane were lost when these polysilanes were pyrolyzed to 800°C (36,202). The pyrolysis of a THF-soluble, extensive cross-linked "polymethylsilane" $[(MeSiH)_{0.4}(MeSi)_{0.6}]_n$, obtained by sodium condensation of $MeSiHCl_2$, left a ceramic residue in 60% up to 1000°C. Less cross-linked polymer $[(MeSiH)_x(MeSi)_y]_n$ ($x = 0.65$-0.85, $y = 1 - x$) obtained by this method gave only a ceramic residue yield of 15-20% under same conditions (203).

Chemical analysis of the ceramic material heated to 1100°C corresponds to the formula $Si_1C_{0.9}H_{<0.1}O_{<0.1}$. However, ^{29}Si NMR spectra of all ceramic products obtained in this study show no NMR peaks that would correspond to either SiO_x or free Si, which can be easily identified according to published data (210). The source of the oxygen found in the chemical analysis is probably the result of handling. Within the limits of analyses, these results suggest that pyrolysis of polymethylsilane leads to essentially pure SiC. In contrast, the ceramic residue obtained from pyrolysis of $[(MeSiH)_{0.4}(MeSi)_{0.6}]_n$ contains 26 wt% free Si (203), while the ceramic residue obtained from polydimethylsilane precursor contains 18 wt% free C (202). Other carbon-rich polymers usually generate more carbon-rich ceramic products (202).

The theoretical SiC yield for polymethylsilane is 91%, so more than 10% of the polymer must have been driven off as volatile oligomers. The transformation procedure of

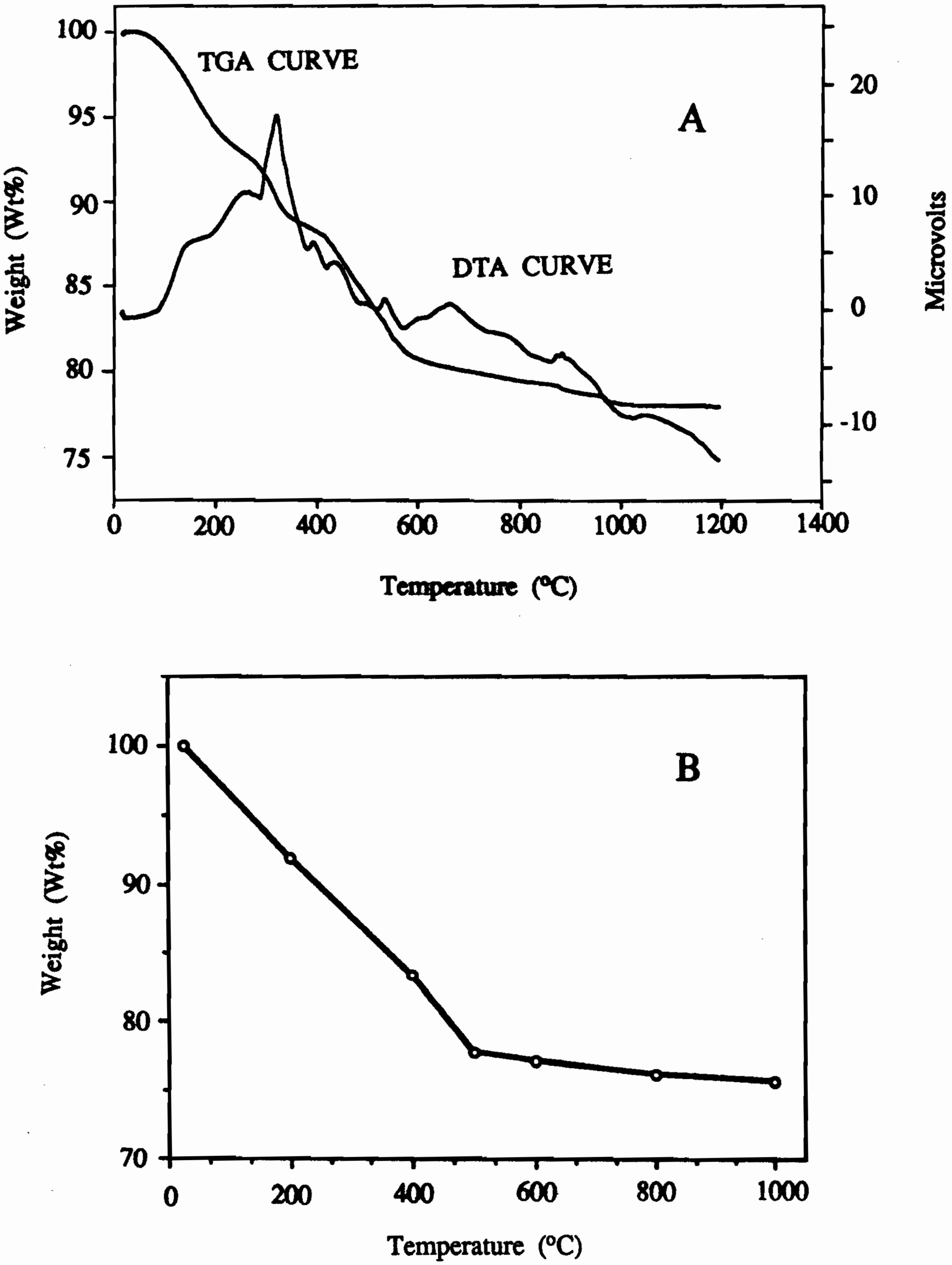

Figure III-11. (A) TGA and DTA curves for polymethylsilane heated at 8°C/min in N_2. (B) Mass loss as a function of pyrolysis temperature for bulk polymethylsilane samples (1 g), heated at 1°C/min in N_2 to selected temperature and held for 0.5 h.

polymethylsilane into ceramic during pyrolysis from room temperature to 1300°C has been followed by solid state ^{29}Si NMR and diffuse reflectance infrared Fourier transform spectroscopy (DRIFT). The ^{29}Si NMR spectra and DRIFT spectra, obtained from the samples generated in the bulk pyrolysis studies, are shown in Figures III-12 and III-13 respectively. Two important features seen in Fig. III-12 are the disappearance of the starting polymer by 400°C and the formation of the rather sharp peaks at 1000°C. At 400°C, the PMS peak at -63 ppm has almost vanished and a broad new peak centered at -10 ppm appears. The DRIFT spectrum of the 400°C sample shows a moderately strong peak at 1350 cm^{-1} that can be assigned to the bending vibration of $Si\text{-}CH_2\text{-}Si$ linkages (59). These linkages are known to form during thermal rearrangement of polydimethylsilane to polycarbosilane. Therefore, we can conclude that the 400°C material is a polymer of the type $\text{-}[H_2SiCH_2]_{1-x}[MeSiH]_x\text{-}$. In the 600°C DRIFT spectrum, all evidence of well-defined molecular structure disappears and the only extant features are C-H (2900 cm^{-1}) and Si-H (2100 cm^{-1}) stretching bands which suggest that the 600°C material is hydrogenated SiC. The NMR peak at -10 ppm sharpens with further heating and very narrow, well-defined peaks at -15.4 ppm and -19.7 ppm appear by 1000°C. The same sharp peaks can be observed if the material is heated at 900°C for about 10h. The 1000°C DRIFT spectrum shows only absorptions in the 400 ~ 1000 cm^{-1} region resulting from SiC (211).

According to recent papers on the ^{29}Si NMR spectra of β-SiC and various α-SiC polytypes (210,212), it can be concluded that we are producing β-SiC (-15.7 ppm) containing small amounts of α-SiC based on the ^{29}Si NMR spectra in Fig. III-12b. In other precursor-derived ceramics, the well-defined ^{29}Si NMR peaks, which indicate the formation of crystalline SiC, are generally observed in samples heated to temperatures of 1400°C or greater (213). By comparison, the polymethylsilane precursor used here exhibits crystalline phases at temperatures of <1000°C.

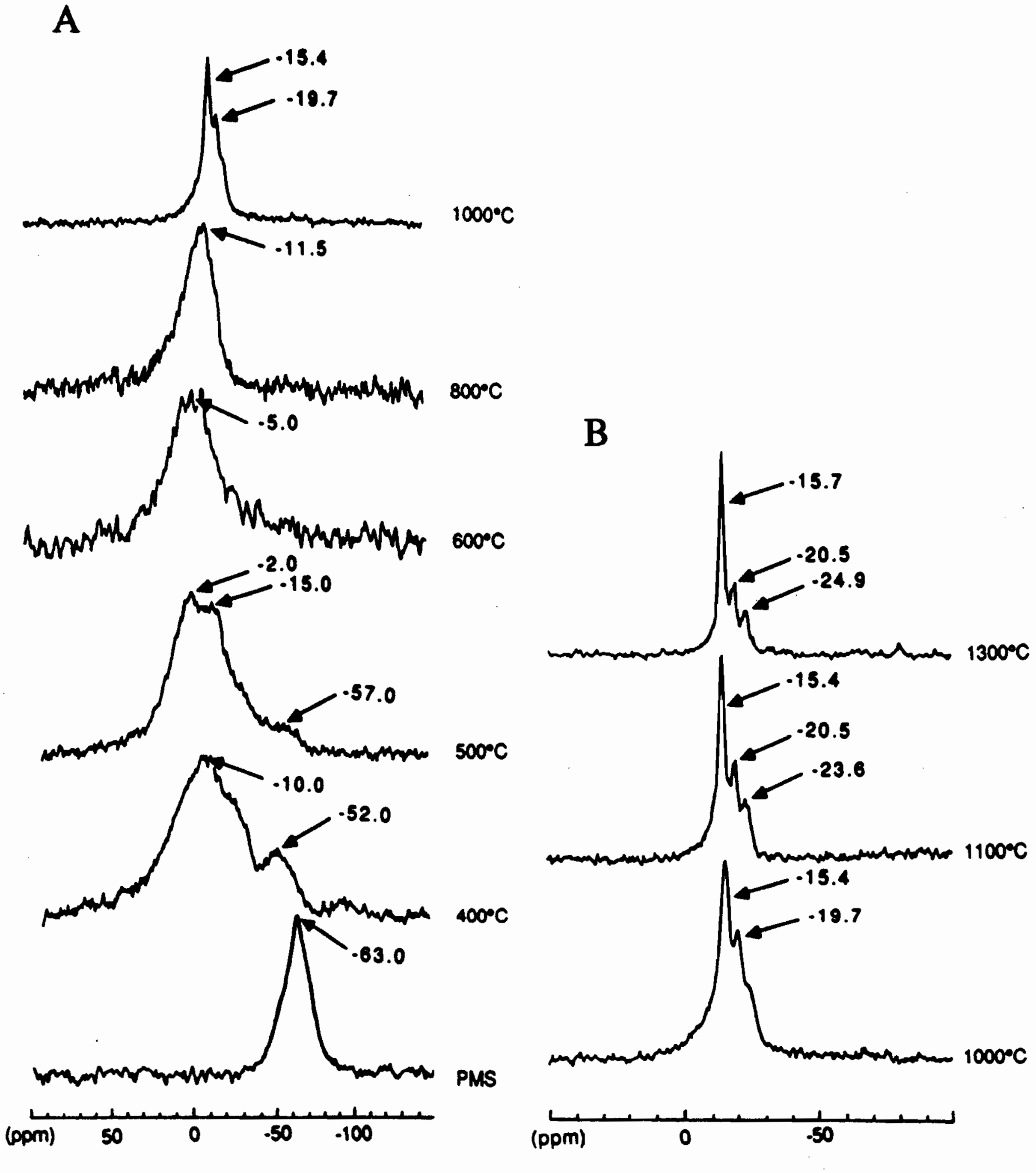

Figure III-12. Solid state ^{29}Si NMR spectra of polymethylsilane heated to selected temperatures. (A) heated at 1°C/min in N_2 from room temperature to selected temperature and held for 0.5 h; (B) heated at 5°C/min in N_2 from 600°C to selected temperature and held for 1 h.

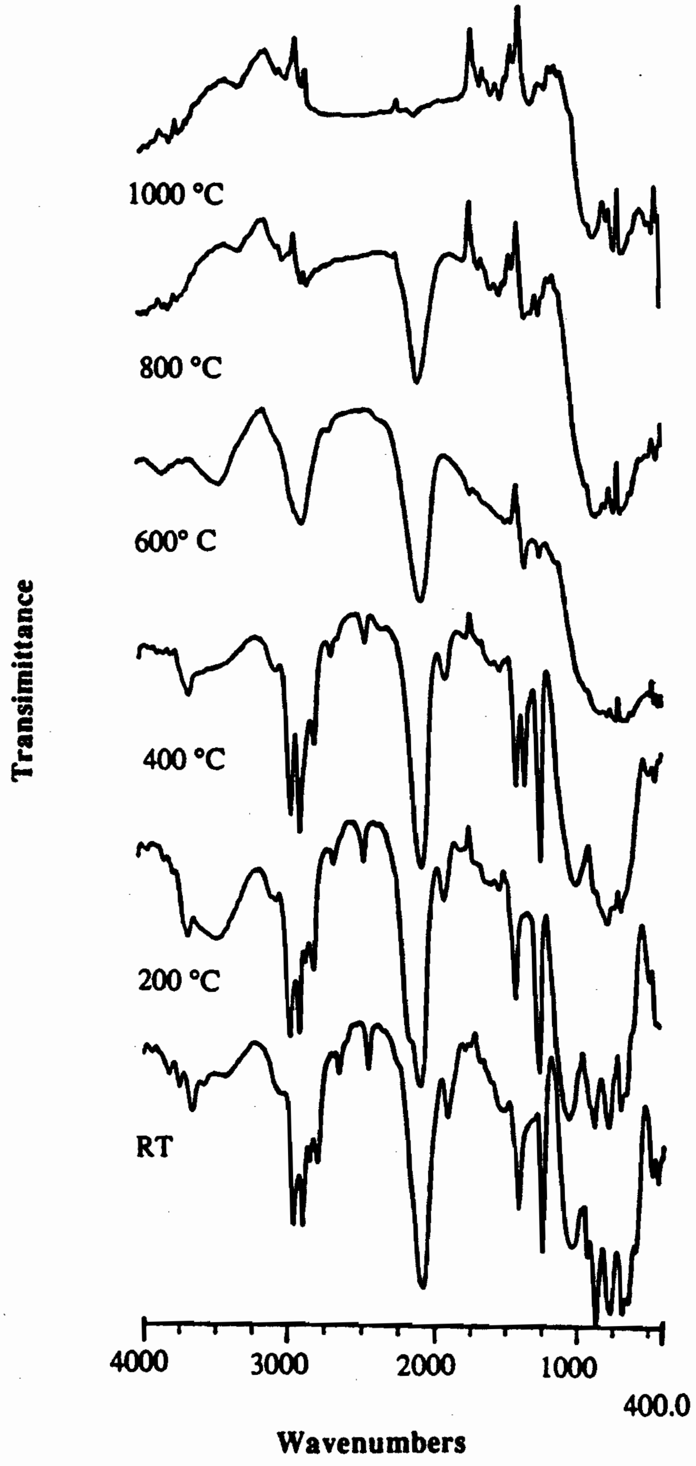

Figure III-13. DRIFT spectra of polymethylsilane heated to selected temperatures. Same conditions as in Figure III-12(A).

III.3 EXPERIMENTAL

III.3.1 General procedures.

The treatments of solvents and the preparations of dimethyltitanocene and dimethylzirconocene have been described before. Methyltrichlorosilane and lithium aluminum hydride were purchased from Aldrich Chemical Co. and used as received. NMR spectra of polymethylsilane were measured in solution on a Varian XL-300 FT spectrometer. Solid state NMR spectra were recorded on a Chemagnetics CMX-300 spectrometer. All NMR spectra were referenced to TMS. IR spectra were recorded on thin films of pure material supported on KBr plates, using an Analect AQS-20 FT-IR spectrophotometer. GPC measurements were made using air-free, chromatographic grade THF solvent with a Varian 5000 Gel Permeation Chromatograph, interfaced to a Varian Vista 402 data station and equipped with a 10^3 Å Ultrastyragel column. The column was calibrated with polystyrene standards. TGA and DTA measurements were made on a PL Thermal Sciences STA-1500 instrument. Because of the air sensitivity of the polymer, all physical measurements were carried out under either nitrogen or argon atmosphere.

III.3.2 Synthesis of methylsilane.

Methyltrichlorosilane (60 ml, 500 mmol) was carefully added to a suspension of lithium aluminum hydride (16 g, 400 mmol) in THF (500 mL) in a 1 L, three necked flask under argon at room temperature. The methylsilane was passed through a condenser and trapped at liquid nitrogen temperature. After completion of the addition, the reactor was stirred at 50°C for a further 3 hours to complete the reaction. The collector was then detached and connected to a 1 L cylinder cooled in liquid nitrogen. the collector was then allowed to warm slowly to the boiling point of methylsilane. Following completion of the transfer, the argon was pumped out of the cylinder, the valve was closed and the cylinder was allowed to warm to room temperature. At room temperature the cylinder pressure was usually 9 to 10 atmospheres (80 - 90% yield).

III.3.3 Polymerization of methylsilane.

The following is a representative experiment for the preparation of polymethylsilane on a 10 g scale. Dimethylzirconocene (200 mg, 0.795 mmol) was dissolved in cyclohexene (25 mL, 244 mmol) in a thick-walled 120 mL Schlenk tube equipped with a magnetic stirrer. After the solution was frozen , the Schlenk tube was evacuated and then connected to the methylsilane cylinder (1 L, 130 psi). The solution was warmed to 45°C and stirred for 8 days. During this time all of the cyclohexene was transformed into cyclohexane and evolution of hydrogen was observed. After a further 8 days, the gas evolution had virtually ceased. At the end of the reaction period, the reactor was carefully vented and the contents were pumped dry, to give a red-orange, viscous grease (15.0 g, 92%). This material was completely soluble in hydrocarbon solvents, but after standing at room temperature for three days it was transformed into an insoluble brittle glass. Samples of the soluble polymer were purified by passing down a 3 × 20 cm Florisil column, and eluting with toluene, to remove the catalyst. The above procedure could be used with either DMT or DMZ as the polymerization catalyst. The polymerization can also be run in the absence of cyclohexene, but in this case, the reaction is slow and there is a considerable pressure of hydrogen at the end of the reaction. All reactions and manipulations were carried out under inert atmosphere.

III.3.4 Pyrolysis of polymethylsilane

The pyrolysis studies were carried out at the University of Washington in collaboration with Prof. Laine's group and with Dr. Florence Babonneau of Université de Pierre et Marie Curie. Data in Figs III-11b and III-13 were provided by Prof. Laine. Spectra in Fig. III-12 were measured by Dr. Babonneau. An insoluble, cross-linked polymethylsilane sample containing 0.2 mole% of "Cp_2Zr" was used for pyrolysis studies. All preparative-scale (1 g) pyrolyses were carried out under an atmosphere of flowing nitrogen in a Lindberg single zone furnace equipped with a Eurotherm temperature controller. Solid state ^{29}Si NMR spectra for pyrolysis products were recorded on a Brüker MSL-400 spectrometer. DRIFT spectra were obtained by using a IBM/Nicolet FTIR-44 spectrophotometer. Elemental analysis of the ceramic material heated to 1100°C was run in Service D'analyse du CNRS, Vernaison, France. Analysis results: Calcd for SiC: C, 29.96; Si, 70.04. Found: C, 25.26; Si, 68.60; O, 2.92; H, < 0.2.

Chapter IV

Dehydrocoupling of diphenylsilane, phenylmethylsilane and butylmethylsilane

IV.1 INTRODUCTION

The dehydrocoupling reaction of secondary silanes in the presence of Wilkinson's catalyst was first reported in 1973 (81). Later, similar results were obtained with a carbenerhodium(I) complex, cis-[RhCl(COD)L^{Me}] (COD = cycloocta-1,5-diene, L^{Me}= :$\overline{\mathrm{CN(Me)(CH_2)_2N}}$Me) or trans-[RhCl$(PPh_3)_2L^{Me}$] as catalyst (82). In these catalyst systems, dimer and trimer can be obtained from phenylmethylsilane, but only dimer can be formed from diphenylsilane. Although a number of other late transition metal complexes have also been examined (83), Wilkinson's catalyst was found to be the best dehydrocoupling catalyst among the studied complexes. Two disadvantages of these late transition metal catalysts are their abilities to promote disproportionation of the Si-C bonds (81-83) and oxygenation of the Si-Si bonds (84).

The metallocene complexes of Ti and Zr have been found to be effective catalysts for the polymerization of primary silanes, but they do not appear to work very well for the dehydrocoupling of secondary silanes. Previously, preliminary studies of dehydrocoupling of diphenylsilane and phenylmethylsilane in this laboratory indicated that dimer is the only coupling product from the diphenylsilane reaction catalyzed by either titanocene or zirconocene (32,33), and a higher oligomer, which was not well characterized, can be obtained from phenylmethylsilane reaction (31). Molecular weight measurement indicated that the phenylmethylsilane oligomer has an average degree of polymerization of four. Recently, Nakano *et al.* (91) reported their results on the dehydrocoupling of diphenylsilane and phenylmethylsilane catalyzed by diphenyltitanocene at higher temperature (110°C), which confirm that dimerization is the only coupling reaction for diphenylsilane, and indicate that dimer and trimer can be obtained from the reaction of phenylmethylsilane under their conditions. On the other hand, Corey *et al.* (214) reported very recently that octamer has been obtained from dehydrocoupling of phenylmethylsilane catalyzed by zirconocene produced *in situ* from Cp_2ZrCl_2 and *n*-BuLi in toluene. Given the uncertainty in defining the products for phenylmethylsilane reaction, it is obvious that further studies are necessary to understand the reaction and confirm the products.

During the last few years, we have also studied the dehydrocoupling reactions of diphenylsilane and phenylmethylsilane in detail. Even though the dehydrocoupling of secondary silanes can not give polymers or higher molecular weight oligomers, it might provide a good synthetic route for functional disilanes and trisilanes that are currently available for only a limited number of systems. In addition, the relative simplicity of the dehydrocoupling of secondary silanes makes these systems, particularly diphenylsilane, easier to follow and more suitable for kinetic and mechanistic studies. The reaction kinetics for the dimerization of diphenylsilane have therefore been studied, together with the reaction profile of the oligomerization of phenylmethylsilane. The reactions of butylmethylsilane have also been studied in the presence of dimethyl-titanocene and -zirconocene catalysts. From these studies, some information about the electronic and steric effects on the reactivity of silanes and the effects of temperature and catalyst concentration on the reaction rate and product distribution was also obtained.

IV.2 RESULTS AND DISCUSSION

IV.2.1 Dehydrocoupling of diphenylsilane.

The dehydrocoupling reaction of diphenylsilane catalyzed by either dimethyl-titanocene or -zirconocene is very simple and gives only one coupling product, 1,1,2,2-tetraphenyldisilane. The assignment of the disilane was made on the basis of a comparison of its IR ($\nu_{Si\text{-}H}$, 2120 cm^{-1} in KBr), ^1H NMR (7.62-7.55 ppm, 8 H, C_6H_5; 7.10-7.03 ppm, 12 H, C_6H_5; 5.48 ppm, 2 H, SiH (C_6D_6)) and m.p. (80.5-81°C) to literature data (82,215). 1,1,2,2-tetraphenyldisilane can be obtained as a crystalline material from the dehydrocoupling reaction. After the reaction had proceeded to some extent, which varies depending on the temperature, the disilane began to precipitate as a crystalline solid. If the reaction time was long enough, the reaction mixture solidified completely. The catalyst could be removed from the disilane by either passing the reaction mixture through a Florisil column or recrystallizing the disilane from hexane.

The dehydrocoupling reaction of diphenylsilane to disilane in the presence of dimethyl-titanocene or -zirconocene can give very high conversion. When the reactions were carried out in neat diphenylsilane at higher catalyst concentrations (3-5 mole%) and temperatures (60-80°C), a conversion of >90% could be obtained after a long reaction time. Such a high conversion was not achieved with Wilkinson's catalyst (81).

A. Titanocene catalyzed reaction.

In titanocene catalyzed reactions, 1 equivalent of diphenylmethylsilane was always produced from the initial reaction of dimethyltitanocene with diphenylsilane. This methylation reaction has been observed in all reactions of dimethyltitanocene with silanes. The dimerization reaction of diphenylsilane was very slow compared to the polymerization reaction of phenylsilane. In a typical reaction with 5 mole% of catalyst in neat silane at room temperature, only 40% of starting diphenylsilane was transformed into dimer after 24 hours. The reaction rate and conversion of diphenylsilane can vary as functions of temperature and concentrations of silane and catalyst. Some typical reaction profiles for the titanocene catalyzed dehydrocoupling reaction of diphenylsilane at different catalyst concentrations and temperatures are shown in Figures IV-1 and IV-2 respectively. It can be seen from these figures that higher temperatures and catalyst concentrations resulted in higher reaction rates and conversions. However, the influences of both temperature and catalyst concentration on the reaction rate are not very remarkable.

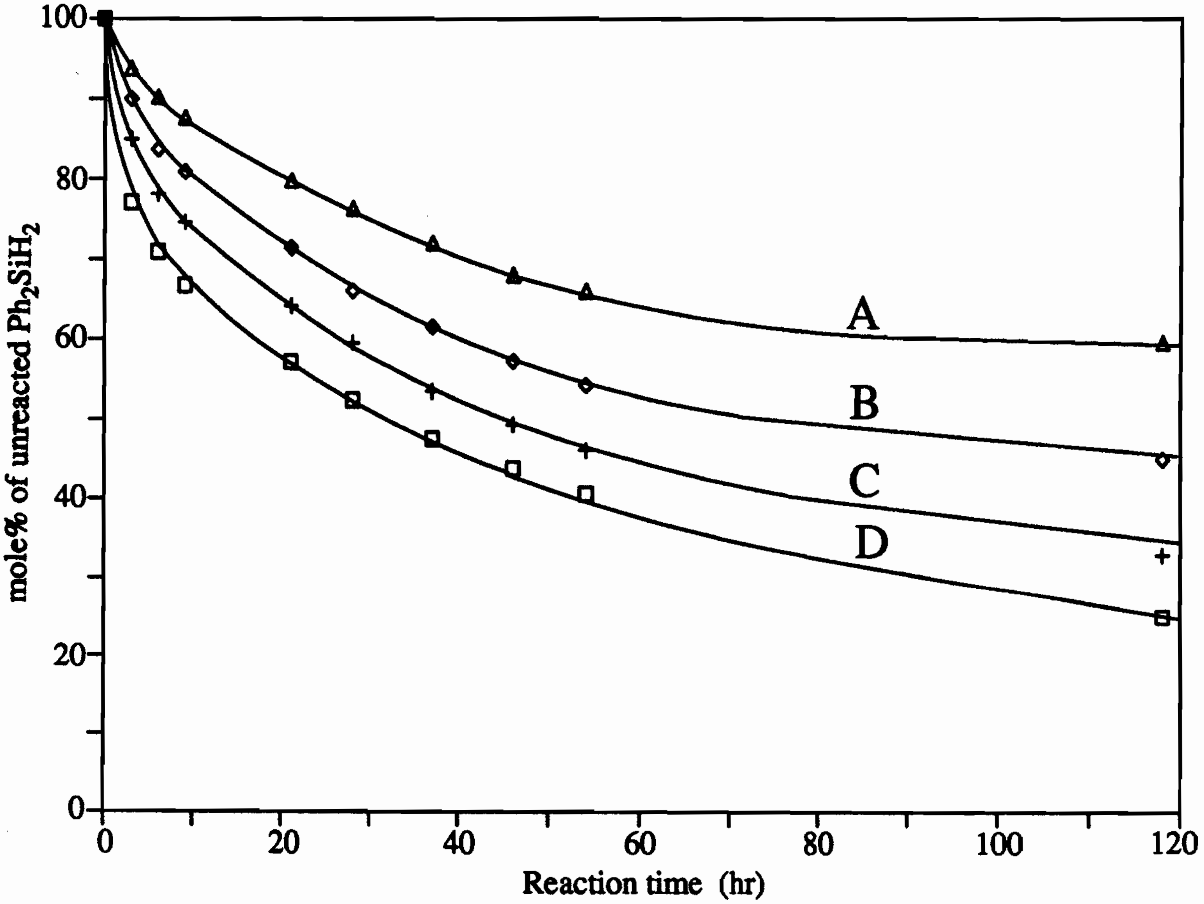

Figure IV-1. Reaction profiles for the titanocene catalyzed dehydrocoupling of Ph_2SiH_2 at different catalyst concentrations. (A) 0.037 M; (B) 0.075 M; (C) 0.15 M and (D) 0.30 M DMT in neat silane at 40°C.

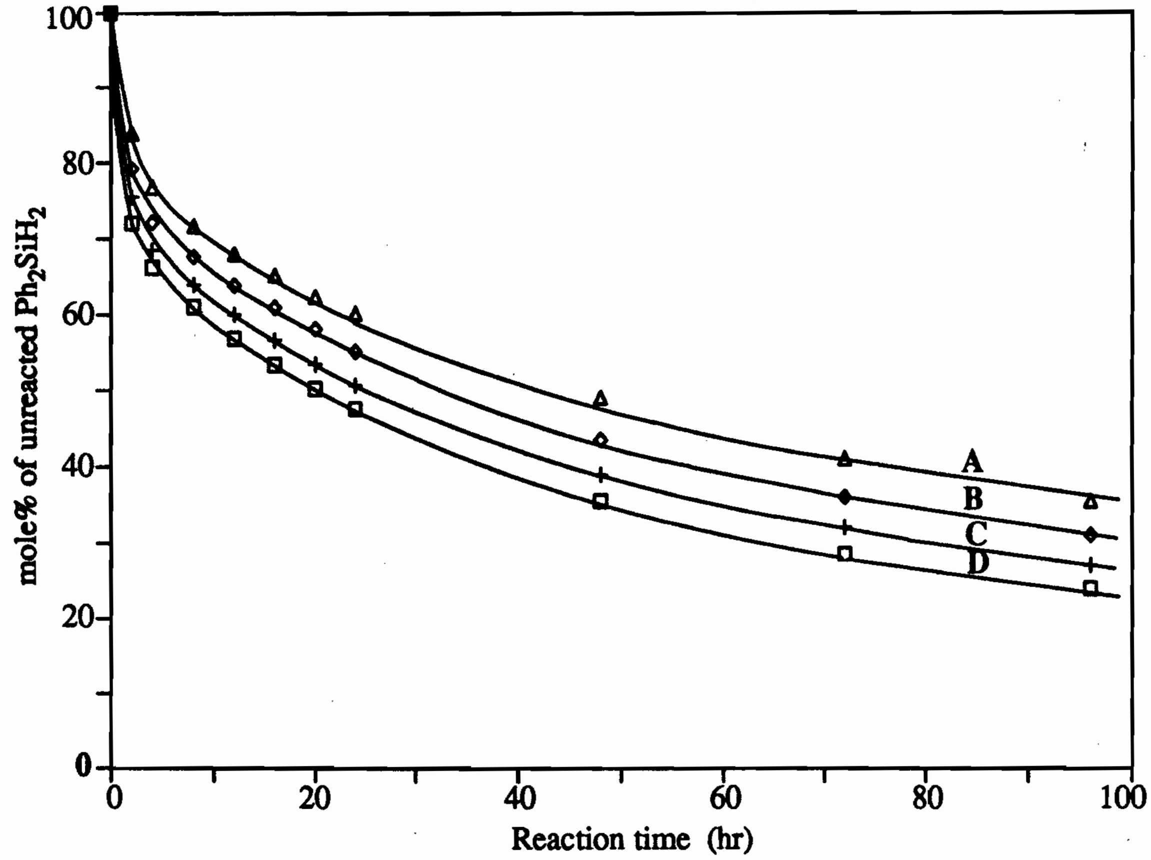

Figure IV-2. reaction profiles for the titanocene catalyzed dehydrocoupling of Ph_2SiH_2 at different temperatures. (A) 20°C; (B) 40°C; (C) 60°C; (D) 80°C. [cat.] = 0.27 M in neat silane (5.4 M).

A kinetic study indicates that the dimerization of diphenylsilane in the presence of catalytic amounts of dimethyltitanocene becomes a second order reaction with respect to the silane after a period of 2~3 hours. Some typical second-order plots (1/[Ph_2SiH_2] vs. time) for the dimerization reaction of diphenylsilane at different temperatures are shown in Figure IV-3. The kinetic data for a number of reactions under different conditions are summarized in Table IV-1. The rate constant k' in Table IV-1, which was measured from the second-order plot, is for the following rate law:

$$R_d = k'[\text{silane}]^2 \qquad (\text{IV-1})$$

Where R_d is the reaction rate of the dimerization of diphenylsilane. The concentration of active catalyst was supposed to remain constant effectively throughout

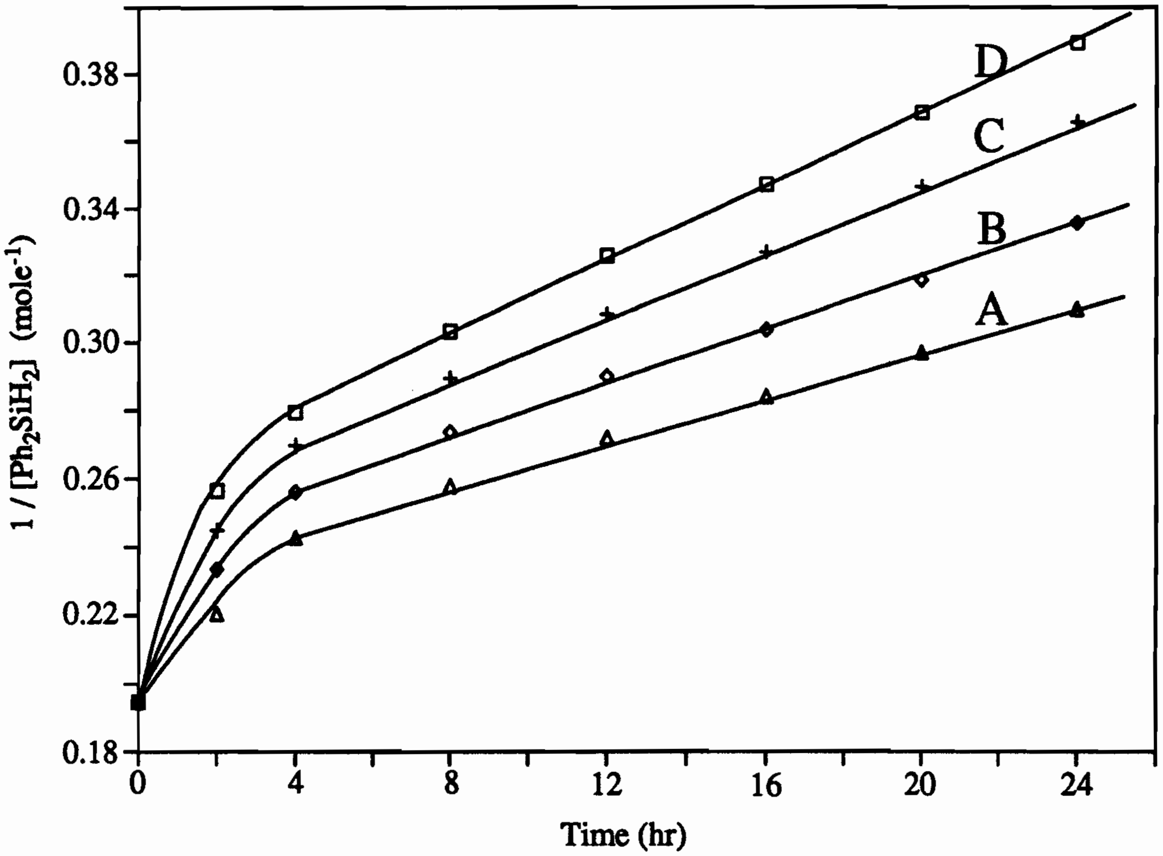

Figure IV-3. Second-order plots for the titanocene catalyzed dehydrocoupling reaction of Ph_2SiH_2 at different temperatures. (A) 20°C; (B) 40°C; (C) 60°C; (D) 80°C. [cat.] = 0.27 M in neat silane (5.4 M). The data point at $t = 0$ is calculated by subtracting the catalyst concentration from silane concentration.

most time of the reaction except the initial stages (2~3 h.) and thus was combined into k' as a constant factor. From these kinetic results, two points should be noted:

Firstly, the reaction rate of the dimerization of diphenylsilane increases slowly with increasing catalyst concentration. When the catalyst concentration is doubled, the rate constant k' only increases by 35% averagely. This suggests that not all the titanocene species, but only a part of them in the reaction system are active catalyst, and the ratio of the active catalyst to total titanocene species decreases with the increase in the total concentration of titanocene compounds.

Secondly, the reaction rate also increases with the increase in temperature, but the

Table IV-1. Kinetic data for titanocene catalyzed dehydrocoupling reactions of diphenylsilane[a]

No.	Temperature (°C)	$[Cp_2TiMe_2]$ (M)	$10^5 k'$ ($M^{-1}{\cdot}s^{-1}$)
1	40	0.30	6.66
2	40	0.15	5.61
3	40	0.075	4.34
4	40	0.037	2.67
5	20	0.27	5.45
6	40	0.27	6.55
7	60	0.27	7.99
8	80	0.27	9.15

[a] All experiments were carried out in neat silane, [silane] = 5.4 M.

effect of temperature on reaction rate seems to be much less than is generally observed for most chemical reactions. When the temperature was increased by 20 degree, the rate constant k' increased only by about 20%. The reason for such a temperature effect is not very clear. The most likely possibility is that the concentration of the active catalyst decreased with the increase in temperature. Another possibility is the reactivity of the active catalyst decreased with increasing temperature. The latter case might happen if the structure of the active catalyst or intermediate changes with temperature. It is also possible that the activation energy for the titanocene catalyzed reaction is low. However, it is difficult to estimate the actual activation energy because the concentration of the active catalyst has been included in the k' in eq. IV-1 as a constant factor.

Another important feature observed in the dehydrocoupling reaction of diphenylsilane is that the reaction rate is much faster in the earlier stages of the reaction. After about 2-3 hours, the reaction rate becomes steady and kinetic data can be measured. It is believed that the higher reaction rate at the beginning results from higher concentration of the active catalyst during this period. A ^1H NMR study of the stoichiometric reaction of

Cp_2TiMe_2 with Ph_2SiH_2 indicated that Cp_2TiMe_2 was totally transformed into the five membered ring dinuclear silyltitanocene complex $Cp_2Ti(\mu\text{-}H)(\mu\text{-}HSiPh_2)TiCp_2$ (<u>**Vd**</u>) at the onset of reaction. Subsequent to this, most of <u>**Vd**</u> was converted to paramagnetic titanocene complexes slowly, so the concentration of <u>**Vd**</u> decreased gradually during a course of 2-3 hours and then remained constant essentially. After several hours, a black compound along with a small amounts of green color compound was precipitated from the reaction solution. Both compounds are paramagnetic and no NMR spectrum can be obtained. EPR studies indicated that the major component of the reaction products is the mixed valence hydride $(Cp_2TiH)_2H$ (<u>**XI**</u>) (171). From the reaction of Cp_2TiMe_2 with Ph_2SiH_2, the silyltitanocene(III) species can be trapped with trimethylphosphine to give a monomeric complex $Cp_2Ti(SiPh_2H)PMe_3$ (see chapter VI). By comparison of this reaction with the phenylsilane reaction (32), it is believed that the green compound is most probably the silyltitanocene(III) dimer $[Cp_2Ti(\mu\text{-}HSiPh_2)]_2$ (<u>**VIId**</u>). The paramagnetism for such a compound might result from the weak Ti-H bonding due to larger steric bulk of the diphenylsilyl group.

The variation of the concentration of <u>**Vd**</u> with time is very consistent with the variation of the reaction rate. This probably indicates that the dinuclear complex <u>**Vd**</u> is the active catalyst. Many experimental results we have obtained support such an assumption that the five membered ring dinuclear complexes <u>**V**</u> are involved in the catalytic cycle of the dehydrocoupling reaction of hydrosilanes. The detailed discussion of the reaction mechanism and experimental evidence will be given in next chapter. A reasonable candidate for the catalytic cycle in which <u>**Vd**</u> is involved is shown in eq. IV-2, IV-3 and IV-4. In order to account for the production of complex <u>**Vd**</u>, the titanocene moiety, Cp_2Ti, must be involved and remain intact. Since the precise structure of titanocene has not been determined, it is represented as "Cp_2Ti". The existence of "Cp_2Ti" in the dehydrocoupling reaction of phenylsilane has been proved by a number of experiments in early studies

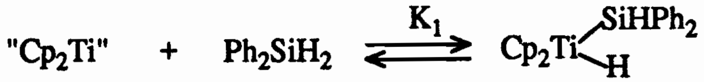

$$\text{"Cp}_2\text{Ti"} + \text{Ph}_2\text{SiH}_2 \overset{K_1}{\rightleftharpoons} \text{Cp}_2\text{Ti}(\text{SiHPh}_2)(\text{H})$$

(IV-2)

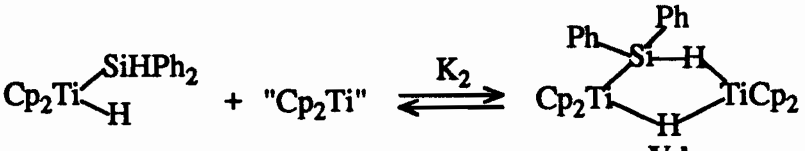

Vd

(IV-3)

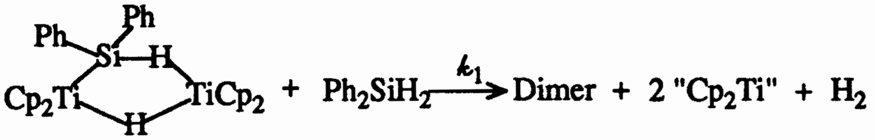

Vd

(IV-4)

(32,148). If it is assumed that equilibria IV-2 and IV-3 are rapidly established and the reaction IV-4 is the rate-controlling step, the concentration of **Vd** is given by

$$[\underline{\text{Vd}}] = K_1K_2[\text{"Cp}_2\text{Ti"}]^2[\text{Ph}_2\text{SiH}_2] \qquad \text{(IV-5)}$$

and then the reaction rate can be expressed as follows:

$$R_d = k_1K_1K_2[\text{"Cp}_2\text{Ti"}]^2\,[\text{Ph}_2\text{SiH}_2]^2 \qquad \text{(IV-6)}$$

When the concentration of the active catalyst remains constant, eq. IV-6 can be reduced to eq. IV-1 with

$$k' = k_1K_1K_2[\text{"Cp}_2\text{Ti"}]^2 \qquad \text{(IV-7)}$$

In fact, experimentally it might be difficult to determine the reaction order with respect to the active catalyst. As mentioned above, during the dehydrocoupling reaction, most of titanium-containing molecules exist in the forms of **VII** and **XI**. The concentration of **Vd** is quite low and does not seem to increase proportionally with the increase in the total concentration of the titanium compounds due to very complicated relations among the compounds in the system.

B. Zirconocene catalyzed reaction.

Dimethylzirconocene exhibits almost identical behavior to dimethyltitanocene in catalyzing the dimerization of diphenylsilane, giving 1,1,2,2-tetraphenyldisilane as the sole dehydrocoupling product. The only difference in reaction products between the two systems is that, in contrast to the DMT catalyzed reaction, only a trace amount of diphenylmethylsilane was produced in the DMZ catalyzed reaction. This probably indicates that the manner in which the catalyst precursor (DMT and DMZ) is transformed into active catalyst species is somewhat different for the two cases. Although DMZ was found to be a more powerful catalyst than DMT for catalyzing the polymerization of phenylsilane, the DMZ catalyzed dimerization of diphenylsilane does not seem to be faster than DMT catalyzed reaction at room temperature. Some typical reaction profiles for DMZ catalyzed dimerization of diphenylsilane at different catalyst concentrations and temperatures are shown in Figures IV-4 and IV-5 respectively. As with the DMT catalyzed reaction described above, the reaction rate of the zirconocene catalyzed dimerization of diphenylsilane also varies as functions of temperature and catalyst concentration. The effect of temperature on the reaction rate in the zirconocene system is much greater than in the titanocene system. So the zirconocene catalyzed reactions at higher temperature are much faster than the titanocene catalyzed reactions under the same conditions, although the reaction rates are comparable at room temperature for both systems.

The kinetic study indicates that the zirconocene catalyzed dimerization of phenylsilane has the same rate law as shown in eq. IV-1 for the titanocene catalyzed reaction. The kinetic data for a number of reactions under different conditions are listed in Table IV-2 and the typical second-order plots for the reactions at different temperatures are shown in Figure IV-6. In order to prove the kinetic results obtained from neat silane reactions, a number of kinetic experiments have also been carried out with toluene as solvent. The results of these experiments are consistent with those of the neat silane

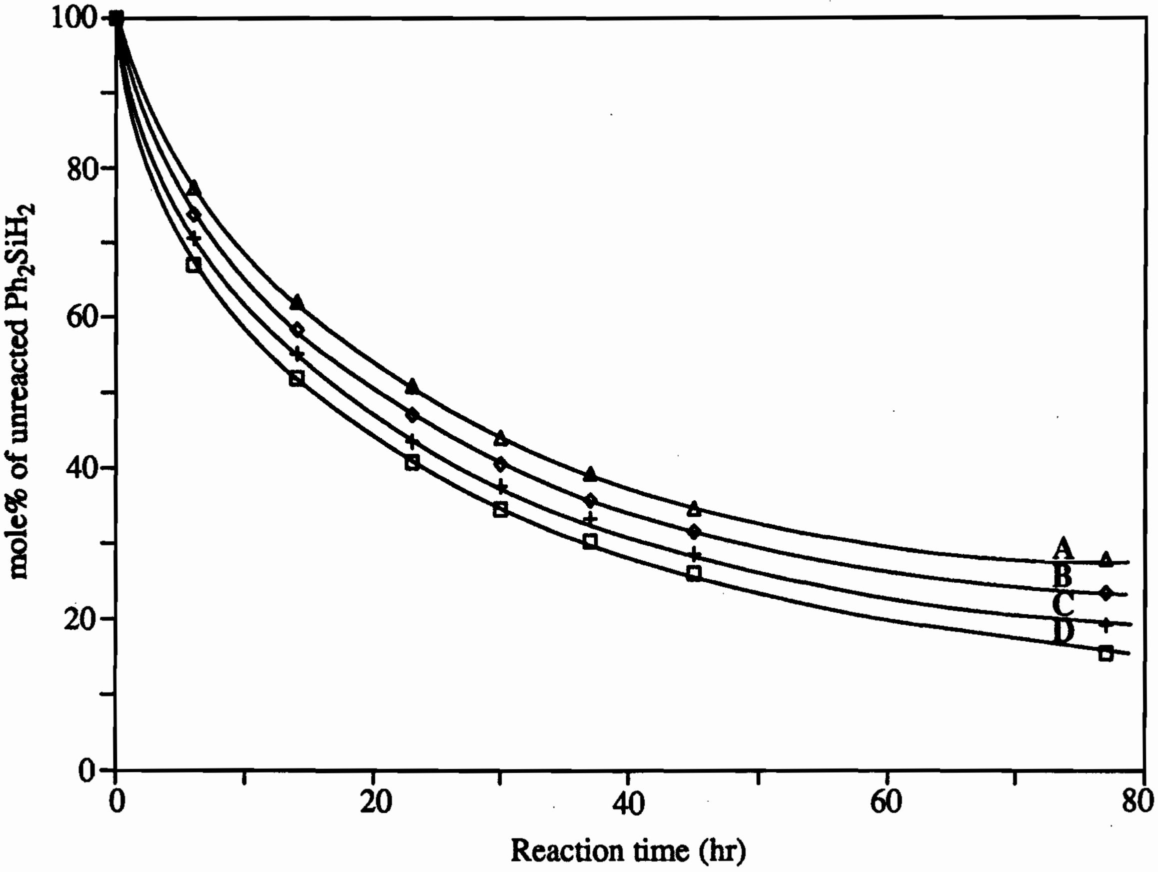

Figure IV-4. Reaction profiles for the zirconocene catalyzed dehydrocoupling of Ph_2SiH_2 at different catalyst concentrations. (A) 0.07 M; (B) 0.14 M; (C) 0.22 M and (D) 0.30 M DMZ in neat silane (5.4 M) at 50°C.

reactions. By comparing the kinetic data in Table IV-2 with those in Table IV-1, it can be seen that the effect of catalyst concentration on the rate constant k' in zirconocene system is even weaker than in the titanocene system. The possible reason for the weak effect of catalyst concentration has been discussed above. The effect of temperature on the rate constant k' in the zirconocene system is much stronger, and seems to be more reasonable than in the titanocene system. The reason for this difference between the two systems is not clear. Several possibilities for the weaker temperature effect in titanocene system has also been discussed above.

Given that the same dehydrocoupling reaction product and rate law were obtained from the two systems, it is very possible that the same reaction mechanism is operating in

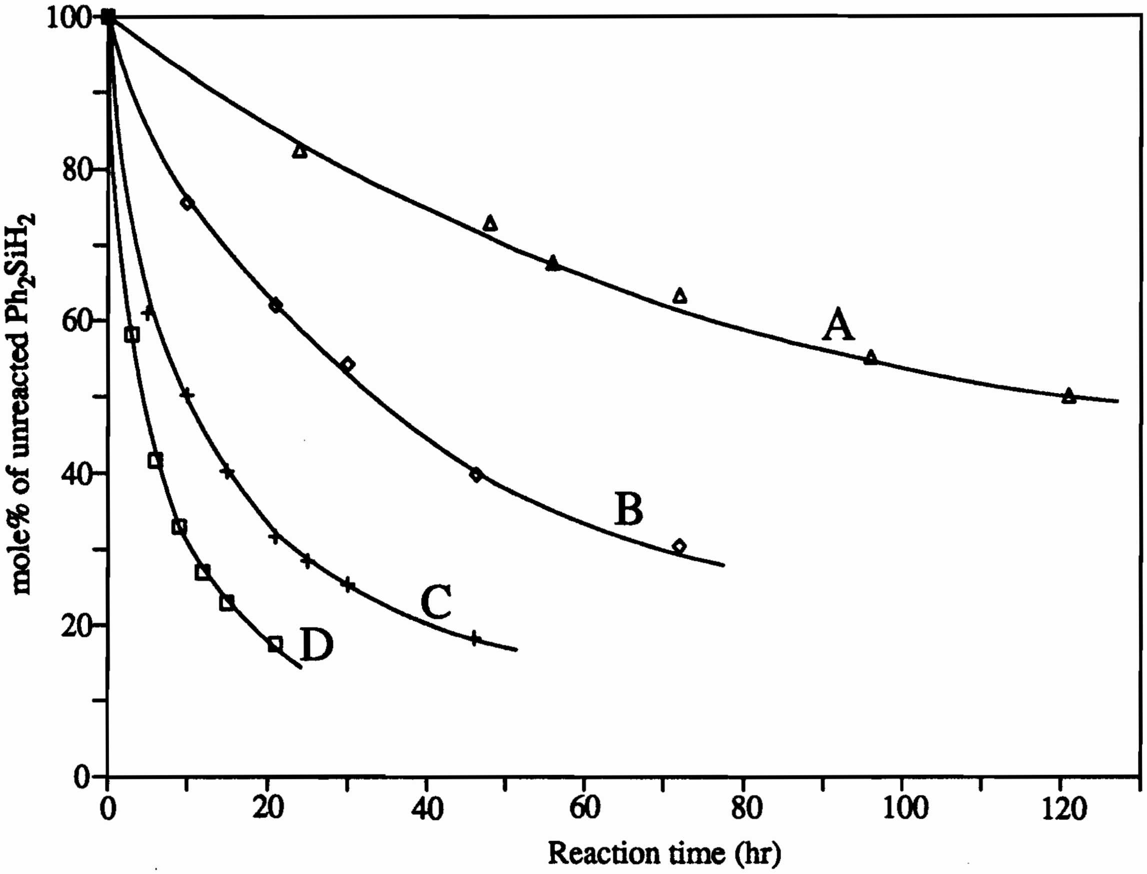

Figure IV-5. Reaction profiles for the zirconocene catalyzed dehydrocoupling of Ph_2SiH_2 at different temperatures. (A) 20°C; (B) 40°C; (C) 60°C; (D) 80°C. [cat.] = 0.27 M in neat silane (5.4 M).

both systems. Although most of the zirconium remains in the form of Zr(IV) species throughout the dehydrocoupling reaction, a hydride resonance in the region of -12 ppm has been observed in the reactions of some secondary silanes with dimethylzirconocene (see chapter V). This resonance is at unusually high field and is almost certainly due to a diamagnetic zirconocene(III) species, most likely a zirconocene analogue of the symmetrical silyltitanocene(III) dimer VII. In earlier studies, weak EPR signals, assigned to a zirconocene analogue of the mixed valence titanocene hydride $(Cp_2TiH)_2H$, were observed during the reaction of dimethylzirconocene with phenylsilane (33). Such EPR signals have also been observed recently in the reactions of other primary and secondary silanes (see chapter V). In addition, the reaction of dimethylzirconocene with a secondary

Table IV-2. Kinetic data for zirconocene catalyzed dehydrocoupling reactions of diphenylsilane

No.	Temperature (°C)	[silane] (M)	[Cp_2ZrMe_2] (M)	$10^5 k'$ ($M^{-1}s^{-1}$)
1	50	5.40[a]	0.30	17.8
2	50	5.40	0.22	16.7
3	50	5.40	0.14	14.6
4	50	5.40	0.07	12.7
5	20	5.40	0.27	2.57
6	40	5.40	0.27	9.79
7	60	5.40	0.27	29.0
8	80	5.40	0.27	70.5
9	60	2.00[b]	0.10	23.9
10	60	2.00	0.08	22.6
11	60	2.00	0.06	21.1

[a] in neat silane, [silane] = 5.40 M. [b] in toluene.

silane or a less reactive primary silane such as methylsilane gave a dark-brown solution, from which a mixture of dark and yellow compounds can be obtained after removing the solvent. ^1H NMR measurement indicated that the dark-brown solution contains considerable amounts of paramagnetic species, which gives rise to weak sample signals and strong solvent signals even though the solution is very concentrated. It was reported that a similar dark-brown solution had been obtained from the reaction of zirconocene dihydride with olefin and the dark species was identified as "Cp_2Zr" (139). The existence of these low valent zirconocene complexes suggests again that the zirconocene catalyzed reaction probably goes through the same mechanism as the titanocene catalyzed reaction, as shown in eq. IV-2, IV-3 and IV-4. Although the key catalyst species in eq. IV-4, a five membered ring bimetallic complex, has not been observed in the zirconocene system, it is possible that such a zirconocene complex is not observable because it is short lived, or paramagnetic. In fact, the titanocene analogue V is paramagnetic in solution (32).

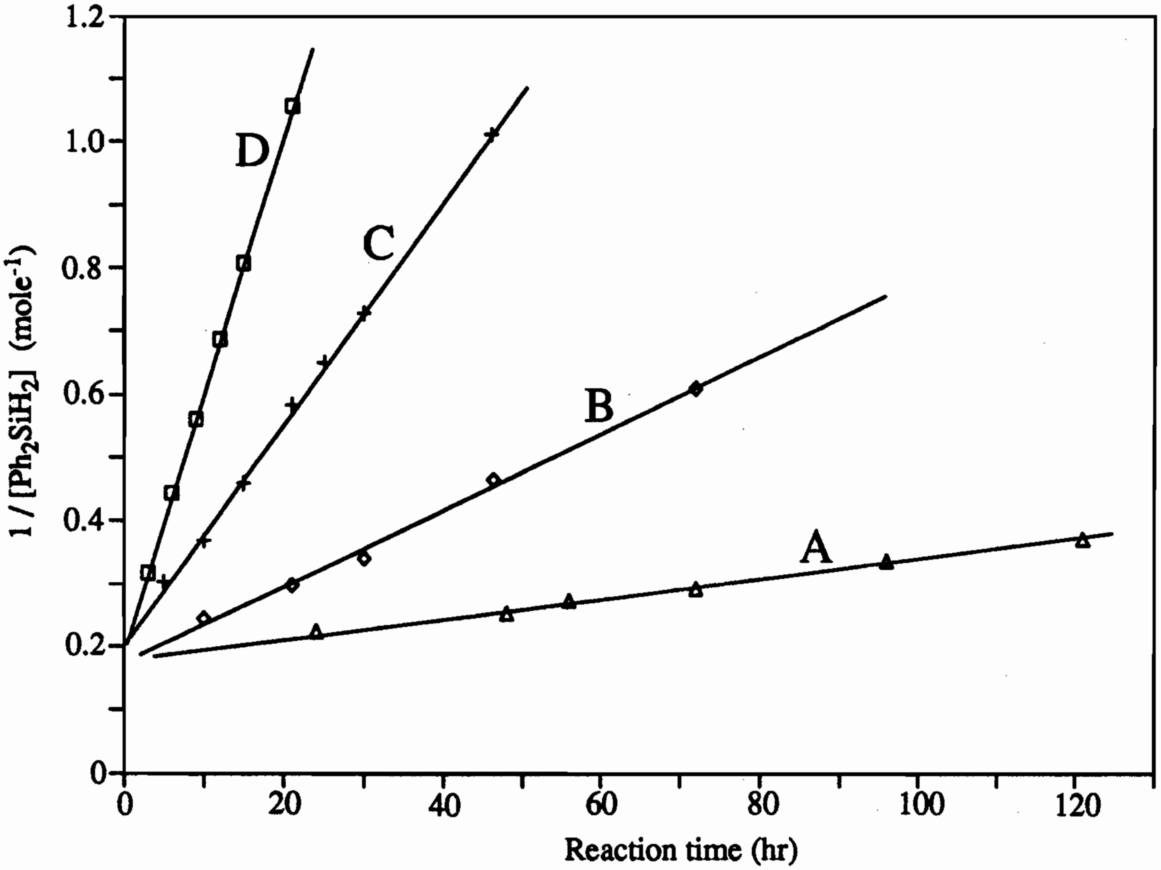

Figure IV-6. Second-order plots for the zirconocene catalyzed dehydrocoupling reaction of Ph_2SiH_2 at different temperatures. (A) 20°C; (B) 40°C; (C) 60°C; (D) 80°C. [cat.] = 0.27 M in neat silane (5.4 M).

Another possible candidate for the reaction mechanism involves a σ-bond metathesis similar to that proposed by Tilley *et al.*(94). The first step of this assumed mechanism is the same as shown in eq. IV-2. The second step, which is presumably the rate-controlling step, is shown in eq. IV-8:

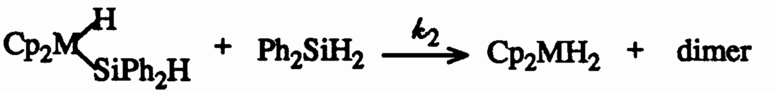

$$Cp_2M\begin{matrix}H\\SiPh_2H\end{matrix} + Ph_2SiH_2 \xrightarrow{k_2} Cp_2MH_2 + \text{dimer} \qquad (IV\text{-}8)$$

Such a mechanism can also give the rate law shown in eq. IV-1. As an alternative to eq. IV-8, σ-bond metathesis between two $Cp_2M(H)SiPh_2H$ molecules, as shown in eq. IV-9, is also possible. Considering that the Si-H bond could probably be activated by the metal toward facile σ-bond metathesis, reaction IV-9 would be more reasonable than IV-8. More detailed discussion will be given in the next chapter.

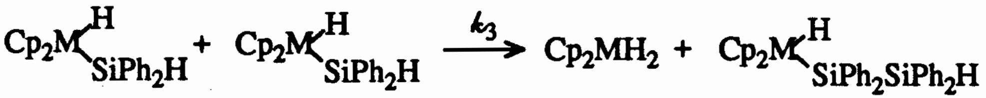

$$\mathrm{Cp_2M}\begin{smallmatrix}\mathrm{H}\\ \mathrm{SiPh_2H}\end{smallmatrix} + \mathrm{Cp_2M}\begin{smallmatrix}\mathrm{H}\\ \mathrm{SiPh_2H}\end{smallmatrix} \xrightarrow{k_3} \mathrm{Cp_2MH_2} + \mathrm{Cp_2M}\begin{smallmatrix}\mathrm{H}\\ \mathrm{SiPh_2SiPh_2H}\end{smallmatrix} \tag{IV-9}$$

C. Trimethyl(cyclopentadienyl)titanium catalyzed reaction.

The catalytic dehydrocoupling of hydrosilanes has been found to be very sensitive to steric bulk of both silane and catalyst (34,90). Corey *et al.* have recently reported that trimer was obtained from the zirconocene catalyzed dehydrocoupling reaction when the two phenyl groups of diphenylsilane are linked in the ortho position by a methylene group and larger oligomers were obtained from the titanocene catalyzed reaction when the two phenyls are tied by a bond instead of a methylene group (85). If the chain length of the coupling product of diphenylsilane is also sensitive to the steric bulk of catalyst, it should be possible to obtain oligomers larger than dimer from the dehydrocoupling reaction when a less sterically bulky catalyst is used. Based on such a consideration, trimethyl(cyclopentadienyl)titanium was tested as a catalyst for the dehydrocoupling of diphenylsilane. Unfortunately, dimer was obtained again as the only product. Moreover, $CpTiMe_3$ showed relatively low catalytic activity towards the dehydrocoupling of diphenylsilane compared to dimethyltitanocene. The results of a number of experiments are shown in Figure IV-7.

To date, only dimer has been obtained from the dehydrocoupling reaction of diphenylsilane catalyzed by a variety of catalysts, including late transition metal complexes (81,82) and early transition metal complexes (32,33,91). It seems that the steric constraint comes from diphenylsilane itself and it is thus impossible to obtain oligomers larger than dimer by changing catalyst.

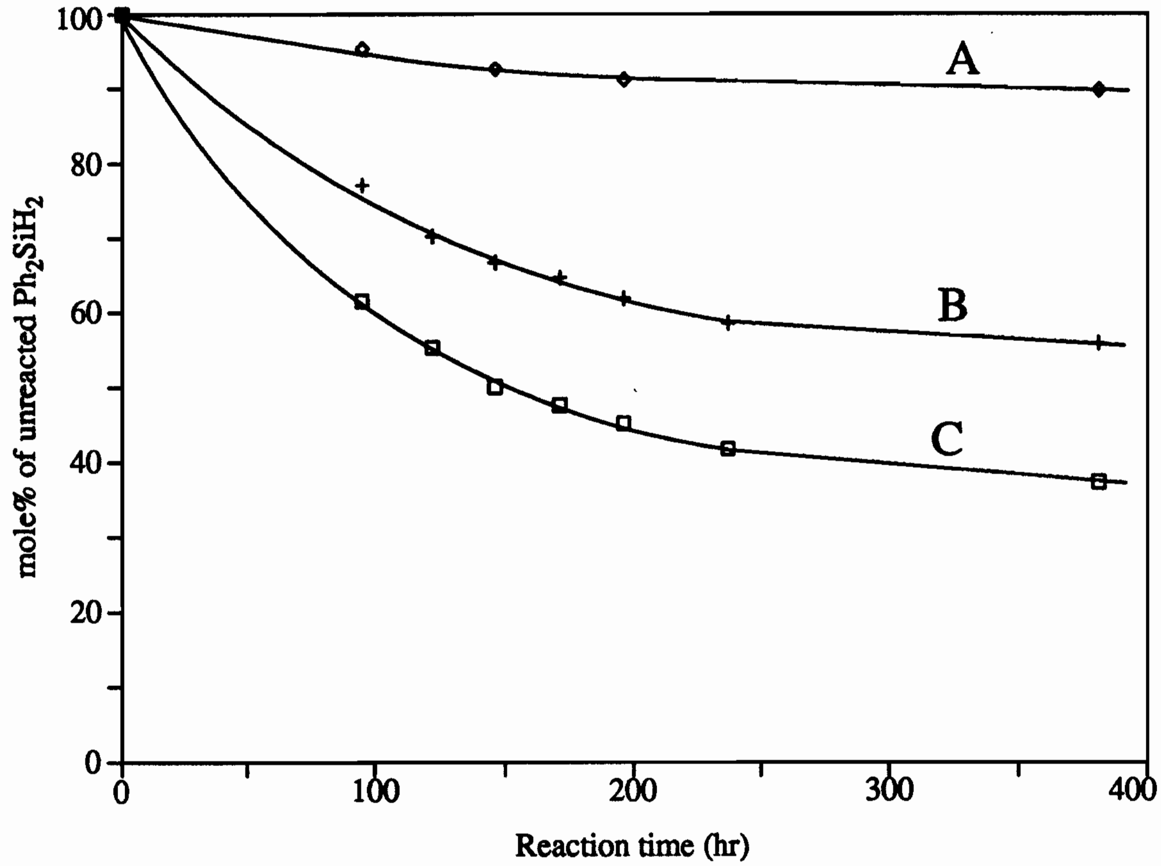

Figure IV-7. Reaction profiles for the dehydrocoupling of Ph_2SiH_2 catalyzed by $CpTiMe_3$ at different temperatures. (A) 20°C; (B) 40°C; (C) 60°C. [cat.] = 0.27 M in neat silane (5.4 M).

IV.2.2 Dehydrocoupling of phenylmethylsilane.

The dehydrocoupling reaction of phenylmethylsilane catalyzed by either dimethyltitanocene or dimethylzirconocene was found to be very slow and gave mainly 1,2-dimethyl-1,2-diphenyldisilane and 1,2,3-trimethyl-1,2,3-triphenyltrisilane as products. No larger oligomers were detected by ^1H NMR and GPC even when the reaction was carried out at 120°C. A number of typical GPC traces are shown in Figure IV-8. The disilane and trisilane give well-separated Si-H ^1H NMR signals and these compounds can be separated very well by GC and GPC, so the reaction can be easily followed. When the reaction was carried out at higher temperatures (≥ 40°C), small amounts of siloxanes were

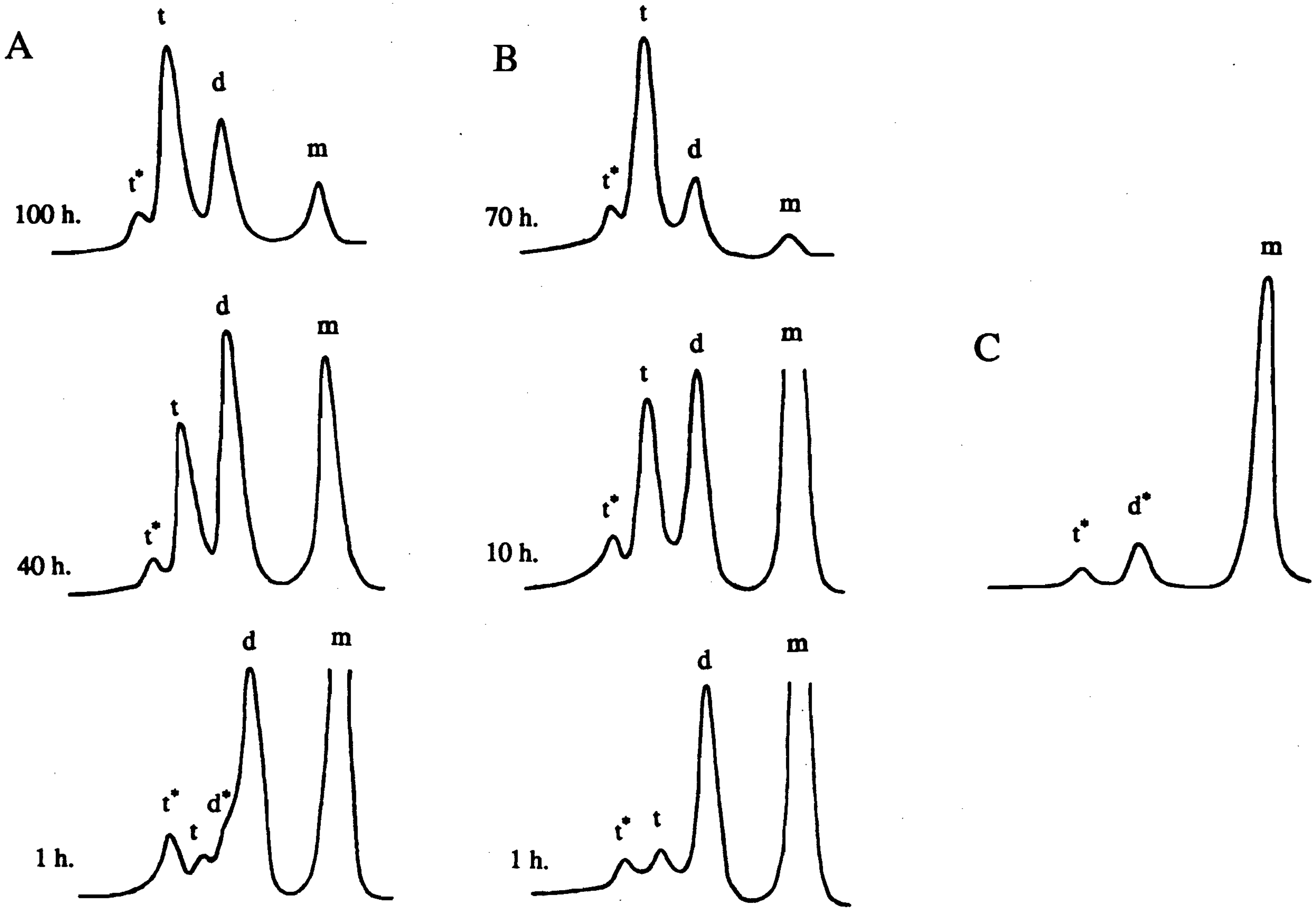

Figure IV-8. GPC traces of (A) titanocene and (B) zirconocene catalyzed $PhMeSiH_2$ dehydrocoupling reaction mixtures at different times, Temp. = 80°C, [Cat.] = 0.218 M; (C) A partially oxidized $PhMeSiH_2$ sample. m - monomer; d - dimer; t - trimer; d^* - disiloxane; t^* - trisiloxane.

usually produced since the phenylmethylsilane and its oligomers are more air sensitive than phenylsilane and diphenylsilane as well as their oligomers. The siloxanes were characterized by ^{1}H NMR and IR. The presence of a broad band in the 1100 cm^{-1} region is characteristic of the siloxanes. Disiloxane and trisiloxane also give distinct Si-H resonances around 5.4 ppm.

The assignments for 1,2-dimethyl-1,2-diphenyldisilane and 1,2,3-trimethyl-1,2,3-triphenyltrisilane were made on the basis of their ^{1}H NMR spectra (including decoupled spectra), GC and GPC traces. There are two diastereomers for the dimer and three diastereomers for the trimer as shown below:

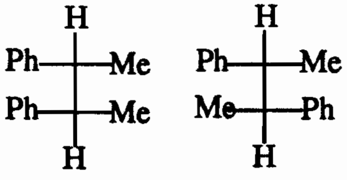

A **B**

Dimer

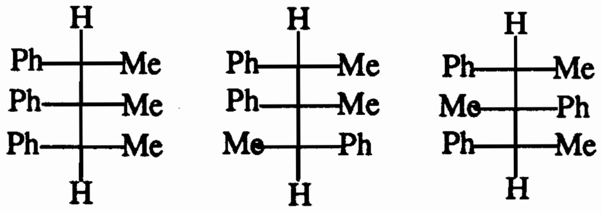

A **B** **C**

Trimer

In the ^{1}H NMR spectrum, all of these stereoisomers can be seen clearly. However, it is difficult to make full ^{1}H NMR assignments for these stereoisomers without separating them. The three diastereomers of the trimer give four sets of Si-H ^{1}H NMR resonances, four sets of C-H resonances for the 1,3-methyl groups and three sets of C-H resonances for the 2-methyl groups. The integral ratio of the C-H resonances of the 2-methyl groups are essentially 1:2:1, which is expected if the relative amount of **A**, **B** and **C** is purely statistical since there are two enantiomers of **B**. The ^{1}H NMR data for these stereoisomers of dimer and trimer as well as for disiloxane and trisiloxane are listed in Table IV-3. The two diastereomers of the dimer can be well separated by GC, while the three isomers of the trimer give one broad peak.

Table IV-3. ^1H NMR data for dimer, trimer and siloxanes[a] from dehydrocoupling reactions of $PhMeSiH_2$

Compound	No. of diastereomers	Si-H	*t*-Me	*m*-Me	^3J (SiH, CH) (Hz)
dimer	2	4.625 (q)	0.337 (d)		4.6
		4.638 (q)	0.347 (d)		4.6
trimer	3	4.711 (q)	0.343 (d)	0.417 (s)	4.6
		4.718 (q)	0.347 (d)	0.427 (s)	4.6
		4.726 (q)	0.378 (d)		4.6
		4.734 (q)	0.381 (d)	0.446 (s)	4.6
disiloxane	2	5.409 (q)	0.333 (d)		3.0
		5.413 (q)			3.0
trisiloxane	3	5.443 (q)	0.363 (d)	0.402 (s)	3.0

[a] NMR chemical shifts, δ(ppm), determined in C_6D_6 with TMS as internal standard. Abbreviations: s, singlet; d, doublet; q, quartet; *t*-Me, methyl group at terminal Si atom; *m*-Me, methyl group at meso- Si atom.

A. Titanocene catalyzed reaction.

The titanocene catalyzed dehydrocoupling reaction of phenylmethylsilane is very slow. Even when the reaction was carried out with 3 mole% of catalyst at 80°C, it required about one week to go to completion. The phenylmethylsilane dehydrocoupling reaction gives dimer and trimer as products in a stepwise fashion. As mentioned above, no evidence for the formation of larger oligomers has been obtained so far from the titanocene catalyzed reactions. By following the reactions under different conditions, it was found that higher temperatures favoured the formation of trimer. When the reaction was conducted at 80°C, 70% of starting phenylmethylsilane could be converted to trisilane at the end of reaction, while only 25% of phenylmethylsilane has been transformed into trisilane at 20°C after 180 hours. The major product in the latter case was dimer (> 40 wt% of the reaction mixture). The facts that a large amount of dimer was accumulated during the dehydrocoupling reaction of phenylmethylsilane and higher temperatures favored the conversion of dimer to trimer indicate that the reactivity of 1,2-diphenyl-1,2-dimethyldisilane is relatively low.

This is in contrast with the phenylsilane reaction where the disilane was found to be much more reactive than monosilane. The lower reactivity of 1,2-diphenyl-1,2-dimethyldisilane is obviously due to its larger steric hindrance and its tertiary structure. It appears that the reactivity decreases rapidly with the increase in steric hindrance from monomer to dimer to trimer because the dimer can be slowly converted to trimer, whereas the trimer seems to be the final product and can not be transformed into larger oligomers under our experimental conditions.

As in the case of the diphenylsilane reaction, the reaction rate increases with increasing temperature and catalyst concentration, but the effects of both temperature and catalyst concentration on the rate of monomer consumption do not appear to be very remarkable although the conversion of dimer to trimer is strongly dependent on temperature. A number of reaction profiles for the titanocene catalyzed dehydrocoupling of phenylmethylsilane at different temperatures and catalyst concentrations are shown in Figures IV-9 and IV-10 respectively.

B. Zirconocene catalyzed reaction.

By following reactions under different conditions, it was found that the zirconocene catalyzed dehydrocoupling reaction of phenylmethylsilane also gives only dimer and trimer as coupling products, even at temperatures as high as 120°C. Although Corey *et al.* reported that oligomers from dimer to octamer have been obtained from the phenylmethylsilane dehydrocoupling reaction with a zirconocene catalyst generated *in situ* by reaction of dichlorozirconocene with butyllithium (214), we did not observe any notable amount of oligomers larger than trimer under our experimental conditions.

The effect of temperature on the reaction rate and product distribution is much more significant for the zirconocene catalyzed reaction than in the titanocene case. As shown in Figures IV-11 and IV-12, the dehydrocoupling reaction did not progress very much at room

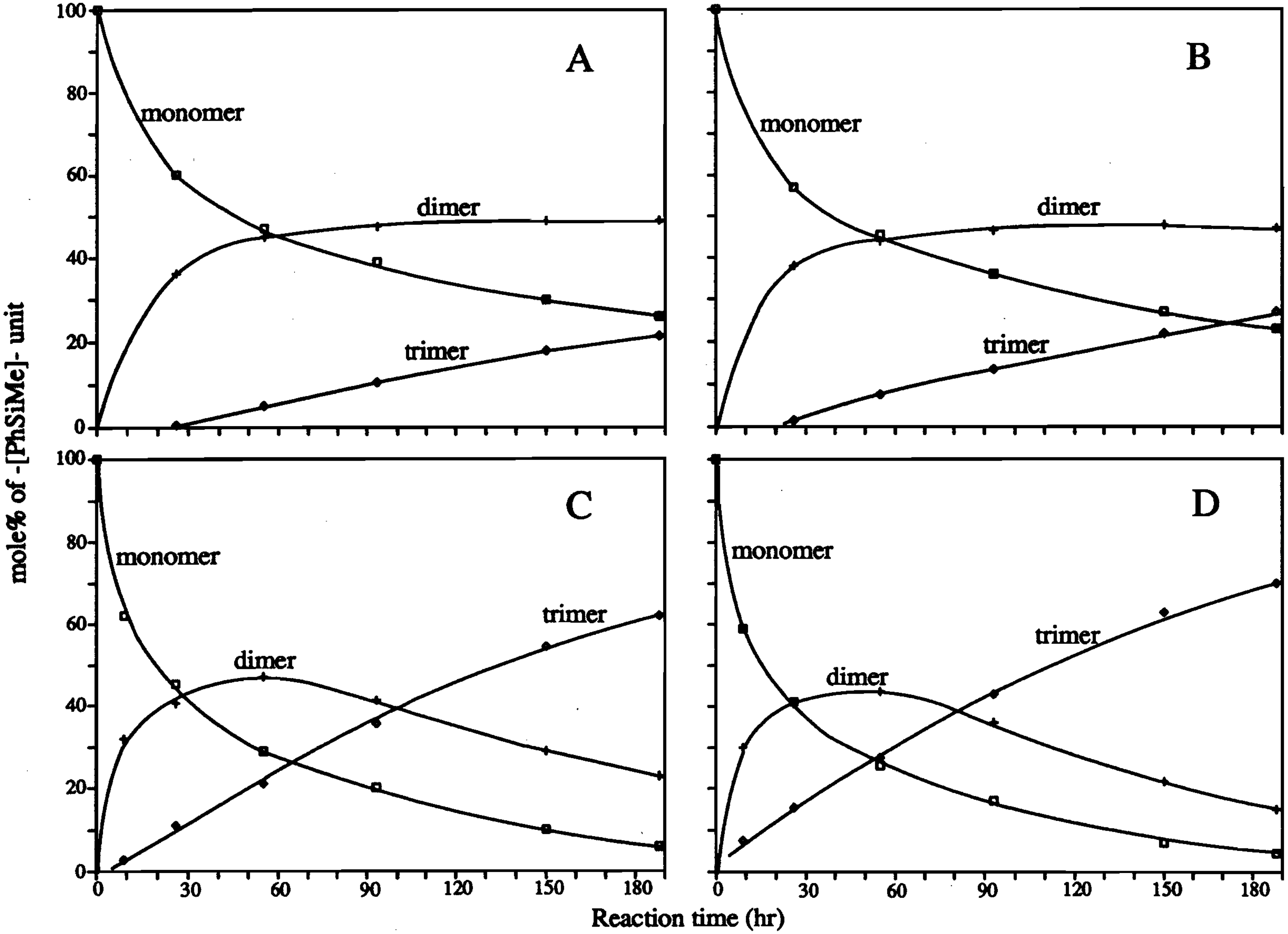

Figure IV-9. Reaction profiles for the titanocene catalyzed dehydrocoupling of $PhMeSiH_2$ at different temperatures. (A) 20°C; (B) 40°C; (C) 60°C; (D) 80°C. [cat.] = 0.218 M in neat silane.

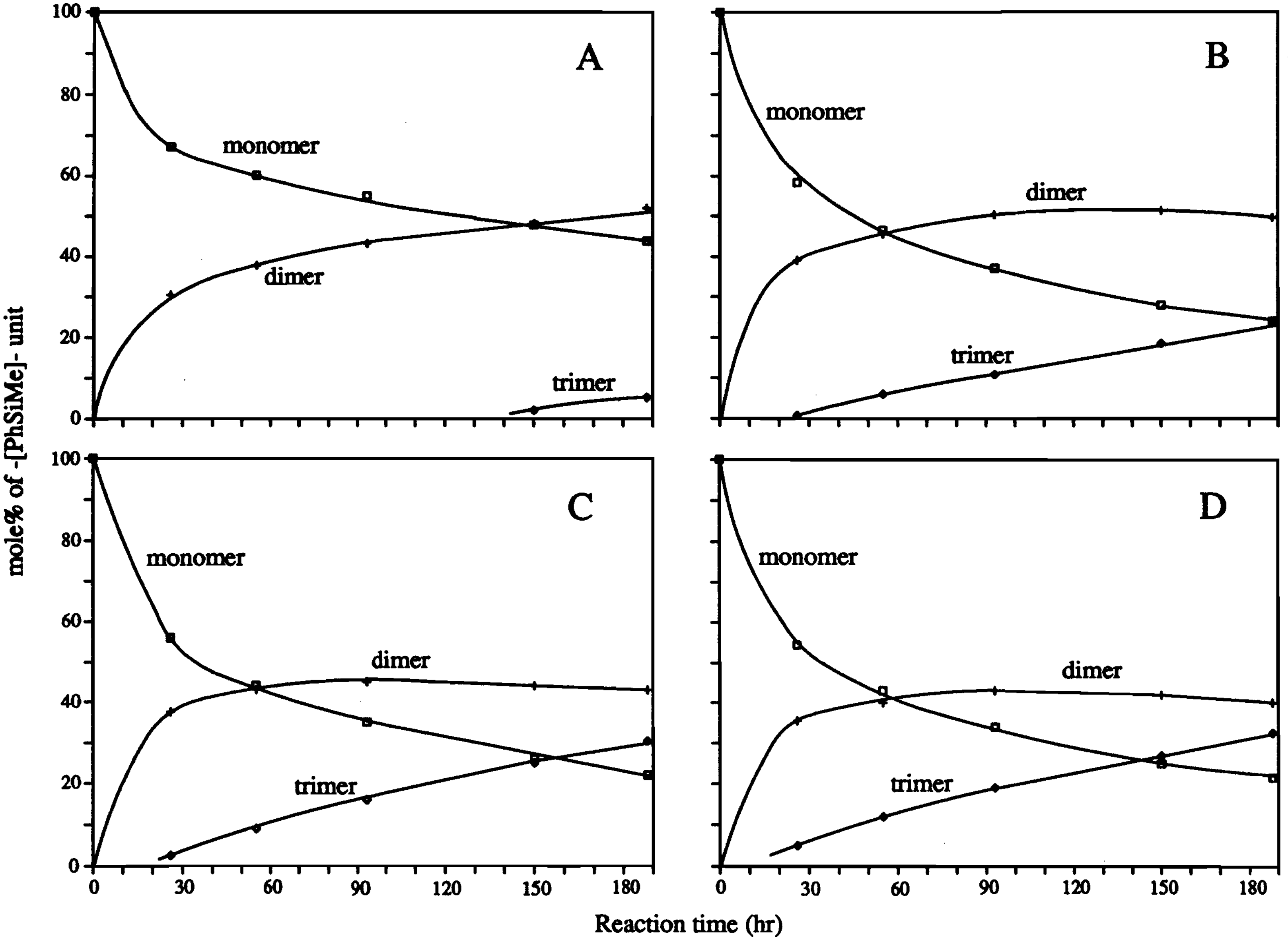

Figure IV-10. Reaction profiles for the titanocene catalyzed dehydrocoupling of $PhMeSiH_2$ at different catalyst concentrations. (A) [cat.] = 0.073 M; (B) [cat.] = 0.146 M; (C) [cat.] = 0.291 M; (D) [cat.] = 0.364 M in neat silane at 40°C.

temperature and only 20% of starting monosilane was converted to disilane. It appears that the catalyst deactivated rapidly at low temperatures. With increasing temperature, the reaction rate and conversion of monosilane increased remarkably. When the reaction was conducted at 80°C, a conversion about 90% could be obtained and ~65% of starting phenylmethylsilane was converted to trimer after about 70 hours.

As discussed in the last section, the smaller temperature effect in the titanocene system is probably due to a decrease in the concentration of active catalyst with increasing temperature. If this is true, the larger temperature effect in the zirconocene system should also be associated with the concentration of active catalyst. It has been found that most of the zirconium species in the catalytic reaction exist in the form of dimeric silylzirconocene(IV)hydride complexes (see chapter V). These dimeric Zr(IV) complexes were found to have little catalytic activity toward the silane dehydrocoupling reaction. It is possible that they dissociate to form active catalyst more easily at higher temperature, and thus the concentration of the active catalyst increases, or at least does not decrease very much, with increasing temperature.

As in the case of the titanocene catalyzed reaction, the reaction rate and conversion increase with increasing the concentration of dimethylzirconocene, but the amplitude of the increase in both the reaction rate and conversion is much smaller than that in the total catalyst concentration. These experimental observations indicate again that the concentration of active catalyst, in both catalytic systems, does not increase proportionally with increasing the total concentration of catalyst.

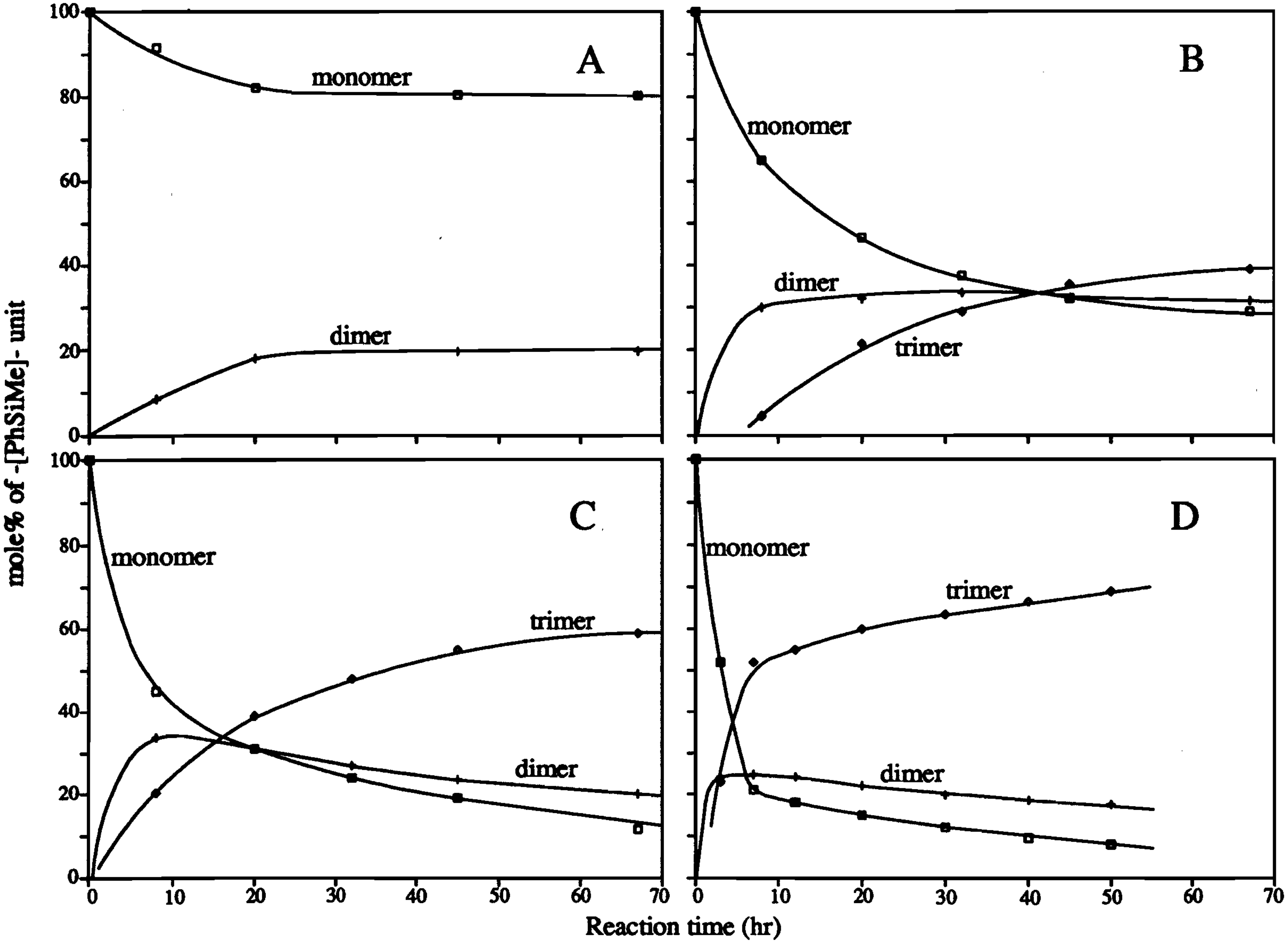

Figure IV-11. Reaction profiles for the zirconocene catalyzed dehydrocoupling of $PhMeSiH_2$ at different temperatures. (A) 20°C; (B) 60°C; (C) 80°C; (D) 120°C. [cat.] = 0.218 M in neat silane.

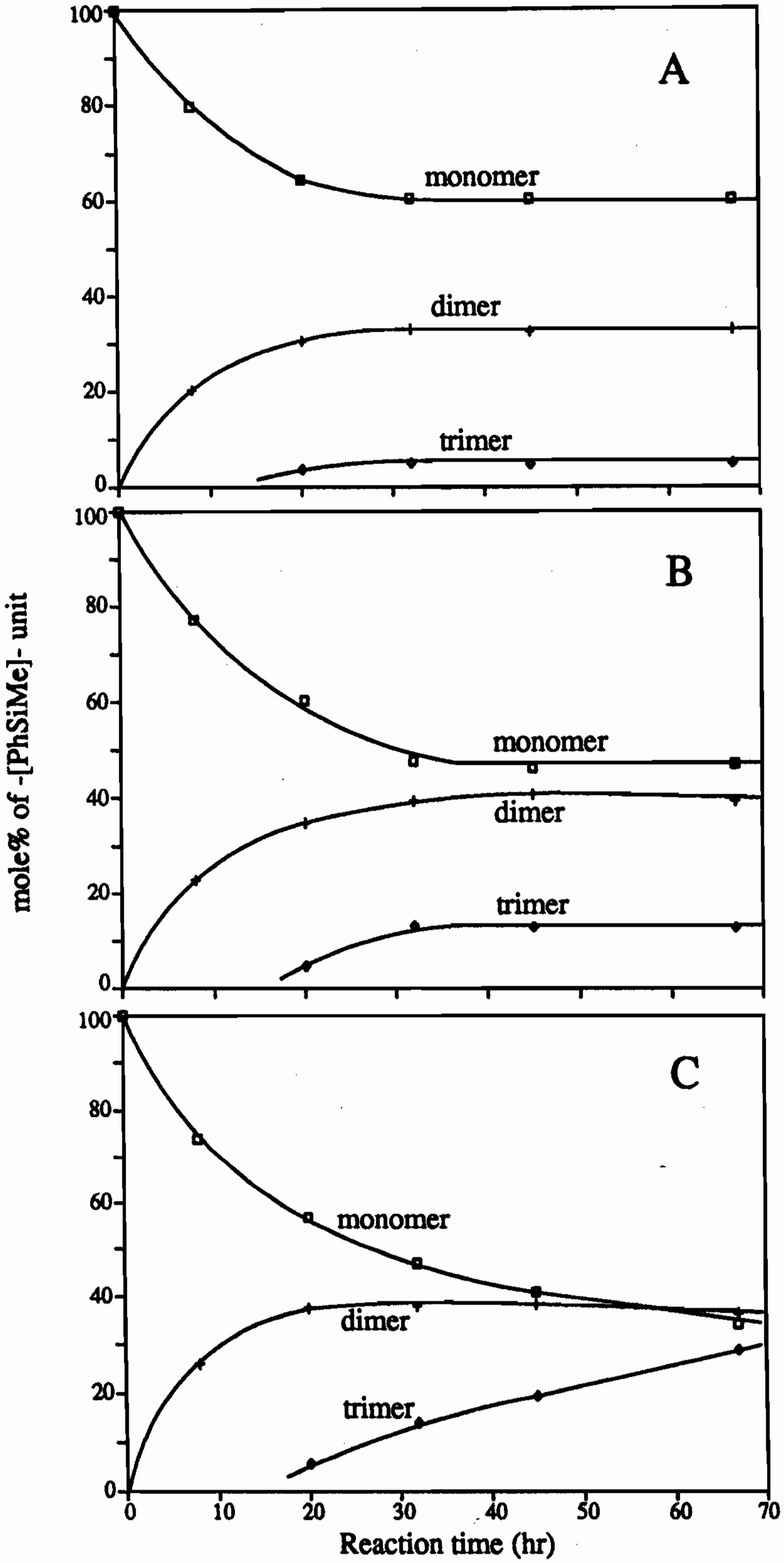

Figure IV-12. Reaction profiles for the zirconocene catalyzed dehydrocoupling of $PhMeSiH_2$ at different catalyst concentrations. (A) 0.073 M; (B) 0.218 M; (C) 0.364 M catalyst in neat silane (7.3 M) at 40°C.

IV.2.3 Observations on the reactions of butylmethylsilane.

In addition to diphenylsilane and phenylmethylsilane, the reactions of *n*-butylmethylsilane in the presence of catalytic amounts of dimethyltitanocene or dimethylzirconocene were also studied under different conditions. Butylmethylsilane is much less reactive than diphenylsilane and phenylmethylsilane. Although it can also transform dimethyltitanocene and dimethylzirconocene to corresponding silyl complexes, no coupling product has been observed from a number of reactions under different conditions, even refluxing for 10 hours in the presence of 3 mole% of catalyst.

It is evident that the low reactivity of butylmethylsilane toward dehydrocoupling reaction is due to both the electronic effect of its two alkyl groups and the larger steric demand of the butyl group than phenyl group. Based on the results we have obtained from the dehydrocoupling reactions of a number of primary and secondary silanes, it can be concluded that the reactivity of a silane depends on both the steric effect and electronic effect of its substituents. The alkyl substituent usually lowers the reactivity of a silane whereas the silyl and aryl substituents enhance the reactivity due to the difference in their electronic effect.

IV.3 EXPERIMENTAL

IV.3.1 General procedures.

All reactions were carried out in Schlenk tubes under argon. The general experimental technigues and procedures as well as the preparations of dimethyltitanocene and dimethylzirconocene have been described previously in chapter II. Trimethyl(cyclopentadienyl)titanium was prepared by a literature method (110). Diphenyldichlorosilane, phenylmethyldichlorosilane and *n*-butylmethyldichlorosilane were purchased from Petrarch Chemical Co. and used as received to prepare dihydrosilanes by literature methods (196). The dehydrocoupling reactions of diphenylsilane were followed by ^{1}H NMR on a Varian T-60 or XL-200 spectrometer and the reactions of phenylmethylsilane and butylmethylsilane were followed on a Varian XL-200 or XL-300 spectrometer. All chemical shifts were referenced to TMS. IR spectra were recorded on an Analect AQS-20 FT-IR spectrophotometer. Gas chromatography analysis of the reaction mixture of phenylmethylsilane was carried out on a Shimadzu GC-8A chromatograph. The detailed experimental conditions have been described before. GPC measurements were performed on a Varian 5000 Gel Permeation Chromatograph, interfaced to a Varian Vista 402 data station and equipped with a 500 Å Ultrastyragel column and a 100 Å Ultrastyragel column. Air-free chromatographic grade THF was used as solvent.

IV.3.2 Dehydrocoupling reactions.

1. Dimerization of diphenylsilane and kinetic studies.

The general experimental procedure for the dimerization reaction of diphenylsilane is the following. Appropriate amounts of catalyst (Cp_2TiMe_2, Cp_2ZrMe_2 or $CpTiMe_3$) were dissolved in either neat diphenylsilane (2 mL) or a solution of diphenylsilane in toluene (2 mL) in a Schlenk tube under argon. The reaction mixture was placed in a constant temperature oil bath with stirring at the temperatures specified in Tables IV-1 and IV-2 as well as Figure IV-7. The reaction was followed by periodic sampling and analysis by ^{1}H NMR and the amounts of monomer and dimer were measured by the integral ratio of their Si-H resonances. When DMT or DMZ was used as catalyst, > 90% of diphenylsilane could be converted to disilane if reaction time is long enough. The disilane was obtained as crystalline material after the monosilane was removed under vacuum, and was purified by either passing it through a Florisil column or recrystallization from hexane.

The reaction order with respect to silane was determined by linearization of concentration function of silane vs. time plots. For all studied reactions catalyzed by DMT or DMZ, a straight line was obtained from the second-order plot for a substantial portion of the reaction, indicating that these reactions are second order with respect to silane. The rate constants given in Tables IV-1 and IV-2 were obtained by measuring the slope of the straight line in the second-order plot. It should be pointed out that, for the titanocene catalyzed reactions, the kinetic data were obtained with the data points measured after these reactions have proceeded for two hours. Some exemplary plots are shown in Figures IV-3 and IV-6.

2. Oligomerization of phenylmethylsilane.

The oligomerization reactions of phenylmethylsilane were conducted in a similar way to the dimerization reactions of diphenylsilane. Generally, appropriate amounts of catalyst (Cp_2TiMe_2 or Cp_2ZrMe_2) were dissolved in neat phenylmethylsilane (2 mL) in a Schlenk tube. The reaction mixture was placed in a constant temperature oil bath, at the temperature specified in Figures IV-9 ~ IV-12, and was periodically sampled and analyzed by ^1H NMR. The concentrations of monomer, dimer and trimer in the phenylmethylsilane oligomerization reaction were followed easily due to the good separation of their resonances.

Chapter V

Reactions of some hydrosilanes with dimethyltitanocene and dimethylzirconocene and discussion of the mechanism of silane dehydrocoupling

V.1 INTRODUCTION

So far, the alkyl, silyl or hydride derivatives of titanocene and zirconocene have been found to be the most active catalysts for the dehydrocoupling reaction of hydrosilanes (32-34,90,92,148), and the dehydrocoupling reactions of a variety of primary and secondary organosilanes catalyzed by these titanocene and zirconocene derivatives have been studied (31,85,88,93,214). From most primary and secondary silanes, except methylsilane, only oligomers consisting of several to tens of silicon atoms can be obtained by the dehydrocoupling reaction. As mentioned in the preceeding chapters, to improve this method, it is very important to understand the reaction mechanism.

Two possible mechanisms, i.e., the metal silylene-based mechanism (34,89) and the σ-bond metathesis mechanism (92), have been suggested, and both of them can explain most of the observed features of the silane dehydrocoupling reaction. However, neither of the two mechanisms has been definitively confirmed or excluded experimentally. For the metal silylene-based mechanism, it is difficult to test due to the absence of any evidence for the existence of early transition metal silylene complexes. On the other hand, for the σ-bond metathesis mechanism, although some σ-bond metathesis reactions involving M-Si, M-H, Si-H and H-H (M = Zr, Hf) have been observed, it appears that further evidences are necessary to confirm the mechanism, especially to confirm the two significant reactions in

$$\text{M-Si} + \text{Si-H} \longrightarrow \text{M-H} + \text{Si-Si} \qquad \text{(V-1)}$$

$$\text{M-H} + \text{Si-H} \longrightarrow \text{M-Si} + H_2 \qquad \text{(V-2)}$$

the mechanism shown in eq. V-1 and V-2. As pointed out in Chapter I, the oligomerization of $PhSiH_3$ in the presence of chloride derivatives of zirconocene and hafnocene are too slow to prove that these chloride derivatives are involved in the catalytic cycle, while such an assumption that these chloride derivatives themselves are active catalysts is the basis of reactions V-1 and V-2 as well as the σ-bond metathesis mechanism. In addition, it is not clear whether or not the reaction V-2 is thermodynamically allowed (209). In a word, the reaction mechanism(s) (there may be more than one mechanism operating) for the dehydrocoupling of silanes is (are) still not very clear and further studies are necessary.

To further understand the dehydrocoupling reaction, the stoichiometric reactions of DMT and DMZ with a number of primary and secondary silanes have been studied and the results will be presented in this chapter. So far, some preliminary catalytic and stoichiometric reactions of a variety of primary and secondary silanes with DMT and DMZ have been studied in this laboratory (31-34,87-90). From these reactions, a number of pieces of evidence that support a bimetallic transition state mechanism for the titanocene catalyzed silane dehydrocoupling reaction have been accumulated. Although this evidence was obtained from the titanocene system, the zirconocene catalyzed reaction appears to be controlled by the same or a closely similar mechanism. In this chapter, the bimetallic transient mechanism will be discussed in detail, and several other possible mechanisms will also be discussed.

V.2 RESULTS AND DISCUSSION

V.2.1 Reactions of several silanes with DMT.

V.2.1.1 Further observations on the reaction of DMT with $PhSiH_3$.

The stoichiometric reactions of DMT with a number of primary organosilanes such as $PhSiH_3$, $BzSiH_3$ and $HxSiH_3$ have been studied previously (148). From these reactions, the dimeric silyl titanocene complexes, $[Cp_2Ti(\mu\text{-}H)(\mu\text{-}HSiHR)TiCp_2]$ **V** and $[Cp_2Ti(\mu\text{-}HSiHR)]_2$ **VII**, and the mixed valence hydride **XI** were obtained. It was noted that the complexes **V** were produced first in these reactions and can be subsequently converted to **VII** in the presence of excess silane. Both **V** and **VII**, if kept in solution, slowly decompose to hydride **XI**. The conversion of **VII** to **V** in solution, especially in THF, was also observed.

In this work, the formation and conversion of **Va** were studied quantitatively by following the reaction of DMT with $PhSiH_3$ by ^1H NMR. The profile of this reaction is shown in Figure V-1. The amount of **XI** was calculated by subtracting the amounts of **Va** and **VIIa** from the total amount of titanocene species. The calculation is reasonable because only these three compounds could be detected by NMR and EPR in this reaction system. From Figure V-1, it can be seen that DMT was totally transformed into **Va** at the onset of reaction. Most of **Va** was subsequently converted to **VIIa** and **XI** along with the formation of oligosilanes and hydrogen evolution. After about 2 hours, the concentrations of **Va**, **VIIa** and **XI** remained constant essentially. This may indicate that these complexes are involved in some kind of cycle. During this period, **Va** only accounted for about 30% of the total titanocene species, and most of the titanocene species were in the form of **VIIa** (~65%).

Complexes **Va** and **XI**, isolated from the reactions of Cp_2TiMe_2 with $PhSiH_3$ (148) and Ph_2SiH_2 (see section V.2.1.4) respectively, were found to be very active catalysts for the silane dehydrocoupling reaction with no induction period. The reactivity of these two complexes is comparable to that of DMT. However, the reactivity of **VIIa** is considerably

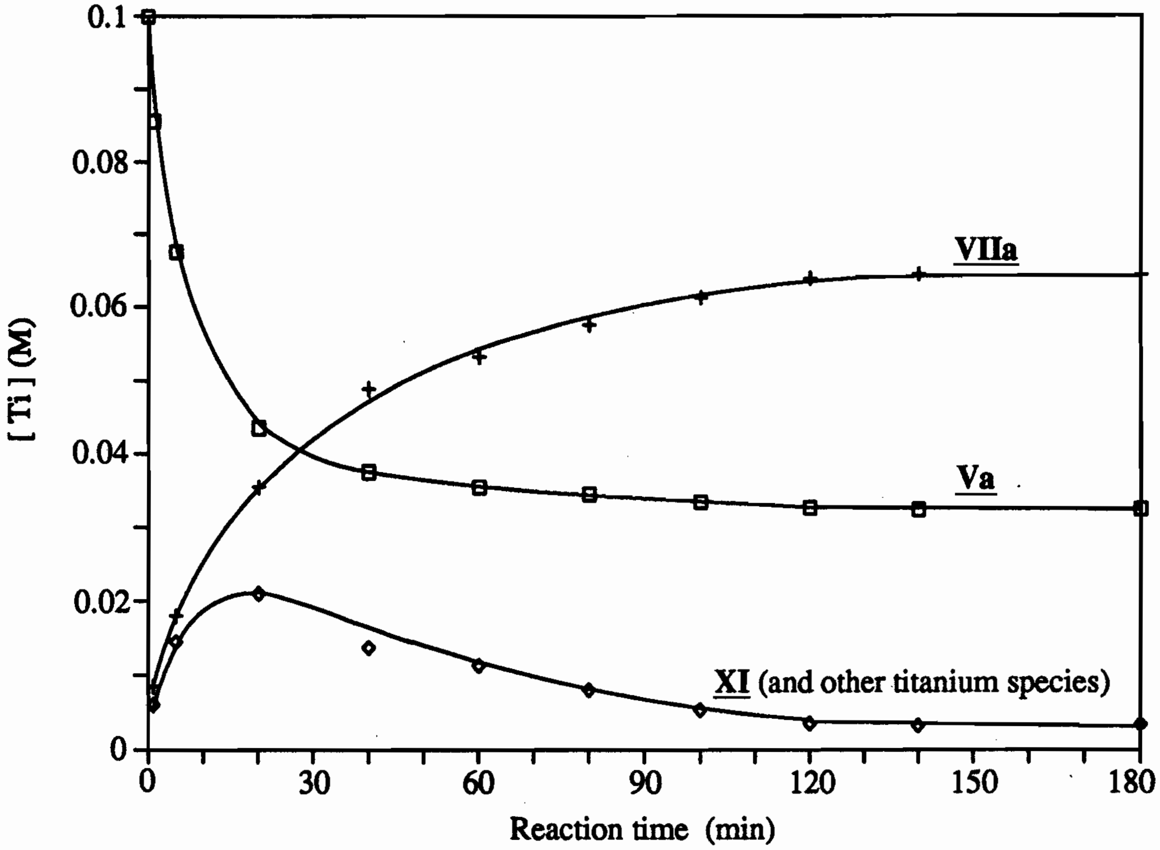

Figure V-1. Evolution of different forms of titanium species in the reaction of DMT with $PhSiH_3$. [DMT] = 0.1 M; [$PhSiH_3$] = 1 M in benzene-d_6 at room temperature. The concentration of XI was calculated by subtracting the amounts of Va and VIIa from the total amount of titanium species.

lower. When VIIa was used as catalyst, the dehydrocoupling reaction of $PhSiH_3$ was very slow at the beginning of reaction, then became faster gradually accompanied by a color change from dark-green to dark-blue. A ^1H NMR study indicated that ~30% of VIIa had been converted to Va after several hours. The conversion of VIIa to Va in the presence of $PhSiH_3$ has been observed previously (148). The above observations indicate that the reaction rate is probably related to the concentration of V. It has also been found that the DMT catalyzed dehydrocoupling reaction of $PhSiH_3$ is very fast at the beginning of reaction, and the reaction rate decreases rapidly with time (Figure II-5). The variation of the reaction rate is once again consistent with the variation of the concentration of V. These results imply that complexes V are probably involved in the catalytic cycle of the silane dehydrocoupling reaction.

V.2.1.2 Reaction of DMT with $MeSiH_3$.

The reaction of DMT with $MeSiH_3$ was found to be similar to the reaction with $PhSiH_3$. ^1H NMR studies indicated that DMT was totally transformed into the five-membered ring complex $Cp_2Ti(\mu-H)(\mu-HSiMeH)TiCp_2$ (Ve) at the beginning of reaction, accompanied by the formation of methane and dimethylsilane. Subsequent to this, most of the complex Ve was gradually converted to the six-membered complex $[Cp_2Ti(\mu-HSiMeH)]_2$ (VIIe) and hydride complex XI along with the dehydrocoupling reaction. After 2 -3 hours, an apparent equilibrium among these species was reached. A reaction profile, which indicates the progress of the conversion of Ve to VIIe and XI, is shown in Figure V-2.

Despite a number of attempts, pure Ve was not isolated from the reaction due to its facile conversion to VIIe in the presence of excess $MeSiH_3$. Ve was always obtained as a mixture with VIIe. Since the solubility and reactivity of $MeSiH_3$ are relatively low, an excess of $MeSiH_3$ must be used to initiate the reaction. It is thus difficult to prepare pure Ve by controlling the stoichiometric ratio of $MeSiH_3$ to DMT.

Pure VIIe was obtained as crystals by the reaction of DMT with $MeSiH_3$ in a dilute solution of DMT (0.24 M) in toluene. Higher concentrations of DMT gave rise to a mixture of Ve and VIIe. Based on its ^1H NMR spectrum (Figure V-3), complex VIIe was found to be present as a mixture of the *cis-* and *trans-* isomers. The ratio of *cis-* to *trans-*isomer is ca. 1.2 : 1 on the basis of their Cp resonances. The NMR assignments were made by comparison of this spectrum with those of the previously characterized analogues, VIIa, VIIb and VIIc (148). As can be seen in Figure V-3, the Cp and terminal Si-H resonances

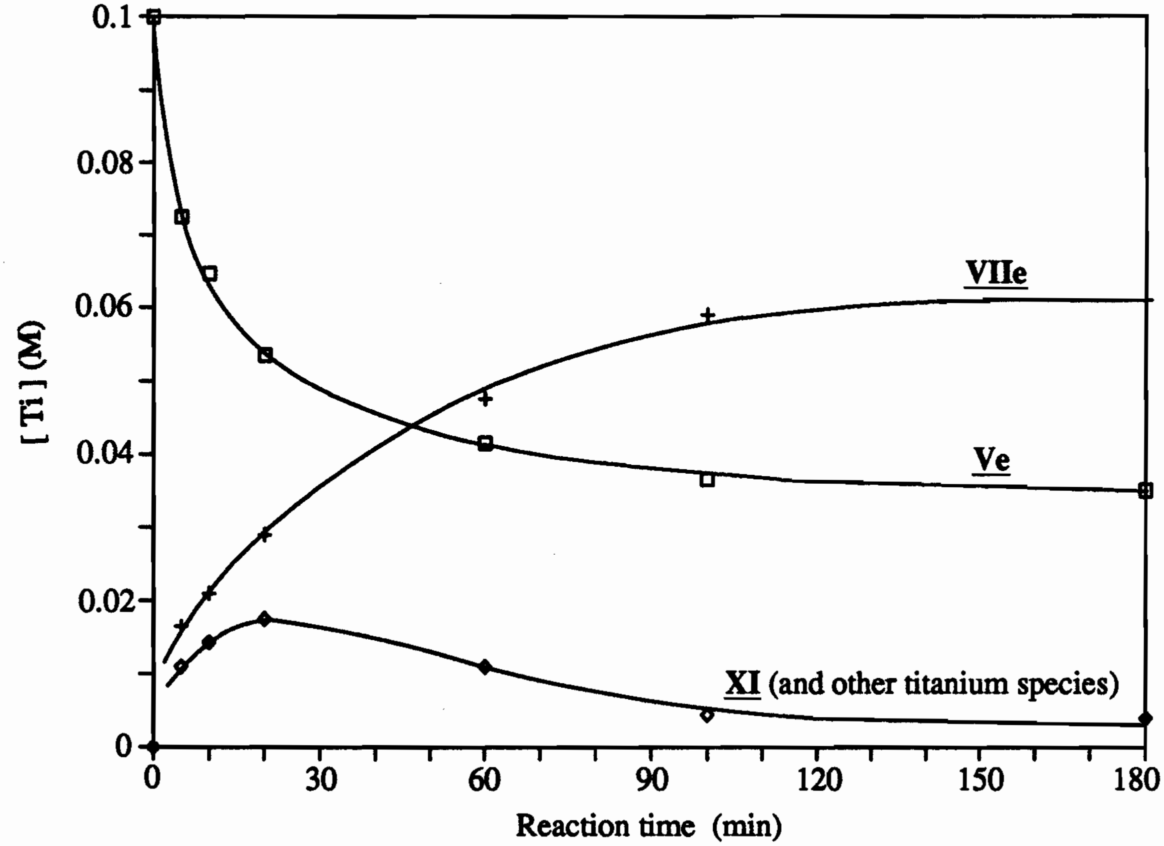

Figure V-2. Evolution of different forms of titanium species in the reaction of DMT with $MeSiH_3$. [DMT] = 0.1 M in benzene-d_6 at room temperature. The concentration of XI was calculated by subtracting the amounts of Ve and VIIe from the total amount of titanium species.

for both isomers are clearly separated from each other, while the CH_3 resonances are partly overlapped and the Si-H-Ti resonances are entirely overlapped.

The ^{1}H NMR spectrum of a mixture of Ve and VIIe is shown in Figure V-4. All the peaks due to Ve in this spectrum show the so called "paramagnetic broadening characteristic" of this type of complex (148). Thus a variable temperature ^{1}H NMR study was performed, the results of which are given in Table V-1. At ambient temperature, in addition to the broad bands at 5.62 and 5.45 ppm due to cyclopentadienyl protons and the broad peak at 0.16 ppm due to methyl protons, broad bands at 3.95 ppm due to the terminal

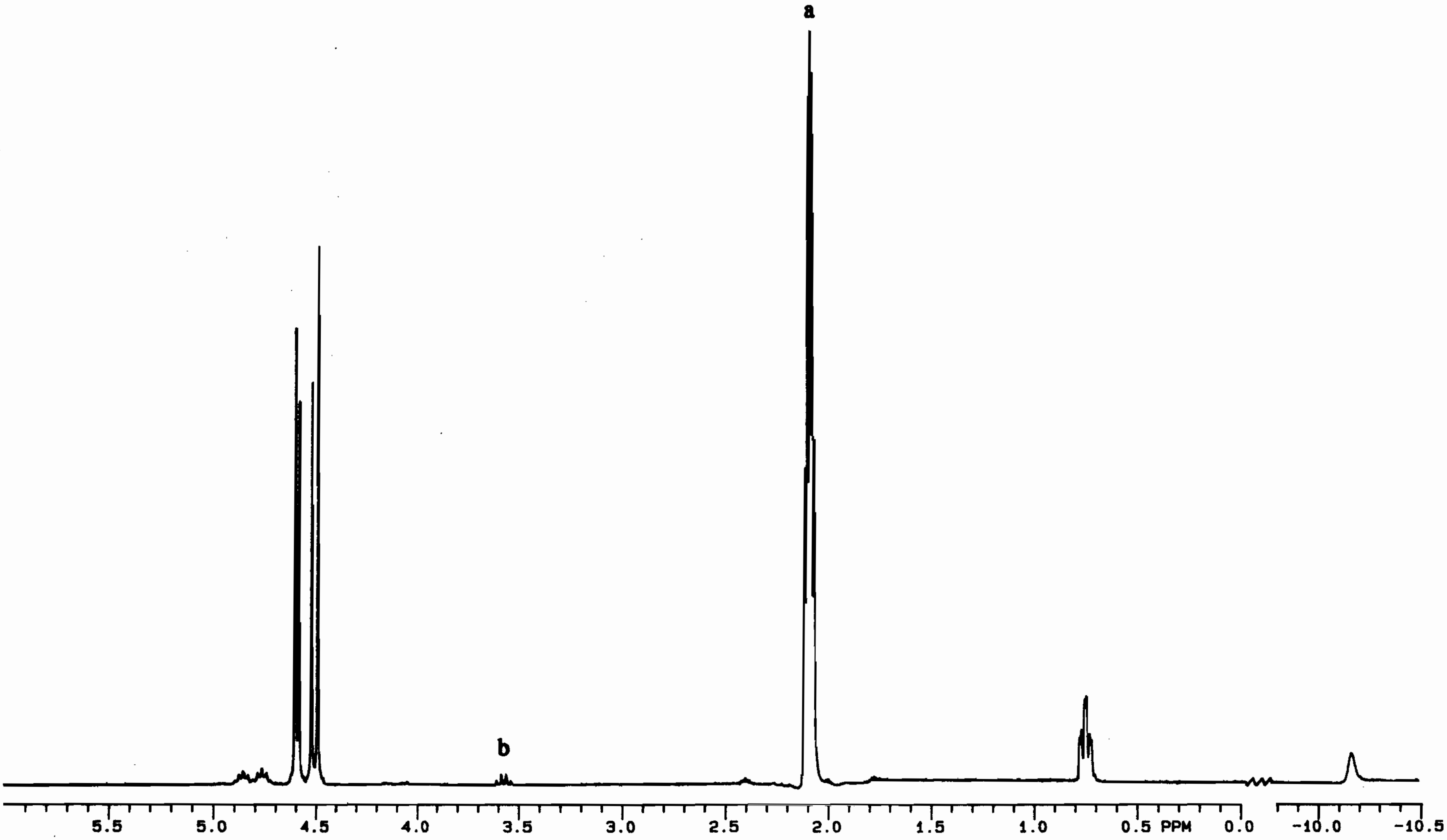

Figure V-3. ^{1}H NMR spectrum of complex <u>VIIe</u> in toluene-d_8 at ambient temperature.
^{a} peaks due to the solvent, ^{b} peaks due to methylsilane.

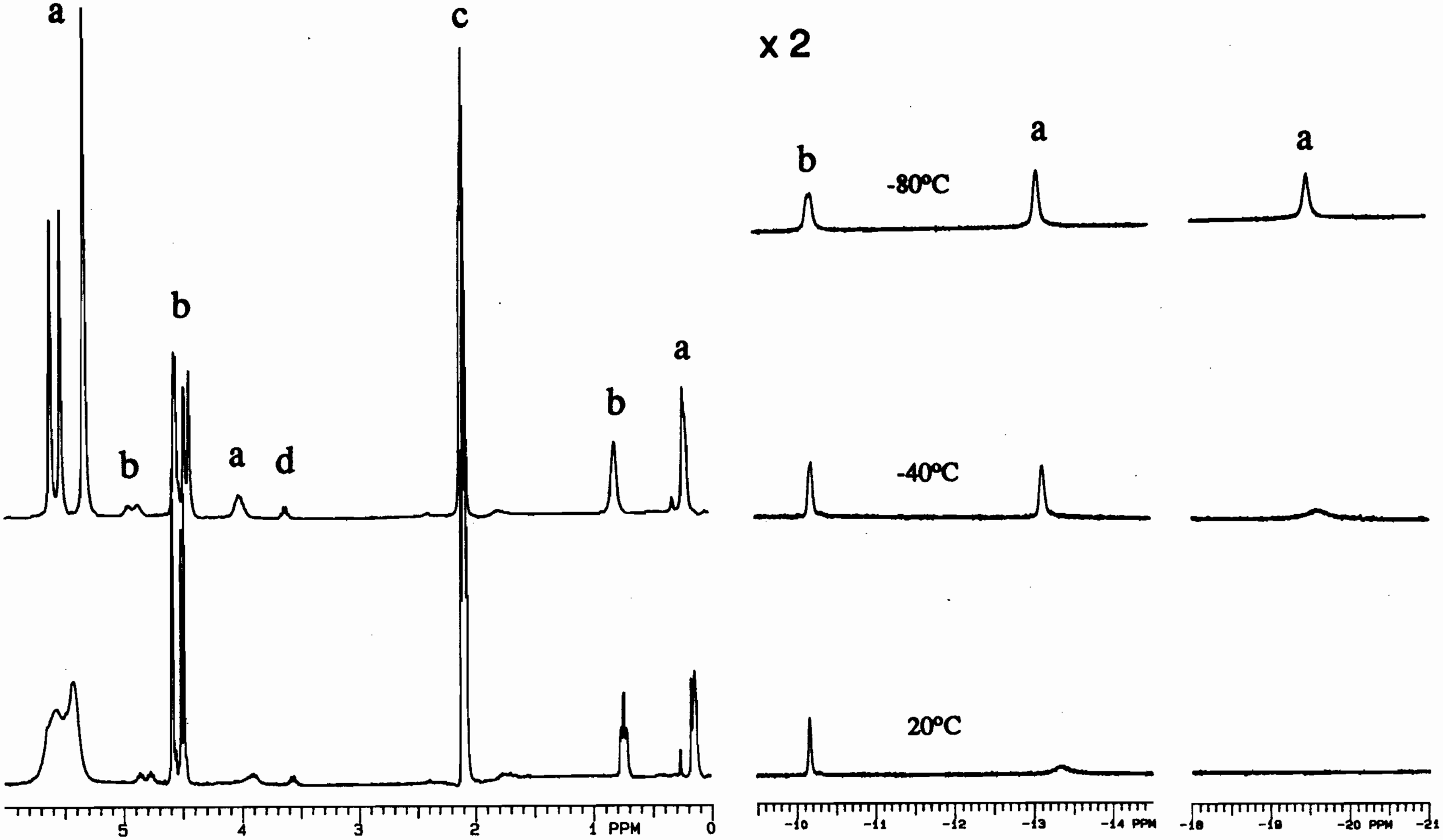

Figure V-4. ^{1}H NMR spectrum of complexes Ve and VIIe in toluene-d_8 at selected temperatures.
[a] peaks due to Ve, [b] peaks due to VIIe, [c] peaks due to the solvent, [d] peaks due to methylsilane.

Table V-1. ^{1}H NMR data for $Cp_2Ti(\mu\text{-}H)(\mu\text{-}HSiMeH)TiCp_2$ (Ve)^{a,b}

Temperature (°C)	C_5H_5	Si-H	CH_3	Si-H-Ti	Ti-H-Ti
20	5.62^c, 5.45^c	3.93^c	0.16	-13.30 (42)^c	^{d}
-40	5.62, 5.53, 5.33^e	4.05 (16)	0.24	-13.12 (14)	-19.62 (50)^c
-80	5.61, 5.52, 5.30^e	4.10 (20)	0.28	-13.09 (16)	-19.50 (16)

^{a} NMR chemical shifts, δ(ppm), measured in toluene-d_8 with TMS as standard.
^{b} numbers in brackets refer to the linewidth at half-height, $\nu_{\frac{1}{2}}$, in Hz.
^{c} broad band. ^{d} peak not observed. ^{e} 2 overlapping singlets.

Si-H and at -13.30 ppm due to the bridging hydride, Si-H-Ti, were also observed for Ve. Upon lowing the temperature, the broad band at 5.65 ppm due to Cp protons was split into two sharp peaks of equal intensity, and other broad bands due to Cp protons and hydrides sharpened considerably. At ca. -40°C a high-field hydride resonance at -19.60 ppm due to Ti-H-Ti appeared. This peak continued to sharpen with decreasing temperature, and eventually became as sharp as the one at -13.30 ppm at -80°C. At this temperature, all peaks due to Ve were found to be as sharp as those due to VIIe, showing no extra "paramagnetic broadening" for Ve relative to VIIe. The broadness of the ^{1}H NMR peaks of complexes V has been suggested to be caused by the presence of a paramagnetic triplet excited state in this type of complex based on the fact that the solutions of complexes V were found to be paramagnetic, and a triplet state in EPR was observed for the solution of Va in toluene (32,148).

V.2.1.3 Reaction of DMT with $BuMeSiH_2$.

The reaction of DMT with $BuMeSiH_2$ was found to be somewhat different from its reactions with primary silanes. Although DMT was also found to be completely transformed into the bimetallic five membered ring complex, $Cp_2Ti(\mu\text{-}H)(\mu\text{-}HSiBuMe)TiCp_2$ (Vf), along with the formation of $BuMe_2SiH$ and CH_4 at the beginning of the reaction, the subsequent conversion of the five-membered ring complex to the six-membered ring complex and the hydride XI (observed in all reactions of DMT with primary silanes) did not occur in this case. The complex Vf was found to be the only observable titanocene complex by ^{1}H NMR, and its concentration in the reaction solution did not change significantly over a period of several hours. EPR study indicated that no hydride XI was produced in this reaction. Considering the nonreactivity of $BuMeSiH_2$ toward the dehydrocoupling reaction, it seems likely that the formation of the six-membered ring complexes VII and the hydride XI is closely related to the dehydrocoupling reaction of silanes. By following reactions of DMT with $PhSiH_3$ and $MeSiH_3$, it has been found that the complexes VII and XI were formed along with the dehydrocoupling of silanes. These observations provide some insights into the mechanism of the silane dehydrocoupling reaction.

The ^{1}H NMR spectra of Vf in toluene-d_8 at different temperatures are shown in Figure V-5. At ambient temperature, four singlets of equal intensity at 5.75, 5.73, 5.52 and 5.50 ppm due to cyclopentadienyl protons and one broad band at -13.75 ppm due to the bridging hydride, Si-H-Ti, were observed. The signals due to methyl and butyl groups overlap with the signals of residual $BuMeSiH_2$ and can not be well assigned. As observed previously with Ve, all peaks due to Vf sharpened on cooling and the resonance due to the bridging hydride, Ti-H-Ti, at -20.15 ppm eventually became visible at about -20°C. The latter peak continued to sharpen with decreasing temperature. The temperature dependence of the ^{1}H NMR spectrum of this type of complex has been discussed in last section.

A very evident paramagnetic broadening effect was observed in this system. In addition to Vf, NMR signals due to $BuMeSiH_2$ and solvent were also broadened. It is interesting to note that the paramagnetic broadening effect increased with increasing the concentration of the sample, as shown in Figure V-6. This indicates that the concentration of the paramagnetic species is proportional to that of Vf. However, it is not clear whether or

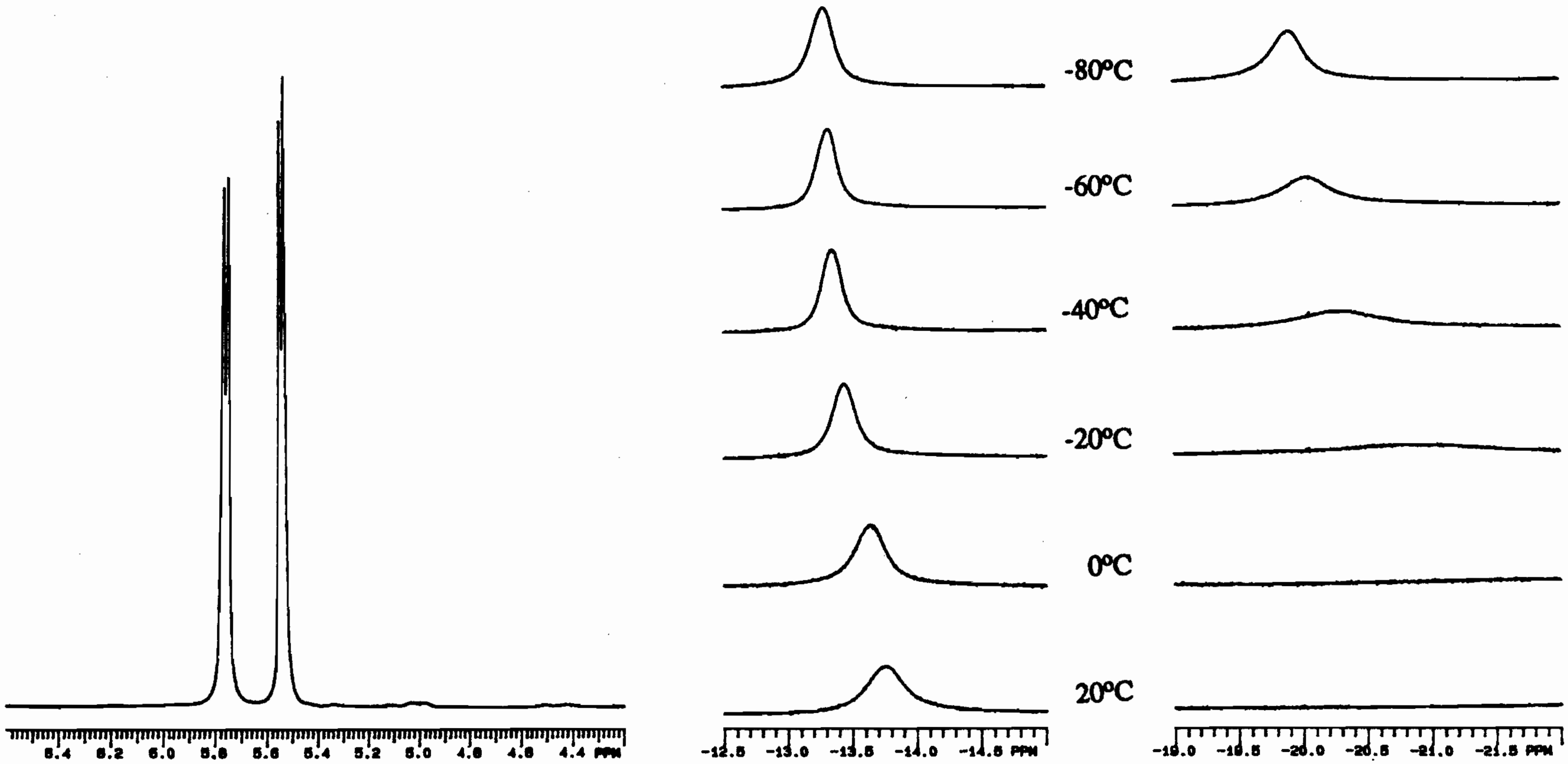

Figure V-5. ^{1}H NMR spectrum of complex Vf in toluene-d_8 at selected temperatures.
[Vf] = 0.1 M.

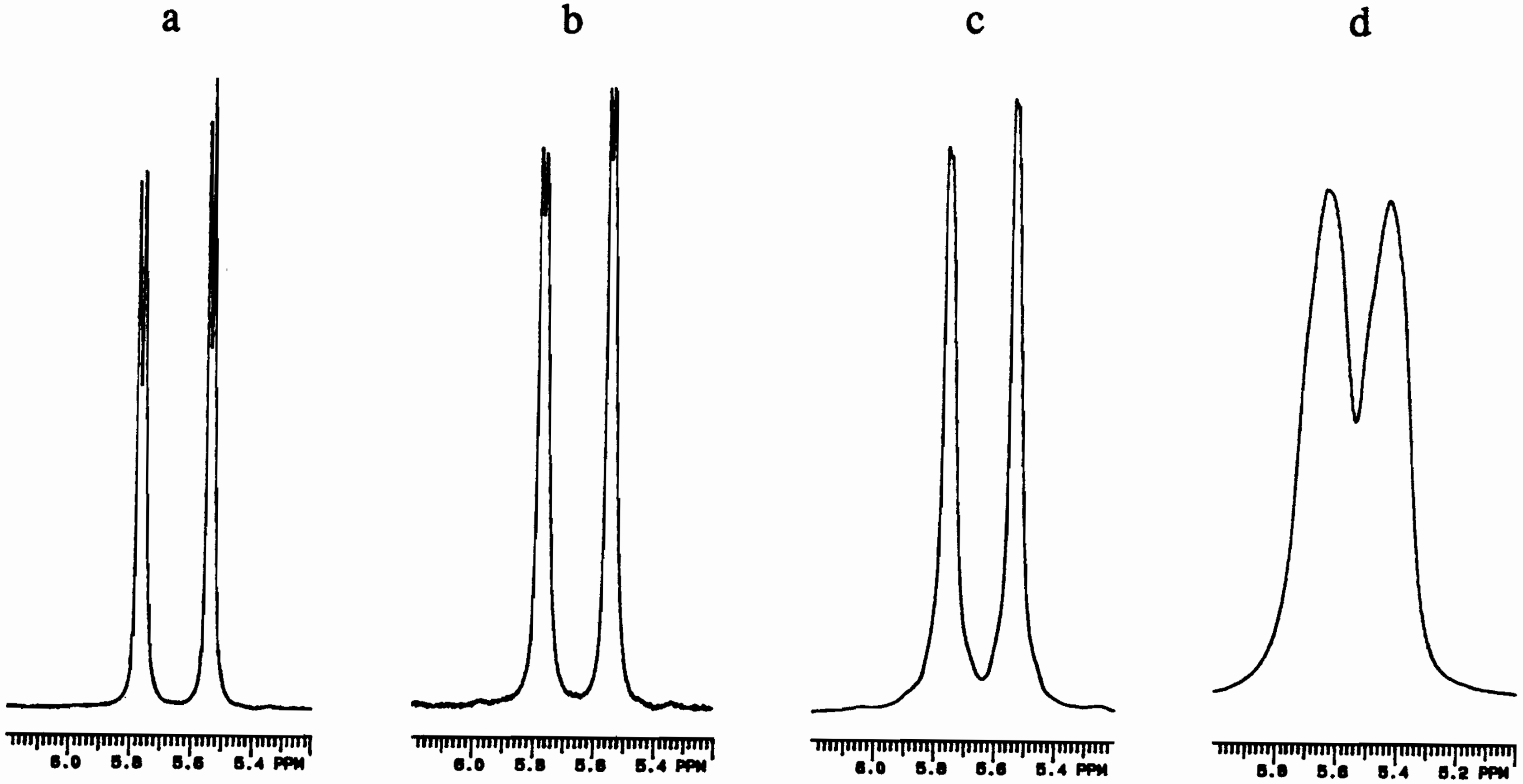

Figure V-6. Cp region of the ^{1}H NMR spectrum of <u>**Vf**</u> in toluene-d_8 at different concentrations. [<u>**Vf**</u>] = 0.1 M (a), 0.2 M (b), 0.3 M (c) and 0.6 M (d).

not Vf itself is the paramagnetic species. It is also possible that the observed paramagnetic effect resulted from some other species formed from the decomposition of Vf.

An EPR study on the solution of Vf in toluene was performed and the spectrum obtained at room temperature exhibits a broad featureless signal at $g_{iso} = 1.984$, which has been observed for all complexes of this type. On lowering the temperature the broad signal becomes broader and the frozen solution spectrum is characteristic of a triplet state molecule (216,217). The triplet state assignment has been confirmed by the observation of the forbidden transition at mid-field (32). As mentioned above, such a triplet species could be either V itself or some other paramagnetic species, such as a solvated "Cp_2Ti". The latter might be more easily formed in the secondary silane systems because the increased steric bulk of the -SiHRR′ group could be expected to promote the dissociation of V according to eq. V-3.

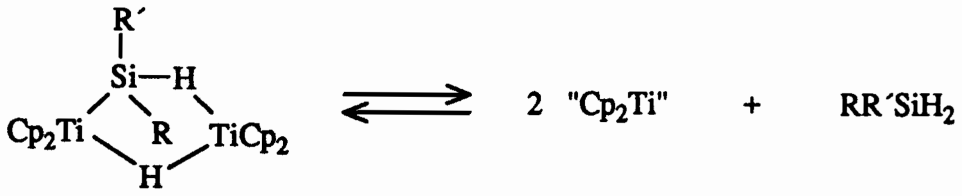

(V-3)

V.2.1.4 Reactions of DMT with Ph_2SiH_2 and $PhMeSiH_2$.

The reactions of DMT with Ph_2SiH_2 and $PhMeSiH_2$ are similar to its reactions with primary silanes. At the onset of reaction, DMT was converted to the five-membered ring complexes, $Cp_2Ti(\mu\text{-}H)(\mu\text{-}HSiPh_2)TiCp_2$ (Vd) and $Cp_2Ti(\mu\text{-}H)(\mu\text{-}HSiPhMe)TiCp_2$ (Vg) respectively, accompanied by a color change from orange to blue/black and the formation of methane and methylated silanes. In both cases, the five-membered ring complex, Vd or Vg, was subsequently transformed into the black hydride XI and a green paramagnetic complex with a slow color change from blue/black to green. Unfortunately, the green complexes could neither be isolated nor be observed by ^1H NMR during reactions, even at

-80°C. On the analogy of reactions with other silanes, the green complexes can be reasonably supposed to be the six-membered ring complexes, $[Cp_2Ti(\mu\text{-}HSiPh_2)]_2$ (**VIId**) and $[Cp_2Ti(\mu\text{-}HSiPhMe)]_2$ (**VIIg**) respectively. The failure to detect these complexes by NMR is probably due to a facile dissociation equilibrium, while the instability of such complexes might result from the weak bonding between Ti and μ-H because of the larger steric bulk of the diorganosilyl groups. Complexes **Vd** and **Vg** were also not isolated, but they could be observed by ^1H NMR in reaction solutions. The ^1H NMR data for **Vd** and **Vg** are given in Tables V-2 and V-3 respectively. In both systems, **XI** was obtained as the only

Table V-2. ^1H NMR data for $Cp_2Ti(\mu\text{-}H)(\mu\text{-}HSiPh_2)TiCp_2$ (**Vd**)[a,b]

Temperature (°C)	C_5H_5		Si-H-Ti	Ti-H-Ti
20	6.16[c],	5.98[c]	d	d
-30	5.94,	5.78	-11.86 (50)	d
-50	5.80,	5.64	-11.78 (40)	d
-80	5.68[c],	5.52[c]	-11.68 (35)	d

[a] NMR chemical shifts, δ(ppm), measured in toluene-d_8 with TMS as standard.
[b] numbers in brackets refer to the linewidth at half-height, $\nu_{\frac{1}{2}}$, in Hz.
[c] broad band. [d] peak not observed.

Table V-3. ^1H NMR data for $Cp_2Ti(\mu\text{-}H)(\mu\text{-}HSiPhMe)TiCp_2$ (**Vg**)[a,b]

Temperature (°C)	C_5H_5			Si-H-Ti	Ti-H-Ti
20	5.78[c],	5.66[c],	5.58[e]	d	d
-30	5.68,	5.58,	5.45[e]	-12.28 (40)	d
-50	5.64,	5.54,	5.41[e]	-12.23 (25)	d
-80	5.61[c],	5.51[c],	5.39[e]	-12.19 (18)	-19.99 (60)

[a] NMR chemical shifts, δ(ppm), measured in toluene-d_8 with TMS as standard.
[b] numbers in brackets refer to the linewidth at half-height, $\nu_{\frac{1}{2}}$, in Hz.
[c] broad band. [d] peak not observed. [e] 2 overlapping broad bands.

isolated compound, which was identified by EPR (171). When reactions were carried out in hexane, XI was easily isolated as a black precipitate. Attempts to grow single crystals were not successful.

The variation in the concentration of the five-membered ring complex with time was followed by ^{1}H NMR in both cases and the results are shown in Figure V-7. In the Ph_2SiH_2 reaction, the concentration of Vd dropped rapidly in the earlier stage of reaction, and then decreased slowly until about 3 hours. After that period, it remained essentially constant, accounting for about 5% of total titanocene species. The $PhMeSiH_2$ reaction showed a similar variation in the concentration of Vg with time. However, the final equilibrium

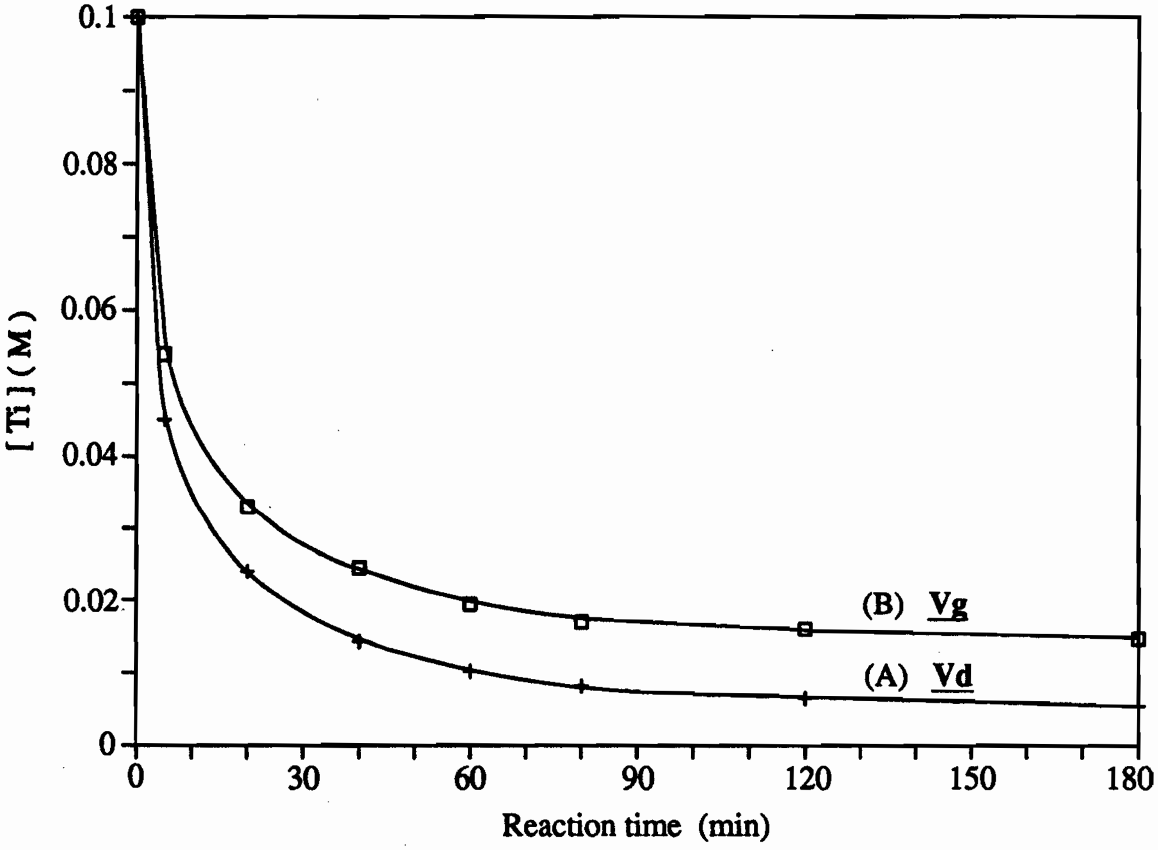

Figure V-7. Evolution of the five-membered ring complexes, Vd and Vg, in the reactions of DMT with (A) Ph_2SiH_2 and (B) $PhMeSiH_2$ respectively. (A) [DMT] = 0.1 M, [Ph_2SiH_2] = 0.7 M; (B) [DMT] = 0.1 M, [$PhMeSiH_2$] = 0.9 M in benzene-d_6.

concentration of Vg (~15% of total titanocene species) is several times higher than that of Vd under the same conditions. Comparing these two reactions to the $PhSiH_3$ reaction, it can be seen that the equilibrium concentration of V decreases with increasing steric bulk of the silyl group in V. ^1H NMR studies on some of the complexes V have also indicated that the stability of these complexes decreases with increasing the steric bulk of the silyl group. For example, the resonance due to the bridged hydride, Si-H-Ti, can be observed at room temperature for primary silane compounds, but can not be observed for the secondary silane compounds Vd and Vg. At lower temperatures, the resonance due to the bridged hydride, Ti-H-Ti, can be observed for most primary and secondary silane compounds, while it can not be observed for Vd even at -80°C. The fact that Vd and Vg were not isolated might be associated to their lower stability.

V.2.2 Reactions of several silanes with DMZ.

V.2.2.1 Reaction of DMZ with $PhSiH_3$.

The reaction of DMZ with $PhSiH_3$ has been studied previously (33) and the first binuclear silylzirconocene hydride VIa has been isolated and characterized. Although VIa was obtained almost quantitatively from this reaction, EPR study of the reaction products of DMZ with $PhSiH_3$ indicated the existence of small amount of paramagnetic species. The observed weak EPR signals, consisting of a doublet and a doublet of triplets, have been assigned tentatively to Cp_2ZrH and $(Cp_2ZrH)_2(\mu\text{-}H)$ (XIII) (33). The latter is a zirconocene analogue of the mixed valence titanocene hydride XI.

In this work the stoichiometric reaction of DMZ with $PhSiH_3$ was followed by ^1H NMR and some new zirconocene species containing bridging Zr-H bonds were observed during the reaction. The $PhSiH_3$ reaction is much faster than the secondary silane reactions under similar conditions. Shortly after the addition of DMZ to $PhSiH_3$ solution in benzene-d_6, the colorless solution turned yellow slowly and then deep orange.

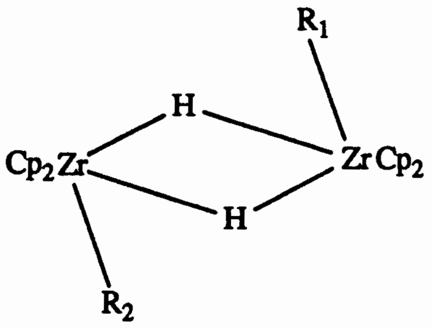

VI

VIa: $R_1 = SiH_2Ph$; $R_2 = SiHMePh$
VIb: $R_1 = R_2 = SiH_2Ph$
VIc: $R_1 = SiH_2Ph$; $R_2 = SiHPhSiH_2Ph$
VId: $R_1 = SiH_2Me$; $R_2 = SiHMe_2$
VIe: $R_1 = R_2 = SiH_2Me$
VIf: $R_1 = SiHMePh$; $R_2 = SiMe_2Ph$
VIg: $R_1 = R_2 = SiHMePh$
VIh: $R_1 = R_2 = SiMe_2Ph$
VIi : $R_1 = SiHPh_2$; $R_2 = SiMePh_2$
VIj : $R_1 = R_2 = SiHPh_2$
VIk: $R_1 = R_2 = SiPh_2SiHPh_2$
VIl: $R_1 = R_2 = SiHBuMe$

Accompanying the color change, the formation of VIa and other dimeric zirconocene hydrides was observed by NMR. During this period, CH_4, H_2, diphenyldisilane and a trace amount of $PhMeSiH_2$ were also observed. After about 2 hours, the DMZ had totally reacted. Based on the ^1H NMR integration of Cp groups, ~ 70% of DMZ was transformed into VIa and only about 3% of DMZ was converted to the symmetrical, dimeric silylzirconocene hydride VIb. In previous studies, it has been found that VIb is a very unstable, unisolable compound (33). This probably is the reason why the unsymmetrical dimer VIa is the major product. VIb was assigned based on its characteristic Cp resonance at 5.39 ppm (33). Other hydride-bridged zirconocene species can only be tentatively assigned on the basis of their high field bridged hydride resonances shown in Figure V-8. The two sets of AB quartets in the region from -2.7 ~ -3.4 ppm might be assigned to the mixed methyl/silyl dimers, XIVa and XIVb, by comparison of this spectrum with those obtained from Ph_2SiH_2 and

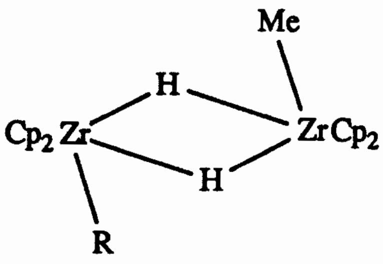

XIV

XIVa: $R = SiH_2Ph$
XIVb: $R = SiHPhSiH_2Ph$
XIVc: $R = SiHMePh$
XIVd: $R = SiHPh_2$
XIVe: $R = SiPh_2SiPh_2H$

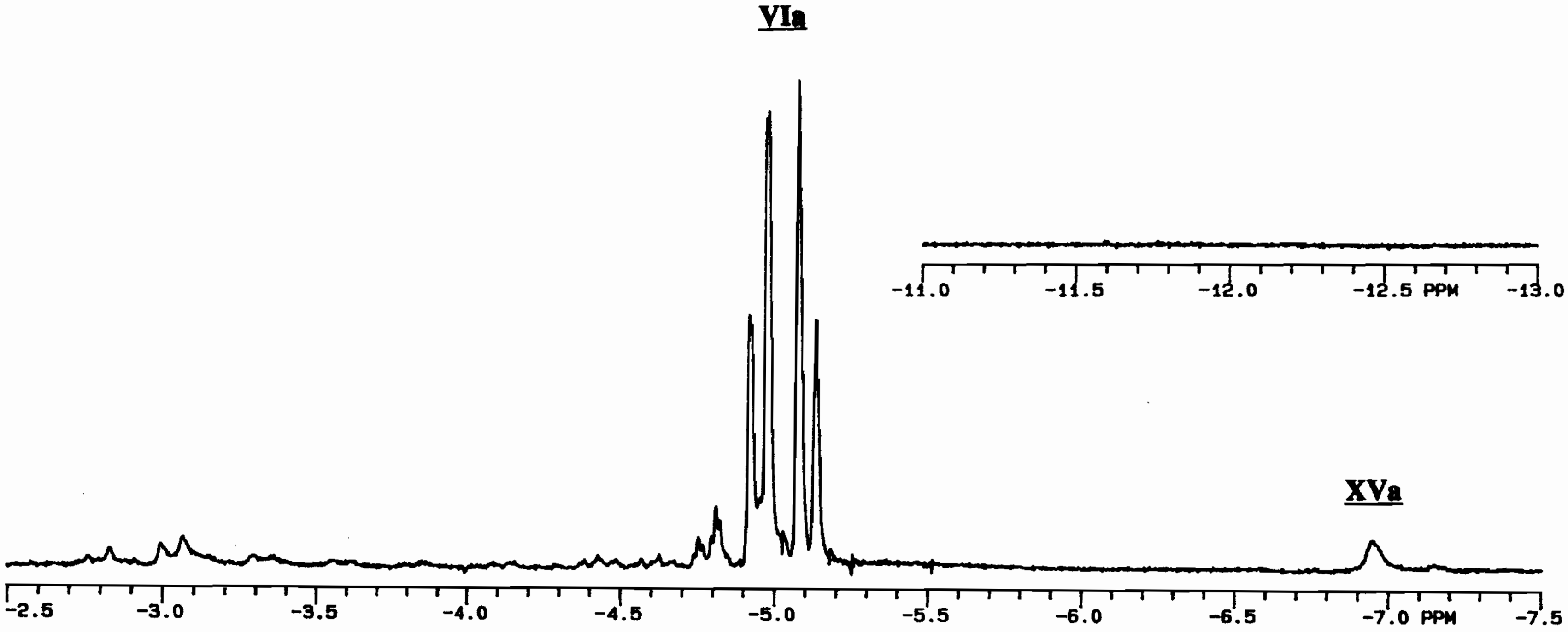

Figure V-8. Zr-H region of the ^{1}H NMR spectrum of the reaction products of DMZ with $PhSiH_3$ in benzene-d_6. $[Cp_2ZrMe_2] = 0.04$ M, $[PhSiH_3] = 0.12$ M, reaction time = 2 h, at room temperature.

$PhMeSiH_2$ reactions. The two compounds account for ca. 10% of the total observable Zr-H species. The doublet of triplets at -4.75 ~ -4.85 ppm is a part of a set of AB quartets, which overlaps with the signal of **VIa**. The triplets result almost certainly from the coupling of the hydride with the two protons in an $-SiH_2Ph$ group. The other part of the AB quartet being at higher field indicates that the R group at another Zr atom in this dimeric complex is a more electron-donating group, most likely a disilyl group, $-SiHPhSiH_2Ph$. This set of resonances may therefore be tentatively assigned to **VIc**. This compound accounts for about 15% of total observable Zr-H species. In contrast to the secondary silane cases described below, no hydride signal around -12 ppm is evident in the $PhSiH_3$ reaction. However, a broad signal at -6.95 ppm is observed in this case. This resonance is at quite high field and is unlikely to be due to a zirconocene(IV) species. On the analogy of secondary silane reactions, such a high field resonance is very likely due to a diamagnetic silylzirconocene(III) dimer (**XVa**) shown as follows:

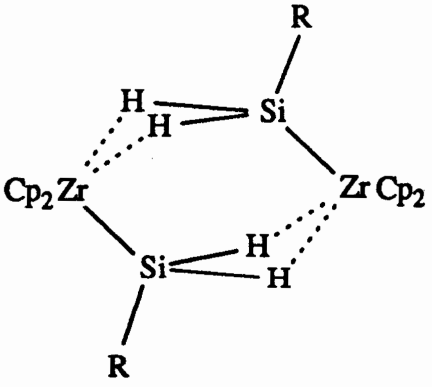

XV

XVa: R = Ph

XVb: R = Me

In an attempt to isolate **VIb**, a reaction solution of DMZ with $PhSiH_3$ in hexane was cooled at -78°C after the color of the solution had changed to pale yellow. A yellow precipitate was formed on the wall of the reactor after two hours. The yellow precipitate converted to a paramagnetic, very air sensitive, dark brown powder when the solvent was removed. The same product can be obtained by reaction of **VIa** with $PhSiH_3$ in similar conditions. This product, in a dilute toluene solution (in a sealed tube) at -20°C, gave first a weak EPR signal consisting of a doublet (g = 1.9846, $A(^1H)$ = 7.13 G), which can be assigned with confidence to Cp_2ZrH, by comparison with reported EPR spectra of this compound obtained in other ways (189,218,219). Upon standing for a while at room temperature, the signal became more intense and the previously observed doublet of triplets (g = 1.9999, $A(^1H_1)$ = 14.60 G, $A(^1H_2)$ = 7.46 G, $A(^{91}Zr)$ = 12.16 G) due to <u>**XIII**</u> appeared simultaneously and grew with time, accompanied by slow gas evolution. Then both signals became weaker and finally disappeared. Upon photolyzing with unfiltered high pressure mercury light, both signals reappeared. It is obvious that neither the mixed valence hydride <u>**XIII**</u> nor the monohydride Cp_2ZrH is the initial dark brown sample. Both of these compounds are produced from either decomposition or reaction of the initial sample. The initial sample is also unlikely to be zirconocene dihydride, Cp_2ZrH_2, since the dihydride has been found to be a diamagnetic, insoluble, white precipitate (179,183) and gives only the doublet EPR signal upon photolysis (189). ^1H NMR study of the dark brown sample at different temperatures indicated that only the signals due to unreacted Cp_2ZrMe_2 and <u>**VIa**</u> can be observed. Based on the above observed experimental phenomena and results, the dark brown compound is probably a silylzirconocene(III) species, most likely a zirconium analogue of the five membered ring titanocene(III) dimer <u>V</u>. <u>V</u> has been found to convert to <u>XI</u> slowly upon standing in solution (148). Such a zirconocene complex was not observed, either by NMR or EPR, perhaps due to a fast dynamic process as shown in eq. V-4.

It is also possible that the dark brown compound is "Cp_2Zr". Although nobody so far

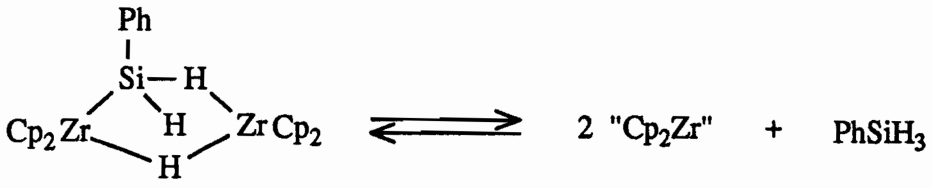

(V-4)

<u>**XVIa**</u>

has observed real "Cp_2Zr", it is almost beyond dispute that such a species is involved in many reactions as a transient intermediate (133,139,178). "Cp_2Zr" has been reported to be an unobservable species by NMR and EPR (172). Based on the reaction process, if the dark brown compound is **XVIa** or "Cp_2Zr", the initially obtained yellow compound probably is **VIb**. The latter could decompose by losing one or two $PhSiH_3$ to give **XVIa** or "Cp_2Zr".

V.2.2.2 Reaction of DMZ with $MeSiH_3$.

The reaction of DMZ with $MeSiH_3$ is quite different from the above discussed reaction with $PhSiH_3$. In the $MeSiH_3$ case, the major products are paramagnetic species and only very weak NMR signals of diamagnetic complexes have been observed. The reaction solution is dark brown in color and gives very strong EPR signals consisting of a doublet, due to Cp_2ZrH, and a doublet of triplets, due to **XIII**. No other EPR signal has been observed. The EPR spectrum is shown in Figure V-9.

In Figure V-10, the Zr-H region ^1H NMR spectrum of the reaction products is shown. It is difficult to make definite assignments for these NMR signals without isolating the compounds. However, it is possible to make some tentative assignments by comparison of this reaction with reactions of other silanes. The signals around -5 ppm are due to hydride bridged silylzirconocene(IV) complexes, while the high field resonance at -11.72 ppm might be due to a dimeric silylzirconocene(III) complex. The sharp singlet at -5.25 ppm and the multiplet at -5.55 ppm could be attributed to symmetrical zirconocene(IV) complexes. The singlet might be due to a tertiary silyl complex, probably a cyclosilyl complex, whereas the multiplet is very likely due to **VIe**. The AB quartet in the region from -5.20 to -5.45 ppm must be due to an unsymmetrical zirconocene(IV) complex, most probably **VId**. The weak, broad resonance at -8.07 ppm is similar to the one at -6.95 ppm observed in $PhSiH_3$ reaction and is probably due to **XVb**.

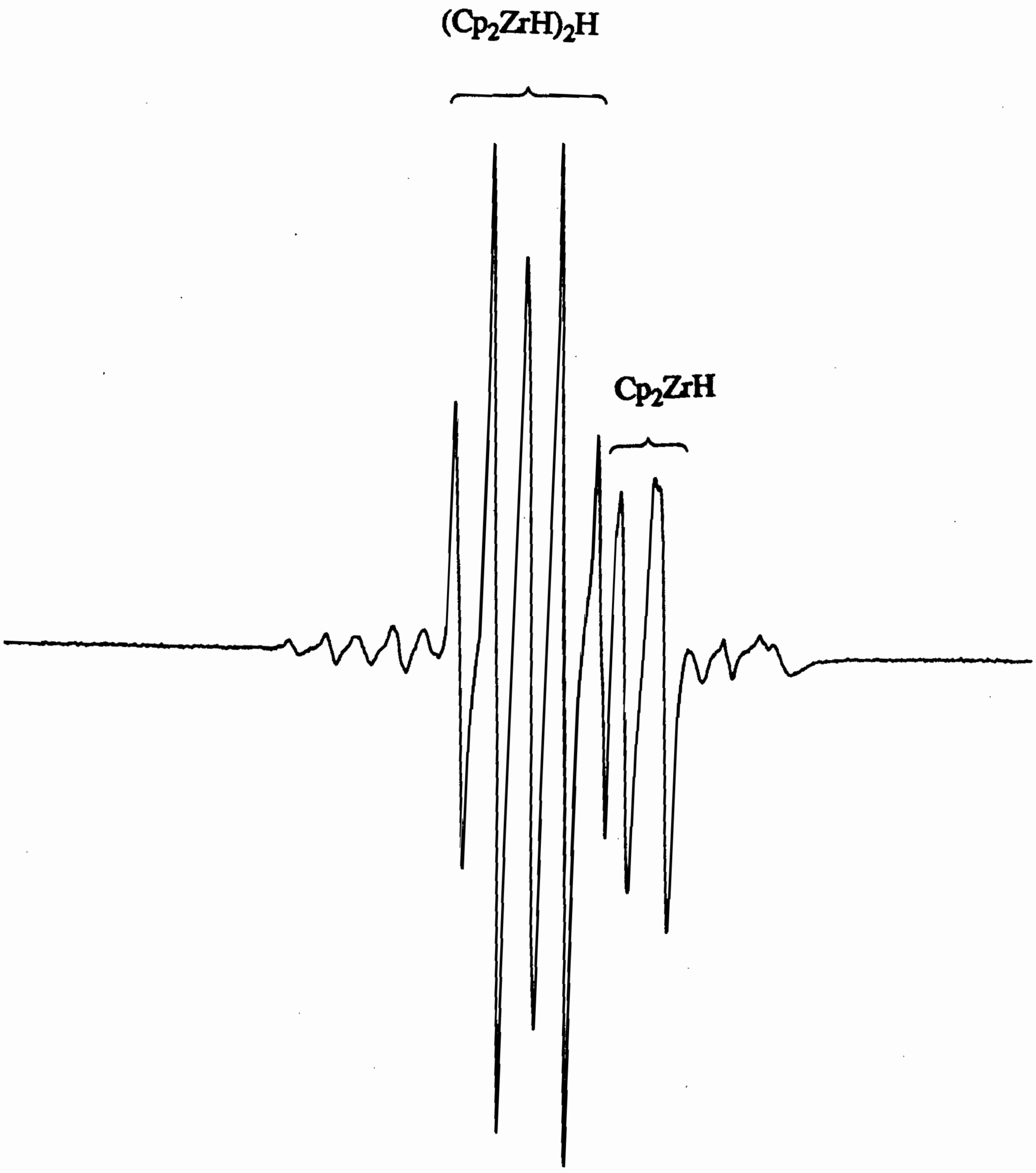

Figure V-9. EPR spectrum of a mixture of $(Cp_2ZrH)_2H$ and Cp_2ZrH in toluene at ambient temperature.

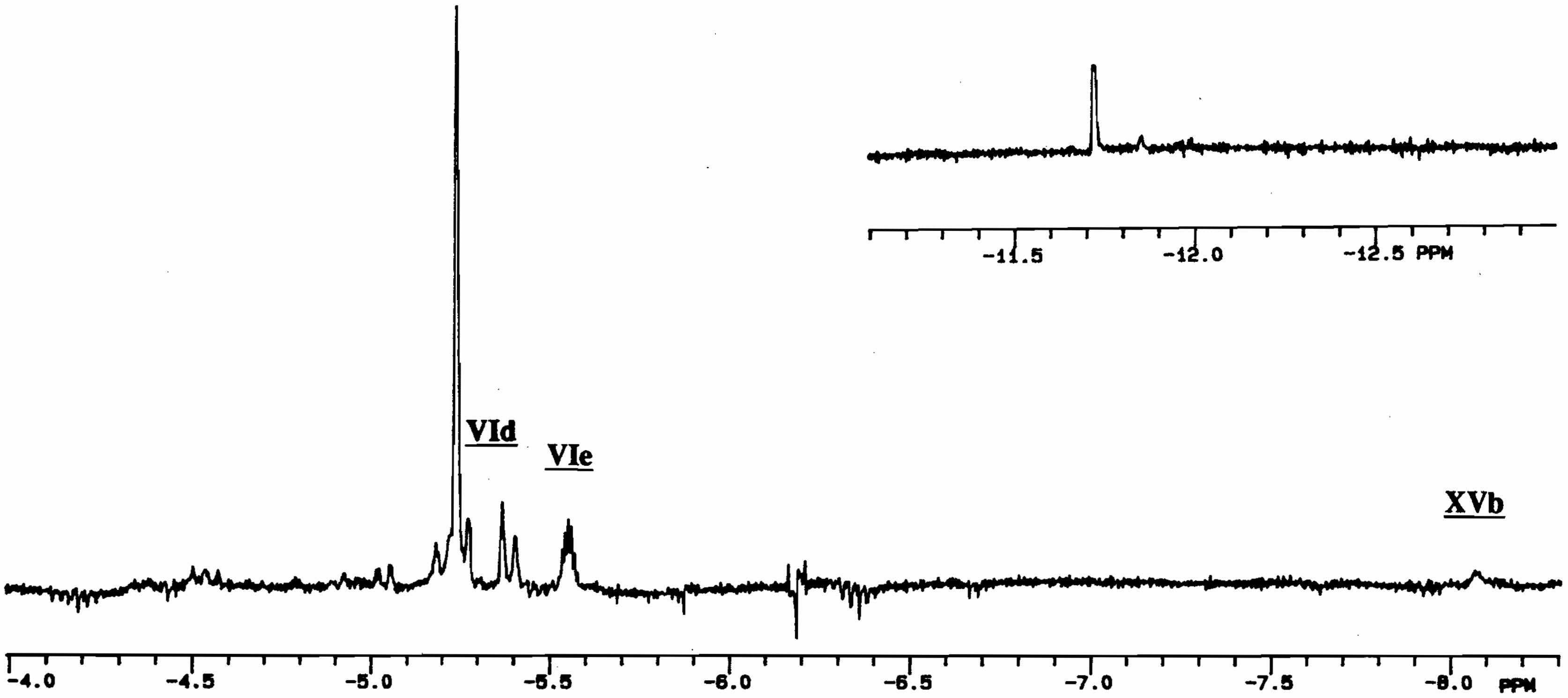

Figure V-10. Zr-H region of the ^{1}H NMR spectrum of the reaction products of DMZ with $MeSiH_3$ in benzene-d_6. $[Cp_2ZrMe_2] = 0.08$ M, $P_{MeSiH3} = 1$ atm, temp. = 50°C, reaction time = 5 h.

V.2.2.3 Reaction of DMZ with $PhMeSiH_2$.

The reaction of $PhMeSiH_2$ with DMZ is much slower than that of $PhSiH_3$, requiring 1 to 2 days to go to completion under the same conditions that lead to complete reaction of $PhSiH_3$ in ca. 1-2 hours. In the reaction of $PhMeSiH_2$, considerable amounts of paramagnetic species are produced and the reaction solution shows dark-brown color. In this case, the unsymmetrical silyl dimer, VIf, is still the major product, but this compound now only accounts for about 55% of the total observed Zr-H species. As a result, more methylated silane, $PhMe_2SiH$, is produced. Although the NMR spectrum of the $PhMeSiH_2$ reaction products is more complicated than that of the $PhSiH_3$ reaction products, assignments for almost all observed Zr-H resonances have been successfully made by following the reaction. The ^1H NMR data for these Zr-H species are given in Table V-4 and the Zr-H region ^1H NMR spectrum of these products is shown in Figure V-11.

In the $PhMeSiH_2$ reaction, a considerable amount (~ 20%) of the mixed methyl/silyl dimer, XIVc, was produced in the early stages of the reaction. With the passage of time, most of XIVc was then converted to other species. The assignment for XIVc was made based on a comparison of this reaction with the Ph_2SiH_2 reaction described below. During the reaction, the mixed hydrido/silyl dimer, XVIIa, was also observed as one of the major products (10-15%). XVIIa is assigned on the basis of its characteristic NMR signals, two

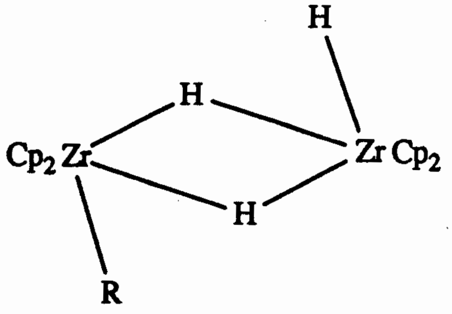

XVII

XVIIa: R = SiHMePh

XVIIb: R = $SiHPh_2$

Table V-4. ^{1}H NMR data for some new compounds from the reaction of DMZ with $PhMeSiH_2$[a]

compound	assignment	chemical shift (δ)	coupling (Hz)
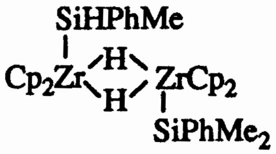 $Cp_2Zr(SiHPhMe)(\mu\text{-}H)_2ZrCp_2(SiPhMe_2)$ (VIf)	C_5H_5	5.24, 5.38, 5.42, 5.49 s	
	SiH	4.88 qd	$^3J = 4.3,\ 2.0$
	PhHSiCH_3	0.60 d	$^3J = 4.3$
	PhSi(CH_3)$_2$	0.52, 0.53 s	
	μ-ZrH	- 4.99 d	$^2J = 11.3$
		- 5.24 dd	$^2J = 11.3,\ ^3J = 2.0$
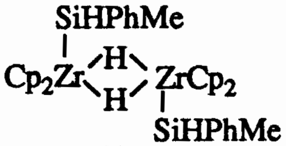 $Cp_2Zr(SiHPhMe)(\mu\text{-}H)_2ZrCp_2(SiHPhMe)$ (VIg)	C_5H_5	5.49, 5.67 s	
	SiH	4.17 qd	$^3J = 4.3,\ 2.2$
	PhHSiCH_3	0.35 d	$^3J = 4.3$
	μ-ZrH	- 4.91 t	$^3J = 2.2$
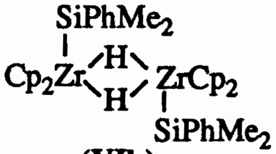 $Cp_2Zr(SiPhMe_2)(\mu\text{-}H)_2ZrCp_2(SiPhMe_2)$ (VIh)	C_5H_5	5.31, 5.46 s	
	PhSi(CH_3)$_2$	0.62, 0.63 s	
	μ-ZrH	- 5.11 s	
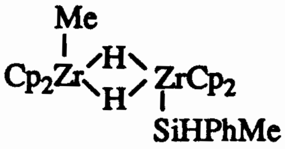 $Cp_2Zr(Me)(\mu\text{-}H)_2ZrCp_2(SiHPhMe)$ (XIVc)	C_5H_5	5.43, 5.44, 5.46, 5.64 s	
	SiH	5.01 qd	$^3J = 4.3,\ 2.0$
	PhHSiCH_3	0.67 d	$^3J = 4.3$
	ZrCH_3	- 0.09 br s	
	μ-ZrH	- 3.19 d	$^2J = 11.8$
		- 3.60 br dd	
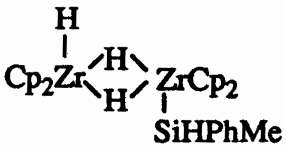 $Cp_2Zr(H)(\mu\text{-}H)_2ZrCp_2(SiHPhMe)$ (XVIIa)	C_5H_5	5.48 (10 H), 5.60, 5.72 s	
	SiH	5.37 qd	$^3J = 4.3,\ 2.1$
	PhHSiCH_3	0.66 d	$^3J = 4.3$
	ZrH	3.73 dd	$^2J = 9.6,\ 4.1$
	μ-ZrH	- 4.15 ddd	$^2J = 11.2, 4.1,\ ^3J = 2.1$
		- 4.61 dd	$^2J = 11.2, 9.6$
$[Cp_2ZrSiHPhMe]_2$ (XVIIIa)	C_5H_5	5.40, 5.44 s	
	SiCH_3	0.16 s	
	Zr-H-Si	- 12.01, - 12.02 (two isomers)	

[a] Spectra recorded at 20°C in benzene-d_6; shifts are in ppm, referenced to TMS.

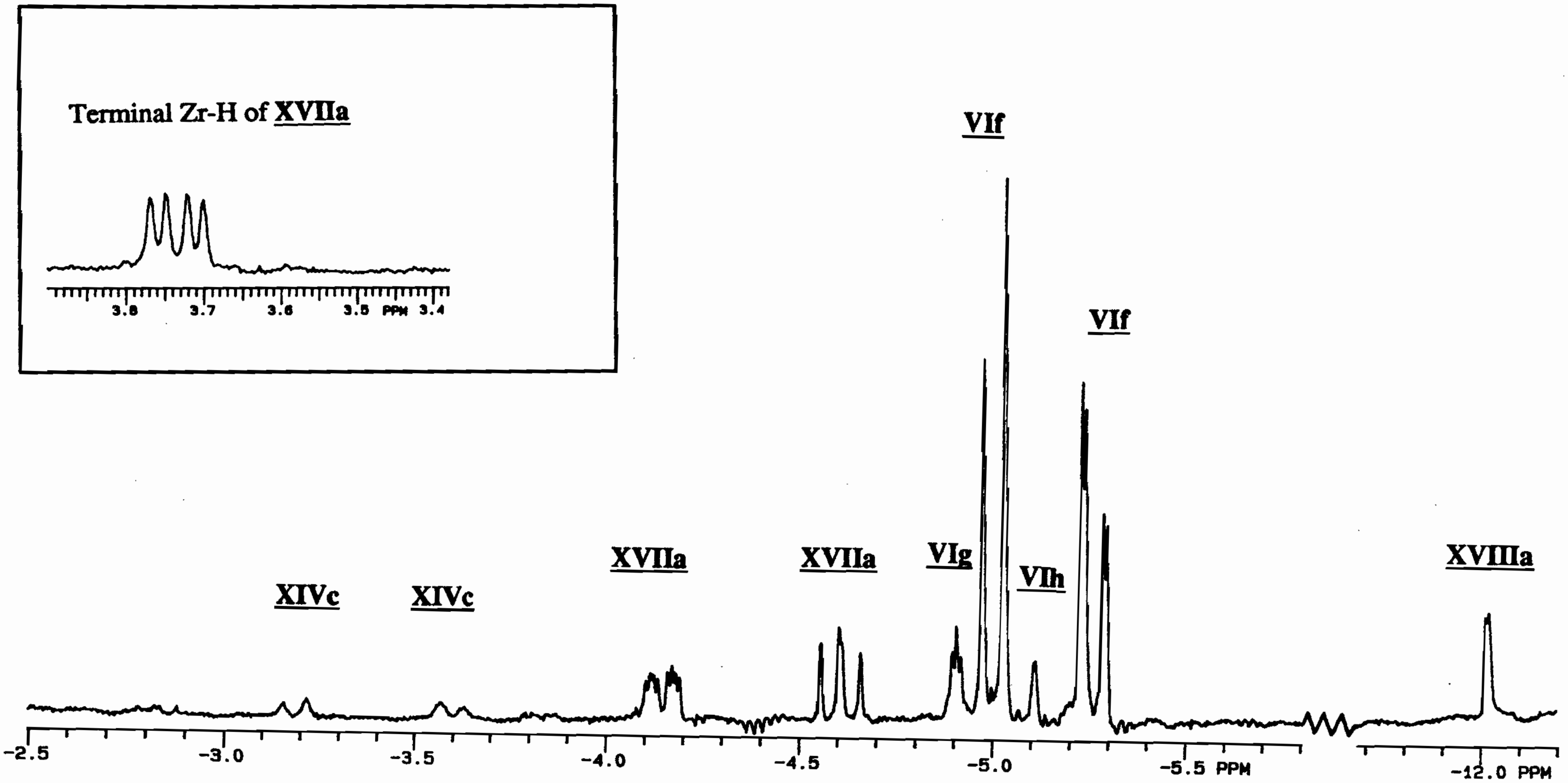

Figure V-11. Zr-H region of the ^{1}H NMR spectrum of the reaction products of DMZ with $PhMeSiH_2$ in benzene-d_6. $[Cp_2ZrMe_2] = 0.08$ M, $[PhMeSiH_2] = 0.24$ M, reaction time = 48 h, at room temperature.

sets of doublet of doublets at 3.73 and -4.61 ppm due to the terminal Zr-H and one of the two bridged Zr-H respectively, and one set of doublet of doublets of doublets at -4.15 ppm due to the other bridged Zr-H which is coupled to the proton in the -SiHPhMe group. In this reaction, small amounts of symmetrical silyl complexes, VIg and VIh, were also observed. A further feature of the spectrum shown in Figure V-11 is the appearance of a hydride resonance in the region of -12 ppm. This resonance is at unusually high field for a Zr-H resonance and is almost certainly due to a diamagnetic zirconocene(III) species, most likely a zirconocene analogue (XVIII) of the titanocene(III) silyl dimer VII. Unfortunately, these kinds of products have thus far resisted attempts at isolation and characterization in the pure state.

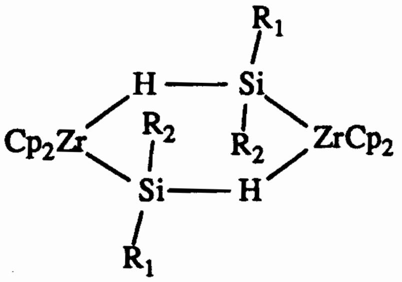

XVIII

XVIIIa: $R_1 = Ph, R_2 = Me$
XVIIIb: $R_1 = R_2 = Ph$
XVIIIc: $R_1 = Bu, R_2 = Me$

Pure VIf has been isolated from the reaction of $PhMeSiH_2$ with DMZ as single crystals. The ^1H NMR spectrum of this complex is shown in Figure V-12. Homonuclear decoupling confirms that the Si-H resonance at 4.88 ppm is coupled to the methyl resonance at 0.597 ppm and bridged Zr-H resonance at -5.24 ppm. The two methyl resonances of equal intensity at 0.529 and 0.518 ppm are due to the two diastereotopic methyls in the $-SiMe_2Ph$ group. The compound appears to give excellent single crystals, but the quality of the obtained X-ray structure is poor due to a severe disorder problem, resulting from the ordered superposition of the two enantiomers of VIf in the crystal. The manner in which the two superposed enantiomers lead to a symmetric electron density map is illustrated in Scheme V-1. An Ortep drawing of VIf showing the atomic numbering scheme is shown in

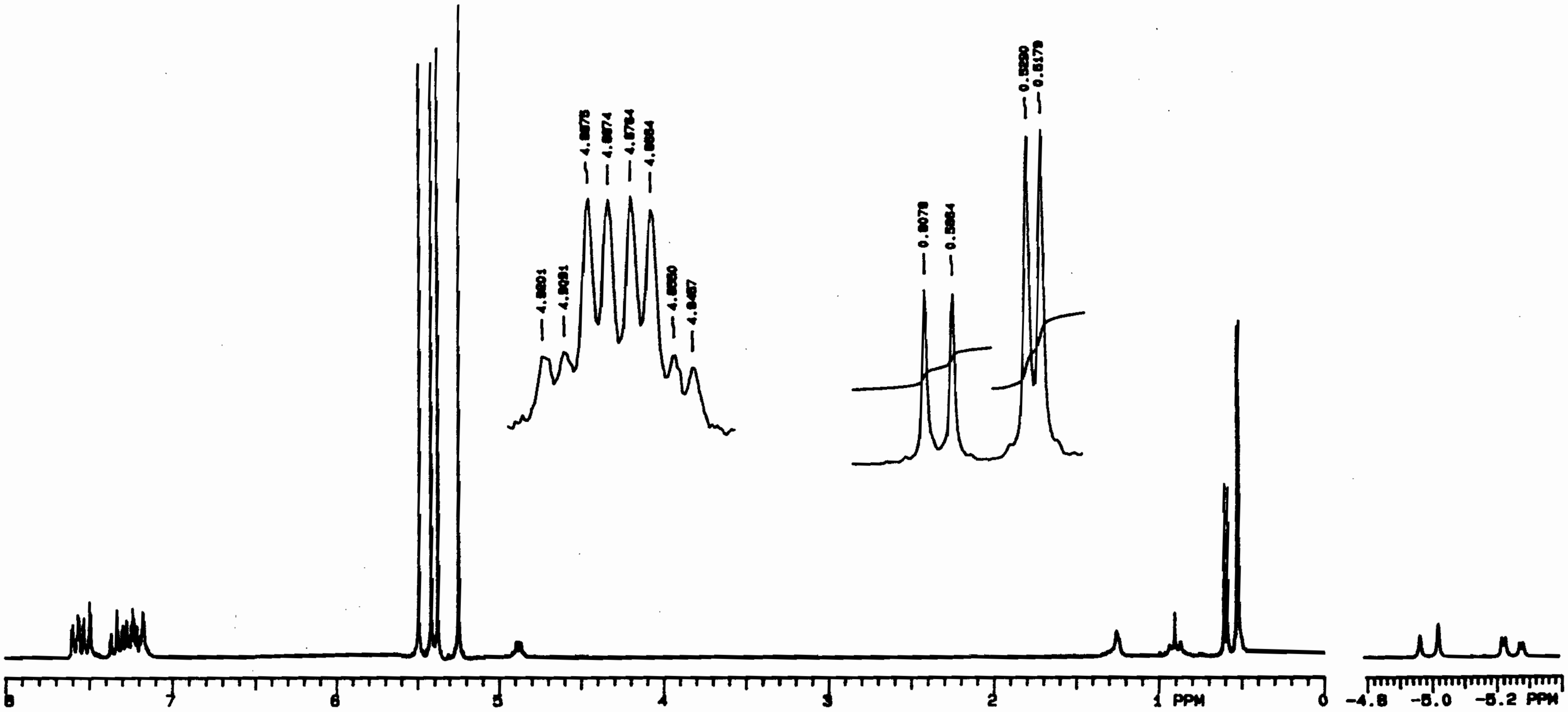

Figure V-12. ^{1}H NMR spectrum of compound <u>VIf</u> in benzene-d_6 at ambient temperature.

Figure V-13 and some selected bond lengths and angles are listed in Table V-5. Complete tables of crystal data, collection and refinement parameters, molecular parameters, atom coordinates and isotropic thermal parameters as well as heavy atom anisotropic thermal parameters are given in Appendix I. Although detailed comparison with other related structures is of questionable utility because of the relative poor precision of the molecular

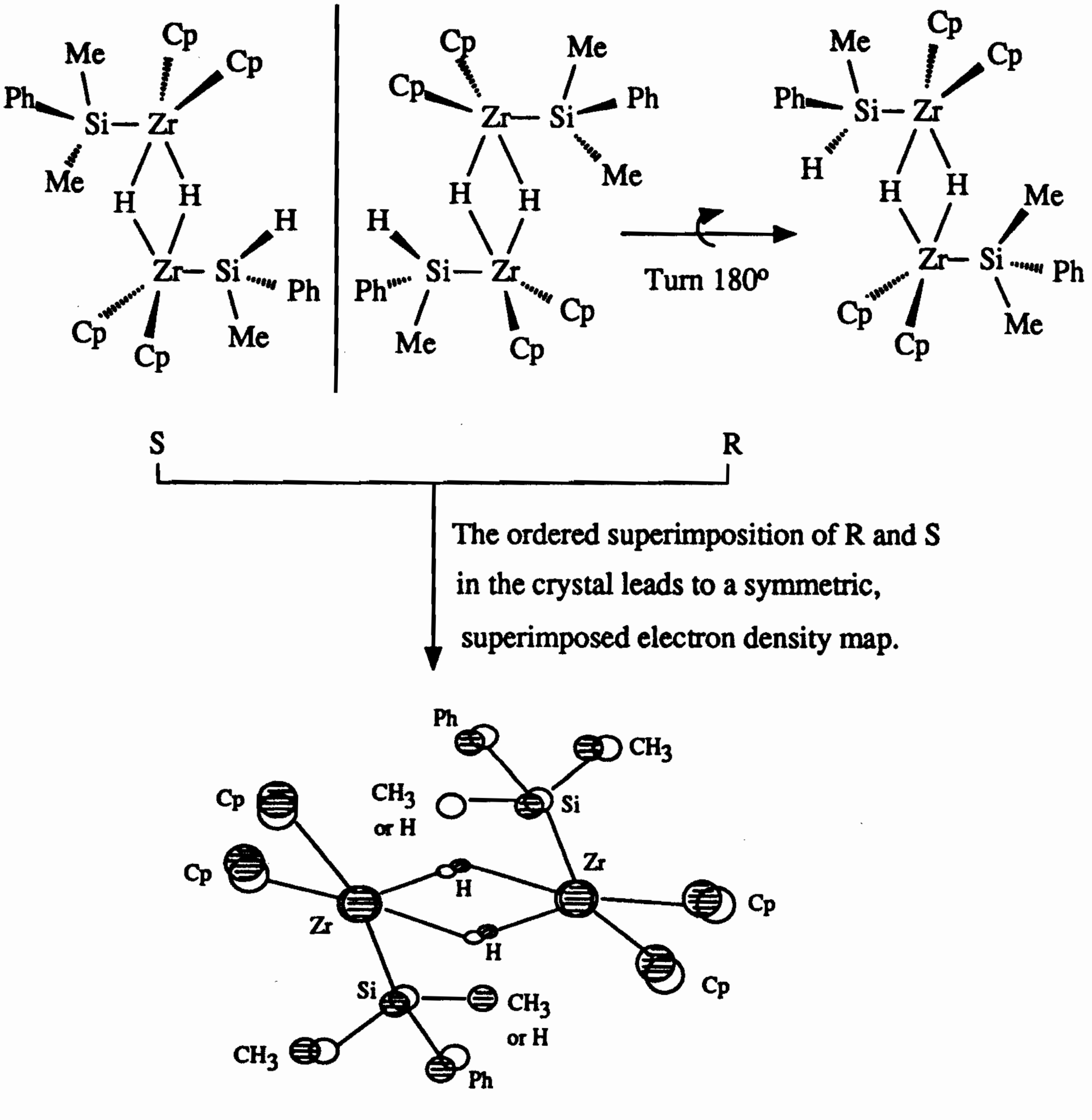

The ordered superimposition of R and S in the crystal leads to a symmetric, superimposed electron density map.

Scheme V-1. The nature of the disorder in compound VIf.

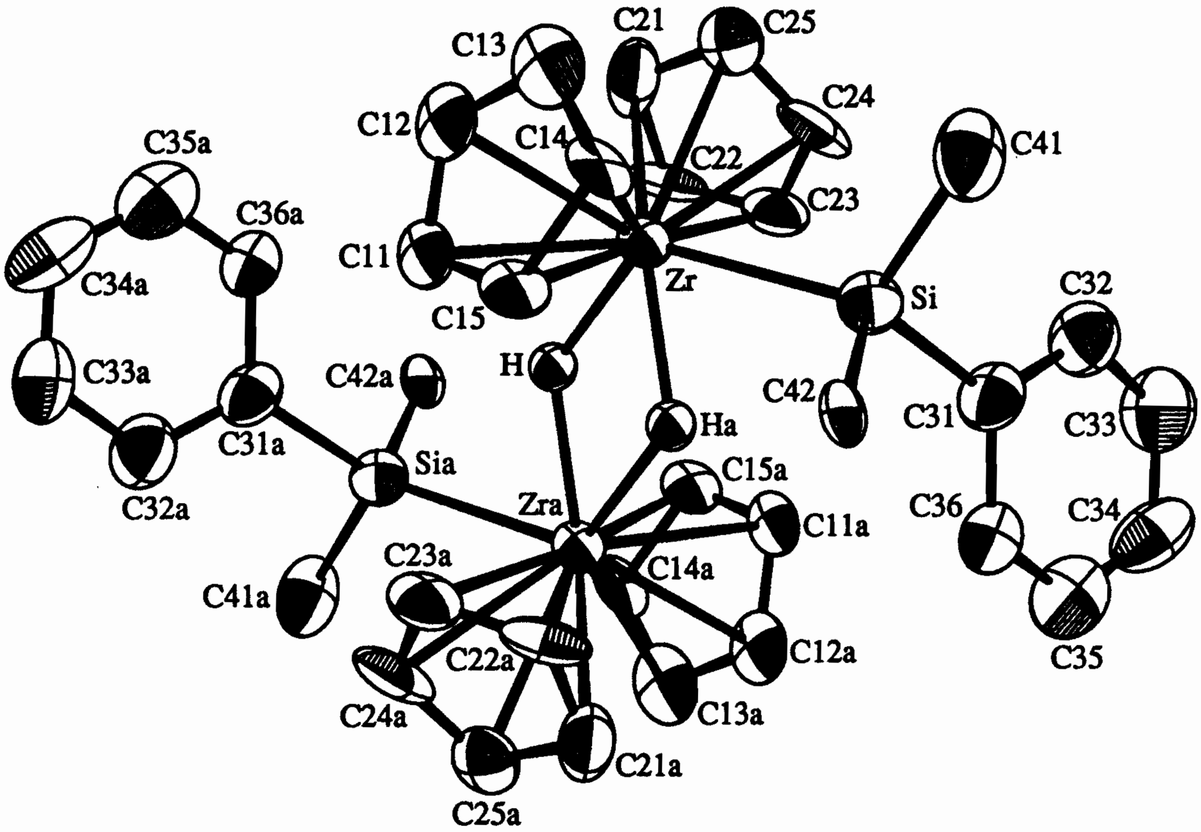

Figure V-13. An ORTEP drawing of $Cp_2Zr(SiPhMe_2)(\mu\text{-}H)_2(HMePhSi)ZrCp_2$ (VIf).

parameters, the structural data are certainly in line with those reported for other bridged Zr(IV) hydrides (184) and Zr(IV) silyl complexes (155). It is more important for us to confirm the overall structure of this type of complex with the X-ray structural data than to obtain the details of their molecular parameters.

In contrast to other examples of this type of complex, VIf was found to be very stable in both solution and the solid state. At ambient temperature, no reaction between VIf and silanes, including primary and secondary silanes, has been observed. Therefore, VIf is completely inactive towards the dehydrocoupling reaction of hydrosilanes under ambient conditions.

Table V-5. Some selected bond lengths and angles for $Cp_2Zr(SiHMePh)(\mu\text{-}H)_2(PhMe_2Si)ZrCp_2$ VIf [a]

	Bond Lengths, Å		
Zr - Si	2.806 (4)	Zr - Zra	3.491 (2)
Zr - H	1.935 (106)	Zr - Ha	1.951 (106)
Zr - Cp(1)	2.223 (13)	Zr - Cp(2)	2.225 (14)
Si - C(31)	1.907 (15)	Si - C(41)	1.885 (18)
Si - C(42)	1.839 (24)		
	Bond Angles, deg		
Si - Zr - Zra	95.6 (1)	Si - Zr - H	121.9 (31)
Si - Zr - Ha	69.8 (31)	H - Zr - Ha	52.1 (55)
Zr - H - Zra	127.9 (55)	Si - Zr - Cp(1)	100.7 (4)
Si - Zr - Cp(2)	100.2 (4)	Cp(1) -Zr - Cp(2)	128.4 (6)
Zr - Si - C(31)	115.1 (5)	Zr - Si - C(41)	116.7 (6)
Zr - Si - C(42)	112.4 (7)		

[a] Cp(n) denotes the centroid of a cyclopentadienyl ring.

V.2.2.4 Reaction of DMZ with Ph_2SiH_2.

The reaction of DMZ with Ph_2SiH_2 is also slow, requiring 1 to 2 days to go to completion under the same conditions as the $PhMeSiH_2$ reaction, and is more complicated than the latter case. In this reaction, the unsymmetrical silyl complex, VIi, only accounts for ca. 10% of the total ^1H NMR observable zirconocene species and the major products are the mixed methyl/silyl dimers, XIVd and XIVe, which account for ca. 30% and 15% of the total observable zirconocene species respectively. Although the reaction is pretty complicated, the assignments for most of the observed zirconocene species have been made by following the reaction and isolating some pure compounds or mixtures of a few species under different conditions. The ^1H NMR data for these zirconocene species are given in Table V-6 and the Zr-H region ^1H NMR spectrum of a reaction mixture is shown in Figure V-14.

Table V-6. ^1H NMR data for some new compounds from the reaction of DMZ with Ph_2SiH_2[a]

compound	assignment	chemical shift (δ)	coupling (Hz)
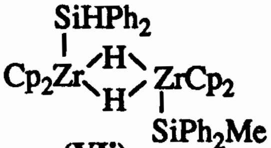 **(VIi)**	C_5H_5	5.449, 5.468 s	
	Si*H*	5.34 d	$^3J = 2.6$
	SiCH_3	0.78 s	
	μ-Zr*H*	- 4.83 d	$^2J = 11.7$
		- 5.10 dd	$^2J = 11.7$, $^3J = 2.6$
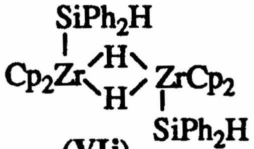 **(VIj)**	C_5H_5	5.471 s	
	Si*H*	5.29 br s	
	μ-Zr*H*	- 4.93 br s	
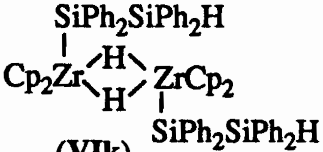 **(VIk)**	C_5H_5	5.484 s	
	μ-Zr*H*	- 4.07 s	
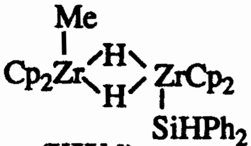 **(XIVd)**	C_5H_5	5.496, 5.509 s	
	Si*H*	5.50 d (overlap with Cp resonance)	
	ZrCH_3	- 0.09 br s	
	μ-Zr*H*	- 3.14 d	$^2J = 12.8$
		- 3.53 dd	$^2J = 12.8$, $^3J = 2.3$
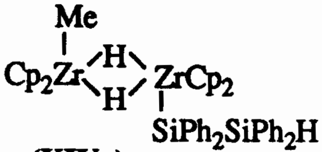 **(XIVe)**	C_5H_5	5.544 br s	
	ZrCH_3	- 0.07 s	
	μ-Zr*H*	- 2.83, - 3.14 d	$^2J = 13.7$
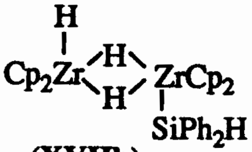 **(XVIIb)**	C_5H_5	5.453, 5.475 s	
	Zr*H*	3.81 dd	$^2J = 9.4$, 3.9
	μ-Zr*H*	- 4.05 ddd	$^2J = 11.6$, 3.9, $^3J = 2.6$
		- 4.51 dd	$^2J = 11.6$, 9.4
$Cp_2Zr(SiHPh_2)Me$	C_5H_5	5.702 s	
	Si*H*	5.14 s	
	ZrCH_3	- 0.28 s	
$[Cp_2ZrSiHPh_2]_2$ **(XVIIIb)**	C_5H_5	5.441 s	
	Zr-*H*-Si	- 12.21 s	

[a] Spectra recorded at 20 °C in benzene-d_6; shifts are in ppm, referenced to TMS.

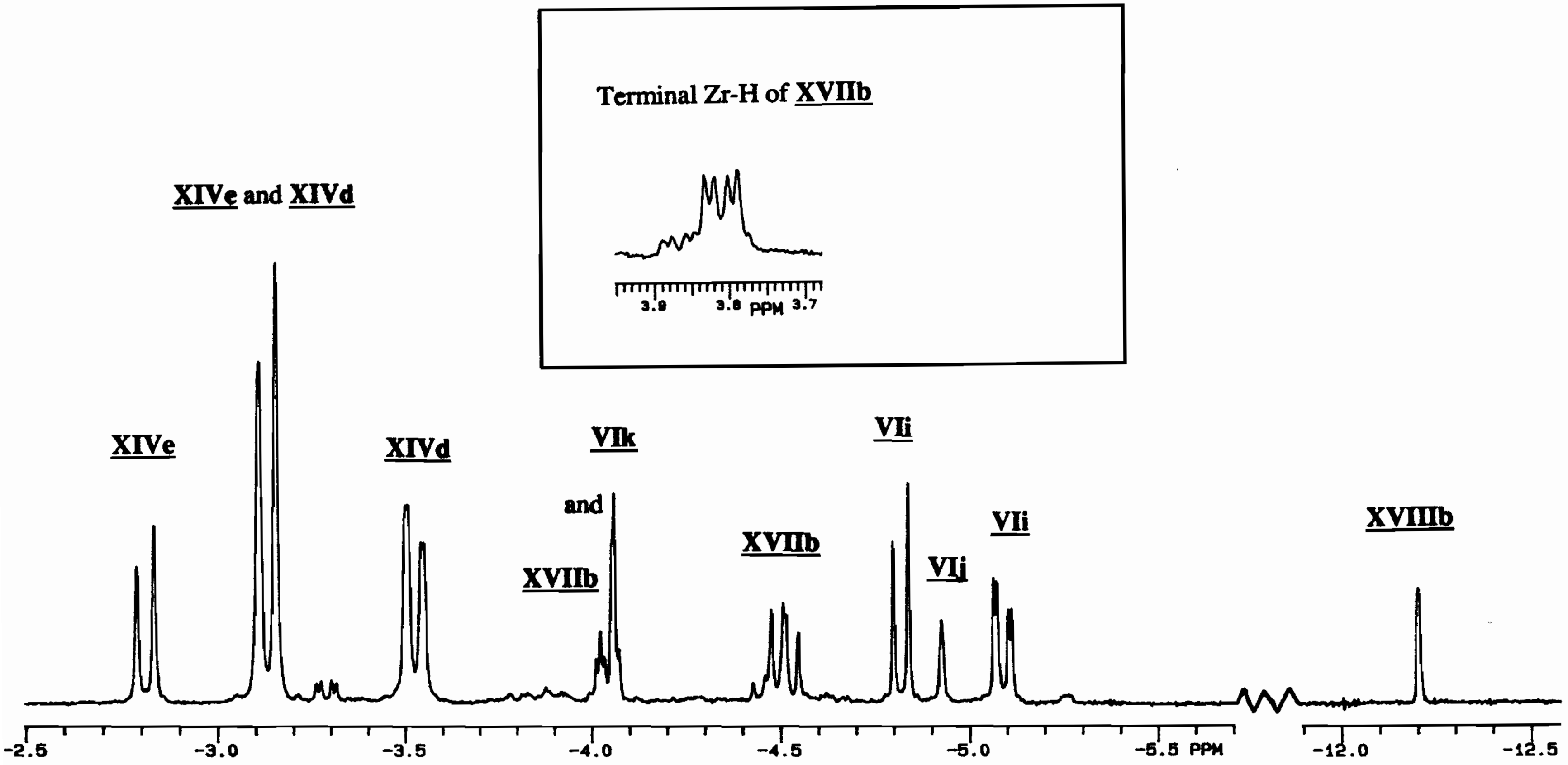

Figure V-14. Zr-H region of the ^{1}H NMR spectrum of the reaction products of DMZ with Ph_2SiH_2 in benzene-d_6. $[Cp_2ZrMe_2]$ = 0.08 M, $[Ph_2SiH_2]$ = 0.24 M, reaction time = 36 h, at room temperature.

In the early stages of a typical reaction, the mixed methyl/silyl dimer, **XIVd**, was produced first. By controlling the reaction conditions carefully, pure **XIVd** has been isolated as microcrystals and its structure is assigned on the basis of its ^1H NMR spectrum, shown in Figure V-15. The Si-H resonance of this compound overlaps with the resonances of Cp groups at 5.50 ppm, which was confirmed by a decoupling experiment (see Fig. V-15). The unsymmetrical silyl dimer **VIi** was produced next and a mixture of **XIVd** and **VIi** was isolated at this stage of the reaction. The ^1H NMR signals of **VIi** are well separated from those of **XIVd** and are readily assigned. The Si-H resonance of **VIi** was also confirmed by a decoupling experiment. With the passage of time, a new mixed methyl/silyl complex was formed with the appearance of an AB quartet at -2.83 and -3.14 ppm. This was followed by a small amount of symmetrical silyl dimer (ca. 3%) with a singlet hydride resonance at -4.07 ppm. Since no corresponding Si-CH_3 resonance has been observed, the two new compounds can only be reasonably assigned to disilyl complexes **XIVe** and **VIk** respectively. As the reaction proceeds, the mixed hydrido/silyl dimer **XVIIb** (ca. 10%) and a small amount of symmetric silyl dimer **VIj** (ca. 3%) were also observed. The assignment for the latter is based on the same reason as mentioned above that no corresponding Si-CH_3 resonance was observed. A high field hydride resonance at -12.2 ppm, probably due to **XVIIIb**, was also observed in the Ph_2SiH_2 reaction. As in the $PhMeSiH_2$ case, the reaction solution became dark-brown in color and showed strong paramagnetism after most of the DMZ had reacted. In addition, a trace of methyl(diphenylsilyl)zirconocene, $Cp_2Zr(SiHPh_2)Me$, was also observed during the reaction. This compound is assigned based on its characteristic Zr-Me resonance at -0.28 ppm (158). A similar NMR signal was also observed in the $PhMeSiH_2$ reaction.

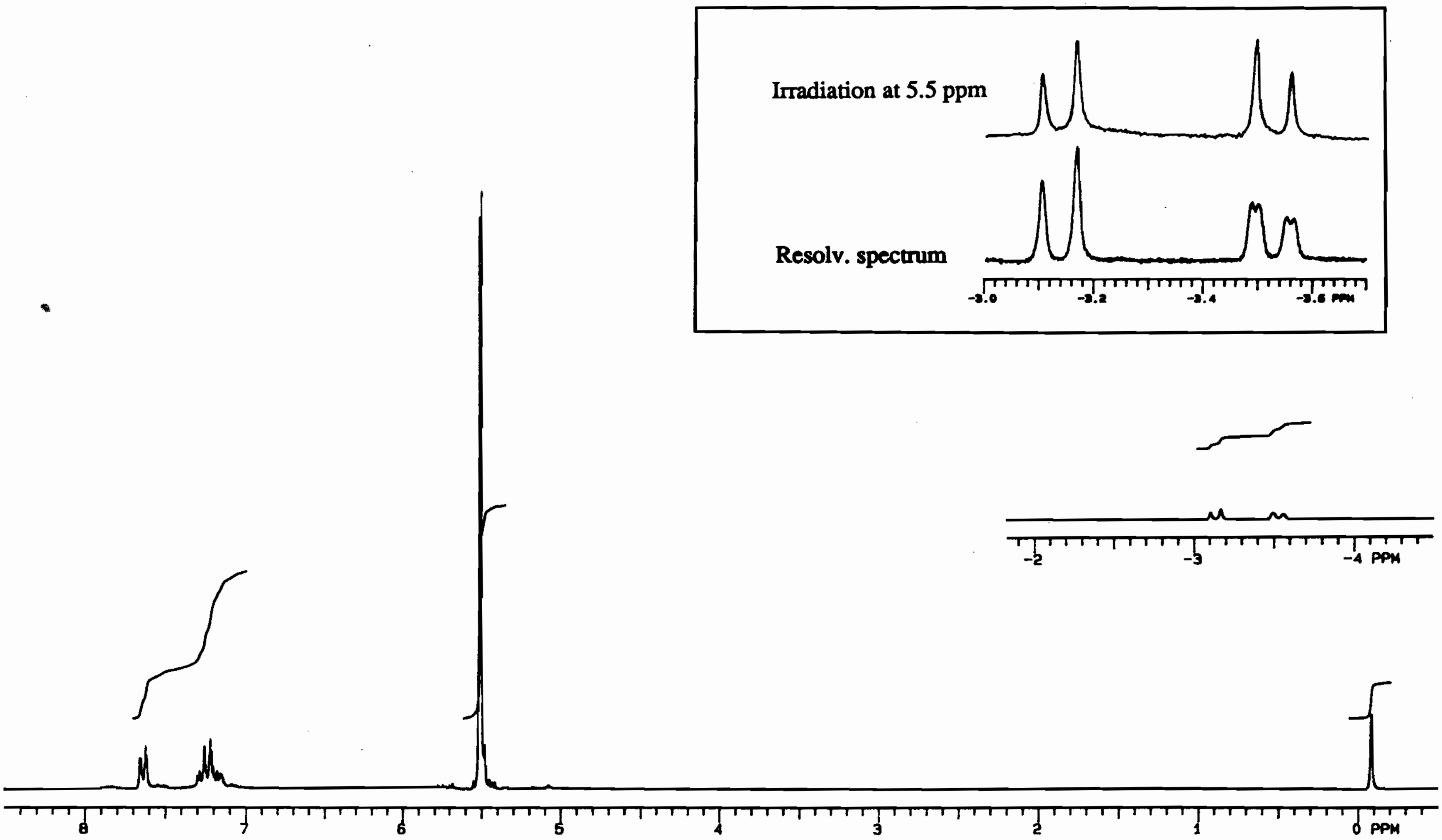

Figure V-15. ^{1}H NMR spectrum of compound XIVd in benzene-d_6 at ambient temperature.

V.2.2.5 Reaction of DMZ with *n*-BuMeSiH$_2$.

n-BuMeSiH$_2$ is much less reactive than PhMeSiH$_2$ or Ph$_2$SiH$_2$ and it requires heating to achieve reasonable reaction rates. In a typical reaction, ~ 50% of DMZ was converted to silyl complexes after the reaction solution was heated at 70°C for 10 hours. In contrast to the PhMeSiH$_2$ and Ph$_2$SiH$_2$ reactions, the ^{1}H NMR spectrum of the BuMeSiH$_2$ reaction products are very simple, as shown in Figure V-16. The unresolved multiplet at -5.70 ppm is due to a symmetrical hydride-bridged dimer, the most likely candidate being **VII**. The high field resonance at -12.07 ppm is assigned tentatively to the symmetrical zirconocene(III) silyl dimer, **XVIIIc** (two isomers). As in the cases of Ph$_2$SiH$_2$, PhMeSiH$_2$ and MeSiH$_3$, the reaction solution of *n*-BuMeSiH$_2$ was also dark-brown in color and showed strong paramagnetism.

In contrast to the reactions of PhSiH$_3$ and PhMeSiH$_2$ where the major products are the unsymmetrical hydride-bridged dimers, the *n*-BuMeSiH$_2$ reaction gives only symmetrical products and no hydride resonance due to an unsymmetrical compound has been observed. As a consequence, the methylated silane, *n*-BuMe$_2$SiH, is produced almost quantitatively. Given the remarkable difference in reaction products for different silanes, it seems clear that the products in these reactions are controlled mainly by their relative stability and the reactivity of silanes, but not by some kind of special mechanism whereby some compounds with particular structure are preferentially formed. More detailed discussion about the reaction products and mechanism will be given later.

V.2.3 Discussion about the mechanism of the silane dehydrocoupling reaction.

V.2.3.1 The dimethyltitanocene catalyzed reaction.

Studies on the dehydrocoupling reactions of organosilanes catalyzed by dialkyl bis(cyclopentadienyl) and bis(indenyl) derivatives of group 4 in our group have indicated that these dehydrocoupling reactions consist of two major stages. The first one is the

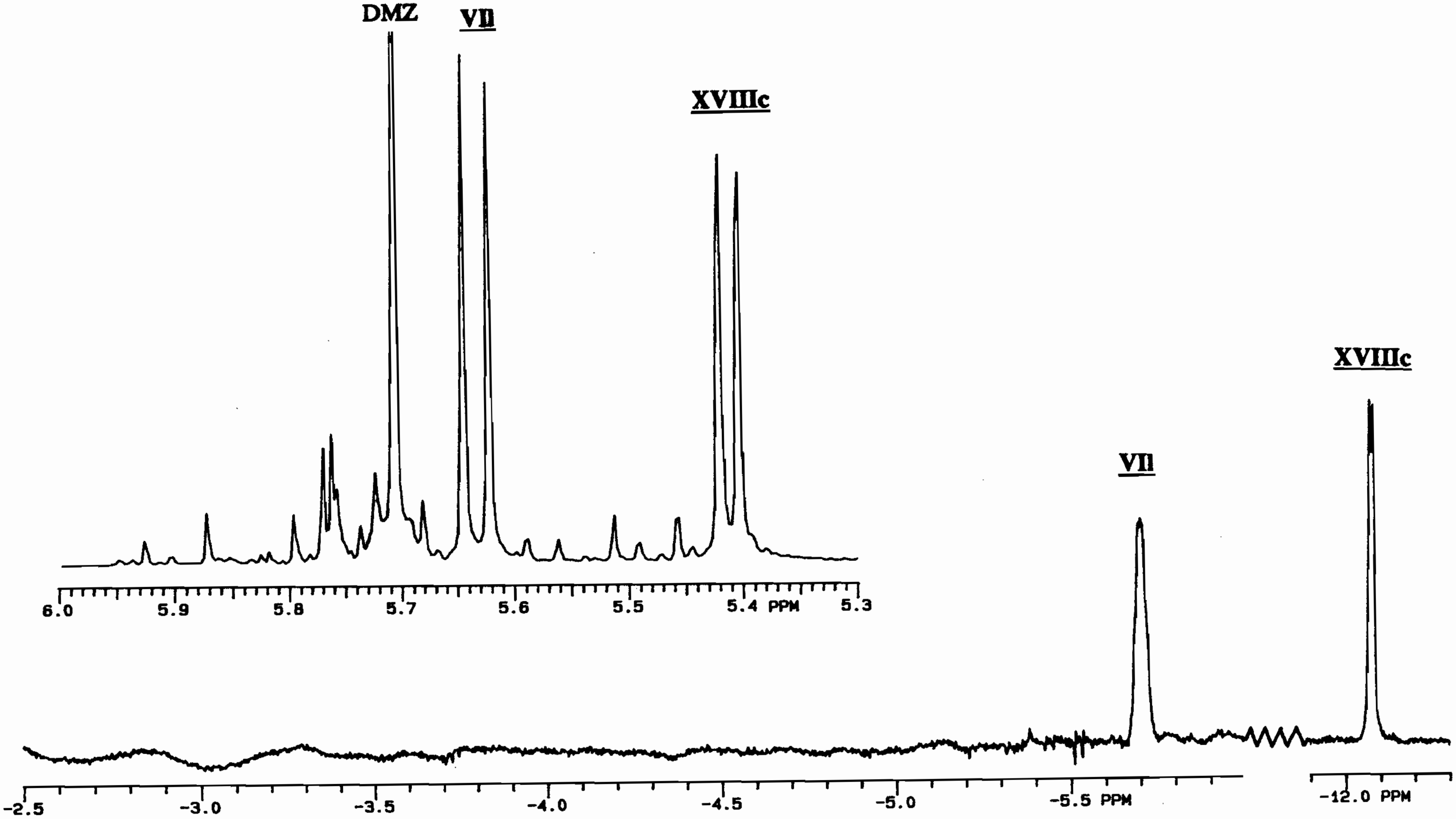

Figure V-16. Cp and Zr-H regions of the ^{1}H NMR spectrum of the reaction products of DMZ with $BuMeSiH_2$ in benzene-d_6. $[Cp_2ZrMe_2] = 0.08$ M, $[BuMeSiH_2] = 0.24$ M, reaction time = 10 h, temp. = 70°C.

initiation stage whereby the dialkyl complex is transformed into an active catalyst, and the second one is the propagation stage. In some cases, the dialkyl complex shows no catalytic activity because of the failure of the starting complex to be converted to an active species (90,92). It is therefore important to understand the mechanisms of both stages.

A. Mechanism in the initiation stage.

So far, all the experimental observations on the catalytic and stoichiometric reactions of DMT with a variety of primary and secondary organosilanes indicate that DMT is completely transformed into the titanium(III) species V at the onset of reaction, accompanied by the formation of 1 equivalent of methane and methylated silane. Usually, an induction period lasting from a few seconds to a few minutes is observed. Sometimes, however, the induction period can be as long as hours. Once the reaction is initiated, the complete conversion of DMT to V occurs very rapidly. Previous studies have indicated that the evolved methane obtains its proton from the silane. Based on these observations, the reactions in the initiation stage can be expressed as follows:

$$Cp_2Ti(CH_3)_2 \;+\; RR'SiH_2 \longrightarrow \text{"}Cp_2Ti\text{"} \;+\; RR'MeSiH \;+\; CH_4 \qquad (V\text{-}5)$$

$$2\ \text{"}Cp_2Ti\text{"} \;+\; RR'SiH_2 \rightleftharpoons Cp_2Ti(\mu\text{-}H)(\mu\text{-}HSiRR')TiCp_2 \qquad (V\text{-}6)$$

Where the $RR'SiH_2$ can be a primary or a secondary organosilane. It has been postulated (148) that Reaction V-5 may occur via either a σ-bond metathesis route as shown in Scheme V-2 or a free radical reaction process as shown in Scheme V-3. However, neither of the Schemes V-2 and V-3 can account for the experimental observations very well. In terms of the σ-bond metathesis reaction in Scheme V-2, one can not understand why an induction period is usually observed. In addition, reaction V-5 is so fast that Cp_2TiMe_2 is completely converted to V in a twinkling once the reaction has been initiated. It seems that

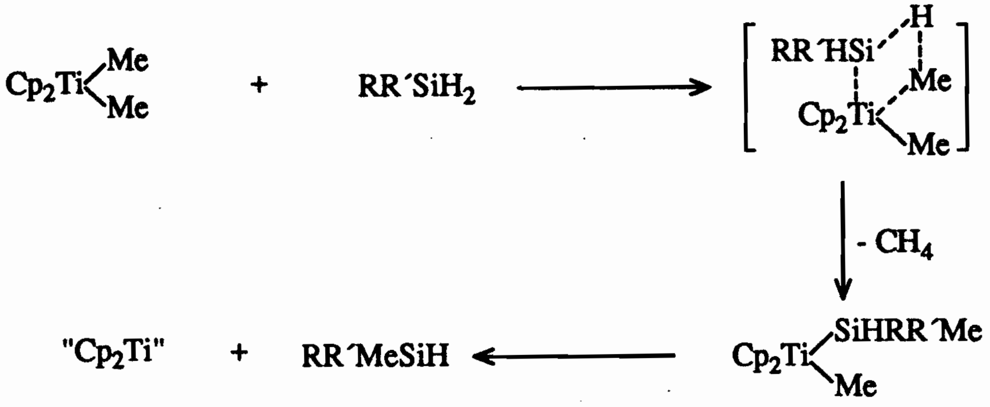

Scheme V-2

$$\mathrm{Cp_2TiMe_2} \xrightarrow{h\nu} \mathrm{Cp_2Ti^{III}Me} + \bullet\mathrm{Me}$$

$$2\ \mathrm{Cp_2Ti^{III}Me} \xrightarrow{\Delta} [\mathrm{Cp_2Ti^{III}Me}]_2$$

$$[\mathrm{Cp_2Ti^{III}Me}]_2 \xrightarrow{h\nu} 2\ \text{"}\mathrm{Cp_2Ti}\text{"} + 2\ \bullet\mathrm{Me}$$

$$\bullet\mathrm{Me} + \mathrm{RR'SiH_2} \longrightarrow \mathrm{CH_4} + \bullet\mathrm{SiRR'H}$$

$$\bullet\mathrm{SiRR'H} + \mathrm{Cp_2TiMe_2} \longrightarrow \mathrm{RR'MeSiH} + \mathrm{Cp_2Ti^{III}Me}$$

Scheme V-3

these features of the reaction could be accounted for better by the free radical reaction mechanism. However, given the fact that the products of the initiation reaction are pretty simple, the free radical reaction mechanism seems also unlikely because more complicated products would be expected from such a free radical reaction system. The subsequent silane dehydrocoupling reaction shows clearly a stepwise fashion and no evidence of any free radical reaction, indicating also that the initiation reaction is unlikely to be a free radical reaction.

Observations on the initiation reaction indicate that the induction period is related to several factors. Lower concentrations of DMT and inefficient drying and degassing of the silane and solvent will lead to a longer induction period. Addition of a trace of reacted DMT (with a silane) to a mixture of DMT and an organosilane initiates the reaction immediately. It seems that some kind of low valent titanocene species is the key initiator of the reaction. It has been found before that Cp^*_2Ti is an initiator of the reaction of $Cp^*_2TiMe_2$ with H_2 (143). The reaction of DMT with a hydrosilane is very similar to the one with H_2, and thus it is possible that the titanocene "Cp_2Ti" is the initiator of the reactions of DMT with silanes. In fact, it appears that only "Cp_2Ti" could be such a species which can not only be produced first in these reactions and exist in the reacted solutions, but also possess the ability to initiate and catalyze these reactions. Based on the above mentioned experimental observations and these considerations, it is very possible that reaction V-5 is completed via a "Cp_2Ti" catalyzed, autoaccelerated reaction mechanism as shown in Scheme V-4. The initial "Cp_2Ti" may be produced by the σ-bond metathesis reaction shown in Scheme V-2. Such a reaction has been observed when Ph_3GeH, instead of organosilanes, was used as substrate (220). In this system, $Cp_2Ti(GePh_3)Me$ was slowly, but quantitatively produced. It is also possible that the initial "Cp_2Ti" comes from the decomposition of DMT given the fact that DMT is very heat and light sensitive. If there is a trace of H_2O or O_2 in the reaction system, the initial produced "Cp_2Ti" will be oxidized. The reaction can be initiated only when all H_2O and O_2 have be consumed. This is probably the reason why an induction period can be observed in this kind of reaction. Although the supposed intermediates, $Cp_2Ti(H)Me$ and $Cp_2Ti(SiHRR')Me$, in Scheme V-4 were not observed directly, their zirconocene analogues have been observed in the reactions of DMZ with Ph_2SiH_2 and $PhMeSiH_2$. It is believed that the two systems follow essentially the same mechanism.

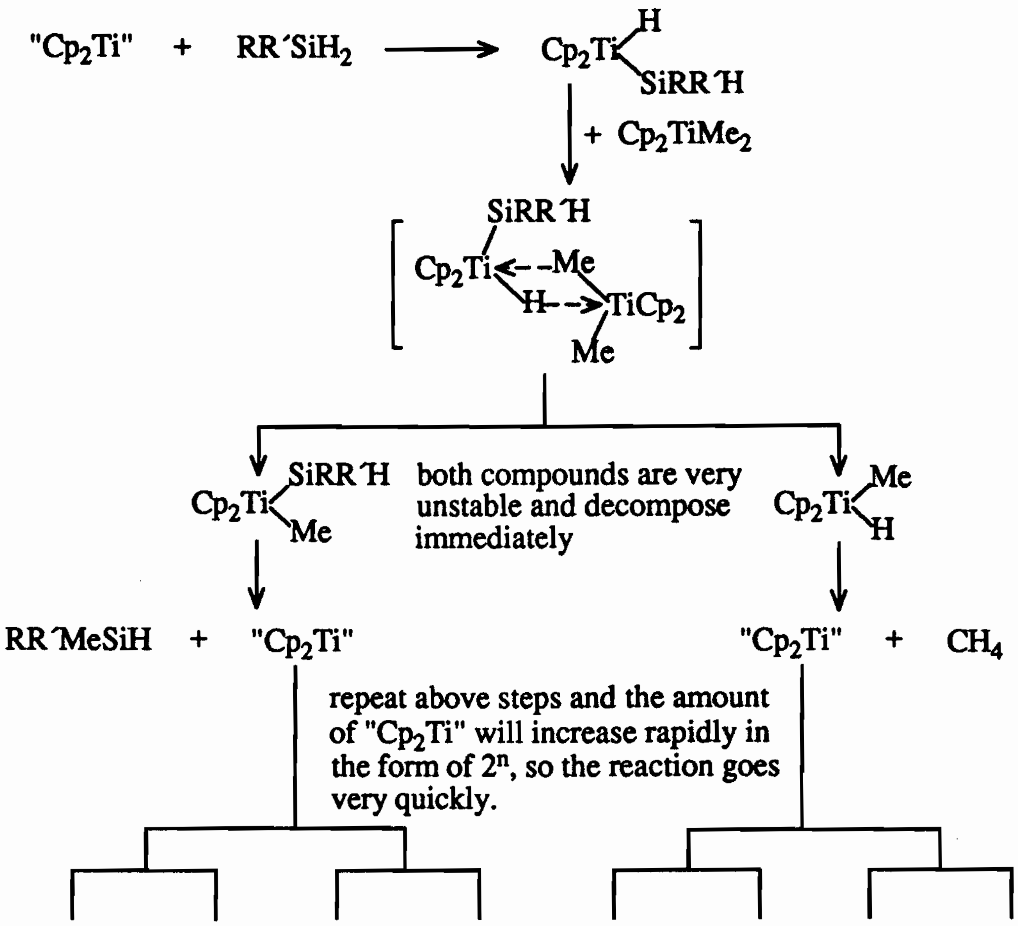

Scheme V-4. A possible mechanism for the initiation stage of the reaction of dimethyltitanocene with hydrosilanes.

B. Mechanism in the propagation stage.

During the last few years, a large number of catalytic and stoichiometric reactions of DMT with a variety of primary and secondary organosilanes have been studied in this laboratory. From these studies, a number of pieces of evidence, which suggest that the five-membered ring complex V is involved in the catalytic cycle of the silane dehydrocoupling reaction, have been accumulated. These include:

1). V is always produced first in the reactions of DMT with primary and secondary organosilanes. Then most of it is slowly transformed into the six membered ring complex, VII, and the hydride complex, XI, accompanied by the dehydrocoupling reaction of silanes. The isolated V has been found to be a very active catalyst for the polymerization of $PhSiH_3$. A kinetic study on the dimerization of Ph_2SiH_2 has also demonstrated that the decrease in reaction rate with time is very consistent with the variation of the concentration of Vd, indicating that the reaction rate is proportional to the concentration of Vd (see Chapter IV).

In previous studies of oligomerization of germanes (34), the diphenylgermyl analogue of V has also been found to be a very powerful catalyst for the tetramerization of diphenylgermane. It is believed that the same mechanism applies to both silane and germane systems.

2). The reaction of DMT with $BuMeSiH_2$ gives the five membered ring complex, Vf, as the major titanocene-containing product. However, no dehydrocoupling reaction has been observed in this system. This result may be attributed to the fact that the reactivity of $BuMeSiH_2$ is too low to undergo the dehydrocoupling reaction although the "active catalyst" Vf can be produced. This reaction indicates again that the conversion of V to VII and XI is related to the dehydrocoupling reaction.

3). In a reaction of $Cp^*{}_2TiMe_2$ with $PhSiH_3$, $Cp^*{}_2TiMe_2$ was reduced to a low valence titanium complex, probably $Cp^*{}_2Ti$, by which the ^1H NMR signals of $PhSiH_3$ were broadened (90). Such a selective line broadening of the silane protons has been attributed to a dynamic process as shown in eq. II-1. In this reaction, however, none of the intermediates V, VII and XI was detected, and no polymerization reaction was observed. Again, whether or not the polymerization can occur is associated with whether or not these bimetallic intermediates can be formed.

4). An earlier study (87) on the titanocene catalyzed co-hydrogenation and hydrosilation of norbornene by $PhSiH_3$ indicated that the reaction at low catalyst concentrations (~0.004 M) gave results significantly different from those obtained at higher (~0.02 M) catalyst concentrations. At low catalyst concentrations, silylated norbornanes

(>50% yield) were obtained as major products. Under these conditions, none of Va, VIIa and XI was observed. At higher catalyst concentrations, rapid conversion of DMT to Va, VIIa and XI occurred and the catalytic reaction produced mainly polysilane and norbornane in about 80% yields, and silylated norbornanes in about 20% yield. These results indicate once again that the polymerization of silanes is related to these bimetallic complexes.

Based on these results, it is believed that V might be an essential intermediate in the catalytic cycle. A possible mechanism involving V is presented in Scheme V-5. From the structural point of view, such a bimetallic transition state mechanism is reasonable. The Ti-H-Ti and Si-H-Ti bridges in V are electron deficient, three-centre, two-electron bonds. The Ti(H)(HSi)Ti five membered ring in V might have three possible valence structures as shown below:

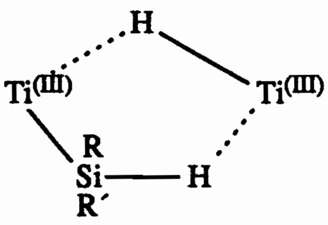

V(a)

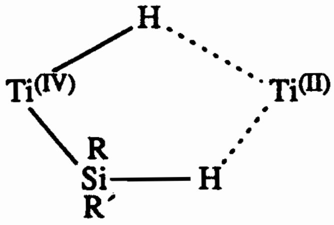

V(b)

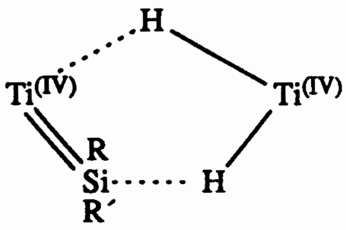

V(c)

From these valence structures, it can be expected that the bridged Ti-H-Ti and Si-H-Ti bonds in V should be quite weak and the Ti-Si bond should be slightly stronger than a normal Ti-Si single bond. The weakness of the Ti-H-Ti and Si-H-Ti has been demonstrated by their temperature dependent ^{1}H NMR signals, and the slightly stronger Ti-Si bond seems to be reflected by comparison of the Ti-Si bond distance (2.61(2) Å) in Va (32) to those in $Cp_2TiCl(SiMe_3)$ (2.67(1) Å) (152) and $Cp_2Ti(SiH_2Ph)(PMe_3)$ (2.650(1) Å). According to the structural feature of V, several possible reactions could be expected. One is the dissociation of V into two titanium(III) species. This kind of reaction has been

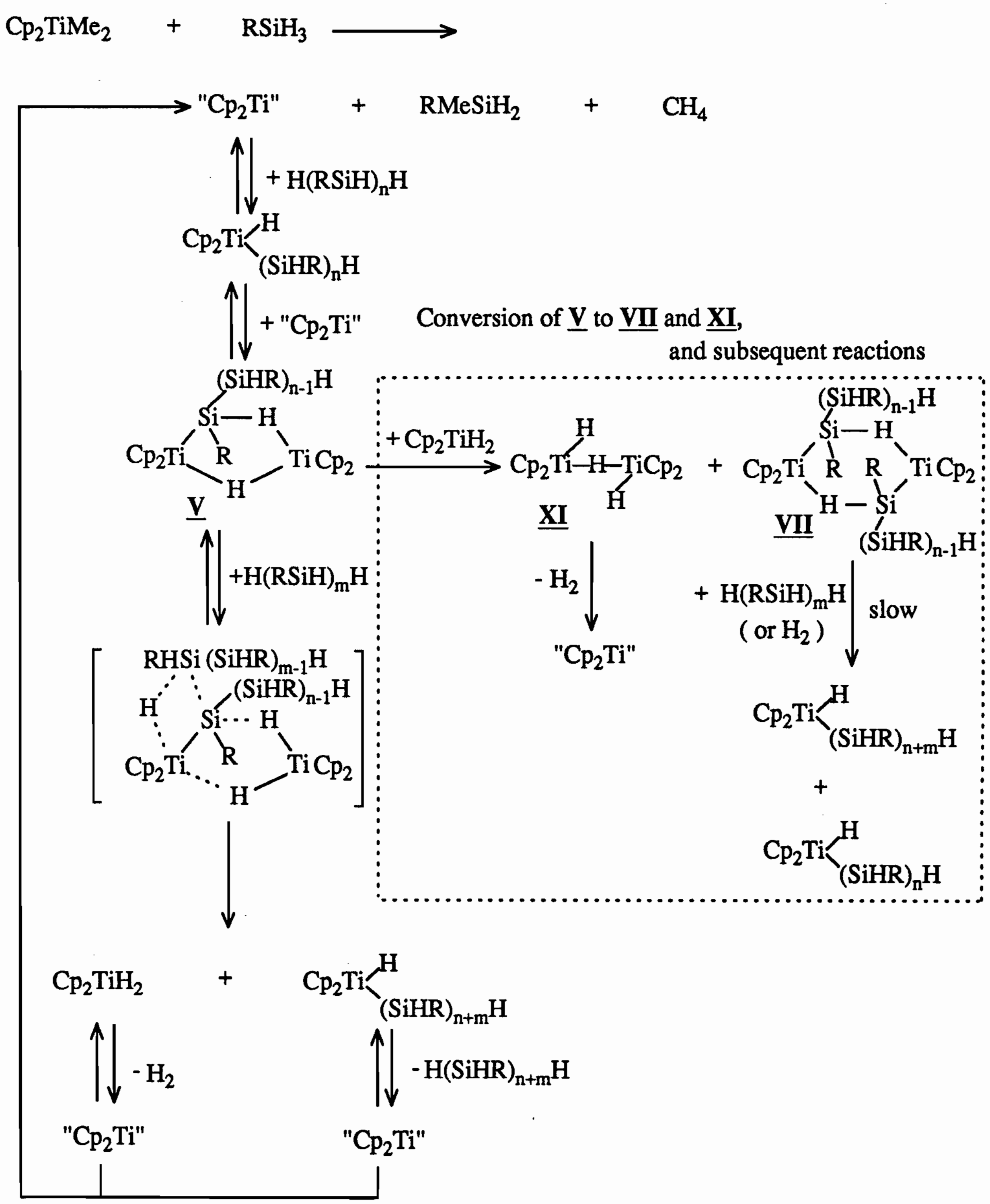

Scheme V-5a. Proposed mechanism for titanocene catalyzed silane dehydrocoupling reaction. Where $RSiH_3$ is a primary silane.

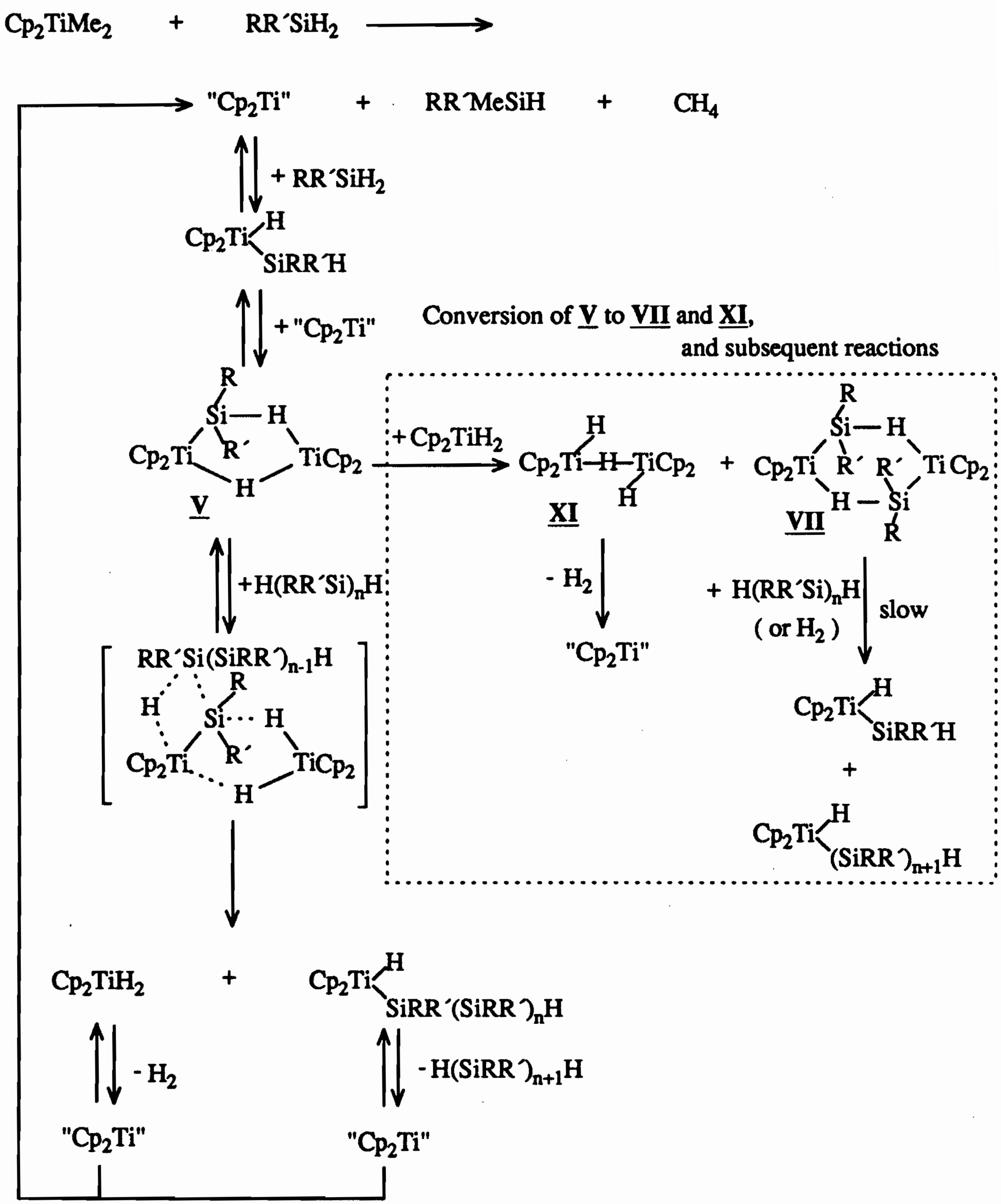

Scheme V-5b. Proposed mechanism for titanocene catalyzed silane dehydrocoupling reaction. Where RR´SiH$_2$ is a secondary silane.

observed by carrying out the reactions of DMT with some primary and secondary silanes in the presence of pyridine or trimethylphosphine. From these reactions, Ti(III) complexes of the type $Cp_2Ti(SiRR'H)L$ (where L = Py, PMe_3) were obtained. Details about these reactions will be given in the next chapter. The conversion of **V** to **VII** and **XI** gives another example of this kind of reaction. Another reaction is the dissociation of **V** into "Cp_2Ti" and silane in the reverse sense of eq. V-6. Such a reaction has been proved by the complete conversion of **Va** to $Cp_2Ti(CO)_2$ and $PhSiH_3$ upon bubbling CO into the solution of **Va** (148). A third reaction of **V** is the Si-Si bond forming step in Scheme V-5. As discussed above, in **V** the Si-H bond and Ti-H bond are relatively weak, while the Ti-Si bond might be slightly stronger than a normal Ti-Si single bond, more or less like a metal-silylene bond. In terms of these structural features, such a Si-Si bond forming reaction is reasonable and understandable. In fact, **V** might be considered as a metal-silylene-like intermediate and such a reaction is therefore a metal-silylene-like reaction. Of course, it also has the elements of σ-bond metatheses at the Ti and Si atoms of **V**.

The bimetallic transition state mechanism shown in Scheme V-5 can explain most of the observed experimental phenomena and results. In return, many of the experimental results can be taken as further evidences to support the mechanism. Some typical examples are given as follows:

1). When the pure six membered ring complex **VIIa** was used as catalyst, the polymerization of $PhSiH_3$ was very slow at the beginning of reaction and then became faster and faster with time, accompanied by a color change from dark green to dark blue, the typical color of **Va**. A ^1H NMR study indicated that about 30% of **VIIa** had converted to **Va** after several hours. We attribute the acceleration of the reaction to the increase in concentration of **Va**.

2). From both previous (34) and present studies of oligomerization of primary silanes, it was found that the major cyclization reaction occurs after the essentially complete conversion of the monomers to linear polysilanes, i.e. the cyclosilanes are produced mainly from the linear polysilanes by a backbiting depolymerization reaction. A possible mechanism for the depolymerization reaction is shown in eq. V-7. From such a reaction,

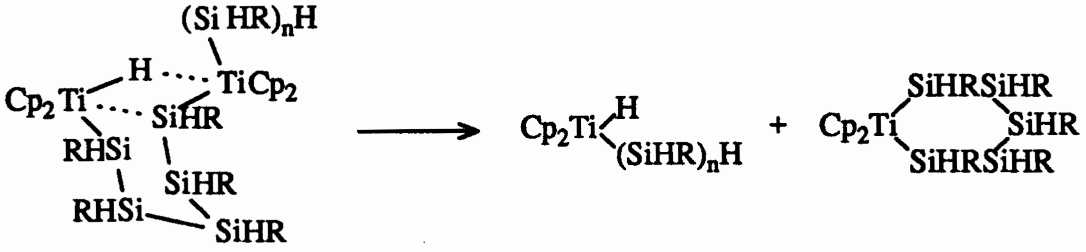

(V-7)

cyclopentasilane would be expected to be produced preferentially. ^{1}H NMR studies have demonstrated that the Si-H resonances of the cyclosilanes formed from the backbiting cyclization extend remarkably towards lower field relative to the Si-H resonances of the cyclosilanes formed during the polymerization (Fig. II-7), which probably indicates that considerable amounts of smaller cyclics are produced in the backbiting cyclization reaction since the Si-H resonance shifts to lower fields for smaller cyclosilanes (221,222). The backbiting cyclization does not occur very much during the chain propagation reaction, probably because most of the catalyst molecules exist in dimeric form during this period. After the chain propagation reaction, the polysilane chain is probably too long to form the dimeric V and thus the chain propagation stops and the backbiting depolymerization occurs. The formation of cyclosilanes during the chain propagation is most likely the result of an intramolecular closure as shown in eq. V-8. This process obviously has a high probability

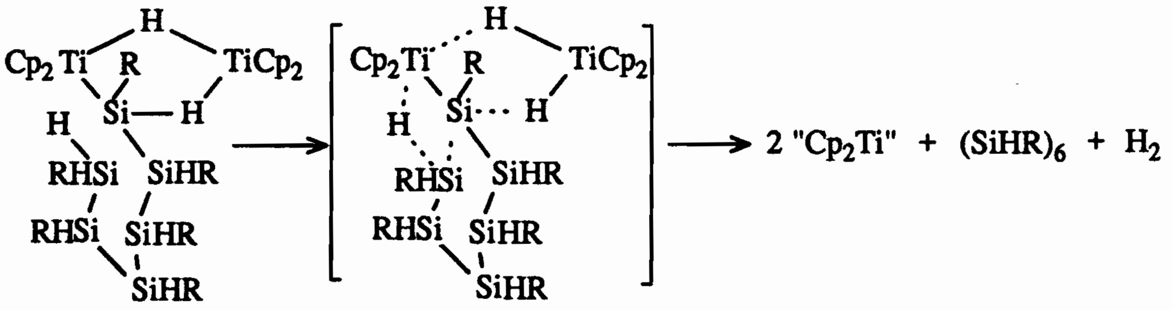

(V-8)

when the silicon chain is about 6 atoms long.

3). When the titanocene catalyzed silane dehydrocoupling reaction is carried out in the presence of an olefin, the evolution of H_2 is completely suppressed and the co-hydrogenation of the olefin takes place. Such a result can be well explained in terms of the bimetallic mechanism. As can be seen from Scheme V-5, in the catalytic cycle, the dihydride complex, Cp_2TiH_2, is formed first, and the H_2 is then liberated from it. The dihydride complex Cp_2MH_2 (M = Ti, Zr) is exactly the active intermediate in the catalyzed hydrogenation reaction of olefin (139,186,223,224). Therefore, if there is any olefin in the reaction system, it will react with Cp_2TiH_2 immediately once the latter is produced. Otherwise, if the dehydrocoupling reaction goes through a mechanism whereby the H_2 is liberated first, it is questionable whether or not the evolution of H_2 can be completely suppressed.

4). The polymerization of 1,2-diphenyldisilane in the presence of titanocene catalyst gives tetrasilane as the main initial product and only a small amount of monosilane is produced during the reaction. However, it was found that most of the disilane is converted to monosilane and 1,2,3-triphenyltrisilane first in the presence of bis(indenyl)titanium catalyst (225). It seems clear that the former reaction proceeds mainly by dehydrocoupling, while the latter goes predominantly through a catalytic redistribution route, probably as the one shown in eq. V-9. The difference between the two systems perhaps results from the larger steric bulk of the bis(indenyl) complex. As discussed above, if V is a necessary intermediate for the dehydrocoupling reaction, the large steric hindrance of the indenyl ligands probably obstructs the formation of such an intermediate in the latter case, and thus the reaction proceeds via a less sterically constrained route.

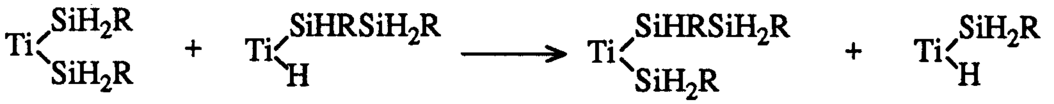

$$\mathrm{Ti}{<}^{\mathrm{SiH_2R}}_{\mathrm{SiH_2R}} + \mathrm{Ti}{<}^{\mathrm{SiHRSiH_2R}}_{\mathrm{H}} \longrightarrow \mathrm{Ti}{<}^{\mathrm{SiHRSiH_2R}}_{\mathrm{SiH_2R}} + \mathrm{Ti}{<}^{\mathrm{SiH_2R}}_{\mathrm{H}} \qquad (\text{V-9})$$

5). It was mentioned in Chapter II that the steric effects of the two reacting silanes in a catalytic cycle are different. If one of the two reacting silanes is monomer or dimer, the dehydrocoupling reaction is fast even though the other is a larger oligomer such as hexamer or still larger. However, if both of the two reacting silanes are trimer or larger oligomer, the reaction is slow. Such results can be reasonably accounted for in terms of the bimetallic transition state mechanism. As seen from Scheme V-5, the two reacting silanes in a catalytic cycle play different roles. One reacts with "Cp_2Ti" to form the intermediate V, while the other reacts with V to give the coupling product. By using molecular models, it can be seen that the steric effect of the silane forming V on the dehydrocoupling reaction increases with chain length more rapidly than that of the latter, the coming silane molecule, especially when the chain length increases from dimer to trimer.

6). According to the mechanism shown in Scheme V-5, a tertiary silane can not dehydrocouple with itself or another tertiary silane, but should be able to couple with a primary or a secondary silane if it's reactivity is high enough and steric hindrance is low enough. This is consistent with experimental observations. The stepwise oligomerization of $PhMeSiH_2$ to dimer and trimer gives a typical example of the dehydrocoupling between a secondary silane and a tertiary silane.

7). Such a mechanism can account for the kinetic results obtained from the dehydrocoupling of Ph_2SiH_2. The kinetic results have been discussed in some detail in the previous chapter. Here we are going to discuss the influence of the catalyst concentration on the reaction rate of the dimerization of Ph_2SiH_2. In the catalytic reaction system, the titanocene species exists mainly in the form of **VIId**, while **Vd** is the active catalyst. These two complexes can convert to each other in the presence of silane. Other titanocene species can be easily converted to **Vd** and do not seem to be important factors to affect the catalytic activity. The conversion of **Vd** to **VIId** may proceed through eq. V-10 and V-11, whereas the reversion of **VIId** to **Vd** probably takes place according to eq. V-12 and V-13 based on

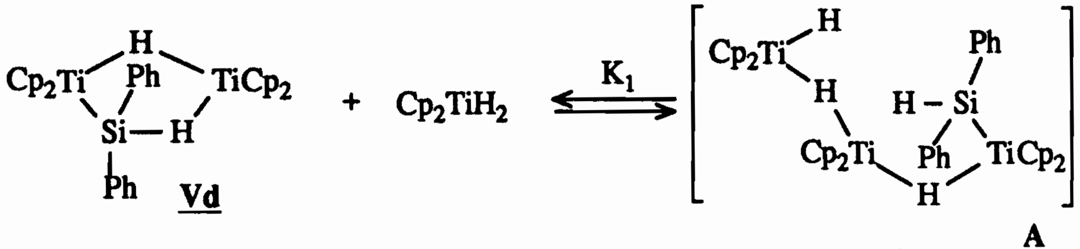

(V-10)

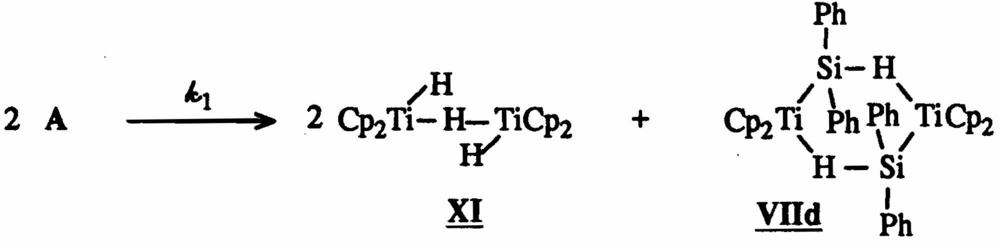

(V-11)

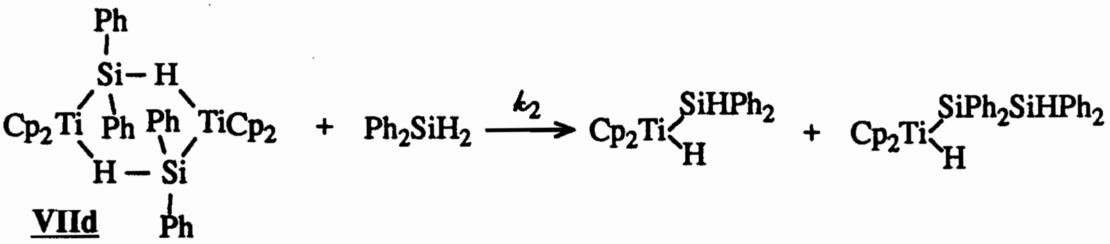

(V-12)

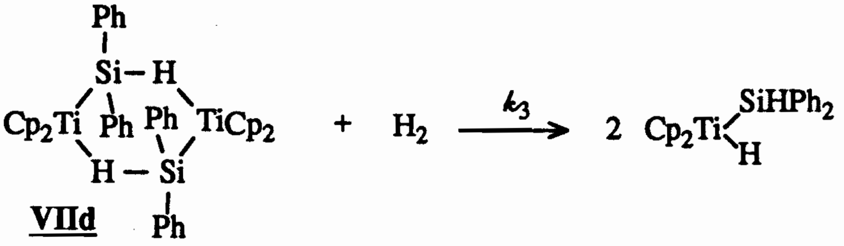

(V-13)

our experimental observations. The reaction rates for the formation (R_f) and consumption (R_c) of **VIId** can be expressed by eq. V-14 and V-15 respectively. When the equilibrium between **Vd** and **VIId** is reached, we have eq. V-16. Under constant concentrations of silane and H_2, eq. V-16 can be reduced to eq. V-17. According to such an equation, if the concentration of **VIId** is doubled by increasing the total catalyst concentration, the concentration of **Vd** can increase at most by 40% even though the concentration of Cp_2TiH_2 is supposed to be constant. If the concentration of Cp_2TiH_2 increases in the same way as that of **Vd**, only an increase of 20% in the concentration of **Vd** can be expected when the concentration of **VIId** is doubled. Experimentally, an average increase of 35% in rate constant was obtained when the total catalyst concentration was doubled.

$$R_f = k_1 [A]^2 = k_1 K_1 [\underline{Vd}]^2 [Cp_2TiH_2]^2 \quad (V\text{-}14)$$

$$R_c = [\underline{VIId}] (k_2 [Ph_2SiH_2] + k_3 [H_2]) \quad (V\text{-}15)$$

$$k_1 K_1 [\underline{Vd}]^2 [Cp_2TiH_2]^2 = [\underline{VIId}] (k_2 [Ph_2SiH_2] + k_3 [H_2]) \quad (V\text{-}16)$$

$$[\underline{Vd}]^2 [Cp_2TiH_2]^2 = K [\underline{VIId}] \quad (V\text{-}17)$$

V.2.3.2 The dimethylzirconocene catalyzed reaction.

All experimental results obtained so far indicate that DMZ exhibits almost identical behavior to DMT in catalyzing the dehydrocoupling of primary and secondary organosilanes. The same dehydrocoupling products are produced from secondary silanes by both catalysts, and the same rate law has been determined in the dimerization of Ph_2SiH_2 catalyzed by both DMT and DMZ. The molecular weights and molecular weight distributions of the polymers produced from primary silanes by the two catalysts are also remarkably similar. These similarities between the two systems imply that the reaction mechanism is probably the same or similar for both systems. Although most of the zirconium remains in the form of NMR-observable Zr(IV) species throughout the reactions with most primary and secondary silanes, lower valent zirconium species, the paramagnetic mixed-valence zirconocene hydride <u>XIII</u> and diamagnetic zirconocene(III)silyl dimer <u>XVIII</u>, have been observed during these reactions. The existence of these lower valent zirconocene analogues of titanocene complexes <u>VII</u> and <u>XI</u> suggests again that the same mechanism might apply to both catalytic systems. Although the five membered ring bimetallic complex, the key active intermediate in Scheme V-5, has not been observed in the zirconocene system, it is possible that such a zirconocene intermediate is not observable because of some kind of dynamic process as discussed above in section V.2.2.1.

On the basis of our experimental observations on the catalytic and stoichiometric reactions of DMZ with a number of primary and secondary organosilanes, it is believed that DMZ is converted to active catalyst by silanes in a similar way to DMT. As in the case of DMT, the direct reaction between DMZ and silane, as shown in Scheme V-2, is necessary at the beginning of the reaction to produce the initial "Cp_2Zr". Following this initial reaction, an initiation process similar to the one shown in Scheme V-4 could be expected. However, the situation of the DMZ system is a little bit more complicated than that of the DMT system. In contrast to the titanocene catalyzed reaction, the zirconocene catalyzed reaction exhibits an autoacceleration in the course of the reaction, but no obvious induction period. The conversion of DMZ is much slower relative to the initiation reaction of DMT, consequently, considerable amounts of dehydrocoupling products have been produced before the conversion of DMZ is completed. These produced oligomers can also react with DMZ, and thus make the DMZ system more complicated. In addition, the mixed hydrido/silyl dimers observed in several reactions must be formed from the reaction of Cp_2ZrH_2 with a silylzirconocene hydride, while the former is produced from the dehydrocoupling reaction. In almost all studied reactions, it was found that most of the DMZ is gradually converted to a variety of hydride bridged Zr(IV) complexes. The conversion of DMZ to these complexes can be accounted for by following reactions.

Initial reactions:

$$Cp_2ZrMe_2 + RR'SiH_2 \longrightarrow Cp_2Zr(RR'SiH)Me + CH_4 \qquad (V\text{-}18)$$

$$Cp_2Zr(RR'SiH)Me \longrightarrow \text{"}Cp_2Zr\text{"} + RR'MeSiH \qquad (V\text{-}19)$$

Following reactions:

$$\text{"}Cp_2Zr\text{"} + RR'SiH_2 \rightleftharpoons Cp_2Zr(H)(SiHRR') \qquad \text{(V-20)}$$

$$\text{"}Cp_2Zr\text{"} + RR'MeSiH \rightleftharpoons Cp_2Zr(H)(SiMeRR') \qquad \text{(V-21)}$$

$$Cp_2Zr(H)(SiHRR') + Cp_2ZrMe_2 \longrightarrow Cp_2Zr(RR'SiH)Me + Cp_2Zr(H)Me \qquad \text{(V-22)}$$

$$Cp_2Zr(H)Me \longrightarrow \text{"}Cp_2Zr\text{"} + CH_4 \qquad \text{(V-23)}$$

$$Cp_2Zr(H)(SiHRR') + Cp_2Zr(H)(SiMeRR') \rightleftharpoons \text{unsymmetrical dimer } \underline{\text{VI}} \qquad \text{(V-24)}$$

$$2 \quad Cp_2Zr(H)(SiHRR') \rightleftharpoons \text{symmetrical dimer } \underline{\text{VI}} \qquad \text{(V-25)}$$

$$2 \quad Cp_2Zr(H)(SiMeRR') \rightleftharpoons \text{symmetrical dimer } \underline{\text{VI}} \qquad \text{(V-26)}$$

$$Cp_2Zr(H)(SiHRR') + Cp_2Zr(H)Me \rightleftharpoons \text{mixed methyl/silyl dimer } \underline{\text{XIV}} \qquad \text{(V-27)}$$

$$Cp_2Zr(H)(SiMeRR') + Cp_2Zr(H)Me \rightleftharpoons \text{mixed methyl/silyl dimer } \underline{\text{XIV}} \qquad \text{(V-28)}$$

$$Cp_2Zr(H)(SiHRR') + Cp_2ZrH_2 \rightleftharpoons \text{mixed hydrido/silyl dimer } \underline{\text{XVII}} \qquad \text{(V-29)}$$

From these reactions, it would be expected that the major reaction products of DMZ with a silane should be those complexes which are more stable relative to others. As seen in section V.2.2, the major reaction products of various silanes with DMZ differ greatly. This indicates that the relative stabilities of different types of complexes vary according to the differences in reactivity and steric hindrance of the silanes. Since most of zirconocene species exist in the form of hydride bridged dimeric complexes, and these dimeric complexes are quite stable in solution, the concentrations of the monomeric hydride complexes must be relatively low throughout these reactions, and thus it would be expected that the reaction V-22 proceeds slowly. In addition, the products of this reaction, $Cp_2Zr(Me)SiRR'H$ and $Cp_2Zr(H)Me$ (form dimeric complexes), are more stable than their titanium analogues based on the fact that the former can be observed but the latter can not. This might be another factor which slows down the conversion of DMZ.

The mixed valence hydride XIII and the six-membered ring complexes XVIII are probably formed mainly in the same way as proposed for their titanium analogues in Scheme V-5. However, it is possible that XVIII can also be formed via hydride bridged complexes VI in a pathway as shown in eq. V-30. Such a reaction can explain the formation of XVIIIc in the $BuMeSiH_2$ system where the dehydrocoupling does not occur.

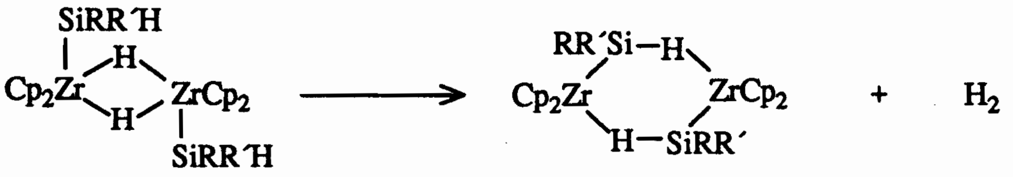

(V-30)

For the propagation process, since the zirconocene system is very similar to the titanocene system, it is believed that the bimetallic transition state mechanism shown in Scheme V-5 probably also operates in the zirconocene system. Although such a mechanism is proposed based mainly on experimental observations on the titanium system, it can also explain almost all experimental observations on the zirconium system.

Although the bimetallic transition state mechanism is currently preferred, it is still believed that these systems are too poorly understood to prematurely discard several other plausible mechanisms. Among these are the intermediacy of silylene complexes (89), σ-bond metathesis proposed by Woo and Tilley (92), and σ-bond metathesis between two silyl complexes as shown in reaction V-31 (209). These mechanisms, especially the σ-bond

$$ZrSiRR'H + ZrSiRR'H \longrightarrow ZrH + ZrSiRR'SiRR'H \qquad (V\text{-}31)$$

metathesis mechanism proposed by Woo and Tilley, can also explain most of our observations if it is assumed that $Cp_2MH(SiRR'H)$ (where M = Ti, Zr) is the key species. It is also possible that more than one mechanism is simultaneously operative in these systems.

V.3 EXPERIMENTAL

The general experimental techniques for purifying solvents, synthesis of reactants and catalysts, and carrying out reactions are the same as described in previous chapters. EPR measurements were carried out by Dr. Edmond Samuel of Laboratoire de Chimie Organométallique de l 'ENSCP, France. The data collection, refinement and resolution of the structure of VIf were carried out by Dr. Zhongsheng Jin of Laboratory 26, Changchun Institute of Applied Chemistry, Academia Sinica, PRC.

V.3.1 Reactions of primary and secondary silanes with DMT.

All of these reactions were followed by ^1H NMR. The standard conditions for these reactions are as follows: To a solution of DMT (10 mg, 0.048 mmol) in degassed benzene-d_6 (0.42 mL) containing 1 drop of cyclohexane as calibrant, the appropriate silane (0.06 mL), other than methylsilane, was added. The reaction mixture was sealed in an NMR tube, placed in the temperature controlled cavity of a 200 or 300 MHz FT-NMR spectrometer, and the concentrations of complexes V and VII with the passage of time were estimated by the integrations of their Cp resonances. In the case of methylsilane, the same amount of DMT was dissolved in 0.48 mL of benzene-d_6. The methylsilane gas was bubbled into the solution until the reaction was initiated, then the NMR tube was sealed and the reaction was followed in the same way as other reactions.

V.3.2 Synthesis of complexes VIIe and Ve.

$MeSiH_3$ was bubbled into a solution of DMT (100 mg, 0.48 mmol) in toluene (2 mL). Within a few minutes a rapid color change from orange to blue/black occurred, accompanied by rapid gas evolution. The reaction solution was left under the atmosphere of $MeSiH_3$ for 24 hours to complete the conversion of **Ve** to **VIIe**. The supernatant liquid was then decanted and the crystals were washed three times with 2 mL portions of cold toluene and dried under vacuum to give **VIIe** (34 mg, 63%). ^1H NMR study indicated that the sample is quite pure, but satisfied analyses were not obtained. Anal. Calcd for $C_{22}H_{30}Si_2Ti_2$: C, 59.19; H, 6.77; Si, 12.58; Ti, 21.46. found: C, 55.57; H, 6.25; Si, 9.94; Ti, 21.87. ^1H NMR (in toluene-d_8): *cis*-isomer: Cp, 4.594 and 4.492 ppm; Si-H (terminal), 4.777 ppm (m), $^2J_{H,H}$ = 4.48 Hz; $^3J_{H,H}$ = 4.50 Hz; CH_3, 0.765 ppm (dd), $^3J_{H,\mu\text{-}H}$ = 1.85 Hz; Si-H-Ti, -10.16 ppm (broad, s); *trans*-isomer: Cp, 4.586 and 4.518 ppm; Si-H (terminal), 4.866 ppm (m), $^2J_{H,H}$ = 4.48 Hz; $^3J_{H,H}$ = 4.50 Hz; CH_3, 0.739 ppm (dd), $^3J_{H,\mu\text{-}H}$ = 1.85 Hz; Si-H-Ti, -10.16 ppm (broad, s). The spectral parameters for Si-H (terminal) and CH_3 resonances are cited for the spectra observed while decoupling at 0.765, 0.739 and -10.16 ppm respectively.

Despite a number of attempts, pure **Ve** was not isolated due to its facile conversion to **VIIe**. **Ve** was therefore obtained as a mixture with **VIIe**. In a typical experiment, $MeSiH_3$ was bubbled into a solution of DMT (200 mg, 0.96 mmol) in toluene (2 mL). After the color change from orange to blue, a black powder was precipitated very soon. the supernatant liquid was decanted immediately and the residual precipitate was dried under vacuum. The ratio of **Ve** to **VIIe** in the mixture varies as a function of reaction time.

V.3.3 Synthesis of complex Vf.

DMT (150 mg, 0.72 mmol) was dissolved in pure *n*-$BuMeSiH_2$ (1mL, 6.7 mmol) in a Schlenk tube. The solution changed color rapidly from orange to ink-blue, accompanied by rapid gas evolution. After about 30 minutes, the supernatant liquid was decanted and the residual precipitate was washed three times with 2 mL portions of cold hexanes and vacuum dried to give a black powder (102 mg, 62%). ^{1}H NMR study indicated that <u>Vf</u> is the only observable compound in the product. However, satisfactory analysis was not obtained. Anal. Calcd for $C_{25}H_{34}SiTi_2$: C, 65.50; H, 7.48; Si, 6.13; Ti, 20.90. Found: C, 62.70; H, 7.01; Si, 5.31; Ti, 20.64.

<u>Vf</u> can only be isolated from the reaction of DMT with neat $BuMeSiH_2$ due to its lower solubility in this system than in common organic solvents, such as toluene, benzene, hexane, pentane, diethyl ether, THF etc. In these organic solvents, it was found that <u>Vf</u> is too soluble to be isolated.

V.3.4 Reactions of primary and secondary silanes with DMZ.

The standard conditions for the stoichiometric reactions of DMZ with different silanes were as follows: DMZ (10 mg, 0.04 mmol) was dissolved in a mixture of degassed benzene-d_6 (0.5 mL) and the appropriate silane (0.12 mmol). The reaction mixture was sealed in an NMR tube and the reaction was followed by ^{1}H NMR on a 200 or 300 MHz FT-NMR spectrometer. For the $BuMeSiH_2$ reaction, the reaction mixture was heated to 70°C to achieve a reasonable reaction rate. In the case of methylsilane, the reaction was carried out at 50°C in a Schlenk tube under an atmosphere of $MeSiH_3$ and the reaction progress was monitored periodically by NMR.

V.3.5 Synthesis of complexes <u>VIf</u> and <u>XIVd</u>.

These two compounds were prepared by the same method. DMZ (200 mg, 0.80 mmol) was dissolved in degassed *n*-hexane (4.0 mL) containing the appropriate silane (2.4 mmol). The solution slowly changed color from colorless to orange with a slow gas evolution and the formation of orange crystals over a period of several hours. The supernatant liquid was decanted and the crystals were washed several times with *n*-hexane and dried under vacuum. <u>VIf</u> was obtained as well formed crystals 155 mg, 58%). Anal.

Calcd for $C_{35}H_{42}Si_2Zr_2$: C, 59.94; H, 6.04; Si, 8.01; Zr, 26.01. Found: C, 58.53; H, 6.02; Si, 5.77; Zr, 26.94. **XIVd** was also obtained as crystals (119 mg, 21%), but the quality of the crystals is not good enough for X-ray crystal structure determination. It should be pointed out that pure **XIVd** (based on ^1H NMR spectrum) was isolated only one time. Attempts to repeat the experiment were not successful, and thus we did not obtained enough amount of **XIVd** for elemental analysis.

V.3.6 X-ray crystal structure of compound VIf.

A crystal of dimensions 0.1 x 0.2 x 0.4 mm was sealed in a thin walled capillary. Diffraction measurements were carried out on a Nicolet R3M/E diffractometer. Computations were performed using the SHELXTL system (226) adapted on an Eclipse S/140 computer. The space group $P2_1/c$ was established by systematic absences in the complete data set ($0k0$, $k = 2n + 1$ and $h0l$, $l = 2n + 1$). The intensity data were corrected for absorption and Lorentz-polarization effects. The positions of the independent zirconium and silicon atoms were deduced from the E-map. The positions of all other independent non-hydrogen atoms were determined from difference Fourier synthesis and the dimeric structure of the compound was confirmed at this point. After a refinement of the positional and thermal parameters of the non-hydrogen atoms by least squares, all of the hydrogen atoms were calculated from difference Fourier synthesis and refined with isotropic thermal parameters. The largest peak corresponded to the bridging hydrides. Finally, all non-hydrogen atoms were refined by full matrix least squares with anisotropic thermal parameters. All atoms other than silicon and zirconium were severely distorted and the electron density for C_{42} showed 1/2 occupancy at the two sites of the dimer, indicating that the crystal contains a pair of enantiomers of **VIf** and the disorder problem results from the ordered superposition of the two enantiomers. The final least squares refinement converged to $R = 0.082$ and $R_w = 0.083$.

Chapter VI

Reactions of some silanes with dimethyltitanocene in the presence of pyridine and trimethylphosphine — Synthesis and structure of some novel bis(cyclopentadienyl)titanium(III) silyl complexes

VI.1 INTRODUCTION

In earlier studies on the properties of complexes <u>**Va**</u> and <u>**VIIa**</u> (32), <u>**VIIa**</u> was found to undergo reaction with tetrahydrofuran (THF) to give a highly unstable, paramagnetic species, which on the basis of its EPR spectrum was presumed to be the monomeric THF complex $[Cp_2Ti(SiH_2Ph)(THF)]$ (<u>**XIX**</u>), as shown in equation VI-1. Because of its

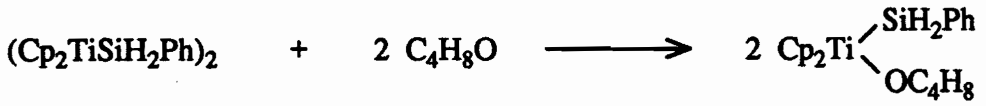

$$(Cp_2TiSiH_2Ph)_2 \quad + \quad 2\ C_4H_8O \longrightarrow 2\ Cp_2Ti\begin{matrix} \diagup SiH_2Ph \\ \diagdown OC_4H_8 \end{matrix} \qquad \text{(VI-1)}$$

<u>**VIIa**</u> <u>**XIX**</u>

instability, compound <u>**XIX**</u> was not isolated as a solid. However, the easy cleavage of <u>**VIIa**</u> by the weak donor ligand THF suggested the possibility that stable complexes might be obtained using other stronger nucleophiles. It is very interesting to study such reactions for the reasons to be mentioned below.

Firstly, further information about the mechanism of the silane dehydrocoupling reaction might be obtained from these kinds of reactions, particularly for the secondary silane reactions. As mentioned in earlier chapters, complexes <u>**V**</u> and <u>**VII**</u> could not be isolated from reactions of DMT with secondary silanes, and <u>**VII**</u> could not even be observed. It is believed that the instability of these compounds could result from weak Ti-H bonding because of the larger steric bulk of the diorganosilyl groups. If the reactions of DMT with secondary silanes are carried out in the presence of a stronger donor ligand, complexes V and VII might be trapped in the form of $Cp_2Ti(SiHRR')L$ (where L is a neutral donor ligand) and thus can be observed indirectly.

Secondly, silyl complexes of earlier transition elements have attracted considerable interest in recent years due to the relevance of such complexes as catalysts for the dehydrocoupling of organosilanes (32,33,84), hydrosilylation of olefins (86), ketones (227) and other unsaturated compounds (156,158), and as silicon analogs of carbene and carbyne complexes (228). In many catalytic reactions, it is believed that low-valent metal compounds are involved in the catalytic cycles. However, these have rarely been isolated and thoroughly identified. In the case of titanium compounds, to our knowledge, only a few silyl titanium(III) compounds have been fully identified (32).

In addition, Woo and Tilley (92,94) have recently reported that some silylzirconocene chloride complexes having only one available σ-bond are active catalysts for silane dehydrocoupling reaction. It is therefore interesting to test the catalytic activity of other monosilyl-titanocene and -zirconocene complexes which have only one σ-bond available for the silane dehydrocoupling reaction.

Based on the above considerations, a study of the reactions of dimethyltitanocene with several silanes in the presence of pyridine (Py) and trimethylphosphine (PMe_3) was undertaken. From these reactions several silyltitanocene(III) complexes, $Cp_2Ti(SiRR'H)L$ (where L = Py or PMe_3; R = Ph; R'= Ph, Me, $SiPhH_2$ or H; or R = Me; R'= H), have been isolated and identified by EPR. Some of them have been structurally characterized by X-ray crystallography.

VI.2 RESULTS AND DISCUSSION

VI.2.1 Reactions of several silanes with DMT in the presence of PMe_3.

The reactions of a variety of organosilanes with DMT in the absence of a donor ligand have been discussed in previous chapters. In all these cases, the reaction mixture turns color from orange to intense royal blue at the beginning of the reaction, and then the color may change slowly to dark-blue or dark-green depending on the property of the silane. NMR and EPR studies indicate that the initial royal blue product is **V**, which is converted to **VII** and **XI** accompanying the silane dehydrocoupling reaction. This behavior of these reactions is unaffected by the addition of triphenylphosphine, but is completely changed by the addition of trimethylphosphine. In the presence of trimethylphosphine, the reaction solution turns color slowly from orange to dark violet and a violet product can be obtained by choosing appropriate reaction conditions. In the cases of $PhSiH_3$, Ph_2SiH_2 and $PhMeSiH_2$, well-formed crystals suitable for X-ray diffraction studies have been obtained by carefully controlling the reaction conditions. In the cases of $MeSiH_3$ and PhH_2SiSiH_2Ph, products were obtained as purple microcrystalline solid. Attempts to grow single crystals suitable for X-ray crystallography were not successful. The *n*-$BuMeSiH_2$ reaction gave a very soluble product and it could not be isolated as solid material.

The products obtained from these reactions have been well identified to be compounds $Cp_2Ti(SiRR'H)PMe_3$ (**XX**) by EPR and X-ray crystallography. All of these compounds decomposed in solution, so that purification by recrystallization was prohibited. Most of the compounds are very soluble in aromatic hydrocarbon, but very insoluble in saturated hydrocarbon, so the choice of reaction solvent is critical. It was found that the best reaction medium is a saturated hydrocarbon, such as pentane or hexane, from which **XX** could be obtained in high yield (>95%). However, the quality of the crystals can be improved by the addition of a small amount of aromatic hydrocarbon. Too much aromatic hydrocarbon can lead to failure of the complex to crystallize because of excessive

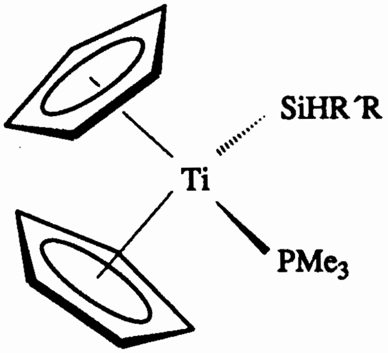

XX

XXa : R = Ph; R′= Ph
XXb : R = Ph; R′= Me
XXc : R = Ph; R′= H
XXd : R = Ph; R′= SiH$_2$Ph
XXe : R = Me; R′= H

solubility.

The reactions of secondary silanes with dimethyltitanocene resemble those of the primary silanes, in that the color change is the same and complexes V and XI are observed in all reactions. However, only for the primary silanes, have complexes VII been obtained. Further, although titanocene-based catalysts can also dehydrocouple secondary silanes, the rates are orders of magnitude slower than the reactions of primary silanes. It is therefore significant that the secondary silyltitanocene phosphine complexes XXa and XXb can be isolated, since this confirms that the path of the reactions of primary and secondary silanes is essentially the same.

The influence of the steric bulk of the phosphine ligands is evident. The phosphine complexes can be prepared with trimethyl or triethylphosphine (229) (cone angles $\theta = 118$ and 132° respectively (230)), but cannot be obtained with bulkier phosphines, such as triphenyl, triisopropyl, and tricyclohexylphosphines ($\theta = 145$, 160 and 172° respectively (230)). The silane dehydrocoupling reaction was found to be completely suppressed in the presence of trimethylphosphine at room temperature, while triphenylphosphine did not seem to have any evident effect on the normal reaction course for the production of the bimetallic complexes V and VII and for the silane dehydrocoupling. Based on these observations, it could be concluded that these silyltitanocene(III) phosphine complexes are not active catalysts for silane dehydrocoupling although they have a Ti-Si σ-bond available. It is possible that the large steric bulk of the tertiary phosphine blocks access to potential participants in a σ-bond metathesis at the Ti-Si bond.

VI.2.2 Reactions of several silanes with DMT in the presence of pyridine.

As in the case of trimethylphosphine, the reaction course of DMT with silanes is entirely altered by the addition of pyridine. However, the reactions in the presence of pyridine are slightly more complicated than those in the presence of trimethylphosphine. When $PhSiH_3$ or Ph_2SiH_2 was used as reactant, the reaction mixture changed color first to blue for a while, then to blue-violet slowly with gas evolution. The blue color species was isolated by cooling the reaction solution with dry ice immediately after the initial color change and confirmed to be V by NMR. During the course of the color change, violet needle-shaped crystals were precipitated. Visual inspection, EPR studies and elemental analysis indicate that the products obtained from the two reaction systems are pyridine analogues of XX, silyltitanocene(III) pyridine complexes XXI. Unfortunately, the crystals for both compounds are a little bit too small to do X-ray diffraction studies. Attempts to grow larger crystals have not been successful.

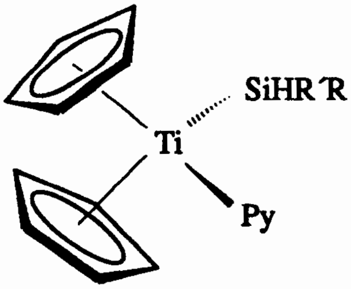

XXI

XXIa : R = Ph; R′ = H

XXIb : R = Ph; R′ = Ph

The reactions of $PhMeSiH_2$ and n-$BuMeSiH_2$ with DMT in the presence of pyridine were found to be very different from the reactions of $PhSiH_3$ and Ph_2SiH_2. Instead of the complexes of the type XXI, a pyridyl bridged titanocene dimer, bis(cyclopentadienyl)-titanium(III)(μ-H)(μ-N,C-pyridyl)bis(cyclopentadienyl)titanium(III) (XXII) was obtained from these reactions. In these cases, the color changed in the same way at the beginning of the reactions as in the cases of $PhSiH_3$ and Ph_2SiH_2. After the initial color change from orange to blue, however, the reaction mixture was slowly transformed into a dark brown solution, from which brownish black needle-shaped crystals were slowly precipitated at -20°C. The extreme instability of the brownish products, from both $PhMeSiH_2$ and n-$BuMeSiH_2$ reaction systems, precluded recrystallization and they have not yet been obtained analytically pure. Both products are paramagnetic in solution and no NMR bands due to them have been observed. The same EPR spectrum was observed for both products, which indicates that the same compound might have been obtained from both systems. However, the EPR spectrum consists of only a featureless singlet and gives no structural information. Fortunately, the crystals obtained directly from the reaction of $PhMeSiH_2$ were of sufficiently high quality for the structure to be determined by X-ray crystallography.

As in the case of trimethylphosphine, the silane dehydrocoupling reaction was also found to be suppressed in the presence of pyridine and 4-methylpyridine, while 2,6-dimethylpyridine showed little influence on the silane dehydrocoupling reaction. In the latter case, no complex of the type XXI or XXII could be obtained. On the basis of the above observations, it seems likely that the formation of XX and XXI kills the catalytic activity of the titanocene species, and the σ-bond metathesis reaction between the Ti-Si bond of XX or XXI and the Si-H bond of a silane, by which the Si-Si bond could be formed, does not occur in these systems.

The present results provide strong evidence for the existence of the equilibria shown in eqs. VI-2 and VI-3. In the absence of a donor ligand L, the equilibrium VI-2 shifts to the

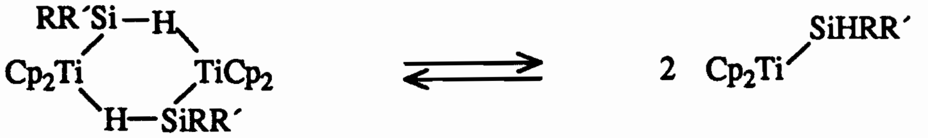

(VI-2)

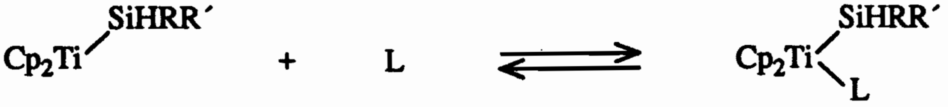

(VI-3)

left to give the bimetallic complexes VII. In the presence of an appropriate donor ligand, such as pyridine or trimethylphosphine, the equilibrium VI-3 shifts to the right to produce the monometallic silyltitanocene(III) complexes XX or XXI. The influence of steric bulk of both the silyl and the donor ligands on the equilibria is very evident. As mentioned above, XX and XXI cannot be formed and the overall equilibria shift towards the left when bulkier donor ligands are used, whereas bulkier silyl groups prevent the formation of VII. Based on our studies on the reactions of DMT with silanes in the presence and absence of a donor ligand, it is very possible that the coordinatively unsaturated species $Cp_2Ti(SiHRR')$ is produced from the dissociation of V, which has been found to be formed first in these reactions. The dissociation of V might be prompted by a donor ligand as shown in Scheme VI-1, or by Cp_2TiH_2 as shown in Scheme V-5 in the absence of any donor ligand. It was found that the addition of trimethylphosphine to a solution of Va in toluene gives rise to an immediate colour change from blue to violet, the typical colour of XX. The spontaneous dissociation of V might be slow since Vf was found to be quite stable in solution. In this special case, the dehydrocoupling reaction does not occur and thus Cp_2TiH_2 may not be produced according to the proposed mechanism shown in Scheme V-5.

The genesis of the pyridyl bridged complex XXII could take place through a number of plausible routes. One would be reaction of a molecule of hydridopyridyltitanocene(IV)

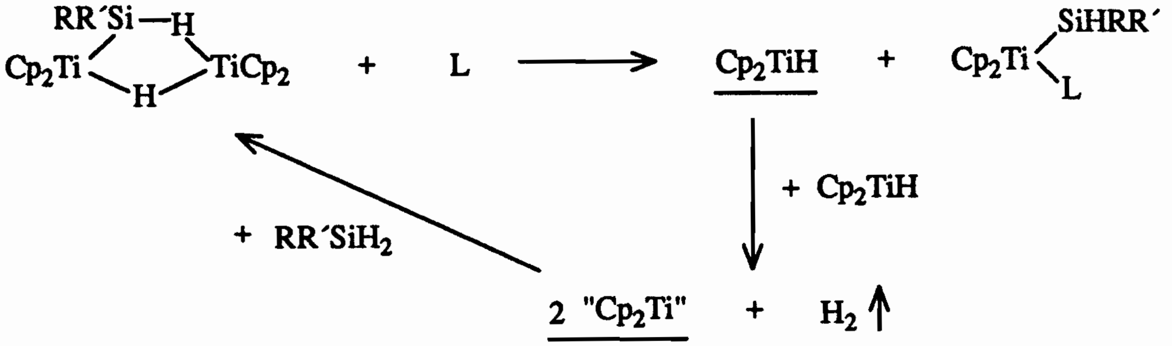

Scheme VI-1. Proposed procedure for the formation of $Cp_2Ti(SiHRRH)L$.

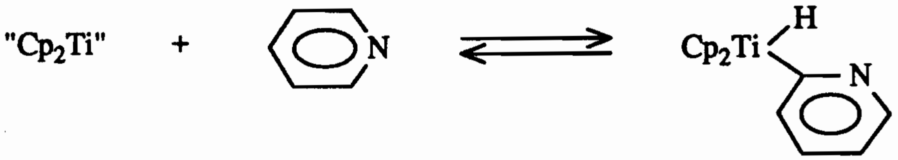

(VI-4)

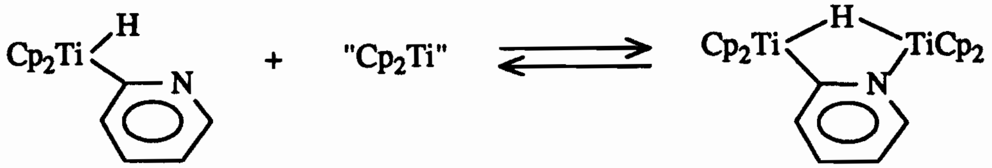

(VI-5)

with titanocene, with the hydridopyridyltitanocene(IV) being produced by a concerted oxidative addition of a pyridine C-H bond to titanocene as shown in eqs. VI-4 and VI-5. A similar process was earlier proposed to explain the formation of V. As discussed in previous chapters, titanocene must be produced as a necessary intermediate in the reactions of DMT with silanes. It is possible that the pyridine competes effectively with the phenylmethylsilane or butylmethylsilane for a key intermediate, resulting in the formation of a pyridyl, rather than a silyl product. The more reactive silanes such as phenylsilane and diphenylsilane would presumably react preferentially with the titanocene intermediate, leading ultimately to the formation of the silyltitanocene(III) pyridine complexes. An equally plausible alternative would be the prior formation of (η^2-C,N-pyridyl)titanocene(III), followed by reaction with hydridotitanocene(III) as shown in eq. VI-6. The (η^2-C,N-pyridyl)titanocene(III) may be produced from the decomposition

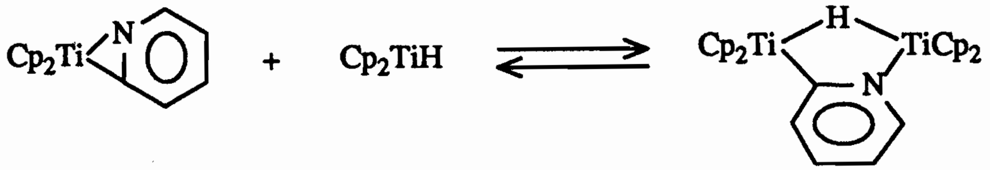

(VI-6)

of silyltitanocene(III) pyridine complexes by the intramolecular σ-bond metathesis reaction shown in eq.VI-7. A similar process was previously proposed by Klei and Teuben (231) for

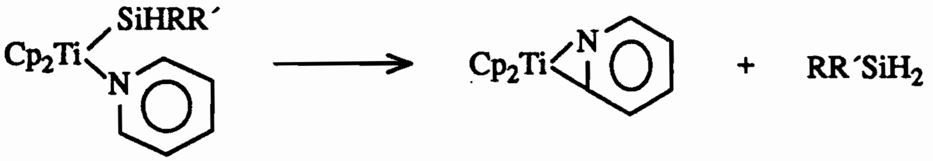

(VI-7)

the decomposition of alkyltitanocene(III) pyridine complexes. A number of other examples of ortho-metallation of pyridine by early transition metal complexes have recently been reported (232-234). The reaction mechanism seems to be similar in all these systems.

VI.2.3 Molecular structures of silyltitanocene(III) trimethylphosphine complexes <u>XXa</u>, <u>XXb</u> and <u>XXc</u>.

Compounds <u>XXa</u>, <u>XXb</u> and <u>XXc</u> were obtained directly as large, well-formed crystals and their molecular structures were determined by X-ray diffraction. To our knowledge, these are the first examples of structures of Ti(III) complexes containing a simple Ti-M σ-bond, where M is a group 14 atom. Although alkyltitanocene(III) complexes have been prepared and their chemistry extensively studied (231,235,236), no X-ray crystallographic study has been reported.

Complete tables of crystal data, collection and refinement parameters, molecular parameters, atom coordinates and isotropic thermal parameters, as well as heavy atom anisotropic thermal parameters for these compounds are given in Appendixes II, III and IV. Their molecular structures are shown in the form of ORTEP diagrams in Figures VI-1, VI-2 and VI-3, while some selected bond lengths and angles are listed in Table VI-1. The major structural parameters of these complexes are in good agreement with each other and all of their structural features conform more or less to expectations. The increase in the P-Ti-Si angle from the primary silyl complex XXc to the secondary silyl complexes XXa and XXb

Table VI-1. Selected bond lengths and bond angles for XXa, XXb and XXc[a].

Compound XXa		Compound XXb		Compound XXc	
		Bond Lengths, Å			
Ti-Si	2.652(1)	Ti-Si	2.646(2)	Ti-Si	2.650(1)
Ti-P	2.609(1)	Ti-P	2.567(2)	Ti-P	2.580(1)
Ti-Cp(1)	2.054(2)	Ti-Cp(1)	2.03(1)	Ti-Cp(1)	2.065(5)
Ti-Cp(2)	2.058(2)	Ti-Cp(2)	2.07(1)	Ti-Cp(2)	2.048(4)
Si-C(31)	1.900(2)	Si-C(19)	1.893(9)	Si-C(31)	1.907(5)
Si-C(41)	1.918(3)	Si-C(20)	1.85(2)		
		Bond Angles, deg			
P-Ti-Si	84.8(1)	P-Ti-Si	84.9(1)	P-Ti-Si	80.9(1)
P-Ti-Cp(1)	107.6(2)	P-Ti-Cp(1)	108.5(5)	P-Ti-Cp(1)	107.1(2)
P-Ti-Cp(2)	106.5(1)	P-Ti-Cp(2)	104.5(4)	P-Ti-Cp(2)	106.9(2)
Si-Ti-Cp(1)	107.7(1)	Si-Ti-Cp(1)	107.4(5)	Si-Ti-Cp(1)	106.2(2)
Si-Ti-Cp(2)	103.3(1)	Si-Ti-Cp(2)	104.1(4)	Si-Ti-Cp(2)	107.0(1)
Ti-P-C(1)	118.6(1)	Ti-P-C(11)	117.0(5)	Ti-P-C(1)	119.0(2)
Ti-P-C(2)	119.7(1)	Ti-P-C(12)	118.5(5)	Ti-P-C(2)	117.9(2)
Ti-P-C(3)	113.5(1)	Ti-P-C(13)	114.0(3)	Ti-P-C(3)	114.3(2)
Ti-Si-C(41)	116.8(1)	Ti-Si-C(19)	111.6(2)	Ti-Si-C(31)	115.5(1)
Ti-Si-C(31)	121.3(1)	Ti-Si-C(20)	121.4(5)	Cp(1)-Ti-Cp(2)	135.4(2)
Cp(1)-Ti-Cp(2)	135.4(1)	Cp(1)-Ti-Cp(2)	135.8(7)		

[a] Cp(n) denotes the centroid of a cyclopentadienyl ring.

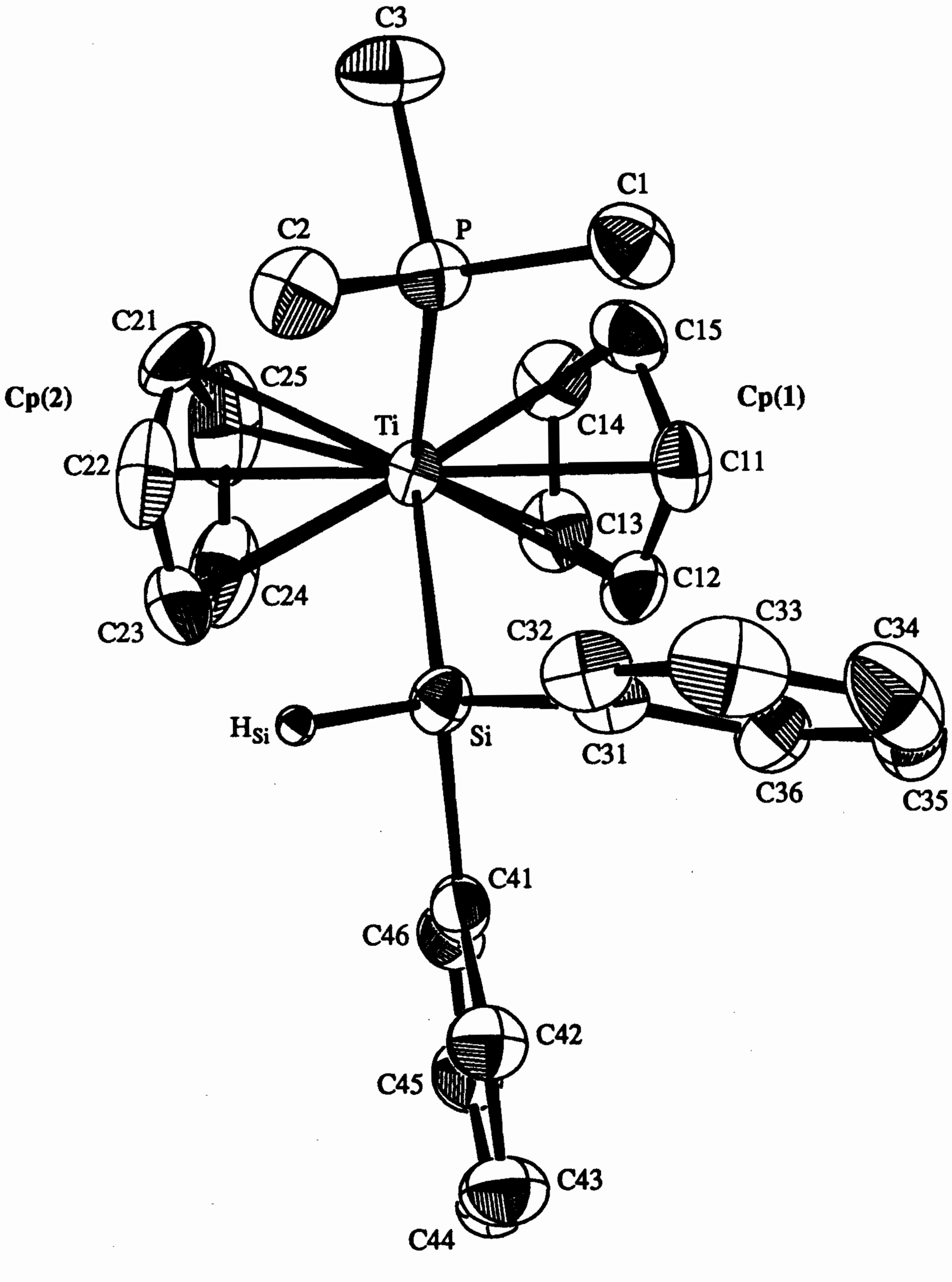

Figure VI-1. ORTEP of $Cp_2Ti(SiHPh_2)PMe_3$, XXa.

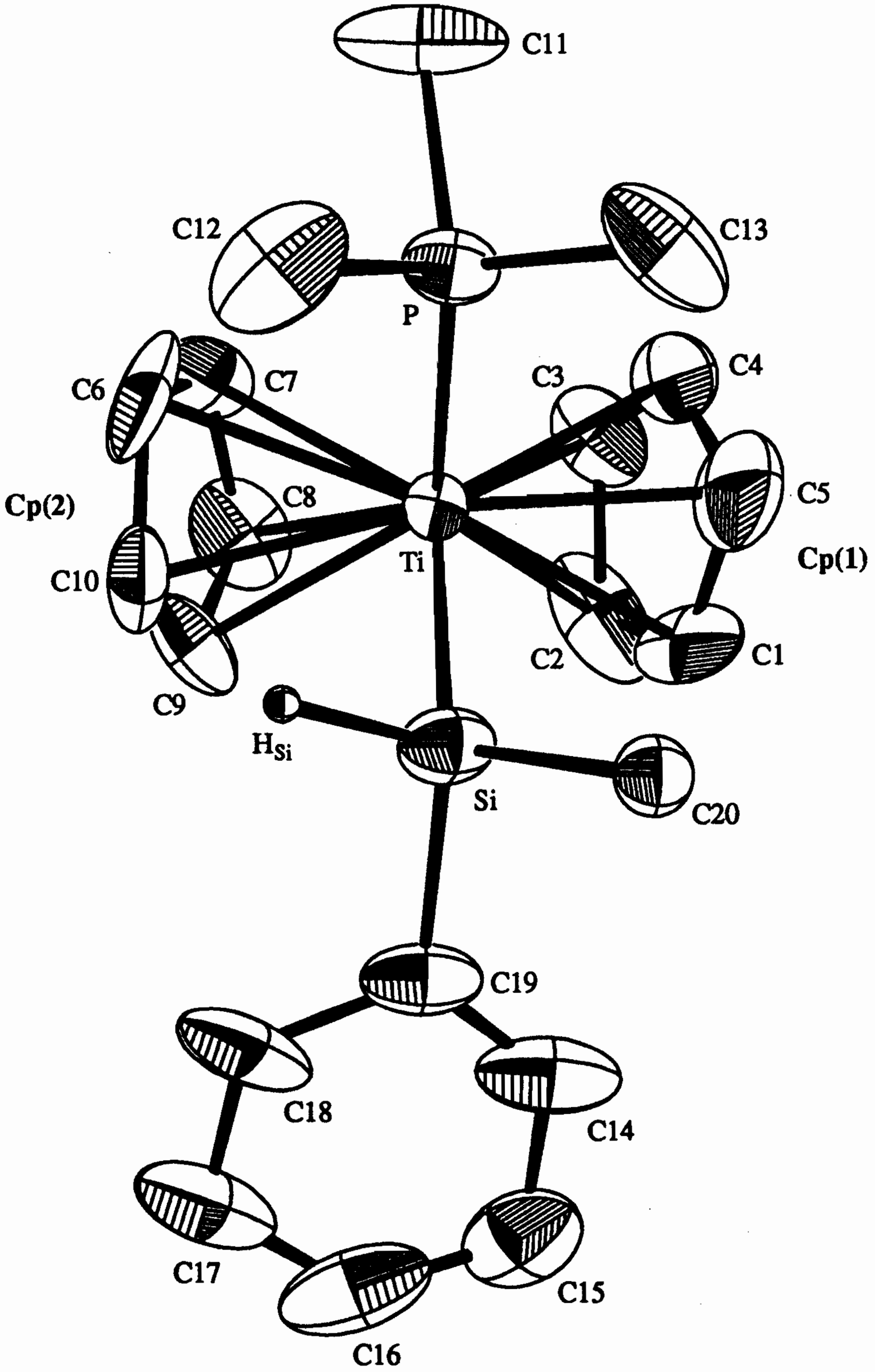

Figure VI-2. ORTEP of $Cp_2Ti(SiHMePh)PMe_3$, XXb.

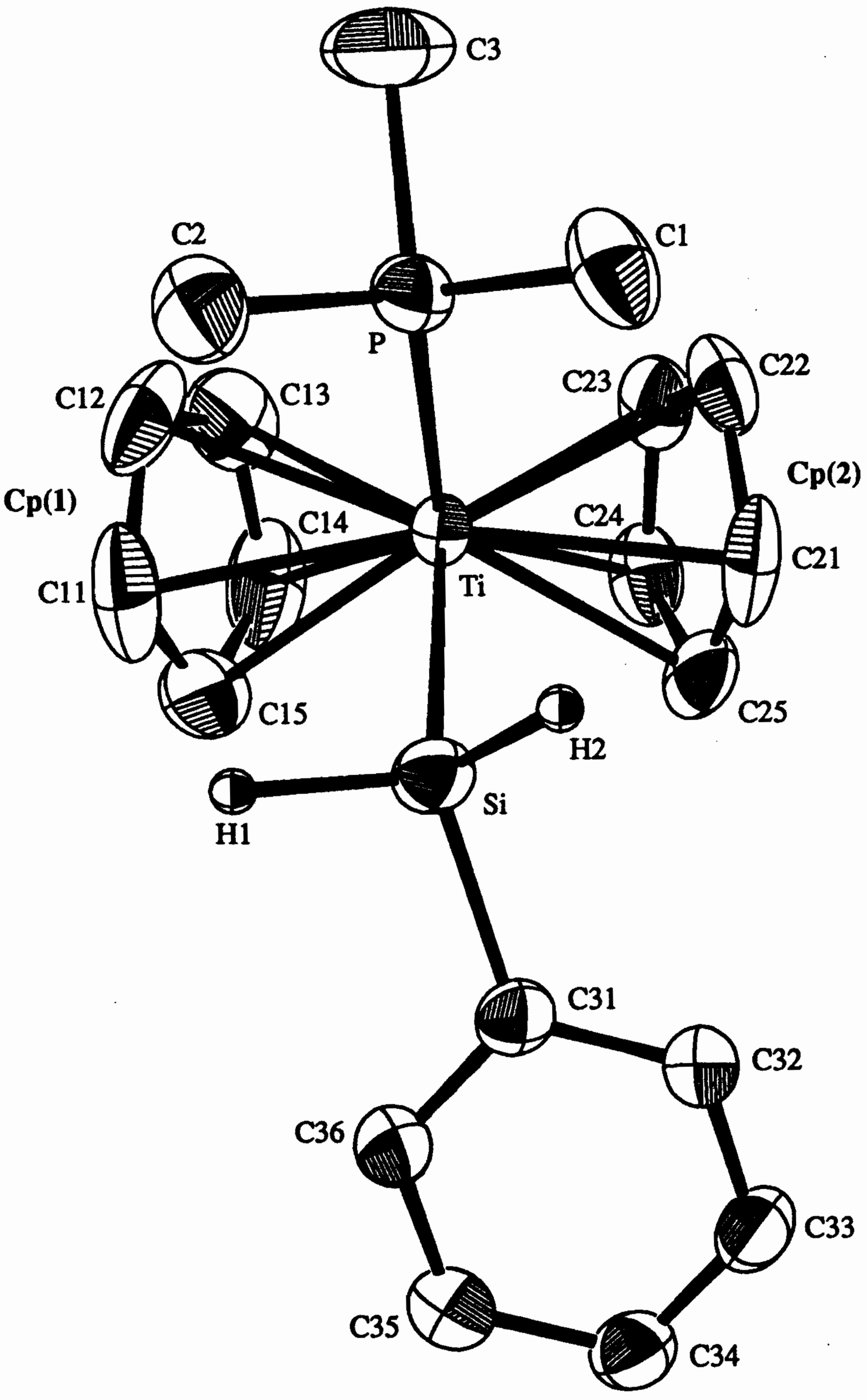

Figure VI-3. ORTEP of $Cp_2Ti(SiH_2Ph)PMe_3$, XXc.

could result from increased steric repulsion in the secondary silyl compounds.

The observed small P-Ti-Si angle in these complexes is consistent with the values reported for other titanocene(III) complexes (237,238). For the purpose of comparison, the essential structural parameters of a number of Cp_2TiL_2-type complexes possessing phosphine or silyl ligands are listed in Table VI-2. In the d^0 complex $Cp_2Ti(SiMe_3)Cl$, the L-Ti-L angle (87(1)°) is larger than that in the d^1 complexes (80.4-84.9°). This is in accord with Hoffmann's prediction that as the number of d electrons increases, the L-Ti-L angle decreases (108). However, the L-Ti-L angles of the d^2 complexes (88.2-92.9°) are actually larger than those of the d^1 complexes.

Table VI-2. Selected bond lengths and bond angles of a number of titanocene complexes containing silyl or phosphine ligands.

Compounds	Ti-P	Ti-Si	Ti-Cp[a]	Cp-Ti-Cp	L-Ti-L[b]	Ref.
$Cp_2Ti(PMe_3)(CO)$	2.544(1)		2.04 2.04	136.9	88.2(1)	237
$Cp_2Ti(PMe_3)_2$	2.524(4) 2.527(3)		2.05 2.06	133.2 134.3	91.5(2) 92.9(1)	239
$Cp_2TiCl(PMe_3)$	2.599(2)		2.07 2.06	132.3	80.4(1)	237
$Cp_2TiCl(PMe_2SiMe_3)$	2.639(1)		2.07 2.07	132.1	81.2(1)	238
$Cp_2TiCl(SiMe_3)$		2.67(1)		132	87(1)	152

[a] Cp denotes the centroid of the cyclopentadienyl ring; [b] L = ligand other than Cp.

The observed values for Ti(III)-P distances in this work correspond closely to the values of other titanocene phosphine complexes in various oxidation states (237-239). The Ti-Si bond lengths in these silylphosphine complexes (2.646-2.652 Å) are close to that in $Cp_2Ti(SiMe_3)Cl$. It is interesting to note that the Ti-Si distances in these monomeric complexes are slightly longer than those observed in bimetallic complexes Va (2.61(2) Å) and VIIa (2.604(2) and 2.583(2) Å) (32). As discussed in previous chapters, the Ti-Si bond in the bimetallic complexes might possess more or less metal-silylene bond character.

The Cp(1)-Ti-Cp(2) angles (135.4-135.8°) observed in these silylphosphine complexes are very close to each other although the Cp-Ti(III) distances (2.048-2.065 Å) are affected obviously by the silyl groups due to steric reason. It is undoubted that the Cp-Ti-Cp angle and Cp-Ti distance of titanocene derivatives are related to the oxidation state of titanium and the nature of the ligands L. Hoffmann et al. (108) have predicted that an increase in the π-accepter character of L will reduce the electron density on the titanium, and should be accompanied by a decrease in the Cp-Ti-Cp angle. The data observed for titanocene(III) compounds seem to be consistent with this prediction. The Cp-Ti-Cp angle for titanocene(III) chloride (237,238) and for complexes Va and VIIa (32) are smaller than those for complexes XXa, XXb and XXc. In all of the former cases the titanium is expected to be less electron rich than it is in latter complexes (in the case of the chloride because of the high electron withdrawing effect of the chlorine; in the case of the bridged silyl complexes because of the three-center, two-electron bridges).

In XXa one of the phenyl groups occupies more or less the same position as the phenyl groups in XXb and XXc. Probably because of a crystal packing effect or steric constraint, however, the plane of the phenyl group in former case is parallel to those of the Cp groups whereas it is vertical in latter cases. The second phenyl group in XXa, although much closer to the phosphine ligand, avoids contact by twisting out of the P-Ti-Si plane. However, the unusually large Ti-Si-C(31) angle (121.3°) suggests that some tilting of the diphenylsilyl moiety away from the phosphine and Cp(1) groups is also necessary to avoid excessive steric interaction. The same is true for compound XXb. In addition, the Si atom in the phenylmethylsilyl group of XXb is a chiral center and thus there are two stereoisomers for XXb. The two isomers cocrystallize in the ratio of 0.71 : 0.29, which results in the disorder of the methyl group and the hydrogen at the Si atom.

VI.2.4 The molecular structure of complex XXII.

The pyridyl-bridged titanocene(III) complex XXII was also characterized by X-ray crystallography. An ORTEP drawing of this molecule is shown in Fig. VI-4, and some selected bond distances and angles are given in Table VI-3. Complete tables of crystal data, collection and refinement parameters, molecular parameters, atom coordinates and isotropic thermal parameters, as well as heavy atom anisotropic thermal parameters for XXII are given in Appendix V. Compound XXII cocrystallizes with pyridine and the crystal contains half a molecule of disordered pyridine per molecule of XXII. A crystallographic packing diagram is shown in Fig. VI-5.

Although the formation of XXII in these systems is quite surprising, the geometry of XXII, with the hydride and pyridyl group in the equatorial plane of the two titanocene

Table VI-3. Selected bond distances and bond angles for complex XXII [a].

Bond Lengths, Å			
Ti(1)-Ti(2)	3.597(1)	Ti(2)-N	2.212(4)
Ti(1)-C(11)	2.230(6)	Ti(1)-H_{Ti}	1.941(16)
Ti(2)-H_{Ti}	1.981(23)	Ti(1)-Cp(1)	2.090(6)
Ti(1)-Cp(2)	2.086(6)	Ti(2)-Cp(3)	2.090(6)
Ti(2)-Cp(4)	2.090(6)		
Bond Angles, deg			
H_{Ti}-Ti(1)-C(11)	83.1(9)	H_{Ti}-Ti(2)-N	83.3(8)
Ti(1)-H_{Ti}-Ti(2)	133.0(16)	Ti(1)-C(11)-N	120.4(3)
Ti(2)-N-C(11)	120.0(4)	Cp(1)-T(1)-Cp(2)	131.8(2)
Cp(3)-Ti(2)-Cp(4)	132.7(2)	H_{Ti}-Ti(1)-Cp(1)	108.6(9)
H_{Ti}-Ti(1)-Cp(2)	107.0(10)	H_{Ti}-Ti(2)-Cp(3)	107.5(9)
H_{Ti}-Ti(2)-Cp(4)	107.9(9)	C(11)-Ti(1)-Cp(1)	108.0(2)
C(11)-Ti(1)-Cp(2)	107.5(2)	N-Ti(2)-Cp(3)	107.4(2)
N-Ti(2)-Cp(4)	106.9(2)		

[a] Cp(n) denotes the centroid of a cyclopentadienyl ring.

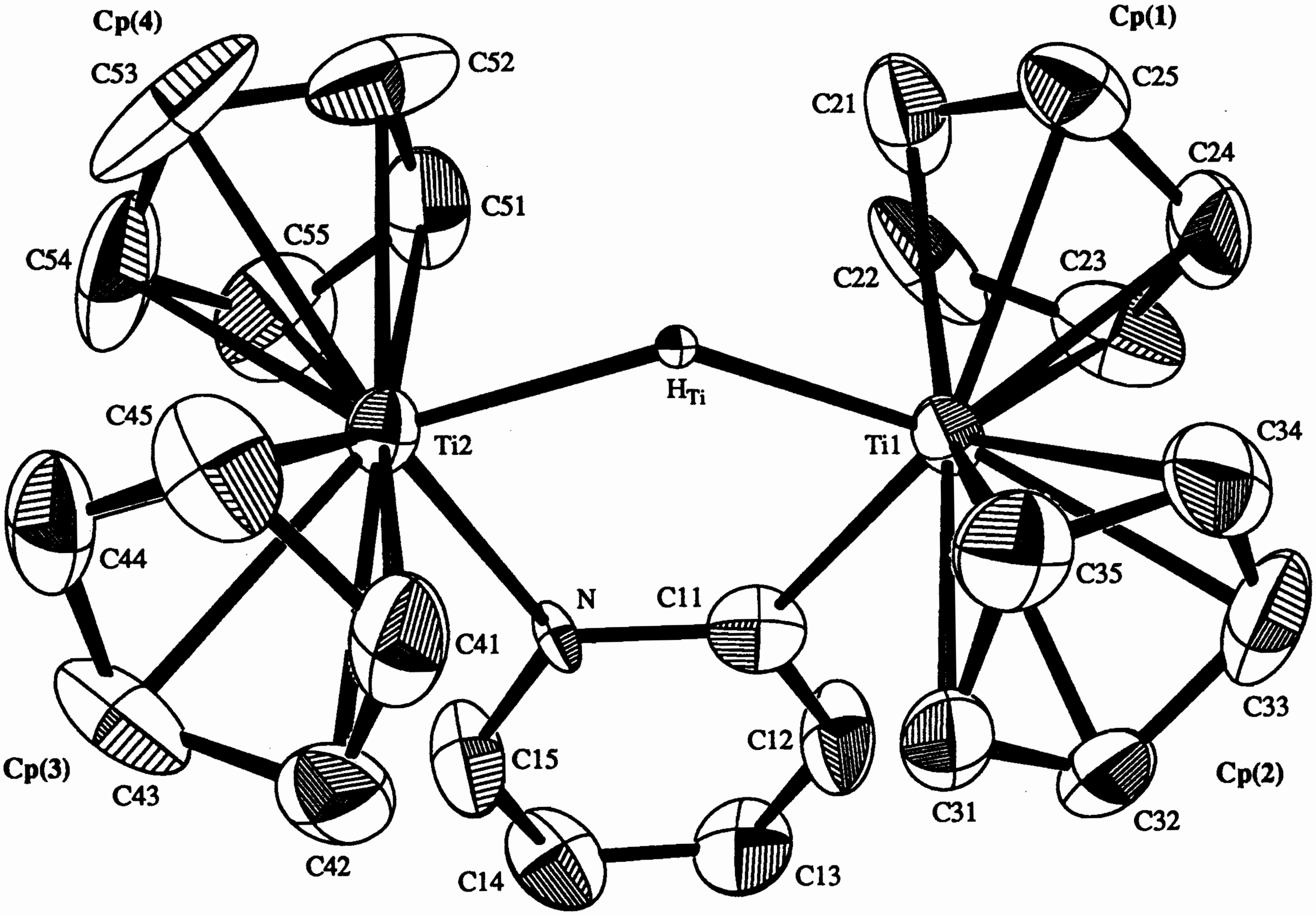

Figure VI-4. ORTEP of $Cp_2Ti(\mu\text{-}H)(\mu\text{-}N,C\text{-}Py)TiCp_2$, XXII.

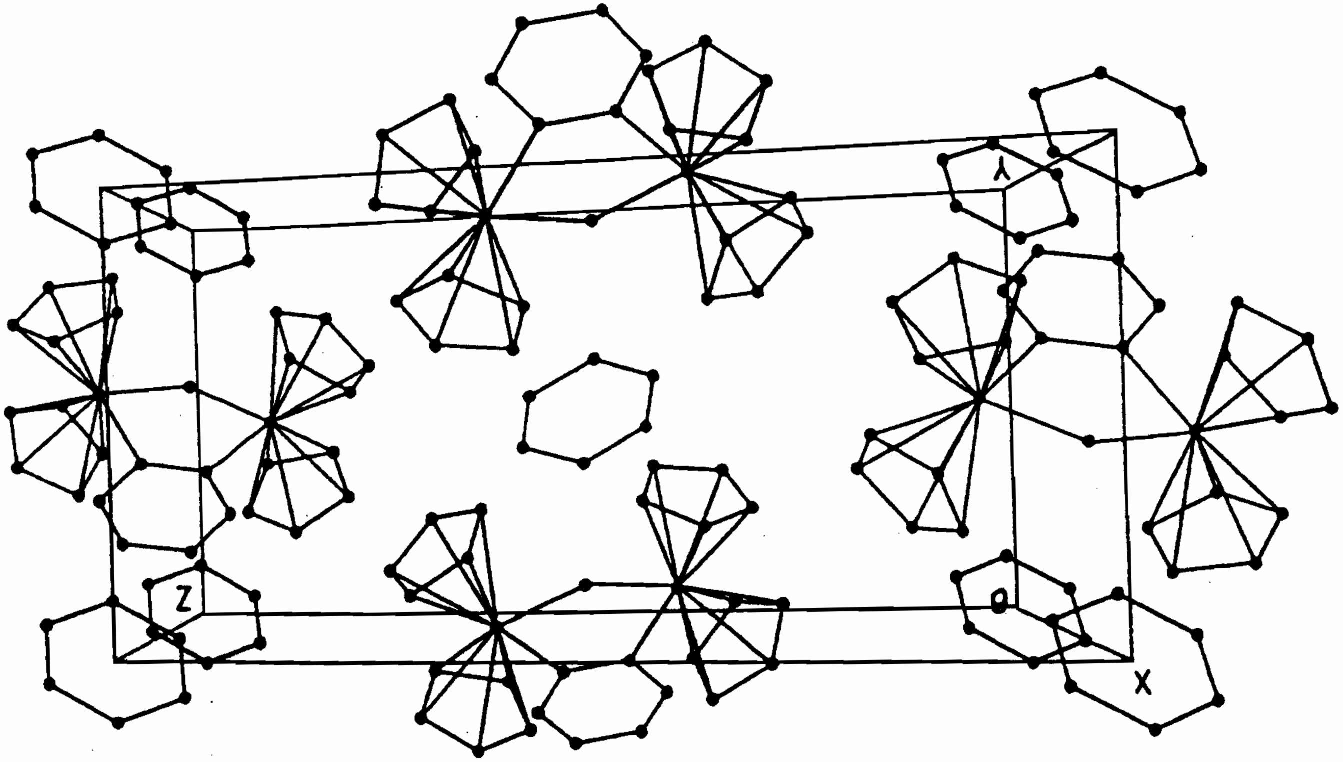

Figure VI-5. A packing diagram of <u>XXII</u>, showing the pyridine of crystallization.

fragments, does not seem to be unusual. From a structural point of view, complex **XXII** might be considered to be similar to the five-membered ring silyltitanocene complexes **V**. As in **V**, there is a bridged hydride between the two Ti atoms in **XXII** and the oxidation state of both Ti atoms is formally Ti(III). The Ti-H bond distances in **XXII** (1.94 and 1.98 Å) are comparable to that in **Va** (1.97 Å). The Cp-Ti distances (2.09 Å) and Cp-Ti-Cp angles (131.8 and 132.7°) in **XXII** are slightly larger than the corresponding values (2.05 to 2.06 Å; 130.6 and 131.1°) in **Va** (32), probably because the titanium in **XXII** is more electron rich than it is in **Va**. The Ti-C(11) distance (2.230 Å) is slightly longer than the distances (2.18 to 2.19 Å) found for sp^2-C ligands bound to titanocene (240,241). The Ti-N distance (2.212 Å) is close to the Ti-N distance in dimeric titanocene(III) pyrazole complex (2.206 Å) (242) and slightly longer than that in bipyridyltitanocene (2.14 Å) (243). The Ti-C distance is longer than the Ti-N distance, which is expected and consistent with those reported for $Cp^*_2Sc(\eta^2\text{-N,C-NC}_5H_4)$ (233) and $Cp_2Zr(\eta^2\text{-N,C-picolyl})(PMe_3)^+$ (234).

VI.2.5 EPR studies on some titanocene(III) complexes.

All of the complexes described in this chapter are paramagnetic, and thus it is not possible for these complexes to be characterized by NMR spectroscopy. Although some of them have been characterized by single crystal X-ray diffraction techniques, most complexes cannot be obtained as good single crystals suitable for x-ray crystallography. Fortunately, most of these paramagnetic complexes give well-resolved isotropic EPR spectra in solution, which provides a powerful means for these compounds to be identified.

VI.2.5.1 EPR spectra of some silyltitanocene trimethylphosphine complexes.

All of the studied silytitanocene(III) trimethylphosphine complexes give well-resolved isotropic EPR spectra in toluene solution. The spectra exhibit hyperfine interaction of the unpaired electron with phosphorus (I = $^1/_2$; 100%) and with the α-hydrogens (I = $^1/_2$; 99.9%) of the silyl ligand, as well as with ^{47}Ti (I = $^5/_2$; 7.3%) and ^{49}Ti (I = $^7/_2$; 5.5%) isotopes. Therefore, the spectra are diagnostic of the presence of a primary silyl (triplet) or secondary silyl (doublet) group. The EPR spectra of XXa to XXe are shown in Figures VI-6 and VI-7, and the coupling constants and *g* values for these complexes are listed in Table VI-4. All of these spectra were obtained at -20°C. The assignment of the coupling of the unpaired electron to the silyl hydrogen was also confirmed by reaction with $PhSiD_3$, which yielded the expected spectrum consisting only of a doublet, due to loss of resolution of the superhyperfine interaction with the deuterium nuclei.

Table VI-4. EPR parameters for some silyltitanocene phosphine complexes.[a,b]

Compound	*A*(P)	*A*(H)	*A*(Ti)	*g*(iso)
$Cp_2Ti(PMe_3)SiHPh_2$	29.9	2.6	8.3	1.9976
$Cp_2Ti(PMe_3)SiHMePh$	29.0	2.9	8.4	1.9966
$Cp_2Ti(PMe_3)SiH_2Ph$	29.3	3.2	8.7	1.9944
$Cp_2Ti(PMe_3)SiHPhSiH_2Ph$	28.8	3.2	7.6	1.9959
$Cp_2Ti(PMe_3)SiH_2Me$	30.7	3.2	8.2	1.9951

[a] All EPR measurements were made at -20°C.
[b] Hyperfine coupling constants in Gauss (1 G = 0.1 mT).

When trimethylphosphine was added to a solution of VIIa in toluene, the color changed from blue to violet and the same EPR spectrum was obtained as with XXc. This result indicates that the silyltitanocene(III) phosphine complexes can be formed directly from the reactions of complexes VII with phosphines, even when they could not be isolated from such reaction systems.

EPR studies revealed that these silyltitanocene(III) phosphine complexes decompose in solution at room temperature. As mentioned above, the superhyperfine interaction with

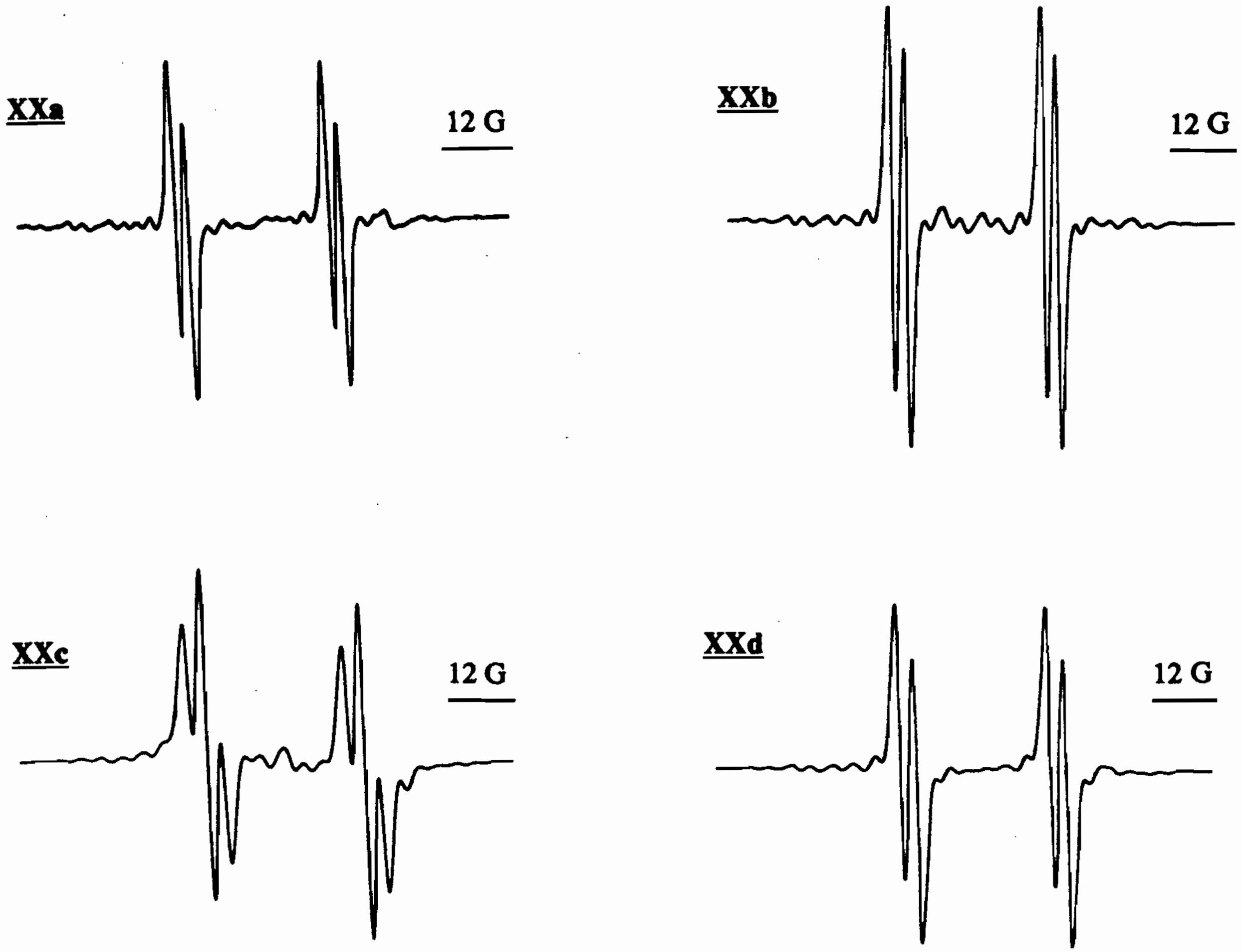

Figure VI-6. EPR spectra of XXa to XXd in toluene at 250 K.

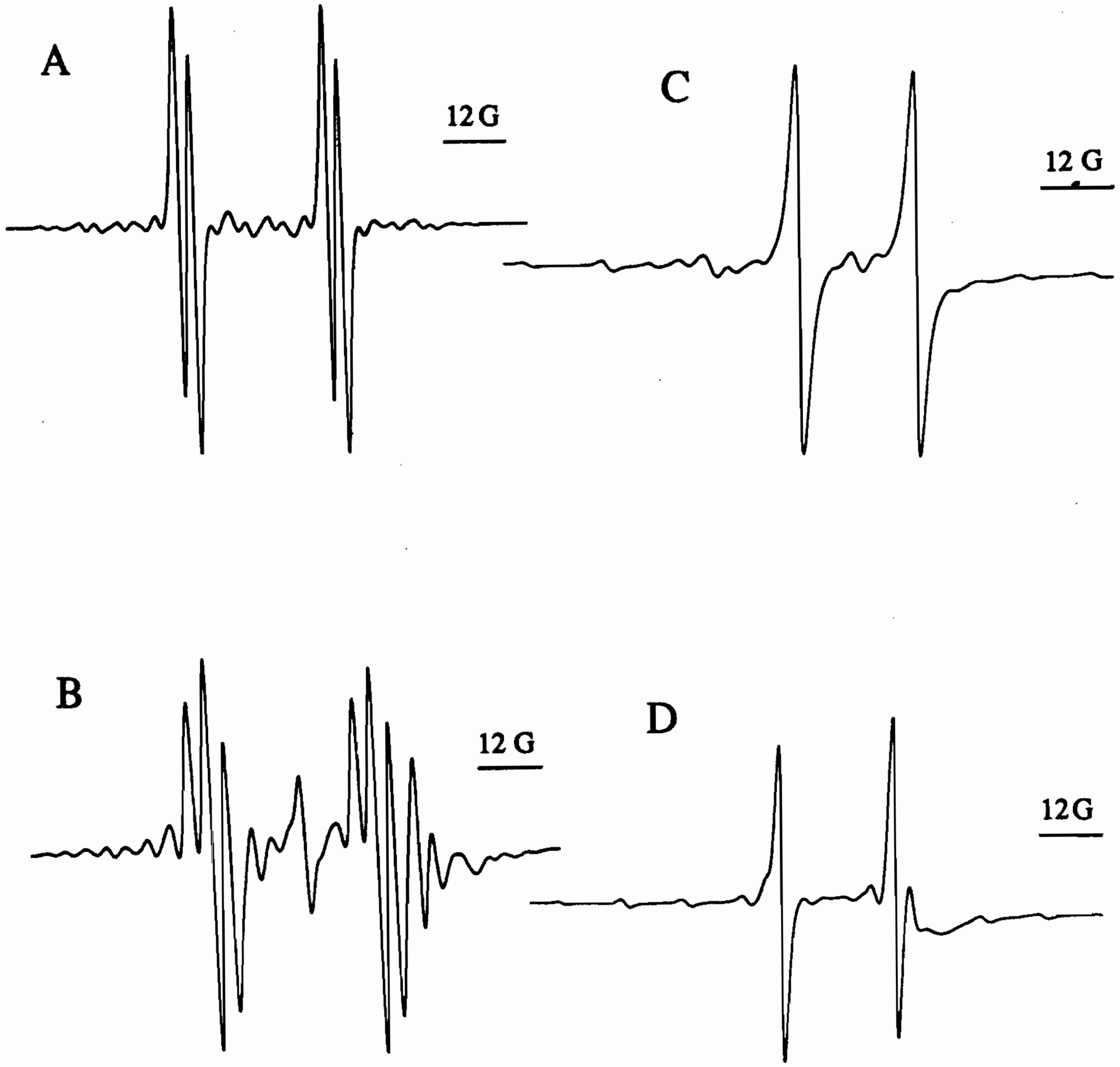

Figure VI-7. EPR spectra of <u>XXb</u> (Top) and <u>XXe</u> (Bottom) in toluene at 250 K (A and B) and room temperature (C and D).

the silyl proton was observed clearly at -20°C for the silylphosphine complexes. However, after the sample solutions were warmed to room temperature and left for a few hours, the superhyperfine coupling with the silyl proton was lost. Meanwhile, the hyperfine coupling constant with phosphorus was considerably reduced whereas the hyperfine coupling constant with titanium was increased, which indicates that the unpaired electron is less located on P, and more located on Ti for the decomposed complexes. As example the EPR spectra of **XXb** and **XXe** in toluene at -20°C and room temperature are shown in Figure VI-7. For all of the studied silyltitanocene(III) trimethylphosphine complexes, the same EPR spectrum (g_{iso}= 1.989, A(P) = 18.2 G, A(Ti) = 12 G) was observed at room temperature. From the above observations, it is obvious that the decomposition product of these silylphosphine complexes is a titanocene(III) phosphine complex, the most likely candidate being $Cp_2\overline{TiCH_2P}Me_2$. However, it is difficult to make a definite assignment for such a paramagnetic species without isolation and characterization in the pure state. Attempts to isolate the decomposition product were not successful.

VI.2.5.2 EPR spectra of silyltitanocene pyridine complexes XXIa and XXIb.

So far, we have not isolated large enough single crystals of the silyltitanocene(III) pyridine complexes for X-ray crystal structure determination. The pyridine compounds could not be well characterized by elemental analysis, probably because of their high instability. However, their EPR spectra give strong indications about their structure. The EPR spectra of **XXIa** and **XXIb** are shown in Fig. VI-8. For both compounds, the EPR spectrum consists of a multiplet due to hyperfine interaction of the unpaired electron with pyridine ^{14}N (99.63%; I = 1) and silyl proton nuclei, as well as with ^{47}Ti and ^{49}Ti isotopes. Because of the closeness in the values of the hyperfine coupling constants A(N) and A(H), the phenylsilyl compound **XXIa** exhibits a central quintet spectrum (g_{iso} = 1.988, A(H) = 2.3, A(N) = 2.3, A(Ti) = 10.3) and the diphenylsilyl compound **XXIb** gives a central quartet

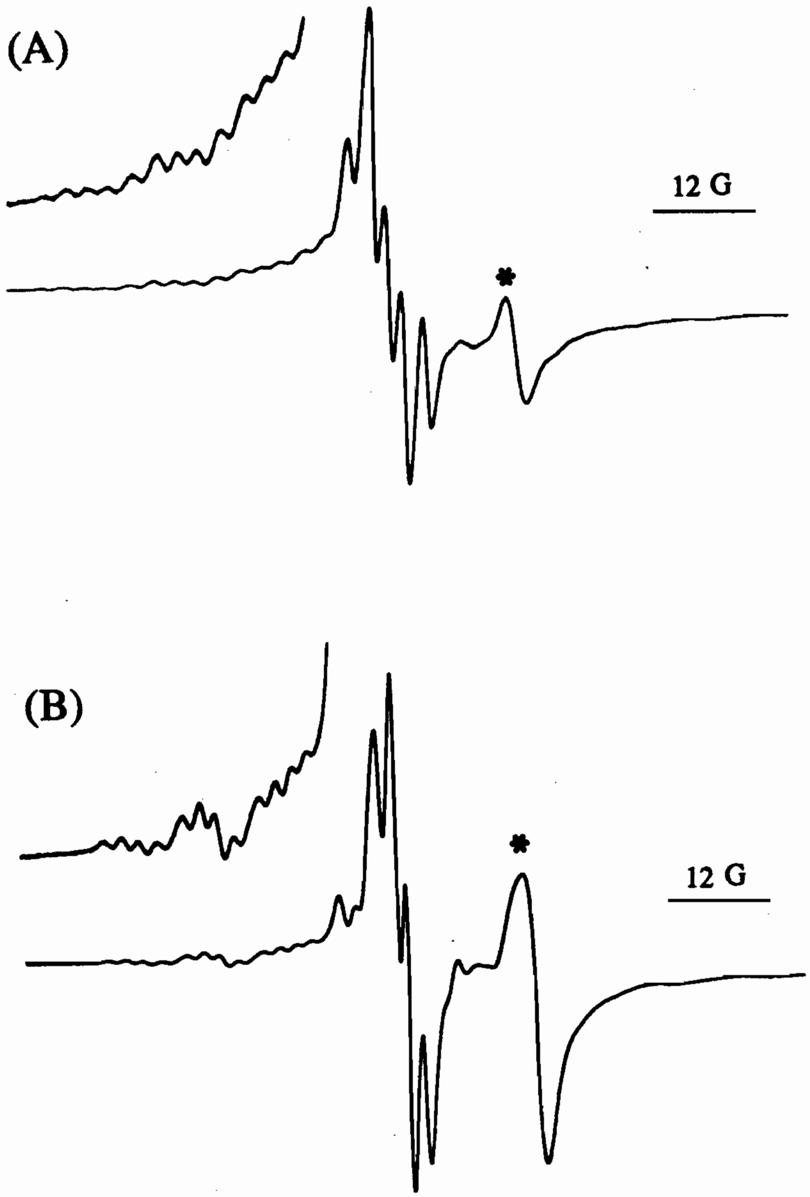

Figure VI-8. EPR spectra of (A) <u>XXIa</u> and (B) <u>XXIb</u> in toluene at 250 K. Gain, 15; modulation intensity, 0.2 G. The high field signal marked with an asterisk is due to an impurity.

spectrum. These spectra are not very well-resolved and thus it is difficult to estimate accurate values of the hyperfine coupling constants A(N) and A(H). The A(N) value for **XXIa** was measured from its deuterated analogue. The absence of resolution can be attributed to the low values of the hyperfine coupling constants and the closeness of A(N) and A(H).

The hyperfine interaction with ^{14}N has been rarely observed in paramagnetic early transition cyclopentadienyl compounds. To our knowledge, ^{14}N hyperfine splitting has been reported only in a few cases of titanocene(III) compounds with nitrogen-containing ligands (216). It was absent in most of this kind of previously studied titanocene(III) compounds (216,244).

VI.2.5.3 EPR study on the pyridyl-bridged titanocene(III) complex XXII.

Given the bimetallic structure of compound **XXII**, it would be expected that **XXII** itself could be either a diamagnetic species due to strong antiferromagnetic coupling between the two Ti(III) ions, as in the case of **VIIa** (32), or a paramagnetic species with a populated triplet state (S = 1) as reported by Stucky et al. for a series of binuclear titanocene(III) complexes (216,244). NMR and EPR studies indicate that the solution of **XXII** in a hydrocarbon solvent is paramagnetic. In contrast to complexes **V**, no NMR signals due to **XXII** were observed in solution while **V** are observable in solution by NMR although they are very similar from the structural point of view. On the other hand, a broad featureless singlet EPR signal (g_{iso}= 1.984), shown in Fig. VI-9, was observed from the solution of **XXII** in toluene, which is exactly the same as that obtained from a toluene solution of **Vf**. Such a broad featureless singlet EPR signal has also be observed previously from the solution of **Va** (32). Based on these observations, it is obvious that the broad featureless singlet EPR signal is unlikely due to complexes **XXII**, **Vf** and **Va** themselves because it is almost certainly impossible for these different compounds to give the same

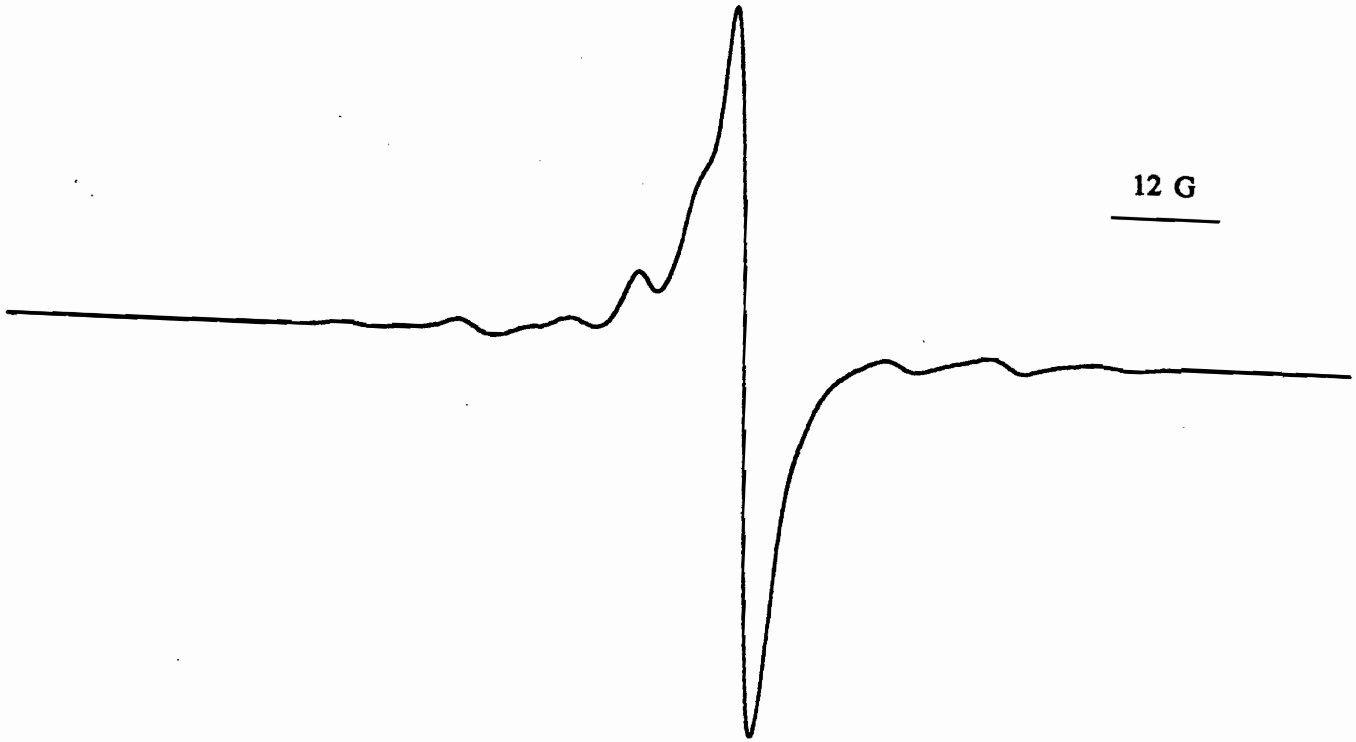

Figure VI-9. EPR spectrum of the solution of <u>**XXII**</u> in toluene at 250 K.

EPR signal. Such an EPR signal is very likely due to a common decomposition product of these complexes. The most possible candidate for such a species is some kind of solvated "titanocene". A similar broad singlet EPR signal due to solvated "titanocene" in THF (g_{iso}= 1.980) has been previously reported (245).

According to theoretical studies carried out by Hoffmann et al. (108), titanocene(II) complexes of the type Cp_2TiL_2 could be either diamagnetic singlet state species or paramagnetic triplet state species depending on the separation between $1a_1$ and b_2 orbitals (see Figs. I-2 and I-3), while the orbital separation is a function of the identity of the L ligands. Such a prediction has been proved by the fact that $Cp_2Ti(CO)_2$ (246) and $Cp_2Ti(PMe_3)_2$ (239) have been found to be diamagnetic while the bipyridyl complex $Cp_2Ti(bpy)$ is paramagnetic (243). The bipyridyl complex $Cp_2Ti(bpy)$ gives a broad singlet EPR signal at room temperature whereas a spectrum exhibiting fine structure, due to a zero-field splitting produced by the spin-spin interactions of the two unpaired electrons, is obtained in frozen toluene. Similar triplet-state features have also been observed for **Va**, **Vf** and **XXII** in frozen toluene. Based on the experimental observations and the above argument, the observed EPR signal is possibly due to a titanocene(II) species of the type $Cp_2Ti(solv)$ or $Cp_2Ti(solv)_2$. As discussed in previous chapters, although titanocene "Cp_2Ti" itself has not been isolated so far, a number of experimental results obtained in the reaction systems of DMT with silanes indicate that intact "titanocene" must exist in some form in reaction solutions.

VI.3. EXPERIMENTAL

All manipulations were performed under argon. The general experimental techniques for purifying solvents, synthesis of reactants, and carrying out reactions are the same as described in previous chapters. All of the compounds described in this chapter decomposed when put in solution, so that purification by recrystallization was prohibited. Analyses had to be performed on crystals obtained directly from the reaction. In fact, even purified transition-metal organosilicon compounds often give unsatisfactory analyses (247-249).

VI.3.1 Preparations of silyltitanocene phosphine complexes XXa to XXe.

Dimethyltitanocene (50 mg, 0.24 mmol) was dissolved in a 1:4 (v/v) mixture of toluene and *n*-hexane (total 5 mL) containing trimethylphosphine (0.34 mmol) and diphenylsilane (0.13 mL, 0.72 mmol). During a period of several hours, the solution slowly changed color from orange to dark violet with a slow gas evolution and the formation of violet crystals of $Cp_2Ti(SiHPh_2)(PMe_3)$ (XXa). The supernatant liquid was decanted and the crystals were washed several times with hexane (yield: 98 mg, 93%). Anal. Calcd for $C_{25}H_{30}PSiTi$: C, 68.49; H, 6.85. Found: C, 67.55; H, 6.57.

Compounds XXb to XXd were prepared under conditions identical with those described for XXa, using the appropriate silane (0.72 mmol) instead of diphenylsilane. XXb (yield: 79 mg, 88%) and XXc (yield: 78 mg, 90%) were obtained as good crystals suitable for X-ray crystallography while XXd (yield: 89 mg, 79%) was obtained as microcrystalline solid. The results of elemental analysis for XXb and XXc are as follows: XXb: Calcd for $C_{20}H_{28}PSiTi$: C, 63.83; H, 7.45. Found: C, 62.58; H, 7.91. XXc: Calcd for $C_{19}H_{26}PSiTi$: C, 63.15; H, 7.25. Found: C, 62.42; H, 6.78. A modified method was used to prepare the methylsilyl complex $Cp_2Ti(SiH_2Me)(PMe_3)$ (XXe) by carrying out the reaction in a thick-walled Schlenk tube under methylsilane atmosphere (30 psi). XXe was obtained as microcrystalline purple solid (yield: 47 mg, 65%). Pure samples for **XXd** and **XXe** were not obtained despite several attempts.

VI.3.2 Preparations of silyltitanocene pyridine complexes XXIa and XXIb.

The pyridine complexes **XXIa** and **XXIb** were prepared in a similar way to that used for the preparations of trimethylphosphine complexes. Typically, Dimethyltitanocene (50 mg, 0.24 mmol) was dissolved in a 1:4 (v/v) mixture of toluene and *n*-hexane (total 5 mL) containing pyridine (0.10 mL, 1.2 mmol) and phenylsilane (0.09 mL, 0.72 mmol). During a period of about one hour, the solution slowly changed color from orange to dark violet, accompanied by a slow gas evolution and the formation of violet needle-shaped crystals of $Cp_2Ti(SiH_2Ph)Py$ (**XXIa**). The crystals were separated from the reaction solution and washed several times with hexane (yield: 76 mg, 87%). Anal. Calcd for $C_{21}H_{22}NSiTi$: C, 69.22; H, 6.09; N, 3.84; Si, 7.71; Ti, 13.15. Found: C, 68.17; H, 6.09; N, 3.22; Si, 7.92; Ti, 13.61. The diphenylsilyl complex **XXIb** was prepared under conditions identical with those used for **XXIa**. In this case, 0.13 mL of diphenylsilane (0.72 mmol) was used instead of phenylsilane. **XXIb** was also obtained as thin violet needles (yield: 96 mg,91%). Anal. Calcd for $C_{27}H_{26}NSiTi$: C, 73.62; H, 5.95; N, 3.18; Si, 6.37; Ti, 10.87. Found: C, 72.83; H, 5.99; N, 3.22; Si, 5.98; Ti, 10.26.

VI.3.3 Preparation of the pyridyl-bridged titanocene(III) complex XXII.

Dimethyltitanocene (50 mg, 0.24 mmol) was added to a solution of phenylmethylsilane (0.30 mL, 2.18 mmol) and pyridine (0.56 mL, 7.00 mmol) in hexane/toluene (8 : 1; 4.5 mL). the solution slowly changed color from orange to dark brown, accompanied by a slow gas evolution. After about two hours, the color change and gas evolution stopped and the dark brown solution was then put in a -20°C refrigerator. Several hours late, brownish black needle-shaped crystals (34 mg, 45%) were obtained.

Anal. Calcd for $C_{24}H_{25}Ti_2N$: C, 65.84; H, 5.76; N, 3.20; Ti, 21.88. Found: C, 63.27; H, 5.12; N, 3.04; Ti, 22.33. The elemental analysis result indicates that the free pyridine in the crystal lattice has been lost after long time evacuation.

VI.3.4 EPR measurements.

All EPR measurements were carried out by Dr. E. Samuel and Mme. Josette Hénique at the Ecole Nationale Superieure de Chimie de Paris. The EPR spectra were recorded on a Bruker ER 220D spectrometer equipped with an Aspect 2000 computer and a ER 4144 variable-temperature unit. The magnetic field was calibrated with a Bruker BNM 12 gaussmeter. The microwave frequency was measured with a Systron Donner frequency counter. The solutions for EPR measurements were prepared by dissolving crystalline compounds in toluene below -20°C and the measurements were made at -20°C. If the solutions were warmed to, or prepared at room temperature, all of the studied compounds had decomposed before measurements could be made.

VI.3.5 X-ray diffraction analysis.

The structure determinations for <u>**XXa**</u>, <u>**XXc**</u> and <u>**XXII**</u> were carried out in P. R. China by Dr. Zhongsheng Jin of Laboratory 26, Changchun Institute of Applied Chemistry. Diffraction measurements for these compounds were carried out on a Nicolet R3M/E diffractometer. Computations were performed using the SHELXTL (226) system adapted to an Eclipse S/140 computer. The data collection for <u>**XXb**</u> was carried out at Crystallitics Company on a Syntex P21 diffractometer, and the structure was solved using SHELXTL and refined in TEXSAN by Dr. Jim Britten at McGill. Complete tables of crystal data, data collection and refinement parameters, molecular parameters, atom coordinates, isotropic thermal parameters and heavy atom anisotropic thermal parameters for <u>**XXa**</u>, <u>**XXb**</u>, <u>**XXc**</u> and <u>**XXII**</u> are given in Appendixes II, III, IV and V respectively.

A. Compounds XXa and XXc.

A single crystal of XXa (0.08 × 0.40 × 0.44 mm) was sealed under argon in a thin-walled capillary. Intensity data were collected at room temperature on a Nicolet R3M/E diffractometer with graphite monochromator and Mo Kα radiation. The space group $P2_1/c$ was established by systematic absences in the complete data set ($0k0$, $k = 2n + 1$ and $h0l$, $l = 2n + 1$). The intensity data were corrected for absorption and Lorentz-polarization effects. The position of the Ti atom was deduced by the direct method. The remaining non-hydrogen atoms were located in difference Fourier syntheses and were refined by full-matrix least-squares and anisotropic thermal parameters. The hydrogen atoms were calculated by difference Fourier syntheses and fixed in their ideal positions with isotropic thermal refinements. The final least-squares refinement converged to $R = 0.030$ and $R_w = 0.030$.

A single crystal of XXc, approximately 0.2 × 0.3 × 0.5 mm, was sealed under argon in a thin-walled glass capillary. Intensity data were collected at room temperature on a Nicolet R3M/E diffractometer with graphite monochromator and Mo Kα radiation. Systematic absences in the complete data set ($0k0$, $k = 2n + 1$) indicated space group $P2_1$ or $P2_1/m$. However, the structure was only solvable for $P2_1$. The intensity data were corrected for absorption and Lorentz-polarization effects. The position of the Ti atom was directly derived from the Patterson map. The remaining non-hydrogen atoms were located in difference Fourier syntheses and were refined by full-matrix least-squares and anisotropic thermal parameters. The hydrogen atoms were calculated by difference Fourier syntheses and fixed in their ideal positions with isotropic thermal refinements. The final least-squares refinement converged to $R = 0.038$ and $R_w = 0.041$.

B. Compound XXb.

A single crystal of **XXb** suitable for X-ray diffraction studies was sealed under argon in a thin-walled glass capillary. Intensity data were collected on a Syntex P21 diffractometer using Mo Kα radiation. The space group $P2_12_12_1$ was established by systematic absences. No absorption correction was applied due to regular crystal shape. The position of the Ti atom was deduced from a Patterson map and remaining non-hydrogen atoms were derived from difference Fourier syntheses. All non-hydrogen atoms were refined anisotropically with full-matrix least-squares methods. The hydrogen atoms were calculated and fixed in idealized positions. The Me/H disorder on Si was refined with C(20) and C(21) having a common isotropic temperature factor and refined occupancy (0.71 and 0.29 for C(20) and C(21) respectively). The final least-squares refinement resulted in R = 0.052 and $R_w = 0.038$.

C. Compound XXII.

A single crystal of **XXII** (0.2 × 0.3 × 0.4 mm) was sealed under argon in a thin-walled glass capillary. Intensity data were collected at room temperature on a Nicolet R3M/E diffractometer with graphite monochromator and Mo Kα radiation. The space group $P2_1/n$ was established by systematic absences in the complete data set ($0k0$, $k = 2n + 1$ and $h0l$, $h + l = 2n + 1$). The intensity data were corrected for absorption and Lorentz-polarization effects. The positions of the Ti atoms were deduced by the direct method. The remaining non-hydrogen atoms were located in difference Fourier syntheses. All non-hydrogen atoms were refined by full-matrix least-squares and anisotropic thermal parameters. The bridging hydrogen atom was located on the E map after full-matrix least-squares refinements and anisotropic refinements of all non-hydrogen atoms. All other hydrogen atoms were calculated and fixed in their ideal positions with isotropic thermal refinements. The final least-squares refinement converged to R = 0.053 and $R_w = 0.037$.

CONTRIBUTIONS TO ORIGINAL KNOWLEDGE

1. The dehydrocoupling of phenylsilane in the presence of DMT or DMZ was proved to be a step-wise reaction, not a chain reaction. Dimer, trimer and other small oligomers were detected during the dehydrocoupling reaction.
2. High molecular weight polymethylsilane was prepared for the first time. The pyrolysis of polymethylsilane gives high yields of near stoichiometric SiC.
3. The dehydrocoupling of a number of secondary organosilanes, including Ph_2SiH_2, $PhMeSiH_2$ and n-$BuMeSiH_2$, and the kinetics of the dimerization of Ph_2SiH_2 were studied.
4. Stoichiometric reactions of DMT and DMZ with a variety of organosilanes were investigated. Some new dimeric silylzirconium complexes, $Cp_2ZrR^1(\mu\text{-}H)_2R^2ZrCp_2$ (where R^1 is a silyl group, R^2 can be H, Me, or a silyl group) and $[Cp_2ZrSiRR'H]_2$ (where R = Ph, R′ = Ph, Me, H; R = Me, R′ = Bu, Me, H), were isolated, or observed by following the reactions by ^1H NMR.
5. A bimetallic transition state mechanism for the titanocene catalyzed silane dehydrocoupling reaction is proposed.
6. Some novel silyl titanocene(III) complexes of the type $Cp_2Ti(R)L$, where R is a silyl group, L = PMe_3 or Py, were synthesized and characterized by EPR and X-ray crystallography.
7. The pyridyl-bridged titanocene(III) complex $Cp_2Ti(\mu\text{-}H)(\mu\text{-}N,C\text{-}Py)TiCp_2$ was isolated and structurally characterized. It is the only known example of this type of pyridyl-bridged transition metal complex.

SUGGESTIONS FOR FURTHER WORK

1. It was found that the silyltitanocene(III) trimethylphosphine and pyridine complexes decompose in solution to form new titanocene(III) complexes. The decomposition products, however, have not been isolated and remain unclear. It might be interesting to isolate these complexes and study their chemical properties.
2. Polymer attached Cp_2TiMe_2 was found to be more effective than unattached Cp_2TiMe_2 as catalyst for the hydrogenation of olefins (224). It is therefore believed that the active catalyst in this kind of reaction is a mononuclear titanocene species. It is probably also interesting to test the catalytic activity of the polymer attached Cp_2TiMe_2 and Cp_2ZrMe_2 for the silane dehydrocoupling reaction, from which some information about the reaction mechanism might be obtained.
3. A variety of dimeric silylzirconium complexes, $Cp_2ZrR^1(\mu\text{-}H)_2R^2ZrCp_2$, where R^1 is a silyl group, R^2 can be H, Me, or a silyl group, have been observed during the reactions of DMZ with a number of organosilanes. However, only a few of them have been isolated. It is possible to isolate these complexes by choosing suitable experimental conditions. In addition, our attempts to obtain a high quality crystal structure of this type of compound have not been successful due to the disorder problem of the unsymmetrical compounds. It is more likely that a high quality single crystal of the symmetrical compound could be obtained from reactions of silanes with Cp_2ZrH_2 or Cp_2ZrR_2 (where R should be a more sterically bulky alkyl group than methyl group).
4. In a preliminary study, not described in this thesis, Cp_2HfMe_2, generated *in situ* by the reaction of Cp_2HfCl_2 with methyllithium, was found to be an active catalyst for the dehydrocoupling of organosilanes. So far, none of the catalytic and stoichiometric reactions of Cp_2HfMe_2 with organosilanes has been studied in detail

although the catalytic activity of $Cp^*_2HfH_2$ and several silyl derivatives of hafnocene chloride $CpCp^*Hf(SiR_3)Cl$ (R = Me, Ph, $SiMe_3$) for the silane dehydrocoupling reaction has been investigated by Tilley *et al.* (92,94). It would be expected that a series of new silylhafnocene complexes can be obtained from the stoichiometric reactions.

REFERENCES

1. H.R. Allcock, *Chem. Eng. News* **1985**, *63*, 22.
2. C. Friedel and J.M. Crafts, *C.R. Acad. Sci. Paris* **1863**, *56*, 590.
3. C. Friedel and A. Ladenburg, *C.R. Hebd. Seances Acad. Sci.* **1869**, *68*, 920.
4. R. West, Organopolysilanes, in *Comprehensive Organometallic Chemistry*, G. Wilkinson, F.G.A. Stone and E.W. Abel, Eds., Pergamon Press, Oxford, 1983, Vol.9, p.365-397.
5. F.S. Kipping and J.E. Sands, *J. Chem. Soc.* **1921**, *119*, 830.
6. F.S. Kipping, *J. Chem. Soc.* **1924**, *125*, 2291.
7. H. Gilman and G.L. Schwebke, *J. Am. Chem. Soc.* **1964**, *86*, 2693.
8. H. Gilman and G.L. Schwebke, *J. Organomet. Chem.* **1965**, *3*, 382.
9. C.A. Burkhard, *J. Am. Chem. Soc.* **1949**, *71*, 963.
10. S. Yajima, J. Hayashi and M. Omori, *Chem. Lett.* **1975**, 931.
11. S. Yajima, K. Okamura and J. Hayashi, *Chem. Lett.* **1975**, 1209.
12. R. West and E. Carberry, *Science* **1975**, *189*, 179 and refs. therein.
13. R. West, L. Brough and W. Wojnowski, *Inorg. Synth.* **1979**, *19*, 265.
14. L. Brough and R. West, J. Organomet. Chem. **1980**, *194*, 139.
15. H. Watanabe and Y. Nagai, in *Organosilicon and Bioorganosilicon Chemistry*, H. Sakurai, Ed., Ellis Horwood Ltd.: London, 1985, Chapter 9, and refs. therein.
16. L.F. Brough, K. Matsumura and R. West, *Angew, Chem. Int. Ed. Engl.* **1979**, *18*, 955.
17. L.F. Brough and R. West, *J. Am. Chem. Soc.* **1981**, *103*, 3049.
18. C.W. Carlson, K. Matsumura and R. West, *J. Organomet. Chem.* **1980**, *194*, C5.
19. H. Watanabe, T. Muraoka, M. Kageyama and Y. Nagai, *Chem. Lett.* **1980**, 753.
20. H. Watanabe, T Muraoka, M. Kageyama and Y. Nagai, *J. Organomet. Chem.* **1981**,

216, C45.

21. C.W. Carlson, X.H. Zhang and R. West, *Organometallics* **1983**, *2*, 453.
22. C.W. Carlson, K.J. haller, X.H. Zhang and R. West, *J. Am. Chem. Soc.* **1984**, *106*, 5521.
23. J.P. Wesson, T.C. Williams, *J. Polym. Sci., Polym. Chem. Ed.* **1980**, *18*, 959.
24. J.P. Wesson, T.C. Williams, *J. Polym. Sci., Polym. Chem. Ed.* **1981**, *19*, 65.
25. R. West, L.D. David, P.I. Djurovich, K.L. Stearly, K.S.V. Srinivasan, J.H. Yu, *J. Am. Chem. Soc.* **1981**, *103*, 7352.
26. L. David, R. West, *U.S. Patent* 4,324,901, 1982.
27. R. West, U.S. Patent 4,260,780, 1981.
28. R.E. Trujillo, *J. Organomet. Chem.* **1980**, *198*, C27.
29. R. West, *J. Organomet. Chem.* **1986**, *300*, 327.
30. R.D. Miller, J. Michl, *Chem. Rev.* **1989**, *89*, 1359.
31. C.T. Aitken, J.F. Harrod, E. Samuel, *J. Organomet. Chem.* **1985**, *279*, C11.
32. C.T. Aitken, J.F. Harrod, E. Samuel, *J. Am. Chem. Soc.* **1986**, *108*, 4059.
33. C.T. Aitken, J.F. Harrod, E. Samuel, *Can. J. Chem.* **1986**, *64*, 1677.
34. J.F. Harrod, in *Inorganic and Organometallic Polymers,* M. Zeldin, K. J. Wynne, H. R. Allcock, Eds., ACS Symposium Series 360, American Chemical Society: Washington, DC, 1988, Chapter 7.
35. J.P. Wesson, T.C. Williams, *J. Polym. Sci., Polym. Chem. Ed.* **1979**, *17*, 2833.
36. R. West, L.D. David, H. Yu, R. Sinclair, *Am. Ceram. Soc. Bull.* **1983**, *62*, 825 and 899.
37. P. Trefonas III, P.I. Djurovich, X.H. Zhang, R. West, R.D. Miller, D. Hofer, *J. Polym. Sci., Polym. Lett. Ed.* **1983**, *21*, 819.
38. X.H. Zhang, R. West, *J. Polym. Sci., Polym. Chem. Ed.* **1984**, *22*, 195.
39. X.H. Zhang, R. West, *J. Polym. Sci., Polym. Chem. Ed.* **1984**, *22*, 225.

40. J.M. Ziegler, L.A. Harrah, A.W. Johnson, *SPIE* **1985**, *539*, 166.

41. D.C. Hofer, K. Jain, R.D. Miller, *IBM Tech. Disclos. Bull.* **1984**, *26*, 166.

42. R. West, X.H. Zhang, P.I. Djurovich, H. Stuger, in *Science of Ceramic Chemical Processing*, L.L. Hench, D.R. Ulrich, Eds., Willey: New York, 1986, p.337-344.

43. K. Matyjaszewski, Y.L. Chen, H.K. Kim, in *Inorganic and Organometallic polymers,* M. Zeldin, K.J. Wynne, H.R. Allcock, Eds., ACS Symposium Series 360, American Chemical Society: Washington, DC, 1988, Chapter 6.

44. H.K. Kim, K. Matyjaszewski, *J. Am. Chem. Soc.* **1988**, *110,* 3321.

45. P.A. Bianconi, T.D. Weidman, *J. Am. Chem. Soc.* **1988**, *110,* 2342.

46. H.K. Kim, K. Matyjaszewski, *Polym. Prepr.* **1989**, *30*, 131.

47. R.D. Miller, J.F. Rabolt, R. Sooriyakumaran, et al., in *Inorganic and Organometallic polymers,* M. Zeldin, K.J. Wynne, H.R. Allcock, Eds., ACS Symposium Series 360, American Chemical Society: Washington, DC, 1988, Chapter 4.

48. K. Sakamoto, K. Obata, H. Hirata, M. nakajima, H. Sakurai, *J. Am. Chem. Soc.* **1989**, *111*, 7641.

49. M. Cypryk, Y. Gupta, K. Matyjaszewski, *J. Am. Chem. Soc.* **1991**, *113*, 1046.

50. M. Stolka, H.J. Yuh, K. McGrane, D.M. Pai, *J. Polym. Sci., Polym. Chem. Ed.* **1987**, *25*, 823.

51. R.G. Kepler, J.M. Zeigler, L.A. Harrah, S.R. Kurtz, *Phys. Rev. B* **1987**, *35*, 2818.

52. A.R. Wolf, R. West, D.G. Peterson, *"Polysilanes: A New Class of Vinyl Photoinitiators"*, presented to 18th Organosilicon Symposium, Schenectady, NY, April 4, 1984.

53. D. Hofer, R.D. Miller, G.C. Willson, *Proc. SPIE Int. Soc. Opt. Eng.* **1984**, *469*, 16, and 108.

54. R.D. Miller, D. Hofer, G.N. Fickes, G. Wilson,E.E. Marinero, P. Trefonas, R. West,

Polym. Eng. Sci. **1986**, *26*, 1129.

55. R.D. Miller, G. Wallraff, N. Clecak, et al., *Polym. Eng. Sci.* **1989**, *29*, 882.
56. G.N. Taylor, M.Y. Hellman, T.M. Wolf, J.M. Zeigler, *Proc. SPIE* **1988**, *920*, 274.
57. K. Kajzar, J. Messier, C. Rosilio, *J. Appl. Phys.* **1986**, *60*, 3040.
58. J. C. Baumert, G.C. Bjorklund, D.H. Lundt, M.C. Jurich, H. Looser, R.d. Miller, et al., *Appl. Phys. Lett.* **1988**, *53*, 1147.
59. S. Yajima, Y. Hasegawa, J. Hayashi, M. Ijmura, *J. Mater. Sci.*, **1978**, *13*, 2569.
60. R. West, in *Ultrastructure Processing of Ceramics, Glasses and Composites*, L. Hench, D.R. Ulrich, Eds., Wiley: New York, 1984, Chapter 19, R.H. Baney, Chapter 20, C.H. Beatty, Chapter 22.
61. R. West, J. Maxka, *Polym. Prepr.* **1987**, *28*, 387.
62. A.R. Wolff, I. Nozue, J. Maxka, R. West, *J. Polym. Sci., Polym. Chem. Ed.* **1988**, *26*, 701.
63. P.M. Cotts, R.D. Miller, P.T. Trefonas, R. West, G.N. Fickes, *Macromolecules* **1987**, *20*, 1047.
64. P. Trefonas, R. West, R.D. Miller, D. Hofer, *J. Polym. Sci., Polym. Lett. Ed.* **1983**, *21*, 823.
65. R. West, I.D. David, P.I. Djurovitch, K.L. Stearley, K.S.V. Srinivasan, H. Yu, *J. Am. Chem. Soc.* **1981**, *103*, 1352.
66. X.H. Zhang, R. West, *J. Polym. Sci.* **1984**, *22*, 159, and 255.
67. P. Trefonas, J.R. Damewood, R. West, R.D. Miller, *Organometallics* **1985**, *4*, 1318.
68. L.A. Harrah, J.M. Zeigler, *J. Polym. Sci., Polym. Lett. Ed.* **1985**, *23*, 209.
69. R.D. Miller, D. Hofer, J. Rabolt, G.N. Fickes, *J. Am. Chem. Soc.* **1985**, *107*, 2172.
70. H. Kuzmany, J. Rabolt, B.L. Farmer, R.D. Miller, *J. Chem. Phys.* **1986**, *85*, 7413.
71. A.J. Lovinger, F.C. Schilling, F.A. Bovey, J.M. Zeigler, *Macromolecules* **1986**, *19*, 2657.

72. H. Naarman, N. Theophilou, L. Geral, J. Sledz, F. Schien, *German Patent* DE3634281, 1988; *Chem. Abstr.* **1988**, *109*, 120989u.

73. A. Usuki, M. Murase, *Jpn Kokai Tokkyo Koho* JP62 59,632 [87 59,632]; *Chem. Abstr.* **1987**, *107*, 218592u.

74. M. Fujino, *Chem. Phys. Lett.* **1987**, *136*, 451.

75. L.M. Samuel, P.N. Sanda, R.D. Miller, *Chem. Phys. Lett.* **1989**, *159*, 227.

76. P. Trefonas, R. West, R.D. Miller, *J. Am. Chem. Soc.* **1985**, *107*, 2737.

77. R. West, X.H. Zhang, P.I. Djurovich, H. Stuger, In *Science of Ceramic Chemical Processing*, L.L. Hench, D.R. Ulrich, Eds., Willey: New York, 1986, Chapter 36.

78. R. West, A.R. Wolff, D.J. Peterson, *J. Radiat. Curing* **1986**, *13*, 35.

79. A.R. Wolff, R. West, *Appl. Organomet. Chem.* **1987**, *1*, 7.

80. R.D. Miller, S.A. MacDonald, *J. Imaging Sci.* **1987**, *31*, 43.

81. I. Ojima, S.I. Inaba, T. Kogure, Y. Nagai, *J. Organomet. Chem.* **1973**, *55*, C7.

82. M.F. Lappert, R.K. Maskell, *J. Organomet. Chem.* **1984**, *264*, 217.

83. K.A. Brown-Wensley, *Organometallics* **1987**, *6*, 1590.

84. J.Y. Corey, L.S. Chang, E.R. Corey, *Organometallics* **1987**, *6*, 1595.

85. L.S. Chang, J.Y. Corey, *Organometallics* **1989**, *8*, 1885.

86. M. Tanaka, T. Kobayashi, T. Hayashi, T. Sakakura, *Appl. Organomet. Chem.* **1988**, *2*, 91.

87. J.F. Harrod, S.S. Yun, *Organometallics* **1987**, *6*, 1381.

88. C.T. Aitken, J.F. Harrod, U.S. Gill, *Can. J. Chem.* **1987**, *65*, 1804.

89. J.F. Harrod, In *Transformation of Organometallics into Common and Exotic Materials: Design and Activation*, R.M. Laine, Ed., NATO ASI Series E, No.141, Martinus Nijhoff: Amsterdam, 1988, p 103.

90. C.T. Aitken, J.P. Barry, F. Gauvin, J.F. Harrod, A. Malek, D. Rousseau, *Organometallics* **1989**, *8*, 1732.

91. T. Nakano, H. Nakamura, Y. Nagai, *Chem. Lett.* **1989**, 83.

92. H.G. Woo, T.D. Tilley, *J. Am. Chem. Soc.* **1989**, *111*, 8043; *Polym. Prepr.* **1990**, *31*, 228.

93. W.H. Campbell, T.K. Hilty, L. Yurga, *Organometallics* **1989**, *8*, 2615.

94. H.G. Woo, T.D. Tilley, *J. Am. Chem. Soc.* **1989**, *111*, 3757.

95. T.D. Tilley, *Comments Inorg. Chem.* **1990**, *10*, 37.

96. K.I. Gell, B. Posin, J. Schwartz, G.M. Williams, *J. Am. Chem. Soc.* **1982**, *104*, 1846.

97. (a) S. Couturier, G. Tainturier, B. Gautheron, *J. organomet. Chem.* **1980**, *195*, 291; (b) S.B. Jones, Ph.D. Thesis, West Virginia University, West Virginia, U.S.A., 1983, P 58-59.

98. I. Hyla-Kryspin, R. Gleiter, C. Kruger, R. Zwettler, G. Erker, *Organometallics* **1990**, *9*, 517 and 524.

99. D.F. Herman, W.K. Nelson, *J. Am. Chem. Soc.* **1952**, *74*, 2693.

100. K. Ziegler, E. Holtzkamp, H. Breil, H. Martin, *Angew. Chem.* **1955**, *67*, 54.

101. T.J. Kealy, P.L. Pauson, *Nature* (London): **1951**, *168*, 1039.

102. S.A. Miller, J.A. Tebboth, J.F. Tremaine, *J. Chem. Soc.* **1952**, 632.

103. G. Wilkinson, M. Rosenblum, M.C. Whiting, R.B. Woodward, *J. Am. Chem. Soc.* **1952**, *74*, 2125.

104. E.O. Fischer, W. Pfab, *Z. Naturforsch* **1952**, *7B*, 377.

105. G. Wilkinson, P.L. Pauson, J.M. Birmingham, F.A. Cotton, *J. Am. Chem. Soc.* **1953**, *75*, 1011.

106. D.J. Cardin, M.F. Lappert, C.L. Raston,P.I. Riley, *Comprehensive Organometallic Chemistry*, G. Wilkinson, F.G.A. Stone and E.W. Abel, Eds., Pergamon Press, Oxford, 1982, Chapter 23.1.

107. Y. Wielstra, S. Gambrarotta, A. Meetsma and J.L. de Boer, *Organometallics* **1989**, *8*, 250.

108. J.W. Lauher, R. Hoffmann, *J. Am. Chem. Soc.* **1976**, *98*, 1729.

109. C.J. Ballhausen, J.P. Dahl, *Acta. Chem. Scand.* **1961**, *15*, 1333.

110. J.E. Bercaw, *J. Am. Chem. Soc.* **1974**, *96*, 5087.

111. T.S. Piper, G. Wilkinson, *J. Inorg. Nucl. Chem.* **1956**, *3*, 104.

112. K. Claus, H. Bestian, *Justus Liebigs Ann. Chem.* **1962**, *654*, 8.

113. E. Samuel, M.D. Rausch, *J. Am. Chem. Soc.* **1973**, *95*, 6264.

114. P.C. Wailes, H. Weigold, A.P. Bell, *J. Organometal. Chem.* **1972**, *34*, 155.

115. L. Summers, R.H. Uloth, A. Holmes, *J. Am. Chem. Soc.* **1955**, *77*, 3604.

116. H. Sinn, F. Patat, *Angew. Chem.* **1963**, *75*, 805.

117. H.C. Beachell, S.A. Butter, *Inorg. Chem.* **1965**, *4*, 1133.

118. B. Wozniak, J.D. Ruddick, G. Wilkinson, *J. Chem. Soc., Part A*, **1971**, 3116.

119. C.P. Boekel, J.H. Teuben, H.J. De Liefde Meijer. *J. Organometal. Chem.* **1975**, *102*, 317.

120. J.X. Mcdermott, M.E. Wilson, G.M. Whitesides, *J. Am. Chem. Soc.* **1976**, *98*, 6529.

121. G. Fachinetti, C. Floriani, *J. Chem. Soc., Chem. Commun.* **1972**, 654.

122. M.D. Rausch, *Pure Appl. Chem.* **1972**, *30*, 523.

123. H.A. Martin, P.J. Lemaire, F. Jellinek, *J. Organometal. Chem.* **1972**, *36*, 93.

124. J.H. Teuben, H.J. De Liefde Meijer, *J. Organometal. Chem.* **1972**, *46*, 313.

125. F.W. Van der Weij, H. Scholtens, J.H. Teuben, *J. Organometal. Chem.* **1977**, *127*, 299.

126. P.C. Wailes, R.S.P. Coutts, H. Weigold, *Organometallic Chemistry of Titanium, Zirconium, and Hafnium*, Academic Press, New York, 1974, P 221.

127. M.J.S. Gynane, J. Jeffery, M.F. Lappert, *J. Chem. Soc., Chem. Commun.* **1978**, 34.

128. G.M. Williams, J. Schwartz, *J. Am. Chem. Soc.* **1982**, *104*, 1122.

129. D.J. Cardin, M.F. Lappert, C.L. Raston, *Chemistry of Organo-zirconium and -hafnium Compounds*, Ellis Horwood Limited, Chichester, 1986, P 279.

130. T. Cuenca, P. Royo, *J. Organometal. Chem.* **1985**, *295*, 159.

131. H.G. Alt, F.P. Di Sanzo, M.D. Rausch, P.C. Uden, *J. Organometal. Chem.* **1976**, *107*, 257.

132. G.J. Erskine, D.A. Wilson, J.D. McCowan, *J. Organometal. Chem.* **1976**, *114*, 119.

133. C.H. Bamford, R.J. Puddephatt, D.M. Slater, *J. Organometal. Chem.* **1978**, *159*, C31.

134. D.J. Cardin, M.F. Lappert, C.L. Raston, P.I.Riley, *Comprehensive Organometallic Chemistry*, G. Wilkinson, F.G.A. Stone and E.W. Abel, Eds., Pergamon Press, Oxford, 1982, Chapter 23.2.

135. J.M. Atkinson, P.B. Brindly, A.G. Davies, J.A. Hawari, *J. Organometal. Chem.* **1984**, *264*, 253.

136. H.G. Alt, M.D. Rausch, *Z. Naturforsch, Teil B* **1975**, *30*, 813.

137. E. Samuel, G. Gianotti, *J. Organometal. Chem.* **1976**, *113*, C17.

138. E. Samuel, *J. Organometal. Chem.* **1980**, *198*, C65.

139. P.C. Wailes, H. Weigold, A.P. Bell, *J. Organometal. Chem.* **1972**, *43*, C32.

140. S.L. Hsu, A.J. Signorelli, G.P. Pez, R.H. Baughman, *J. Chem. Phys.* **1978**, *69*, 106.

141. T. Graczyk, J.F. Harrod, unpublished results.

142. J.E. Bercaw, H.H. Brintzinger, *J. Am. Chem. Soc.* **1969**, *91*, 7301.

143. J.E. Bercaw, R.H. Marvich, L.G. Bell, H.H. Brintzinger, *J. Am. Chem. Soc.* **1972**, *94*, 1219.

144. S. Couturier, B. Gautheron, *J. Organometal. Chem.* **1978**, *157*, C61.

145. H. Weigold, A.P. Bell, R.I. Willing, *J. Organometal. Chem.* **1974**, *73*, 23.

146. R.F. Jordan, C.S. Bajgur, W.E. Dasher, A.L. Rheingold, *Organometallics* **1987**, *6*, 1041.

147. F.D. Miller, R.D. Sanner, *Organometallics* **1988**, *7*, 818.

148. C.T. Aitken, Ph.D. Thesis, McGill University, Quebec, Canada, 1986, Chapter 3.

149. D.J. Cardin, S.A. Keppie, B.M. Kingston, M.F. Lappert, *J. Chem. Soc., Chem. Commun.* **1967**, 1035.

150. E. Hengge, H. Zimmerman, *Angew. Chem. Int. Ed. Engl.* **1968**, *7*, 142.

151. B.M. Kingston and M.F. Lappert, *J Chem. Soc., Dalton Trans.* **1972**, 69.

152. L. Rosch, G. Altnau, W. Erb, J. Pickardt, N. Bruncks, *J. Organometal. Chem.* **1980**, *197*, 51.

153. M.S. Holtman, E.P. Schram, *J. Organometal. Chem.* **1980**, *187*, 147.

154. A.J. Blakeney, J.A. Gladysz, *J. Organometal. Chem.* **1980**, *202*, 263.

155. T.D. Tilley, *Organometallics* **1985**, *4*, 1452.

156. B.K. Campion, J. Falk, T.D. Tilley, *J. Am. Chem. Soc.* **1987**, *109*, 2049.

157. H.F. Elsner, T.D. Tilley, A. L. Rheinglod, S.J. Geib, *J. Organometal. Chem.* **1988**, *358*, 169.

158. D.M. Roddick, R.H. Heyn, T.D. Tilley, *Organometallics* **1989**, *8*, 324.

159. G. Henchen, E. Weiss, *Chem. Ber.* **1973**, *106*, 1747.

160. A.K. Fischer, G. Wilkinson, *J. Inorg. Nucl. Chem.* **1956**, *2*, 149.

161. G.W. Watt, L.J. Baye, *J. Inorg. Nucl. Chem.* **1964**, *26*, 2099.

162. K. Shikata, K. Yokogawa, S. Nakao, K. Azuma, *Kogyo Kagaku Zasshi* **1965**, *68*, 1248.

163. G.W. Watt, L.J. Baye, F.O. Drummond, Jr., *J. Am. Chem. Soc.* **1966**, *88*, 1138.

164. J.J. Salzmann, P. Mosimann, *Helv. Chim. Acta* **1967**, *50*, 1831.

165. F. Calderazzo, J.J. Salzmann, P. Mosimann, *Inorg. Chim. Acta* **1967**, *1*, 65.

166. E.E. van Tamelen, R.B. Fechter, S.W. Schneller, G. Boche, R.H. Greeley, B. Akermark, *J. Am. Chem. Soc.* **1969**, *91*, 1551.

167. H.H. Brintzinger, J.E. Bercaw, *J. Am. Chem. Soc.* **1970**, *92*, 6182.

168. A. Davison, S.S. Wreford, *J. Am. Chem. Soc.* **1974**, *96*, 3017.

169. L.J. Guggenberger, F.N. Tebbe, *J. Am. Chem. Soc.* **1976**, *98*, 4137.

170. J.E. Bercaw, H.H. Brintzinger, *J. Am. Chem. Soc.* **1971**, *93*, 2046.

171. E. Samuel, J.F. Harrod, *J. Am. Chem. Soc.* **1984**, *106*, 1859.

172. G.W. Watt, F.O. Drummond, Jr., *J. Am. Chem. Soc.* **1966**, *88*, 5926.

173. P.C. Wailes, H. Weigold, *J. Organomet. Chem.* **1970**, *24*, 713.

174. P.C. Wailes, H. Weigold, *J. Organomet. Chem.* **1971**, *28*, 91.

175. P.C. Wailes, H. Weigold, A.P. Bell, *J. Organomet. Chem.* **1972**, *43*, C32.

176. H. Alt, M.D. Rausch, *J. Am. Chem. Soc.* **1974**, *96*, 5936.

177. G.P. Pez, C.F. Putnik, S.L. Suib, G.D. Stucky, *J. Am. Chem. Soc.* **1979**, *101*, 6933.

178. K.I. Gell, T.V. Harris, J. Schwartz, *Inorg. Chem.* **1981**, *20*, 481.

179. B.D. James, R.K. Nanda, M.G.H. Wallbridge, *Inorg. Chem.* **1967**, *6*, 1979.

180. P.C. Wailes, H. Weigold, *J. Organomet. Chem.* **1970**, *24*, 405.

181. K.I. Gell, J. Schwartz, *J. Am. Chem. Soc.* **1978**, *100*, 3246.

182. J. Jeffrey, M.F. Lappert, N.T. Luong-Thi, J.L. Atwood, W.E. Hunter, *J. Chem. Soc., Chem. Commun.* **1978**, 1081.

183. D.G. Bickley, N. Hao, P. Bougeard, B.G. Sayer, R.C. Burns, M.J. McGlinchey, *J. Organomet. Chem.* **1983**, *246*, 257.

184. S.B. Jones, J.L. Petersen, *Inorg. Chem.* **1981**, *20*, 2889.

185. J.M. Manriquez, J.E. Bercaw, *J. Am. Chem. Soc.* **1974**, *96*, 6229.

186. J.M. Manriquez, D.R. McAlister, R.D. Sanner, J.E. Bercaw, *J. Am. Chem. Soc.* **1978**, *100*, 2716.

187. E. Samuel, P. maillard, G. Gianotti, *J. Organomet. Chem.* **1977**, *142*, 289.

188. A. Hudson, M.F. Lappert, R. Pichon, *J. Chem. Soc., Chem. Commun.* **1983**, 374.

189. S.B. Jones, J.L. Petersen, *J. Am. Chem. Soc.* **1983**, *105*, 5502.

190. J.M. Kanabus-Kaminska, J.A. Hawari, D. Griller, C. Chatgilialoglu, *J. Am. Chem. Soc.* **1987**, *109*, 5267.

191. R. Walsh, *Accts. Chem. Res.* **1981**, *14*, 246.

192. C.T. Aitken, J.F. Britten, J.F. Harrod and D. Rousseau, in press.

193. B. Cote, M.Sc. Thesis, McGill University, Quebec, Canada, p 47.

194. N.N. Greenwood, A. Earnshaw, In *Chemistry of the Elements*, Pergamon Press, Oxford, 1984.

195. D.L. Shriver, *the Manipulations of Air-Sensitive Compounds*, McGraw-Hill, New York, 1969, p 141.

196. R.A. Benkeser, H. Landesman, D.J. Foster, *J. Am. Chem. Soc.* **1952**, *74*, 648.

197. S. Yajima, *Ceram. Bull.* **1985**, *62*, 993.

198. Y. Hasegawa, K. Okmura, *J. Mater. Sci.* **1983**, *18*, 3633.

199. Y. Hasegawa, K. Okmura, *J. Mater. Sci.* **1985**, *20*, 321.

200. J.P. Wesson, T.C. William, *J. Polym. Sci., Polym. Chem. Ed.* **1981**, *19*, 65.

201. K. Kumar, M.H. Litt, *J. Polym. Sci., Polym. Chem. Ed.* **1988**, *26*, 25.

202. D.J. Carlsson, J.D. Cooney, S. Gauthier, D.J. Worsfold, *J. Am. Ceram. Soc.* **1990**, *73*, 237.

203. D. Seyferth and H. Lang, *Organometallics*, **1991**, *10*, 551.

204. C.L. Schilling, T.C. Williams, U.S. Patent 4,472,591, 1984.

205. K.A. Brown-Wensley, R.A. Sinclair, U.S. Patent 4, 537,942, 1985.

206. D. Seyferth, in *Silicon-Based Polymer Science,* J. M. Zeigler and F. W. G. Fearon Eds, Advances in Chemistry 224, American Chemical Society: Washington, DC, 1990, Chapter 31.

207. C.T. Aitken, J.F. Harrod, A. Malek, E. Samuel, *J. Organomet. Chem.* **1988**, *349*, 285.

208. F.W. Billmeyer, *Textbook of Polymer Science,* 3rd Edition, Wiley: New York, 1984, p 40.

209. Y. Mu, C.T. Aitken, B. Cote, J.F. Harrod, E. Samuel, *Can. J. Chem.* **1991**, *69*, 264.

210. J.S. Hartman, M.F. Richardson, B.L. Sheriff and B.G. Winsborrow, *J. Am. Chem.*

Soc. **1987**, *109*, 6059.

211. Y. Hasegawa, M. Iimura and S. Yajima, *J. Mater. Sci.* **1980**, *15*, 720.

212. K.R. Carduner, S.S. Shinozaki, M.J. Rokosz, C.R. Peters, T.J. Whalen, *J. Am. Ceram. Soc.* **1990**, *73*, 2281.

213. G.D. Sorard, F. Babonneau, J.D. Mackenzie, *J. Mater. Sci.* **1990**, *25*, 3886.

214. J.Y. Corey, X.H. Zhu, T.C. Bedard, *XXIII Organosilicon Symposium*, Midland, MI, April 20-21, 1990, Abstract D1.

215. W. Steudel, H. Gilman, *J. Am. Chem. Soc.* **1960**, *82*, 6129.

216. L.C. Francesconi, D.R. Corbin, D.N. Hendrickson, G.D. Stucky, *Inorg. Chem.* **1978**, *17*, 2078; **1979**, *18*, 3074; **1981**, *20*, 2059.

217. W. Weltner, Jr., *Magnetic Atoms and Molecules*, Van Nostrand Reinhold Company Inc., New York, 1983, Chapter III.

218. R. Choukroun D. Gervais, *J. Chem. Soc.,Chem. Commun.* **1985**, 224.

219. E. Samuel, *Inorg. Chem.* **1983**, *22*, 2967.

220. J.F. Harrod, A. Malek, F.D. Rochon, R. Melanson, *Organometallics*, **1987**, *6*, 2117.

221. E. Hengge, H. Marketz, *Monatshefte für Chemie*, **1970**, *101*, 528.

222. E. Hengge, F. Lunzer, *Monatshefte für Chemie*, **1976**, *107*, 371.

223. J.E. Bercaw, *Adv. Chem. Ser.* **1978**, *167*, 136.

224. W.D. Bonds, Jr., C.H. Brubaker, Jr., E.S. Chandrasekaran, C. Gibbons, R.H. Grubbs, L.C. Kroll, *J. Am. Chem. Soc.* **1975**, *97*, 2128.

225. F. Gauvin, J.F. Harrod, unpublished result.

226. G.M. Sheldrick, SHELXTL, an integrated system for solving, refining and displaying crystal structures from diffraction data, Revision 5; University of Gottingen, Federal Republic of Germany.

227. T. Nakano and Y. Nagai, *Chem. Lett.* **1988**, 481.

228. D.A. Strauss and T.D. Tilley, *J. Am. Chem. Soc.* **1987**, *109*, 5872.

229. E. Samuel, Y. Mu, J.F. Harrod, Y. Dromzee, Y. Jeannin, *J. Am. Chem. Soc.* **1990**, *112*, 3435.

230. C.A. Tolman, *Chem. Rev.* **1977**, *77*, 313.

231. E. Klei and J.H. Teuben, *J. Organomet. Chem.* **1981**, *214*, 53.

232. K.H. den Haan, Y. Wielstra, J.H. Teuben, *Organometallics*, **1987**, *6*, 2053.

233. M.E. Thompson, S.M. Baxter, A.R. Bulls, B.J. Burger, M.C. Nolan, B.D. Santarsiero, W.P. Schaefer, J.E. Bercaw, *J. Am. Chem. Soc.* **1987**, *109*, 203.

234. R.F. Jordan, D.F. Taylor, N.C. Baenziger, *Organometallics*, **1990**, *9*, 1546.

235. E. Klei and J.H. Teuben, *J. Organomet. Chem.* **1980**, *188*, 97.

236. E. Klei, J.H. Telgen, J.H. Teuben, *J. Organomet. Chem.* **1981**, *209*, 297.

237. L.B. Kool, M.D. Rausch, H.G. Alt, M. Herberhold, B. Wolf, U. Thewalt, *J. Organomet. Chem.* **1985**, *297*, 159.

238. R. Payne, J. Hachgenei, G. Fritz, D. Fenske, *Z. Naturforsch.* **1986**, *41b*, 1535.

239. L.B. Kool, M.D. Rausch, H.G. Alt, M. Herberhold, U. Thewalt, B. Wolf, *Angew. Chem., Int. Ed. Engl.* **1985**, *24*, 394.

240. G.P. Pez, *J. Am. Chem. Soc.* **1976**, *98*, 8072.

241. V.V. Bhide, M.F. Ferona, A. Djebli, W.J. Youngs, *Organometallics*, **1990**, *9*, 1766.

242. B.F. Fieselmann and G.D. Stucky, *Inorg. Chem.* **1978**, *17*, 2074.

243. A.M. McPherson, B.F. Fieselmann, D.L. Lichtenberger, G.L. McPherson, G.D. Stucky, *J. Am. Chem. Soc.* **1979**, *101*, 3425.

244. R. Jungst, D. Sekutiwski, J. David, M. Luly, G. Stucky, *Inorg. Chem.* **1977**, *16*, 1645.

245. M. Peng and C.H. Brubaker, Jr. *Inorg. Chim. Acta*, **1978**, *26*, 231.

246. J.L. Atwood, K.F. Stone, H.G. Alt, D.C. Hancir, M.D. Rausch, *J. Organomet. Chem.* **1975**, *96*, C4.

247. J. Arnold, D.N. Shina, T.D. Tilley, *Organometallics*, **1986**, *5*, 2037.

248. D.M. Rodick, T.D. Tilley, A.L. Rheingold, S.J. Geib, *J. Am. Chem. Soc.* **1987**, *109*, 945.

249. J. Arnold, T.D. Tilley, A.L. Rheingold, S.J. Geib, *Organometallics*, 1987, *6*, 473.

APPENDIX I. X-RAY CRYSTAL STRUCTURAL ANALYSIS OF COMPLEX VIf

Table AI-1. Crystal data and data collection parameters for VIf

formula	$Zr_2Si_2C_{35}H_{42}$
fw	701.39
crystal system	monoclinic
space group	$P2_1/c$
a, Å	9.581(6)
b, Å	16.423(5)
c, Å	10.463(5)
β, deg	92.27(5)
V, Å^3	1645(1)
Z	2
F(000)	720
ρ_{calcd}, g/cm^3	1.42
μ(Mo Kα), cm^{-1}	7.2
crystal size, mm	0.1 × 0.2 × 0.4
temp, °C	20
radiation (graphite monochromator)	Mo Kα (λ = 0.71069 Å)
2θ limits, deg	$3 < 2\theta < 50$
scan speed	depending on reflection
no. of reflections collected	3157
no. of reflections used	1379
final no. of parameter	188
R[a]	0.082
Rw[b]	0.083

[a] $R = \Sigma||F_o| - |F_c|| / \Sigma|F_o|$

[b] $Rw = [\Sigma w(|F_o| - |F_c|)^2 / \Sigma wF_o^2]^{1/2}$

Table AI-2. Atomic coordinates and isotropic thermal parameters for VIf

Atom	X	Y	Z	U_{eq}[a]
Zr	0.4735(1)	0.9224(1)	0.1105(1)	0.046(1)
Si	0.7538(4)	0.9116(2)	0.1973(4)	0.059(1)
C(11)	0.40445(18)	0.8393(7)	-0.0838(13)	0.068(6)
C(12)	0.3305(18)	0.8072(8)	0.0174(14)	0.073(6)
C(13)	0.4217(19)	0.7715(9)	0.1040(10)	0.091(7)
C(14)	0.5556(17)	0.7818(7)	0.0602(12)	0.077(5)
C(15)	0.5425(200	0.8232(7)	-0.0621(14)	0.069(5)
C(21)	0.2697(17)	0.9308(14)	0.2542(15)	0.097(8)
C(22)	0.3095(19)	1.0097(10)	0.2326(15)	0.083(7)
C(23)	0.4344(18)	1.0237(8)	0.2890(13)	0.073(6)
C(24)	0.4759(20)	0.9537(14)	0.3452(14)	0.091(8)
C(25)	0.3810(17)	0.8943(11)	0.3274(13)	0.072(6)
C(31)	0.8349(15)	1.0113(9)	0.2574(15)	0.072(5)
C(32)	0.8370(17)	1.0369(11)	0.3847(17)	0.089(7)
C(33)	0.8957(24)	1.1115(14)	0.4207(19)	0.122(9)
C(34)	0.9578(18)	1.1594(11)	0.3359(24)	0.102(9)
C(35)	0.9593(18)	1.1358(11)	0.2131(22)	0.098(8)
C(36)	0.9054(14)	1.0650(80	0.1712(15)	0.066(5)
C(41)	0.7961(19)	0.8337(11)	0.3253(16)	0.097(7)
C(42)	0.8687(23)	0.8768(17)	0.0716(22)	0.055(9)
Ha	0.5880(107)	0.9978(65)	0.0157(105)	0.074(38)

[a] Equivalent isotropic U defined as one third of the trace of the orthogonalized U_{ij} tensor.

Table AI-3. Anisotropic thermal parameters ($Å^2 \times 10^3$) for <u>VIf</u>

Atom	U11	U22	U33	U23	U13	U12
Zr	68(1)	27(1)	43(1)	-1(1)	0(1)	1(1)
Si	69(2)	41(2)	67(2)	2(2)	-1(2)	4(2)
C(11)	111(13)	31(6)	61(9)	-15(6)	-23(9)	-4(7)
C(12)	100(12)	48(7)	71(9)	-7(7)	-8(9)	-29(8)
C(13)	150(15)	33(7)	86(11)	-1(7)	-22(11)	-17(9)
C(14)	147(14)	24(5)	57(8)	-13(5)	-38(8)	32(8)
C(15)	118(13)	25(5)	64(8)	-16(5)	-9(8)	16(7)
C(21)	66(10)	162(21)	64(9)	-31(12)	2(8)	-32(12)
C(22)	118(14)	66(10)	68(10)	0(8)	29(9)	43(10)
C(23)	111(12)	46(8)	62(9)	-9(6)	7(8)	20(8)
C(24)	91(12)	137(18)	45(8)	19(9)	14(8)	49(12)
C(25)	86(11)	75(10)	55(9)	2(7)	15(8)	-16(9)
C(31)	71(9)	50(8)	94(11)	-5(7)	-10(8)	10(7)
C(32)	97(13)	75(10)	93(11)	-11(9)	-6(10)	-9(9)
C(33)	1156(19)	122(16)	86(13)	-50(12)	-8(13)	-37(15)
C(34)	82(12)	61(10)	163(20)	-15(11)	14(13)	-1(9)
C(35)	86(12)	68(10)	139(18)	10(12)	-4(12)	9(9)
C(36)	61(8)	51(7)	84(10)	6(7)	-7(7)	-4(7)
C(41)	94(13)	69(10)	122(15)	7(10)	-40(11)	7(9)
C(42)	41(13)	74(17)	47(14)	4(12)	-19(11)	17(12)

Table AI-4. Selected bond lengths and angles for VIf

Zr-Si	2.806(4)	Zr-C(11)	2.516(14)
Zr-C(12)	2.511(15)	Zr-C(13)	2.529(15)
Zr-C(14)	2.502(12)	Zr-C(15)	2.540(14)
Zr-C(21)	2.515(17)	Zr-C(22)	2.513(17)
Zr-C(23)	2.540(14)	Zr-C(24)	2.507(15)
Zr-C(25)	2.511(15)	Zr-H	1.935(106)
Zr-Ha	1.951(106)	Zr-Zra	3.491(2)
Si-C(31)	1.907(15)	Si-C(41)	1.885(18)
Si-C(42)	1.839(24)	C(11)-C(12)	1.400(21)
C(11)-C(15)	1.358(25)	C(12)-C(13)	1.366(22)
C(13)-C(14)	1.390(24)	C(14)-C(15)	1.450(18)
C(21)-C(22)	1.372(28)	C(21)-C(25)	1.421(23)
C(22)-C(23)	1.333(24)	C(23)-C(24)	1.344(25)
C(24)-C(25)	1.341(27)	C(31)-C(32)	1.396(23)
C(31)-C(36)	1.449(21)	C(32)-C(33)	1.394(29)
C(33)-C(34)	1.343(31)	C(34)-C(35)	1.342(34)
C(35)-C(36)	1.338(23)		

Si-Zr-C(11)	116.4(4)	Si-Zr-C(12)	125.3(4)
Si-Zr-C(13)	97.5(4)	Si-Zr-C(14)	72.8(4)
Si-Zr-C(15)	85.2(4)	Si-Zr-C(21)	124.5(4)
Si-Zr-C(22)	118.8(4)	Si-Zr-C(23)	88.3(4)
Si-Zr-C(24)	74.0(4)	Si-Zr-C(25)	93.6(4)
Si-Zr-H	121.9(31)	Si-Zr-Ha	69.8(31)
Si-Zr-Zra	95.6(1)	H-Zr-Ha	52.1(55)
Zr-H-Zra	127.9(55)	Zr-Si-C(31)	115.1(5)
Zr-Si-C(41)	116.7(6)	Zr-Si-C(42)	112.4(7)
C(31)-Si-C(41)	106.0(7)	C(31)-Si-C(42)	104.8(10)
C(41)-Si-C(42)	100.3(10)	Si-C(31)-C(32)	124.3(12)
Si-C(31)-C(36)	120.8(11)	C(11)-Zr-C(12)	32.3(5)

Table AI-4. Selected bond lengths and angles for VIf (Continued)

C(11)-Zr-C(13)	53.2(5)	C(11)-Zr-C(14)	53.4(4)
C(11)-Zr-C(15)	31.2(6)	C(12)-Zr-C(13)	31.5(5)
C(12)-Zr-C(14)	52.7(5)	C(12)-Zr-C(15)	52.7(5)
C(13)-Zr-C(14)	32.1(5)	C(13)-Zr-C(15)	53.7(5)
C(14)-Zr-C(15)	33.4(4)	C(21)-Zr-C(22)	31.7(6)
C(21)-Zr-C(23)	52.0(6)	C(21)-Zr-C(24)	51.7(6)
C(21)-Zr-C(25)	32.8(5)	C(22)-Zr-C(23)	30.6(5)
C(22)-Zr-C(24)	50.7(6)	C(22)-Zr-C(25)	52.8(5)
C(23)-Zr-C(24)	30.9(6)	C(23)-Zr-C(25)	52.3(5)
C(24)-Zr-C(25)	31.0(6)	C(11)-Zr-C(21)	109.1(6)
C(12)-Zr-C(21)	81.3(6)	C(13)-Zr-C(21)	85.0(7)
C(14)-Zr-C(21)	115.7(6)	C(15)-Zr-C(21)	133.6(6)
C(11)-Zr-C(22)	124.8(5)	C(12)-Zr-C(22)	106.5(6)
C(13)-Zr-C(22)	116.5(6)	C(14)-Zr-C(22)	147.3(5)
C(15)-Zr-C(22)	155.9(6)	C(11)-Zr-C(23)	155.2(5)
C(12)-Zr-C(23)	133.2(5)	C(13)-ZR-C(23)	128.9(5)
C(14)-Zr-C(23)	144.7(4)	C(15)-Zr-C(23)	173.4(6)
C(11)-Zr-C(24)	153.4(6)	C(12)-Zr-C(24)	121.2(6)
C(13)-Zr-C(24)	102.8(6)	C(14)-Zr-C(24)	113.8(6)
C(15)-Zr-C(24)	146.6(6)	C(11)-ZR-C(25)	122.6(5)
C(12)-Zr-C(25)	90.3(5)	C(13)-Zr-C(25)	76.6(6)
C(14)-Zr-C(25)	98.4(5)	C(15)-Zr-C(25)	129.5(5)

APPENDIX II. X-RAY CRYSTAL STRUCTURAL ANALYSIS OF COMPLEX XXa

Table AII-1. Crystal data and data collection parameters for XXa

formula	$C_{25}H_{30}SiPTi$
fw	437.46
crystal system	monoclinic
space group	$P2_1/c$
a, Å	8.734(1)
b, Å	26.192(2)
c, Å	10.289(2)
β, deg	100.97(1)
V, $Å^3$	2310(1)
Z	4
F(000)	928
ρ_{calcd}, g/cm^3	1.26
μ(Mo Kα), cm^{-1}	5.1
crystal size, mm	0.08 × 0.40 × 0.44
temp, °C	20
radiation (graphite monochromator)	Mo Kα (λ = 0.71069 Å)
2θ limits, deg	$3 < 2\theta < 52$
scan speed, deg/min	6
no. of reflections collected	3761
no. of reflections used	2237
final no. of parameter	433
R[a]	0.030
Rw[b]	0.030

[a] $R = \Sigma||F_o| - |F_c|| / \Sigma|F_o|$

[b] $Rw = [\Sigma w(|F_o| - |F_c|)^2 / \Sigma w F_o^2]^{1/2}$

Table AII-2. Atomic coordinates and isotropic thermal parameters for XXa

Atom	X	Y	Z	U_{eq}[a]
Ti	-0.0626(1)	0.3701(1)	0.3143(1)	0.041(1)
P	-0.2756(1)	0.4395(1)	0.2409(1)	0.050(1)
Si	0.0161(1)	0.3877(1)	0.0818(1)	0.044(1)
C(1)	-0.4412(3)	0.4239(1)	0.1111(3)	0.068(1)
C(2)	-0.2199(4)	0.5014(1)	0.1842(3)	0.068(1)
C(3)	-0.3754(4)	0.4595(1)	0.3733(3)	0.081(2)
C(11)	-0.2494(4)	0.3128(1)	0.1973(3)	0.065(1)
C(12)	-0.1064(4)	0.2874(1)	0.2203(3)	0.064(1)
C(13)	-0.0602(4)	0.2814(1)	0.3561(3)	0.070(1)
C(14)	-0.1743(5)	0.3026(2)	0.4169(4)	0.070(1)
C(15)	-0.2914(4)	0.3215(1)	0.3199(4)	0.066(1)
C(21)	0.0251(7)	0.4255(3)	0.4914(6)	0.102(3)
C(22)	0.0956(5)	0.4409(1)	0.3887(4)	0.081(2)
C(23)	0.1930(4)	0.4033(1)	0.3678(3)	0.082(2)
C(24)	0.1872(4)	0.3654(1)	0.4537(4)	0.100(2)
C(25)	0.0822(7)	0.3785(3)	0.5293(5)	0.114(3)
C(31)	-0.1360(3)	0.3889(1)	-0.0771(3)	0.046(1)
C(32)	-0.1860(4)	0.4336(1)	-0.1437(3)	0.060(1)
C(33)	-0.3009(4)	0.4335(1)	-0.2569(3)	0.084(2)
C(34)	-0.3678(4)	0.3889(2)	-0.3066(3)	0.092(2)
C(35)	-0.3167(4)	0.3438(1)	-0.2459(3)	0.075(1)
C(36)	-0.2048(4)	0.3438(1)	-0.1331(3)	0.055(1)
C(41)	0.1708(3)	0.3436(1)	0.0324(3)	0.045(1)
C(42)	0.2090(4)	0.3486(1)	-0.0924(3)	0.059(1)
C(43)	0.3166(4)	0.3178(1)	-0.1344(3)	0.072(1)
C(44)	0.3922(4)	0.2804(1)	-0.0529(3)	0.069(1)
C(45)	0.3590(4)	0.2746(1)	0.0697(3)	0.060(1)
C(46)	0.2509(3)	0.3056(1)	0.1117(3)	0.054(1)

[a] Equivalent isotropic U defined as one third of the trace of the orthogonalized U_{ij} tensor.

Table AII-3. Anisotropic thermal parameters (Å^2 × 10^3) for **XXa**

Atom	U11	U22	U33	U23	U13	U12
Ti	47(1)	36(1)	37(1)	-1(1)	3(1)	-2(1)
P	51(1)	52(1)	46(1)	5(1)	7(1)	6(1)
Si	52(1)	37(1)	43(1)	-1(1)	9(1)	-3(1)
C(1)	53(2)	85(2)	64(2)	9(2)	2(2)	5(2)
C(2)	78(2)	55(2)	69(2)	9(2)	8(2)	7(2)
C(3)	78(3)	102(3)	66(2)	10(2)	22(2)	38(2)
C(11)	71(2)	59(2)	60(2)	4(2)	2(2)	-27(2)
C(12)	80(3)	43(2)	74(2)	-14(2)	27(2)	-17(2)
C(13)	81(2)	37(2)	88(2)	11(2)	9(2)	3(2)
C(14)	93(3)	57(2)	61(2)	14(2)	23(2)	-9(2)
C(15)	60(2)	56(2)	88(3)	8(2)	29(2)	-11(2)
C(21)	70(3)	134(5)	95(4)	-83(4)	-5(3)	12(4)
C(22)	91(3)	54(2)	83(3)	-6(2)	-24(2)	-19(2)
C(23)	48(2)	114(3)	83(2)	-29(2)	6(2)	-23(2)
C(24)	89(3)	71(2)	113(3)	-16(2)	-49(2)	14(2)
C(25)	151(5)	133(4)	40(3)	12(3)	-26(3)	-60(4)
C(31)	49(2)	46(2)	46(2)	2(1)	17(1)	8(1)
C(32)	70(2)	54(2)	57(2)	10(1)	17(2)	9(2)
C(33)	85(3)	98(3)	68(2)	38(2)	11(2)	29(2)
C(34)	59(2)	155(4)	57(2)	26(2)	-5(2)	-11(2)
C(35)	69(2)	102(3)	52(2)	-4(2)	8(2)	-26(2)
C(36)	63(2)	55(2)	48(2)	1(1)	10(2)	1(2)
C(41)	43(2)	49(2)	43(2)	-1(1)	6(1)	-7(1)
C(42)	54(2)	71(2)	53(2)	6(2)	7(2)	9(2)
C(43)	68(2)	97(3)	55(2)	-1(2)	22(2)	8(2)
C(44)	54(2)	78(2)	79(2)	-23(2)	19(2)	6(2)
C(45)	50(2)	61(2)	67(2)	2(2)	4(2)	9(2)
C(46)	49(2)	60(2)	54(2)	2(1)	11(2)	-2(2)

Table AII-4. Selected bond lengths and angles for XXa

Ti-Si	2.652(1)	Ti-P	2.609(1)
Ti-C(11)	2.370(3)	Ti-C(12)	2.373(3)
Ti-C(13)	2.360(3)	Ti-C(14)	2.361(4)
Ti-C(15)	2.378(3)	Ti-C(21)	2.341(6)
Ti-C(22)	2.352(4)	Ti-C(23)	2.361(3)
Ti-C(24)	2.375(3)	Ti-C(25)	2.340(5)
P-C(1)	1.819(3)	P-C(2)	1.819(3)
P-C(3)	1.827(4)	Si-H_{Si}	1.481(19)
Si-C(31)	1.900(2)	Si-C(41)	1.918(3)
C(11)-C(12)	1.395(5)	C(11)-C(15)	1.397(5)
C(12)-C(13)	1.387(5)	C(13)-C(14)	1.390(6)
C(14)-C(15)	1.378(5)	C(21)-C(22)	1.380(8)
C(22)-C(23)	1.345(5)	C(23)-C(24)	1.336(5)
C(24)-C(25)	1.355(8)	C(21)-C(25)	1.355(9)
C(31)-C(32)	1.386(4)	C(32)-C(33)	1.386(4)
C(33)-C(34)	1.360(5)	C(34)-C(35)	1.373(5)
C(35)-C(36)	1.367(4)	C(31)-C(36)	1.397(4)
C(41)-C(42)	1.393(4)	C(42)-C(43)	1.369(5)
C(43)-C(44)	1.374(4)	C(44)-C(45)	1.356(5)
C(45)-C(46)	1.376(4)	C(41)-C(46)	1.388(4)
P-Ti-Si	84.8(1)	P-Ti-C(11)	84.9(1)
P-Ti-C(12)	117.9(1)	P-Ti-C(13)	136.1(1)
P-Ti-C(14)	108.6(1)	P-Ti-C(15)	79.8(1)
P-Ti-C(21)	84.4(1)	P-Ti-C(22)	83.5(1)
P-Ti-C(23)	113.6(1)	P-Ti-C(24)	137.1(1)
P-Ti-C(25)	115.8(2)	Si-Ti-C(11)	85.6(1)
Si-Ti-C(12)	80.8(1)	Si-Ti-C(13)	109.9(1)
Si-Ti-C(14)	137.2(1)	Si-Ti-C(15)	118.6(1)
Si-Ti-C(21)	119.4(2)	Si-Ti-C(22)	83.5(1)
Si-Ti-C(23)	75.5(1)	Si-Ti-C(24)	100.8(1)

Table AII-4. Selected bond lengths and angles for <u>XXa</u> (Continued)

Si-Ti-C(25)	130.5(2)	Ti-P-C(1)	118.6(1)
Ti-P-C(2)	119.7(1)	Ti-P-C(3)	113.5(1)
Ti-Si-H_{Si}	114.7(9)	Ti-Si-C(31)	121.3(1)
Ti-Si-C(41)	116.8(1)	C(31)-Si-H_{Si}	99.5(8)
C(41)-Si-H_{Si}	99.8(9)	C(31)-Si-C(41)	101.2(1)
C(1)-P-C(2)	100.9(1)	C(1)-P-C(3)	100.7(2)
C(2)-P-C(3)	100.3(2)	Si-C(31)-C(32)	122.8(2)
Si-C(31)-C(36)	121.1(2)	Si-C(41)-C(42)	119.4(2)
Si-C(41)-C(46)	125.3(2)	C(11)-Ti-C(21)	151.6(2)
C(12)-Ti-C(21)	152.4(2)	C(13)-Ti-C(21)	118.5(2)
C(14)-Ti-C(21)	102.6(2)	C(15)-Ti-C(21)	117.7(2)
C(11)-Ti-C(22)	165.9(1)	C(12)-Ti-C(22)	153.1(1)
C(13)-Ti-C(22)	137.0(1)	C(14)-Ti-C(22)	135.3(1)
C(15)-Ti-C(22)	149.1(1)	C(11)-Ti-C(23)	151.7(1)
C(12)-Ti-C(23)	120.2(1)	C(13)-Ti-C(23)	110.2(1)
C(14)-Ti-C(23)	128.6(1)	C(15)-Ti-C(23)	162.3(1)
C(11)-Ti-C(24)	137.6(1)	C(12)-Ti-C(24)	104.9(1)
C(13)-Ti-C(24)	82.2(1)	C(14)-Ti-C(24)	95.8(1)
C(15)-Ti-C(24)	129.6(1)	C(11)-Ti-C(25)	137.4(2)
C(12)-Ti-C(25)	119.2(2)	C(13)-Ti-C(25)	86.4(2)
C(14)-Ti-C(25)	81.0(2)	C(15)-Ti-C(25)	109.5(2)

APPENDIX III. X-RAY CRYSTAL STRUCTURAL ANALYSIS OF COMPLEX XXb

Table AIII-1. Crystal data and data collection parameters for XXb

formula	$C_{20}H_{28}SiPTi$
fw	375.40
crystal system	orthorhombic
space group	$P2_12_12_1$
a, Å	9.076(3)
b, Å	12.078(4)
c, Å	18.299(5)
$\alpha = \beta = \gamma$, deg	90
V, $Å^3$	2006(1)
Z	4
F(000)	796
ρ_{calcd}, g/cm^3	1.243
μ(Mo Kα), cm^{-1}	5.56
crystal size, mm	0.4 × 0.4 × 0.4
temp, °C	20
radiation (graphite monochromator)	Mo Kα ($\lambda = 0.71069$ Å)
2θ limits, deg	$3 < 2\theta < 55$
scan speed, deg/min	6
no. of reflections collected	2624
no. of reflections used	1440
final no. of parameter	208
R^a	0.052
Rw^b	0.038

[a] $R = \Sigma||F_o| - |F_c|| / \Sigma|F_o|$

[b] $Rw = [\Sigma w(|F_o| - |F_c|)^2 / \Sigma w F_o^2]^{1/2}$

Table AIII-2. Atomic coordinates and isotropic thermal parameters for XXb

Atom	X	Y	Z	U_{eq}[a]
Ti	0.1102(1)	1.0031(2)	0.5785(1)	0.030(1)
P	-0.1711(2)	0.9846(4)	0.5864(1)	0.045(1)
Si	0.1020(2)	0.9905(4)	0.7228(1)	0.049(1)
C(1)	0.206(3)	1.177(1)	0.609(1)	0.09(1)
C(2)	0.294(2)	1.138(1)	0.550(2)	0.11(1)
C(3)	0.181(2)	1.134(1)	0.492(1)	0.066(9)
C(4)	0.058(2)	1.166(1)	0.520(1)	0.065(9)
C(5)	0.063(3)	1.196(1)	0.588(1)	0.09(1)
C(6)	0.059(2)	0.814(1)	0.544(2)	0.09(1)
C(7)	0.138(3)	0.863(2)	0.487(1)	0.09(1)
C(8)	0.276(2)	0.894(1)	0.513(1)	0.07(1)
C(9)	0.281(2)	0.858(1)	0.581(1)	0.067(9)
C(10)	0.158(2)	0.813(1)	0.604(1)	0.058(8)
C(11)	-0.272(1)	1.099(1)	0.629(1)	0.09(1)
C(12)	-0.247(1)	0.869(1)	0.636(1)	0.09(1)
C(13)	-0.262(1)	0.969(2)	0.4975(4)	0.10(1)
C(14)	0.375(2)	1.075(2)	0.7800(9)	0.08(1)
C(15)	0.526(2)	1.070(1)	0.8068(8)	0.08(1)
C(16)	0.570(2)	0.965(2)	0.8174(9)	0.09(1)
C(17)	0.499(2)	0.866(1)	0.8020(9)	0.09(1)
C(18)	0.358(2)	0.882(1)	0.7762(9)	0.08(1)
C(19)	0.294(1)	0.988(2)	0.7635(4)	0.059(6)
C(20)	0.012(2)	1.099(1)	0.7785(8)	0.055(3)
C(21)	-0.012(4)	0.934(3)	0.789(2)	0.055

[a] Equivalent isotropic U defined as one third of the trace of the orthogonalized U_{ij} tensor.

Table AIII-3. Anisotropic thermal parameters ($Å^2$ × 100) for **XXb**

Atom	U11	U22	U33	U23	U13	U12
Ti	3.40(6)	3.98(6)	3.85(6)	0.6(1)	-0.13(7)	-0.0(1)
P	3.8(1)	8.0(2)	5.1(1)	0.4(2)	0.3(1)	0.1(2)
Si	5.9(1)	8.3(2)	4.2(1)	-0.9(2)	-0.2(1)	0.4(3)
C(1)	14(2)	7(1)	12(2)	5(1)	-7(1)	-8(1)
C(2)	3.8(7)	9(1)	28(3)	9(2)	1(2)	-2(1)
C(3)	8(1)	9(1)	8(1)	4.1(8)	2(1)	0(1)
C(4)	11(1)	5.6(9)	8(1)	3.2(8)	-2(1)	2.3(9)
C(5)	16(2)	5.5(8)	14(2)	1(1)	-2(1)	-3(1)
C(6)	5.2(9)	5(1)	25(3)	-7(1)	2(1)	-1.9(7)
C(7)	15(2)	11(1)	7(1)	-6(1)	-5(1)	7(1)
C(8)	8(1)	11(1)	9(1)	0(1)	4(1)	3(1)
C(9)	7(1)	8(1)	10(1)	1.9(9)	1.0(8)	4.4(8)
C(10)	12(1)	3.2(6)	7(1)	0.2(6)	1(1)	0(1)
C(11)	7(1)	14(1)	12(1)	3(1)	3(1)	6(1)
C(12)	9(1)	13(1)	10(1)	-1(1)	4(1)	-6(1)
C(13)	5.3(6)	25(2)	6.6(6)	3(1)	-1.9(5)	-3(1)
C(14)	7(1)	19(2)	4.9(8)	1(1)	-0.9(8)	-0(1)
C(15)	14(2)	12(1)	5(1)	1(1)	-0(1)	-4(2)
C(16)	12(1)	20(2)	3.8(6)	-2.6(9)	0.5(7)	-4(1)
C(17)	11(1)	19(2)	5.4(8)	-0(1)	-1.3(8)	8(1)
C(18)	10(1)	16(1)	4.8(8)	2.4(9)	-1.4(9)	5(1)
C(19)	5.6(5)	13(1)	3.6(4)	0(1)	-0.1(4)	0(1)
C(20)	7.0(4)					
C(21)	7.0					

Table AIII-4. Selected bond lengths and angles for XXb

Ti-Si	2.646(2)	Ti-P	2.567(2)
Ti-C(1)	2.34(1)	Ti-C(2)	2.39(2)
Ti-C(3)	2.33(1)	Ti-C(4)	2.29(1)
Ti-C(5)	2.37(2)	Ti-C(6)	2.41(1)
Ti-C(7)	2.40(2)	Ti-C(8)	2.33(1)
Ti-C(9)	2.34(1)	Ti-C(10)	2.39(1)
P-C(11)	1.83(2)	P-C(12)	1.81(2)
P-C(13)	1.835(8)	Si-C(19)	1.893(9)
Si-C(20)	1.85(2)	C(1)-C(2)	1.42(3)
C(1)-C(5)	1.38(2)	C(2)-C(3)	1.47(3)
C(3)-C(4)	1.30(2)	C(4)-C(5)	1.28(2)
C(6)-C(7)	1.40(3)	C(6)-C(10)	1.42(2)
C(7)-C(8)	1.39(2)	C(8)-C(9)	1.33(2)
C(9)-C(10)	1.30(2)	C(14)-C(15)	1.46(2)
C(14)-C(19)	1.32(2)	C(15)-C(16)	1.35(2)
C(16)-C(17)	1.39(2)	C(17)-C(18)	1.38(2)
C(18)-C(19)	1.42(2)		

P-Ti-Si	84.86(8)	P-Ti-C(1)	115.8(7)
P-Ti-C(2)	140.0(4)	P-Ti-C(3)	112.0(6)
P-Ti-C(4)	84.0(5)	P-Ti-C(5)	84.3(6)
P-Ti-C(6)	75.0(4)	P-Ti-C(7)	94.7(7)
P-Ti-C(8)	128.4(5)	P-Ti-C(9)	126.2(5)
P-Ti-C(10)	95.0(5)	Si-Ti-C(1)	79.9(5)
Si-Ti-C(2)	106.1(8)	Si-Ti-C(3)	136.5(5)
Si-Ti-C(4)	120.6(5)	Si-Ti-C(5)	88.9(6)
Si-Ti-C(6)	101.5(8)	Si-Ti-C(7)	131.3(6)
Si-Ti-C(8)	120.0(5)	Si-Ti-C(9)	87.3(4)
Si-Ti-C(10)	75.8(3)	Ti-P-C(11)	117.0(5)
Ti-P-C(12)	118.5(5)	Ti-P-C(13)	114.0(3)
Ti-Si-H_{Si}	109.0	Ti-Si-C(19)	111.6(2)

Table AIII-4. Selected bond lengths and angles for **XXb** (Continued)

Ti-Si-C(20)	121.4(5)	C(19)-Si-H_{Si}	109.8
C(20)-Si-H_{Si}	102.7	C(19)-Si-C(20)	101.6(8)
C(11)-P-C(12)	100.6(5)	C(11)-P-C(13)	103.3(7)
C(12)-P-C(13)	101.0(7)	Si-C(19)-C(14)	126(2)
Si-C(19)-C(18)	117(1)	C(1)-Ti-C(6)	169.2(8)
C(1)-Ti-C(7)	139.6(8)	C(1)-Ti-C(8)	112.9(8)
C(1)-Ti-C(9)	114.9(9)	C(1)-Ti-C(10)	138.6(7)
C(2)-Ti-C(6)	136.3(7)	C(2)-Ti-C(7)	104.9(8)
C(2)-Ti-C(8)	79.8(6)	C(2)-Ti-C(9)	93.2(5)
C(2)-Ti-C(10)	124.9(6)	C(3)-Ti-C(6)	121.2(8)
C(3)-Ti-C(7)	88.5(6)	C(3)-Ti-C(8)	81.6(6)
C(3)-Ti-C(9)	109.9(6)	C(3)-Ti-C(10)	137.3(6)
C(4)-Ti-C(6)	130.8(9)	C(4)-Ti-C(7)	107.7(7)
C(4)-Ti-C(8)	112.3(7)	C(4)-Ti-C(9)	142.5(7)
C(4)-Ti-C(10)	163.3(6)	C(5)-Ti-C(6)	155.7(8)
C(5)-Ti-C(7)	139.6(8)	C(5)-Ti-C(8)	135.1(6)
C(5)-Ti-C(9)	148.7(7)	C(5)-Ti-C(10)	164.7(7)

APPENDIX IV. X-RAY CRYSTAL STRUCTURAL ANALYSIS OF COMPLEX XXc

Table AIV-1. Crystal data and data collection parameters for XXc

formula	$C_{19}H_{26}SiPTi$
fw	361.37
crystal system	monoclinic
space group	$P2_1$
a, Å	8.548(2)
b, Å	9.098(2)
c, Å	12.786(2)
β, deg	101.48(2)
V, $Å^3$	974(1)
Z	2
F(000)	382
ρ_{calcd}, g/cm^3	1.23
μ(Mo Kα), cm^{-1}	5.9
crystal size, mm	0.2 × 0.3 × 0.5
temp, °C	20
radiation (graphite monochromator)	Mo Kα (λ = 0.71069 Å)
2θ limits, deg	$3 < 2\theta < 60$
scan speed, deg/min	7
no. of reflections collected	3258
no. of reflections used	2077
final no. of parameter	215
R[a]	0.038
Rw[b]	0.041

[a] $R = \Sigma||F_o| - |F_c|| / \Sigma|F_o|$

[b] $Rw = [\Sigma w(|F_o| - |F_c|)^2 / \Sigma w F_o^2]^{1/2}$

Table AIV-2. Atomic coordinates and isotropic thermal parameters for XXc

Atom	X	Y	Z	U_{eq}[a]
Ti	0.1107(1)	0.5000	0.2657(1)	0.037(1)
P	0.1653(1)	0.7791(1)	0.2748(1)	0.050(1)
Si	0.4203(1)	0.4958(2)	0.2647(1)	0.050(1)
C(1)	0.2256(7)	0.6691(6)	0.1624(4)	0.075(2)
C(2)	0.3159(7)	0.8481(6)	0.3846(4)	0.073(2)
C(3)	-0.0065(8)	0.8909(7)	0.2891(6)	0.105(3)
C(11)	0.2174(7)	0.4741(10)	0.4507(3)	0.094(3)
C(12)	0.0804(9)	0.5549(7)	0.4422(3)	0.092(3)
C(13)	-0.0452(7)	0.4678(9)	0.3978(4)	0.094(3)
C(14)	0.0129(8)	0.3345(8)	0.3801(4)	0.095(3)
C(15)	0.1760(8)	0.3379(7)	0.4119(4)	0.094(3)
C(21)	0.1029(5)	0.5052(8)	0.0806(3)	0.076(2)
C(22)	-0.0340(6)	0.5818(6)	0.0969(3)	0.067(2)
C(23)	-0.1284(5)	0.4831(7)	0.1367(3)	0.065(2)
C(24)	-0.0579(5)	0.3457(6)	0.1426(4)	0.066(2)
C(25)	0.0855(6)	0.3586(7)	0.1097(4)	0.073(2)
C(31)	0.5000(4)	0.3155(5)	0.2200(3)	0.048(1)
C(32)	0.4926(5)	0.2825(6)	0.1126(3)	0.056(1)
C(33)	0.5445(5)	0.1503(6)	0.0802(3)	0.064(2)
C(34)	0.6049(5)	0.0448(5)	0.1522(4)	0.063(2)
C(35)	0.6127(5)	0.0713(6)	0.2592(4)	0.065(2)
C(36)	0.5617(5)	0.2051(6)	0.2914(3)	0.059(1)

[a] Equivalent isotropic U defined as one third of the trace of the orthogonalized U_{ij} tensor.

Table AIV-3. Anisotropic thermal parameters ($\text{Å}^2 \times 10^3$) for XXc

Atom	U11	U22	U33	U23	U13	U12
Ti	39(1)	42(1)	30(1)	-1(1)	7(1)	-2(1)
P	56(1)	43(1)	49(1)	0(1)	4(1)	4(1)
Si	42(1)	56(1)	51(1)	-7(1)	8(1)	4(1)
C(1)	95(3)	63(3)	61(3)	19(2)	-3(2)	-15(3)
C(2)	91(3)	54(3)	66(3)	-6(2)	-2(2)	-9(3)
C(3)	109(5)	73(4)	133(6)	-9(4)	21(4)	40(4)
C(11)	87(3)	157(7)	35(2)	14(3)	8(2)	-30(4)
C(12)	172(6)	68(3)	52(3)	-7(2)	60(4)	-11(4)
C(13)	80(3)	144(7)	71(3)	35(4)	46(3)	26(4)
C(14)	148(6)	87(4)	56(3)	10(3)	33(3)	-46(4)
C(15)	143(6)	84(4)	65(3)	38(3)	43(4)	44(4)
C(21)	61(2)	141(5)	27(1)	-14(3)	9(1)	-38(4)
C(22)	81(3)	67(3)	42(2)	8(2)	-15(2)	-7(2)
C(23)	41(2)	96(4)	52920	-8(3)	-3(1)	-7(3)
C(24)	72(3)	67(3)	53(2)	-4(2)	-3(2)	-26(2)
C(25)	26(3)	98(4)	49(2)	-32(3)	-4(2)	6(3)
C(31)	37(2)	61(3)	49(2)	-2(2)	14(1)	0(2)
C(32)	56(2)	69(3)	45(2)	4(2)	12(2)	13(2)
C(33)	59(2)	84(3)	51(2)	-15(2)	15(2)	6(2)
C(34)	58(2)	63(3)	64(2)	-15(2)	8(2)	9(2)
C(35)	66(3)	65(3)	61(3)	7(2)	9(2)	14(2)
C(36)	52(2)	77(3)	46(2)	-2(2)	6(2)	10(2)

Table AIV-4. Selected bond lengths and angles for <u>XXc</u>

Ti-Si	2.650(1)	Ti-P	2.580(1)
Ti-C(11)	2.371(4)	Ti-C(12)	2.375(5)
Ti-C(13)	2.368(6)	Ti-C(14)	2.365(7)
Ti-C(15)	2.359(6)	Ti-C(21)	2.355(3)
Ti-C(22)	2.383(4)	Ti-C(23)	2.363(4)
Ti-C(24)	2.371(5)	Ti-C(25)	2.347(5)
P-C(1)	1.816(6)	P-C(2)	1.817(5)
P-C(3)	1.825(7)	Si-H(1)	1.468(28)
Si-H(2)	1.467(40)	Si-C(31)	1.907(5)
C(11)-C(12)	1.369(10)	C(11)-C(15)	1.355(11)
C(12)-C(13)	1.364(9)	C(13)-C(14)	1.347(10)
C(14)-C(15)	1.373(10)	C(21)-C(22)	1.412(7)
C(22)-C(23)	1.371(7)	C(23)-C(24)	1.383(8)
C(24)-C(25)	1.377(7)	C(21)-C(25)	1.401(9)
C(31)-C(32)	1.394(5)	C(32)-C(33)	1.375(7)
C(33)-C(34)	1.359(7)	C(34)-C(35)	1.377(7)
C(35)-C(36)	1.383(8)	C(31)-C(36)	1.388(6)
P-Ti-Si	80.9(1)	P-Ti-C(11)	91.3(2)
P-Ti-C(12)	78.7(1)	P-Ti-C(13)	102.2(2)
P-Ti-C(14)	133.0(2)	P-Ti-C(15)	124.6(2)
P-Ti-C(21)	89.7(2)	P-Ti-C(22)	77.9(1)
P-Ti-C(23)	102.6(2)	P-Ti-C(24)	133.9(1)
P-Ti-C(25)	124.3(1)	Si-Ti-C(11)	79.5(2)
Si-Ti-C(12)	107.8(2)	Si-Ti-C(13)	134.9(1)
Si-Ti-C(14)	118.1(2)	Si-Ti-C(15)	85.2(2)
Si-Ti-C(21)	79.9(1)	Si-Ti-C(22)	109.8(1)
Si-Ti-C(23)	136.2(1)	Si-Ti-C(24)	117.6(1)
Si-Ti-C(25)	84.9(1)	Ti-P-C(1)	119.0(2)
Ti-P-C(2)	117.9(2)	Ti-P-C(3)	114.3(2)

Table AIV-4. Selected bond lengths and angles for XXc (Continued)

Ti-Si-H(1)	112.4(16)	Ti-Si-H(2)	110.0(17)
Ti-Si-C(31)	115.5(1)	C(31)-Si-H(1)	102.4(23)
C(31)-Si-H(2)	104.2(16)	H(1)-Si-H(2)	111.8(26)
C(1)-P-C(2)	100.8(2)	C(1)-P-C(3)	100.9(3)
C(2)-P-C(3)	101.0(3)	Si-C(31)-C(32)	122.1(3)
Si-C(31)-C(36)	122.5(3)	C(11)-Ti-C(21)	158.9(2)
C(12)-Ti-C(21)	164.6(2)	C(13)-Ti-C(21)	144.2(2)
C(14)-Ti-C(21)	133.8(2)	C(15)-Ti-C(21)	139.8(2)
C(11)-Ti-C(22)	164.1(2)	C(12)-Ti-C(22)	131.3(2)
C(13)-Ti-C(22)	114.8(2)	C(14)-Ti-C(22)	125.1(2)
C(15)-Ti-C(22)	155.7(2)	C(11)-Ti-C(23)	142.9(2)
C(12)-Ti-C(23)	115.7(2)	C(13)-Ti-C(23)	87.6(2)
C(14)-Ti-C(23)	91.6(2)	C(15)-Ti-C(23)	123.3(2)
C(11)-Ti-C(24)	131.8(2)	C(12)-Ti-C(24)	126.1(2)
C(13)-Ti-C(24)	92.7(2)	C(14)-Ti-C(24)	77.9(2)
C(15)-Ti-C(24)	100(2)	C(11)-Ti-C(25)	138.2(2)
C(12)-Ti-C(25)	156.0(2)	C(13)-Ti-C(25)	124.6(2)
C(14)-Ti-C(25)	101.1(2)	C(15)-Ti-C(25)	107.3(2)

APPENDIX V. X-RAY CRYSTAL STRUCTURAL ANALYSIS OF COMPLEX XXII

Table AV-1. Crystal data and data collection parameters for XXII

formula	$C_{25}H_{25}NTi_2$
fw	435.28
crystal system	monoclinic
space group	$P2_1/n$
a, Å	16.996(10)
b, Å	8.106(4)
c, Å	18.412(7)
β, deg	114.40(3)
V, $Å^3$	2306(1)
Z	4
F(000)	988
ρ_{calcd}, g/cm^3	1.37
μ(Mo Kα), cm^{-1}	7.4
crystal size, mm	0.2 × 0.4 × 0.3
temp, °C	20
radiation (graphite monochromator)	Mo Kα (λ = 0.71069 Å)
2θ limits, deg	$3 < 2\theta < 50$
scan speed, deg/min	6
no. of reflections collected	4063
no. of reflections used	1725
final no. of parameter	284
R[a]	0.053
Rw[b]	0.037

[a] $R = \Sigma||F_o| - |F_c|| / \Sigma|F_o|$

[b] $Rw = [\Sigma w(|F_o| - |F_c|)^2 / \Sigma w F_o^2]^{1/2}$

Table AV-2. Atomic coordinates and isotropic thermal parameters for <u>**XXII**</u>

Atom	X	Y	Z	U_{eq}[a]
Ti(1)	0.7924(1)	0.9240(1)	0.5983(1)	0.038(1)
Ti(2)	0.665(1)	1.0043(1)	0.376(1)	0.039(1)
H_{Ti}	0.7040(15)	0.9000(43)	0.4905(10)	0.015(11)
N	0.109(3)	1.1263(6)	0.4604(3)	0.024(2)
C(11)	0.848(3)	1.1024(6)	0.5406(3)	0.055(3)
C(12)	0.9235(4)	1.1882(8)	0.5844(3)	0.069(4)
C(13)	0.9633(4)	1.2909(8)	0.5528(4)	0.070(4)
C(14)	0.9259(4)	1.3117(8)	0.4714(4)	0.069(4)
C(15)	0.8519(4)	1.2292(8)	0.4294(3)	0.069(4)
C(21)	0.6770(4)	1.0787(9)	0.6103(4)	0.085(4)
C(22)	0.7475(4)	1.1837(7)	0.6329(4)	0.093(5)
C(23)	0.8119(4)	1.1111(8)	0.7047(4)	0.086(4)
C(24)	0.7745(4)	0.9677(8)	0.7183(3)	0.081(4)
C(25)	0.6929(4)	0.9523(8)	0.6599(4)	0.072(4)
C(31)	0.8733(4)	0.7256(7)	0.5629(3)	0.060(3)
C(32)	0.9305(4)	0.7921(7)	0.6351(3)	0.066(3)
C(33)	0.9003(4)	0.7464(9)	0.6917(4)	0.082(4)
C(34)	0.8266(4)	0.6527(8)	0.6547(4)	0.077(4)
C(35)	0.8090(4)	0.6376(7)	0.5759(3)	0.068(4)
C(41)	0.7378(4)	0.7331(7)	0.3725(3)	0.065(3)
C(42)	0.7900(4)	0.8484(7)	0.3544(3)	0.071(4)
C(43)	0.7330(4)	0.9333(8)	0.2856(3)	0.078(4)
C(44)	0.6505(4)	0.8671(8)	0.2648(3)	0.072(4)
C(45)	0.6528(4)	0.7461(7)	0.3167(3)	0.072(4)
C(51)	0.6240(4)	1.2335(9)	0.4239(4)	0.081(4)
C(52)	0.5632(4)	1.1142(10)	0.4014(4)	0.098(5)
C(53)	0.5361(4)	1.0842(10)	0.3206(5)	0.117(5)
C(54)	0.5879(5)	1.1993(10)	0.2993(4)	0.112(5)
C(55)	0.6388(4)	1.2850(8)	0.3631(4)	0.093(5)

[a] Equivalent isotropic U defined as one third of the trace of the orthogonalized U_{ij} tensor.

Table AV-3. Anisotropic thermal parameters ($\AA^2 \times 10^3$) for **XXII**

Atom	U11	U22	U33	U23	U13	U12
Ti(1)	45(1)	39(1)	34(1)	3(1)	19(1)	2(1)
Ti(2)	42(1)	39(1)	31(1)	-3(1)	10(1)	-0(1)
N	35(3)	24(4)	14(3)	-1(3)	13(3)	-9(3)
C(11)	55(4)	47(4)	68(4)	-4(3)	29(3)	-4(3)
C(12)	63(5)	86(6)	38(4)	1(4)	1(4)	-40(5)
C(13)	51(5)	74(6)	78(6)	-6(5)	18(4)	-31(4)
C(14)	86(6)	61(5)	75(5)	-6(5)	47(5)	-34(5)
C(15)	81(5)	80(6)	38(4)	-0(4)	18(4)	-36(5)
C(21)	120(6)	87(6)	65(5)	28(5)	56(5)	53(6)
C(22)	194(8)	35(5)	115(6)	8(5)	128(6)	20(5)
C(23)	110(6)	73(6)	100(6)	-51(5)	69(5)	-31(5)
C(24)	95(5)	115(7)	34(4)	-1(4)	28(4)	24(5)
C(25)	84(5)	73(7)	80(5)	-1(5)	56(5)	6(5)
C(31)	70(5)	63(5)	49(4)	6(4)	27(4)	35(4)
C(32)	45(4)	78(6)	75(5)	28(4)	24(4)	23(4)
C(33)	88(6)	85(7)	50(7)	10(5)	4(5)	43(5)
C(34)	93(6)	63(6)	96(6)	41(5)	59(5)	25(5)
C(35)	75(5)	47(5)	83(5)	11(4)	34(4)	11(4)
C(41)	81(5)	59(5)	42(4)	-16(4)	13(4)	21(4)
C(42)	66(5)	87(6)	66(4)	-30(4)	33(4)	3(4)
C(43)	111(6)	78(6)	81(5)	-21(4)	76(5)	-20(5)
C(44)	94(6)	72(6)	35(4)	-16(4)	12(4)	10(4)
C(45)	106(6)	45(5)	68(5)	-20(4)	41(4)	-23(4)
C(51)	103(7)	84(7)	56(5)	5(5)	32(5)	55(5)
C(52)	47(5)	84(7)	160(8)	23(6)	39(5)	14(5)
C(53)	41(5)	69(7)	162(9)	-45(7)	-38(5)	12(5)
C(54)	120(7)	125(8)	44(5)	1(5)	-12(5)	80(6)
C(55)	107(7)	48(6)	114(7)	29(5)	35(6)	25(5)

Table AV-4. Selected bond lengths and angles for **XXII**

Ti(1)-H_{Ti}	1.941(16)	Ti(2)-H_{Ti}	1.981(23)
Ti(1)-C(11)	2.230(6)	Ti(2)-N	2.212(4)
Ti(1)-C(21)	2.412(8)	Ti(1)-C(22)	2.413(7)
Ti(1)-C(23)	2.391(7)	Ti(1)-C(24)	2.377(7)
Ti(1)-C(25)	2.402(8)	Ti(1)-C(31)	2.373(6)
Ti(1)-C(32)	2.404(6)	Ti(1)-C(33)	2.404(6)
Ti(1)-C(34)	2.399(7)	Ti(1)-C(35)	2.395(6)
Ti(2)-C(41)	2.423(6)	Ti(2)-C(42)	2.440(7)
Ti(2)-C(43)	2.389(7)	Ti(2)-C(44)	2.363(6)
Ti(2)-C(45)	2.408(6)	Ti(2)-C(51)	2.367(8)
Ti(2)-C(52)	2.381(8)	Ti(2)-C(53)	2.418(7)
Ti(2)-C(54)	2.386(7)	Ti(2)-C(55)	2.394(7)
C(11)-N	1.356(6)	C(11)-C(12)	1.377(7)
C(12)-C(13)	1.345(11)	C(13)-C(14)	1.375(9)
C(14)-C(15)	1.349(8)	C(15)-N	1.354(9)
C(21)-C(22)	1.385(10)	C(22)-C(23)	1.448(8)
C(23)-C(24)	1.395(10)	C(24)-C(25)	1.363(7)
C(21)-C(25)	1.324(9)	C(31)-C(32)	1.391(7)
C(32)-C(33)	1.388(11)	C(33)-C(34)	1.380(9)
C(34)-C(35)	1.361(9)	C(31)-C(35)	1.404(9)
C(41)-C(42)	1.419(9)	C(42)-C(43)	1.415(7)
C(43)-C(44)	1.396(9)	C(44)-C(45)	1.358(9)
C(41)-C(45)	1.386(7)	C(51)-C(52)	1.348(10)
C(52)-C(53)	1.385(12)	C(53)-C(54)	1.443(12)
C(54)-C(55)	1.331(9)	C(51)-C(55)	1.314(12)
C(11)-Ti(1)-H_{Ti}	83.1(9)	N-Ti(2)-H_{Ti}	83.3(8)
Ti(1)-H_{Ti}-Ti(2)	133.0(16)	Ti(1)-C(11)-N	120.4(3)
Ti(1)-C(11)-C(12)	121.4(4)	Ti(2)-N-C(11)	120.0(4)
Ti(2)-N-C(15)	123.3(3)	N-C(11)-C(12)	118.1(5)

Table AV-4. Selected bond lengths and angles for XXII (Continued)

C(11)-C(12)-C(13)	124.4(5)	C(12)-C(13)-C(14)	117.4(5)
C(13)-C(14)-C(15)	117.7(7)	C(14)-C(15)-N	125.7(5)
C(15)-N-C(11)	116.8(4)	H_{Ti}-Ti(1)-C(21)	80.3(9)
H_{Ti}-Ti(1)-C(22)	99.3(10)	H_{Ti}-Ti(1)-C(23)	133.5(10)
H_{Ti}-Ti(1)-C(24)	128.6(8)	H_{Ti}-Ti(1)-C(25)	95.5(8)
H_{Ti}-Ti(1)-C(31)	86.6(9)	H_{Ti}-Ti(1)-C(32)	119.7(9)
H_{Ti}-Ti(1)-C(33)	135.2(10)	H_{Ti}-Ti(1)-C(34)	107.3(10)
H_{Ti}-Ti(1)-C(35)	79.8(10)	H_{Ti}-Ti(2)-C(41)	78.7(9)
H_{Ti}-Ti(2)-C(42)	100.4(9)	H_{Ti}-Ti(2)-C(43)	132.9(9)
H_{Ti}-Ti(2)-C(44)	126.3(9)	H_{Ti}-Ti(2)-C(45)	93.2(9)
H_{Ti}-Ti(2)-C(51)	88.5(9)	H_{Ti}-Ti(2)-C(52)	81.3(8)
H_{Ti}-Ti(2)-C(53)	108.2(8)	H_{Ti}-Ti(2)-C(54)	136.1(9)
H_{Ti}-Ti(2)-C(55)	119.5(10)	C(11)-Ti(1)-C(21)	103.4(2)
C(11)-Ti(1)-C(22)	78.7(2)	C(11)-Ti(1)-C(23)	92.2(2)
C(11)-Ti(1)-C(24)	126.2(2)	C(11)-Ti(1)-C(25)	133.4(2)
C(11)-Ti(1)-C(31)	84.1(2)	C(11)-Ti(1)-C(32)	82.1(2)
C(11)-Ti(1)-C(33)	112.3(2)	C(11)-Ti(1)-C(34)	136.6(2)
C(11)-Ti(1)-C(35)	116.2(2)	N-Ti(2)-C(41)	100.2(2)
N-Ti(2)-C(42)	77.1(2)	N-Ti(2)-C(43)	92.4(2)
N-Ti(2)-C(44)	126.5(2)	N-Ti(2)-C(45)	132.1(2)
N-Ti(2)-C(51)	84.5(2)	N-Ti(2)-C(52)	115.4(2)
N-Ti(2)-C(53)	137.0(2)	N-Ti(2)-C(54)	110.0(2)
N-Ti(2)-C(55)	81.5(2)	C(21)-Ti(1)-C(31)	163.9(2)
C(22)-Ti(1)-C(31)	161.0(2)	C(23)-Ti(1)-C(31)	139.1(2)
C(24)-Ti(1)-C(31)	131.8(2)	C(25)-Ti(1)-C(31)	142.5(2)
C(21)-Ti(1)-C(32)	160.0(2)	C(22)-Ti(1)-C(32)	133.8(2)
C(23)-Ti(1)-C(32)	105.3(2)	C(24)-Ti(1)-C(32)	106.8(2)
C(25)-Ti(1)-C(32)	134.6(2)	C(21)-Ti(1)-C(33)	130.8(3)
C(22)-Ti(1)-C(33)	124.3(2)	C(23)-Ti(1)-C(33)	89.3(2)
C(24)-Ti(1)-C(33)	77.1(2)	C(25)-Ti(1)-C(33)	101.3(2)

Table AV-4. Selected bond lengths and angles for XXII (Continued)

C(21)-Ti(1)-C(34)	119.8(3)	C(22)-Ti(1)-C(34)	137.1(3)
C(23)-Ti(1)-C(34)	107.5(2)	C(24)-Ti(1)-C(34)	80.5(2)
C(25)-Ti(1)-C(34)	88.5(3)	C(21)-Ti(1)-C(35)	132.6(2)
C(22)-Ti(1)-C(35)	164.6(3)	C(23)-Ti(1)-C(35)	140.4(2)
C(24)-Ti(1)-C(35)	112.0(2)	C(25)-Ti(1)-C(35)	109.2(2)
C(41)-Ti(1)-C(51)	165.6(3)	C(42)-Ti(1)-C(51)	158.5(2)
C(43)-Ti(1)-C(51)	138.0(2)	C(44)-Ti(1)-C(51)	132.1(2)
C(45)-Ti(1)-C(51)	143.3(2)	C(41)-Ti(1)-C(52)	136.5(2)
C(42)-Ti(1)-C(52)	167.5(2)	C(43)-Ti(1)-C(52)	139.8(2)
C(44)-Ti(1)-C(52)	112.8(2)	C(45)-Ti(1)-C(52)	111.2(2)
C(41)-Ti(1)-C(53)	122.5(2)	C(42)-Ti(1)-C(53)	136.7(2)
C(43)-Ti(1)-C(53)	106.5(3)	C(44)-Ti(1)-C(53)	80.6(3)
C(45)-Ti(1)-C(53)	89.6(2)	C(41)-Ti(1)-C(54)	135.0(2)
C(42)-Ti(1)-C(54)	123.2(3)	C(43)-Ti(1)-C(54)	89.4(2)
C(44)-Ti(1)-C(54)	80.1(2)	C(45)-Ti(1)-C(54)	105.3(2)
C(41)-Ti(1)-C(55)	161.8(3)	C(42)-Ti(1)-C(55)	131.8(3)
C(43)-Ti(1)-C(55)	106.0(3)	C(44)-Ti(1)-C(55)	109.5(2)
C(45)-Ti(1)-C(55)	137.6(2)		